

GRANTECAN S.A.
Version 3.1
OSIRIS USER MANUAL
January 1, 2014

OSIRIS
USER MANUAL

Antonio Cabrera-Lavers, OSIRIS Instrument Specialist¹.

¹ This document is based on a first version of the manual from J. Cepa (Instrument P.I.), and the OSIRIS Instrument Team, under the direction of the Instituto de Astrofísica de Canarias.

TABLE OF CONTENTS

LIST OF ABBREVIATIONS.....	5
1. INSTRUMENT CHARACTERISTICS	6
1.1 OVERVIEW	6
1.1.1 <i>Instrument description</i>	6
1.1.2 <i>OSIRIS focal plane masks</i>	8
1.1.3 <i>Observing modes</i>	9
1.1.4 <i>Main Characteristics</i>	10
1.1.5 <i>Field obscuration and vignetting</i>	11
1.1.6 <i>Field orientation and gap</i>	11
1.1.7 <i>Instrument overheads</i>	12
1.1.8 <i>Environmental conditions</i>	12
1.2 DETECTORS	12
1.2.1 <i>Description</i>	12
1.2.2 <i>OSIRIS standard CCD operation modes</i>	14
1.2.3 <i>OSIRIS CCDs linearity / dark current level / cross-talk</i>	14
1.2.4 <i>Quantum Efficiency</i>	15
1.2.6 <i>CCD windowing</i>	16
2. BROAD BAND IMAGING	17
2.1.1 <i>Sloan broad band filters</i>	17
2.1.1.1 <i>Zeropoints</i>	19
2.1.1.2 <i>Sky background</i>	19
2.1.1.3 <i>Colour corrections</i>	20
2.1.1.4 <i>OSIRIS/GTC Broad Band Imaging efficiency</i>	20
2.2 <i>PHOTOMETRIC UNIFORMITY</i>	22
2.3 <i>SKY FLAT FIELDS</i>	22
2.4 <i>SLOAN PHOTOMETRIC STANDARDS</i>	22
3. TUNABLE FILTER IMAGING	23
3.1 <i>OSIRIS TUNABLE FILTERS DESCRIPTION</i>	23
3.1.1 <i>Introduction to FabryPerot filters (FPFs)</i>	23
3.1.1.1 <i>Performance of an ideal FPF</i>	23
3.1.1.2 <i>Limitations</i>	25
3.1.1.3 <i>Gap-scanning etalons</i>	26
3.1.2 <i>Charge shuffling</i>	28
3.1.3 <i>Order sorters</i>	28
3.1.4 <i>OSIRIS TF Characteristics and Features</i>	28
3.1.4.1 <i>Dimensions</i>	30
3.1.4.2 <i>Coatings</i>	30
3.2 <i>OSIRIS FOV FOR TUNABLE FILTER IMAGING</i>	31
3.2.1 <i>Red Tunable Filter</i>	32
3.2.2 <i>Blue Tunable Filter</i>	33
3.3 <i>OSIRIS TUNABLE FILTER AVAILABLE WIDTHS</i>	35
3.4 <i>ORDER SORTER FILTERS</i>	37
3.5 <i>CALIBRATING THE TF AND TUNING ACCURACY</i>	37
3.5.1 <i>Parallelism</i>	37

3.5.1.1	<i>General considerations</i>	37
3.5.1.2	TF parallelization procedure.....	38
3.5.1.3	Lack of parallelism.....	39
3.5.2	<i>Wavelength calibration</i>	41
3.5.2.1	General considerations	41
3.5.2.2	Calibration using the ICM.....	42
3.5.3	<i>Checking the calibration by using night sky emission lines</i>	43
3.5.4	<i>Tuning accuracy</i>	45
3.5.5	<i>Tuning speed</i>	45
3.6	OBSERVING WITH OSIRIS TUNABLE FILTER	45
3.6.1	<i>Tunable Filter vs. Spectroscopy</i>	45
3.6.2	<i>Observing Strategies</i>	46
3.6.2.1	Selecting off-band wavelengths.....	47
3.6.2.1.1	Continuum subtraction.....	47
3.6.2.2	Deblending lines.....	48
3.6.2.3	On-line FWHM selection	49
3.6.2.4	Deciding target position and orientation.....	50
3.6.2.5	Removing ghosts, cosmic rays and cosmetics	51
3.6.2.5.1	Field masking	53
3.6.2.5.2	Azimuthal dithering pattern	53
3.6.2.5.3	TF tuning dithering pattern	53
3.6.2.6	Tunable tomography.....	53
3.6.2.6.1	Technique	53
3.6.2.7	Band synthesis technique	54
3.6.2.7.1	Technique	54
3.6.2.8	Summary	56
3.6.2.8.1	Sources of instrumental photometric errors.	56
3.6.2.8.2	Preparing an observation: a checklist.....	56
3.7	SPECTROPHOTOMETRIC STANDARDS FOR TF FLUX CALIBRATION	57
3.8	OSIRIS TUNABLE FILTERS GLOBAL EFFICIENCY	57
3.9	POST-PROCESSING TF DATA	58
3.9.1	<i>Calibration images</i>	58
3.9.1.1	Bias.....	58
3.9.1.2	Flat fields.....	58
3.9.2	<i>Night-sky emission line rings</i>	59
3.10	MEDIUM BAND IMAGING WITH TF ORDER SORTERS	60
4.	MEDIUM BAND IMAGING (SHARDS FILTERS)	63
4.1	PHOTON DETECTION EFFICIENCY WITH SHARDS FILTERS	67
5.	FAST IMAGING MODES	68
5.1	FAST PHOTOMETRY	68
5.2	FRAME TRANSFER	69
6.	LONG SLIT SPECTROSCOPY	71
6.1	ACQUISITION IN LONG-SLIT SPECTROSCOPIC MODE.....	72
6.2	FLEXURE.....	73
6.3	FRINGING.....	73
6.4	SPATIAL DISPLACEMENT	74
6.5	ARC LINE MAPS.....	75
6.5.1	<i>Arc-line ghosts</i>	82
6.5.2	<i>Spectral solutions</i>	82
6.5.3	<i>Spectral flat fields</i>	83
6.6	VPHs R2000/R2500 GHOSTING	83
6.7	SECOND ORDER CONTAMINATION	84

6.8	SPECTROPHOTOMETRIC STANDARDS	84
6.9	SPECTROSCOPIC PHOTON DETECTION EFFICIENCY	85
7	MULTI-OBJECT SPECTROSCOPY	86
7.1	GENERAL DESCRIPTION	86
7.2	MOS LIFE CYCLE	87
7.3	MOS MODE PRACTICAL LIMITATIONS	88
7.4	CALIBRATING MOS OBSERVATIONS	89
7.5	DESIGNING MOS MASKS: A SUMMARY	89
7.6	THE MASK DESIGNER TOOL	90
7.6.1.	<i>Starting up</i>	91
7.6.2.	<i>Getting to know the Mask Designer</i>	91
7.6.3.	<i>The graphical user interface</i>	92
7.6.4.	<i>Designing MOS masks step-by-step</i>	97
7.6.4.1.	Example #1: Using an OSIRIS pre-image	97
7.6.4.2.	Example #2: Using equatorial coordinates	100
8	OBSERVING WITH OSIRIS	103
8.1	EXPOSURE TIME CALCULATOR (ETC)	103
8.2	GTC PHASE 2 TOOL	103
9	OSIRIS DATA PROCESSING	105
9.1	OSIRIS / GTC KEYWORDS	105
9.2	ASTROMETRY WITH OSIRIS	116
9.2.1	<i>Input Data</i>	117
9.2.2	<i>Astrometric Solution</i>	117
9.2.3	<i>Mosaic Composition</i>	119
9.2.4	<i>Composing a first-order mosaic from raw data</i>	120
10	OSIRIS OS FILTER CHARACTERISTICS	121
10.1	BLUE TUNABLE FILTER	121
10.2	RED TUNABLE FILTER	126
11	OSIRIS GRISMS/VPH EFFICIENCIES	130
12	OSIRIS INDIVIDUAL ARC LINE MAPS	133
13	OSIRIS SLOAN PHOTOMETRIC STANDARDS	145
14	OSIRIS SPECTROPHOTOMETRIC STANDARDS	147
A.	LIST OF REFERENCE DOCUMENTS	149
B.	REFERENCES	149

LIST OF ABBREVIATIONS

AAO	Anglo Australian Observatory
CCD	Charge Coupled Device
ESAC/INSA	European Science Astronomy Centre / Ingeniería y Servicios Aeroespaciales
ESO	European Southern Observatory
EW	Equivalent Width
FITS	Flexible Image Transport System
FOV	Field Of View
FWHM	Full Width at Half Maximum
GTC	Gran Telescopio Canarias
IAA	Instituto de Astrofísica de Andalucía
IA-UNAM	Instituto de Astronomía – Universidad Nacional Autónoma de México
ICM	Instrument Calibration Module
IDT	Instrument Definition Team
IFCA-UNICAN	Instituto de Física de Cantabria – Universidad de Cantabria
MOS	Multiple Object Spectroscopy
NIR	Near InfraRed
OSIRIS	Optical System for Imaging and low Resolution Integrated Spectroscopy
OS	Order Sorter
PI	Principal Investigator
PSF	Point Spread Function
QE	Quantum Efficiency
S/N	Signal to Noise ratio
TBC	To Be Confirmed
TBD	To Be Defined
TF	Tunable Filter
z	Redshift

1. INSTRUMENT CHARACTERISTICS

1.1 Overview

1.1.1 Instrument description

OSIRIS is the first work-horse imaging and spectroscopic instrument for the GTC. The OSIRIS acronym stands for *Optical System for Imaging and low-intermediate Resolution Integrated Spectroscopy*, which encapsulated in a few words the versatile nature of this instrument that we will describe in this manual.

A key scientific driver in the design of OSIRIS has been the study of star formation indicators in nearby galaxies and more distant objects, back to the furthest observable galaxies with GTC. In particular, star formation in galaxies as a function of redshift is a classical topic and one main objectives of several current projects of instruments for large telescopes both, ground based and aboard satellites.

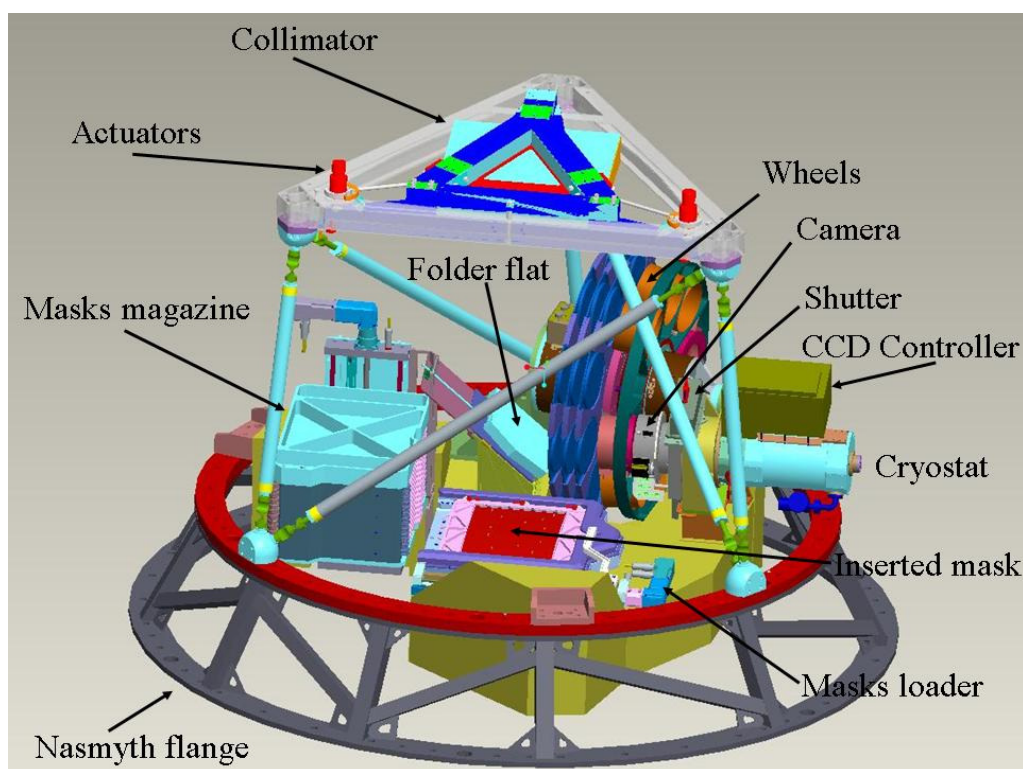


Figure 1.1.- 3D of OSIRIS showing the main subsystems.

OSIRIS is directly attached to the GTC field rotator and guide unit in the GTC Nasmyth-B focal station (Figure 1.1). The instrument optics are designed around the classical concept of collimator plus camera. For reasons of keeping the instrument compact, the optical train is folded and the field is off-axis. Its compact design will allow future migration of the instrument to the Cassegrain focal station. Next we will briefly describe the main components of the instrument, following the light path from the moment the light coming from the telescope enters the instrument through a transparent entrance window.

A masks loader (Figure 1.1) selects and insert/remove masks to/from the telescope focal plane. In addition to user customized masks for multi-object spectroscopy, a number of fixed width long-slit masks are available, as well as a number of special masks to facilitate fast photometry and charge shuffling (see 1.1.2).

Having passed the focal plane, the light reflects off the collimator (Figure 1.1), which is an off-axis quasi-parabolic mirror with elements for support and adjustment. The collimator is open-loop actively controlled to compensate for gravitational flexures of the instrument (Figure 1.1).

The collimated beam next hits a flat fold mirror that directs the light beam towards the filter wheels and the camera optics. Both the collimator and folder are covered with a silver protected coating of high red and blue reflectivity (Figure 1.2).

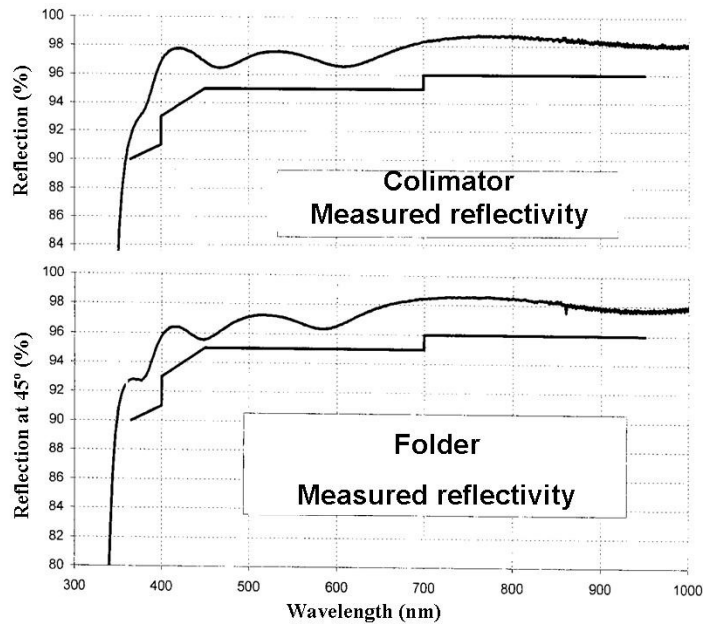


Figure 1.2.- Collimator and folder flat measured reflectivity (curve) with respect to the requirements (straight stepper lines)

Filters, grisms and Tunable Filters (TFs) can be inserted in the collimated beam near the pupil via four filters wheels, three for standard filters and the fourth, at the pupil, for TFs and grisms. Each filter wheel has 9 positions, and the grism wheel holds, apart from the tunable filters, up to 6 dispersive element. Together they allow selecting the adequate combination of these elements for using the different observing modes described in the following subsection. Conventional filters are used for imaging and for order sorting the TFs and grisms. The filters insert into the beam at an angle of 10.5 degrees in order to avoid ghost images.

The all-refractive OSIRIS camera consists of 9 spherical lenses. The last lens is the dewar window. The camera effective focal length of 181 mm provides the required detector scale (0.127 arcsec/pixel) on a flat focal plane that is tilted 1.83 degrees. The shutter is incorporated in between the camera optics.

Light is detected by a mosaic of two detector of 2k×4k red-optimized CCDs in a cryostat.

The instrument control subsystem allows mechanisms, tunable filters and the detector to work in a synchronized fashion. Also, it provide users with mechanisms controls and data processing interfaces. This instrument control is closely integrated with the rest of Telescope Control following the GTC standards. This facilitates a high level of automation of observing sequences.

OSIRIS calibration is performed using spectral lamps provided by the GTC Instrument Calibration Module (ICM), also, external continuum lamps for dome flat fields are available at the telescope.

1.1.2 OSIRIS focal plane masks

The OSIRIS mask holder with 13 positions allows remote changes of focal plane masks such as spectrograph slits, custom-made multi-object masks, or other special-purpose masks. The following masks are available at the instrument:

- Long Slit masks. Available slit widths are: 0.4", 0.6", 0.8", 1.0", 1.2", 1.5", 1.8", 2.5", 3.0", 5.0", 10.0".
- Decentred long slit of 3" width for fast photometry in shuffle mode (Figure 1.3 right).
- Mask of the central 1/3 imaging FOV for TF imaging shuffle (two TF tunings or straddling line, Figure 1.3 left).
- Frame transfer mask, selecting 1/2 of the lines in both detectors (Figure 1.3 middle).
- Mask shading one detector, for avoiding dithering when obtaining TF imaging of bright crowded or extended fields.
- Pinhole masks (for Long Slit and Multi Object Spectroscopy tests).



Figure 1.3.- From left to right, charge shuffling mask selecting the central 1/3 of the detector lines (the central black circular piece is shown just for reference), frame transfer mask selecting the half of the detector exposed, and the fast photometry mask with the decentred slit of 3 arcseconds width.

1.1.3 Observing modes

The following table provides a summary of the different OSIRIS observing modes, that are described further on in this manual.

Mode	Description
Imaging	
Broad band	SDSS and order sorter sets
Narrow band	With Tunable Filters: Blue (450-671 nm) and Red (651-934.5 nm)
Single exposure	One wavelength for line and another for continuum
Scan	A set of exposures at several equidistant & contiguous wavelengths
Medium band	SHARDS private filters set
Spectroscopy	
Long slit	Slit widths defined by available masks
MOS	Using user-customized masks
Standard	Slitlets: sky and object in the same slit
Fast photometry	
Shuffle	Decentered slit plus charge shuffling
Frame transfer	Defining windows and combining with frame transfer

1.1.4 Main Characteristics

The following table summarises the main instrument characteristics.

Total FOV	8.53 × 8.67 arcminutes with small shadowed area in one side (Figure 1.4)
Unvignetted FOV	7.8 × 7.8 arcminutes
Long slit	7.4 arcminutes (long slits length)
MOS FOV	7.5 × 6.0 arcminutes
Plate scale	0.12718 arcsec/pixel (both imaging and spectroscopy) ¹
Image quality	< 0.15'' (80% polychromatic EE)
Distortion	Lower than 2%
Instrument Position Angle	150.540346°
Detector system	Two MAT 4k × 2k (~9.4 arcsec gap ²) from same Si wafer
Broad band	ugriz filter, medium band TF order sorters (OS) and medium band SHARDS filters.
Tunable Filters	Central λ tunable from 450 through 935 nm ³ FWHM tunable from ~4.5 through ~20 Å, depending on λ Lower FWHM is limited by the order-sorting filter, and the higher by the etalon gap range. Tuning time ~10 ms depending on etalon gap. Minimum is ~1 ms Tuning accuracy in λ and FWHM ~1-2 Å
Spectral resolutions	300, 500, 1.000, 2.000, and 2.500. Resolution for 0.6'' slit width. Available spectral ranges R=300 & 500 are limited by second-order light, and higher R by detector.
Long slit widths	Masks of fixed widths from 0.4 through 10.0 arcseconds
MOS (masks)	~30 targets per mask (using classical slits of 15'' length)
Flexures	Less than 1 pixel

¹ This corresponds to the physical pixel size, while the standard operation mode uses 2x2 binning (hence standard operational plate scale is 0.254 arcsec/pixel).

² Physical gap is of ~12 pixels, -binned- (or ~3 arcsec), the gap between photosensitive pixels is of ~37 pixels or 9.4 arcsec. Then, the last quantity is the one to take into account when dithering for covering the gap on the sky.

³ Current IAC calibration facilities allow calibration from 450 through 950 nm only. In the near future it will be expanded for covering the full OSIRIS wavelength range.

1.1.5 Field obscuration and vignetting

As can be appreciated from Figure 1.4, there is an obscuration of the left hand side OSIRIS full FOV of CCD1 due to the edges of the filter wheels and the folder mirror. This was contemplated in the original design and does not affect the specified unvignetted field of view. The obscured area is best avoided, although reliable photometry can be performed on targets located in this region of the detector.

Some vignetting is present in the lower part (lower 250 pixels, binned) of the CCDs, due to filter wheel 1. With the filter in position removed, the vignetting is reduced in CCD1 only (Figure 1.4). In all cases the total unvignetted field of view is 7.8×7.8 arcmin.

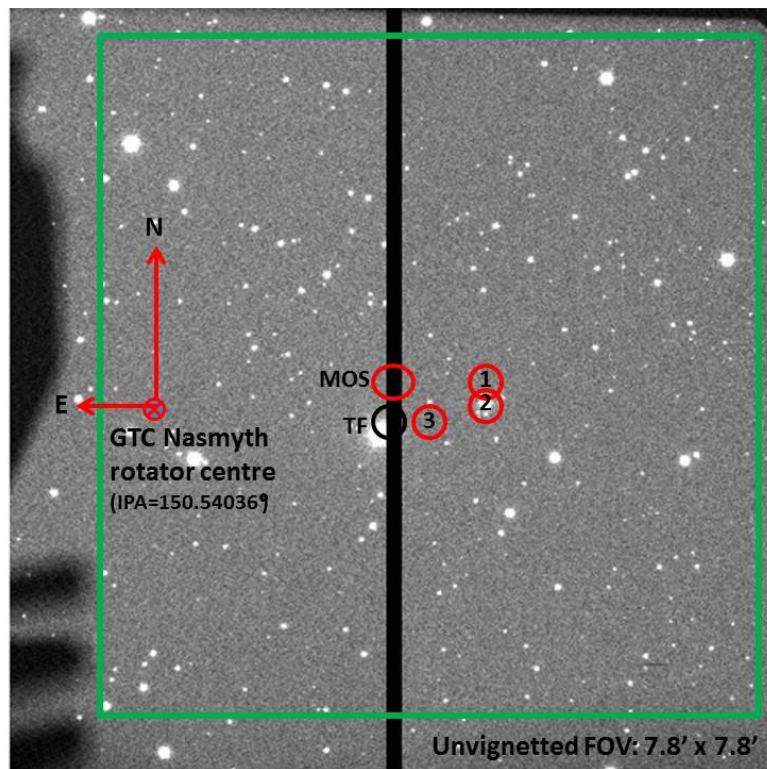


Figure 1.4.- OSIRIS image showing the shadowing produced by the folder mirror and filter wheels on one side of CCD1 (left). Since the instrument is off-axis, the centre of the OSIRIS field does not coincide with GTC pointing centre

Figure 1.4 shows the location of the standard pointing positions for the different observing modes of OSIRIS: Broad Band Imaging (1), Long Slit Spectroscopy (2), and Tunable Filter Imaging (3). The location of the Tunable Filters' optical centre and the MOS reference pointing are also shown.

1.1.6 Field orientation and gap

The OSIRIS instrument position angle within the GTC reference system is 150.540346° . With this orientation, North is up and East left in the images. This value can be retrieved from KEYWORD IPA at image headers. If a different position angle (P.A.) is requested by the user, the resultant IPA would be $150.540346^\circ - \text{P.A.}$ (with P.A. measured from N to E).

The OSIRIS focal plane is imaged by two CCDs that have a narrow gap between them. This gap is 9.4 arcsecs wide. To cover the full field when defining a dithering pattern, steps of 10 arcsecs (or even 12 arcsecs to be more conservative) perpendicular to the gap are recommended.

1.1.7 Instrument overheads

During instrument design, special efforts have been invested in reducing instrument overheads due to configuration changes (observing modes, masks, and filters or grisms) to the minimum. The following table summarizes the typical time it takes to change a component.

Mask change	Filter Change	Grism Change
60 sec	8 sec	10 sec

These times only reflect the mechanical changes of the components and not the overheads for target acquisition in the different modes, auto-guiding and detector readout.

Changing from one TF to the other takes about 13s. Changing TF wavelength tuning takes at most about 0.1 s, usually 0.02 s, depending on the gap differences between the different tunings.

1.1.8 Environmental conditions

OSIRIS is protected from the environment through its fairly air tight enclosure. Dry air flushes the instrument to avoid dust and moisture entering the instrument and depositing on optical surfaces. This air is provided by GTC instrument services and it is not thermally controlled, but its temperature is quite stable. The aim is to minimize temperature and humidity gradients within the instrument so as to ensure best image stability. Even when inside the dome the humidity raises substantially due to weather conditions, the humidity inside OSIRIS is kept stable during several hours.

Temperature changes in GTC structure are transmitted quite fast by conduction to OSIRIS structure via the Nasmyth flange to the GTC rotator. Also, although the attached electronic cabinets are thermally isolated, some heat leaks inside the instrument.

1.2 Detectors

1.2.1 Description

The OSIRIS detector system is composed of a mosaic of two buttable 2Kx4K CCDs to give a total 4Kx4K pixels, 15 microns/pixel. The arrays are MAT-44-82 from Marconi (2 channel each, Frame-Transfer type, 20-1000 kHz readout rate). The software allows driving one or both MAT44-82 CCDs, by one or two outputs each. It is also possible to modify the parallel or serial clocks time, so that it is possible to readout the array from 20 kHz per channel up to the CCD readout limit of 1 MHz. It allows frame transfer mode and binning.

The following table summarises the main OSIRIS detector parameters.

Parameter	Value	Comments
Array size	2048 × 4096	Photosensitive area
Overscan area	[1:24,1:2048]	For bias subtraction
Readout channels ¹	2	Per detector
Shuffle speed	50 μ s/line	Used for skipping lines in window mode as well
Readout speeds	100, 200, 500 kHz	20, 50 & 1 MHz possible (not recommended ²)
RON ³	3.5 e ⁻ @ 100 kHz 4.5 e⁻ @ 200 kHz 8 e ⁻ @ 500 kHz	Nominal are 200 kHz for imaging and spectroscopy & 500 kHz for acquisition
Gain (e ⁻ /ADU)	0.95 @ 200 kHz	
Linearity	Better than 1%	For 1% to 90% full well (see Figure 1.5)
Operating Temp.	148-152 K	
Dark current	2-3 e ⁻ /hour/pixel	
CTE	Vertical >0.999999 Horizontal >0.9999	Measured on grade 5 at laboratory
Binning	2 × 1, 1 × 2 & 2 × 2	Nominal is 2 × 2
Windows	Up to 5 enabled	Copied on both detectors
Frame transfer	Enabled	For fast photometry
Fringing	3% @ 900nm 2% @ 950 nm 4% @ 990 nm	Fringing starts between 850 and 900 nm Measured on grade 5 device at laboratory

¹ Using two channel per detector requires obtaining all images in this configuration and slightly different biases per channel (i.e.: half detector) are obtained

² At 950 kHz the RON is so high that the image is not of scientific use, and at speeds lower/equal than 100 kHz the readout time increases at a cost of no significant reduction of RON

³ RON @ 500 kHz is higher than nominal (~8 e⁻), likely due to EMI.

Readout times can be evaluated in the following way:

Pixels to read / (readout speed x binned pixels x channels used)

For example, reading both 2k × 4k full detectors using two channels per detector with 2 × 2 binning at 500 kHz takes ~2 s.

Please note that this does not consider the time invested in configuring the SDSU (about 5s), clearing the chip before each exposure (about 4s), and transferring and saving the frame on disk (few more seconds).

Then, since an image is started till is fully acquired, for the two CCDs Output A and 2x2 binning, takes 7.8 seconds at 500 kHz readout speed and about 21 s at 200 kHz.

1.2.2 OSIRIS standard CCD operation modes

As it was described in Section 1.2.1, the CCDs control system offers a wide range of readout modes and gain settings, but for the time being the standard observing modes are shown in the table below. In the scientific standard mode the detector linearity is guaranteed up to the full 16 bits signal maximum. Read noise is better than 5 electrons in the standard readout mode used for both imaging and spectroscopy.

The acquisition mode is generally used for test images but not for science data. This mode has a significant high noise pattern so it is not suitable for scientific cases. The following table gives an overview of the main characteristics of the standard readout modes.

	Imaging/Spectroscopy (Standard)	Slow	Acquisition
Readout configuration	CCD1+CCD2_A	CCD1+CCD2_A	CCD1+CCD2_A
Readout velocity	200 kHz	100 kHz	500 kHz
Gain (e⁻/ADU)^(*)	0.95	1.15	1.46
Saturation (ADUs)	65,000	65,000	55,000
Binning (X x Y)	2 x 2	2 x 2	2 x 2
Readout time	21 sec	42 sec	7.8 sec
Actual readout noise	~4.5 e ⁻	~3.5 e ⁻	~8 e ⁻

^(*) Those values are for CCD1. Gain for CCD2 is about 5% lower than these.

A frequent monitoring of the Gain and Readout noise for the standard operation mode of OSIRIS is done for operational purposes, and the values are updated at the OSIRIS site at GTC web page.

IMPORTANT: In order to decrease the overheads during OSIRIS operation, **from semester 2014A onwards the standard readout mode will be 200 kHz in all the observing modes provided by the instrument.** The initial purpose of allowing two different readout speeds was to provide a low readout noise mode for spectroscopic observations, different than the one used for imaging modes. However, the reasonable good performance of OSIRIS CCDs allows to get low readout noise levels either at 100 kHz or 200 kHz, hence the only real difference when using those modes is having different readout times.

1.2.3 OSIRIS CCDs linearity / dark current level / cross-talk

In the OSIRIS standard operation mode, detector linearity is guaranteed up to the full 16 bits signal maximum (Figure 1.5).

During the first months of operation of the instrument (2009), OSIRIS suffered of a very high dark current resulting from an excessive temperature of the CCD that was not correctly reported by the CCD thermometry system. A redesign of the thermal coupling between the

liquid Nitrogen container and the CCD has resulted in a notable improvement of the dark current, which is now at acceptable levels of about 10-12 ADUs/h for a 2 x 2 binned pixel. Hence, since February 2010 no dark images are needed for OSIRIS data analysis.

A slight cross-talk effect between both CCDs in OSIRIS has been measured during instrument commissioning tests. The effect is as small as 2.8×10^{-4} respect to the original signal, hence the effect in the scientific images can be neglected.

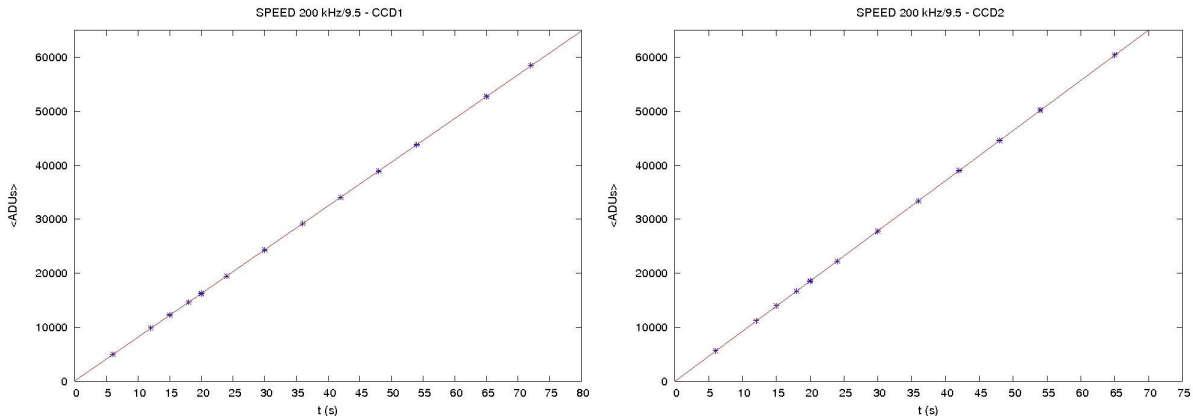


Fig. 1.5.- : Linearity plots for OSIRIS standard readout mode in both CCDs.

Cosmic ray events have been measured in both OSIRIS CCDs, resulting an average of 30 impacts/min, that means around 1800 impacts/h.

1.2.4 Quantum Efficiency

The detectors are optimized for longer wavelengths, but with a low, although reasonable, blue efficiency, of about 20% @ 365nm. Hence observing at these wavelengths is possible, although slow.

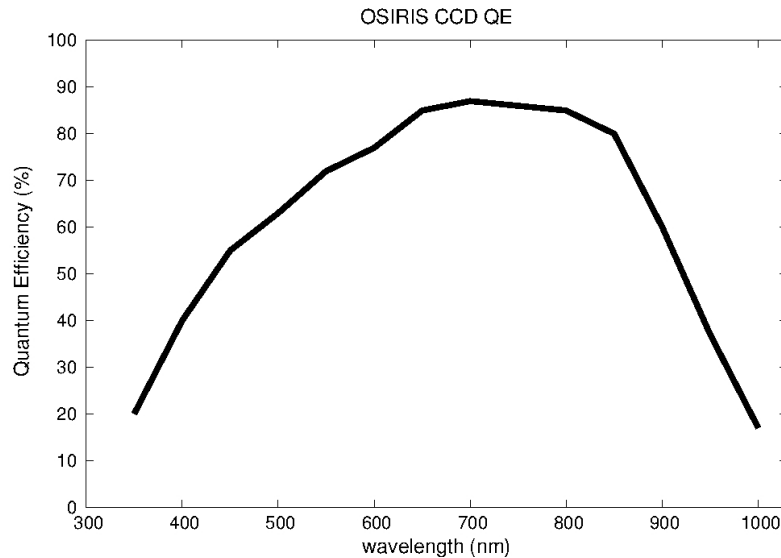


Figure 1.6.-: QE of OSIRIS CCDs.

1.2.6 CCD windowing

OSIRIS CCDs allows to define up to 5 windows at the same time for SIMPLE readout modes, and only a single window for FAST MODES.

There are some restrictions that the user has to take into account when defining those windows:

- All the windows must have the same size.
- No overlap is allowed between different windows.
- Windows must be defined in increasing order of their Y coordinate (that coincides with the readout direction). Therefore, Y coordinates for different windows must not overlap (for example, if a window is defined at [1:200,300:499], any other window must begin at Y=500, or conclude at Y=299).
- Windows are replicated in both CCDs. Hence, if N windows are defined in CCD1, the same windows will appear in CCD2, with the same size and position as those of CCD1. Some cross-talk has been noted between windows in both CCDs, for this reason is highly recommended that only use a single CCD when using windowing in OSIRIS.

The readout speed in windowing mode is defined by the combination of the windows size and CCD readout mode. When windows are read out, the CCD section unused is 'split' at the highest readout speed, hence there is no dependence in the total readout time on the windows location in the CCDs.

In any case, if the user is interested in observing with OSIRIS by using windows, please contact well in advance a GTC staff astronomer, in order to choose what is the most convenient setup for the observing program. At the telescope, the GTC staff astronomer will perform the observations, and all the restrictions and particularities in using the windows will be properly considered.

2. BROAD BAND IMAGING

OSIRIS allows broadband imaging over a FOV of 8.53' x 8.67' (7.8' x 7.8' unvignetted) covering the full spectral range from $\lambda=3650 \text{ \AA}$ to $\lambda=10000 \text{ \AA}$, with a high transmission coefficient in particular at longer wavelengths.

All standard OSIRIS filters have been designed to work in a collimated beam with a tilt angle of 10.5° to avoid ghosts due to back reflections into the detector.

The OSIRIS standard pointing in Broad Band imaging mode is at the CCD2 pixel $(256,1024)^2$ to maximize the available FOV and in order to avoid possible cosmetic effects, which are more abundant in the CCD1. The coordinates introduced by the PI in the Phase-2 tool will be positioned at this central pixel.

2.1.1 Sloan broad band filters

Broad band imaging with OSIRIS covers a spectral range from $\lambda=3650 \text{ \AA}$ to $\lambda=10000 \text{ \AA}$ using the standard Sloan filters $u'(\lambda 3500/600)$, $g'(\lambda 4750/1400)$, $r'(\lambda 6250/1400)$, $i'(\lambda 7700/1500)$ and $z'(\lambda 9100/120)$.

The following table provides the measured parameters at the IAC optical laboratory at ambient temperature at the centre of the filter and with normal incidence. Due to IAC Laboratory limitations, no measures for u' filter are available aside from those provided by the manufacturer.

Filter	Central wavelength (\AA)	FWHM (\AA)	Transmission (%)
u'	—	—	—
g'	4815	1530	82.48
r'	6410	1760	94.14
i'	7705	1510	89.00
z'	9695	2610	97.16

The filters are placed in the collimated beam and close to the pupil of the instrument, at an angle of 10.5° with respect to the optical axis of the instrument. Because of the angle the central wavelength $[\lambda_c(10^\circ)]$ is shifted with respect to the nominal central wavelength $[\lambda_c(0^\circ)]$ and the bandwidth $[\Delta\lambda]$ changes slightly, but the transmission curve shape is hardly altered. Furthermore, depending on the location in the focal plane, the light incident on the filter cover a range of angles between -2° y 22° , with the corresponding shift in wavelength. For the broad-band filters this effect is small as can be seen in the following table.

² Note that those coordinates are binned coordinates, that is the standard operation mode of OSIRIS. When 1×1 binning is used, those values have to be doubled.

The maximum spatial variations of the filters with respect to the centre are:

Filter	Central wavelength (Å)	FWHM (Å)	Transmission (%)
u'	—	—	—
g'	30	40	1.05
r'	30	40	1.36
i'	5	10	1.09
z'	0	0	1.39

The absolute spectral responses for each filter (except u') are provided in Figure 2.1.

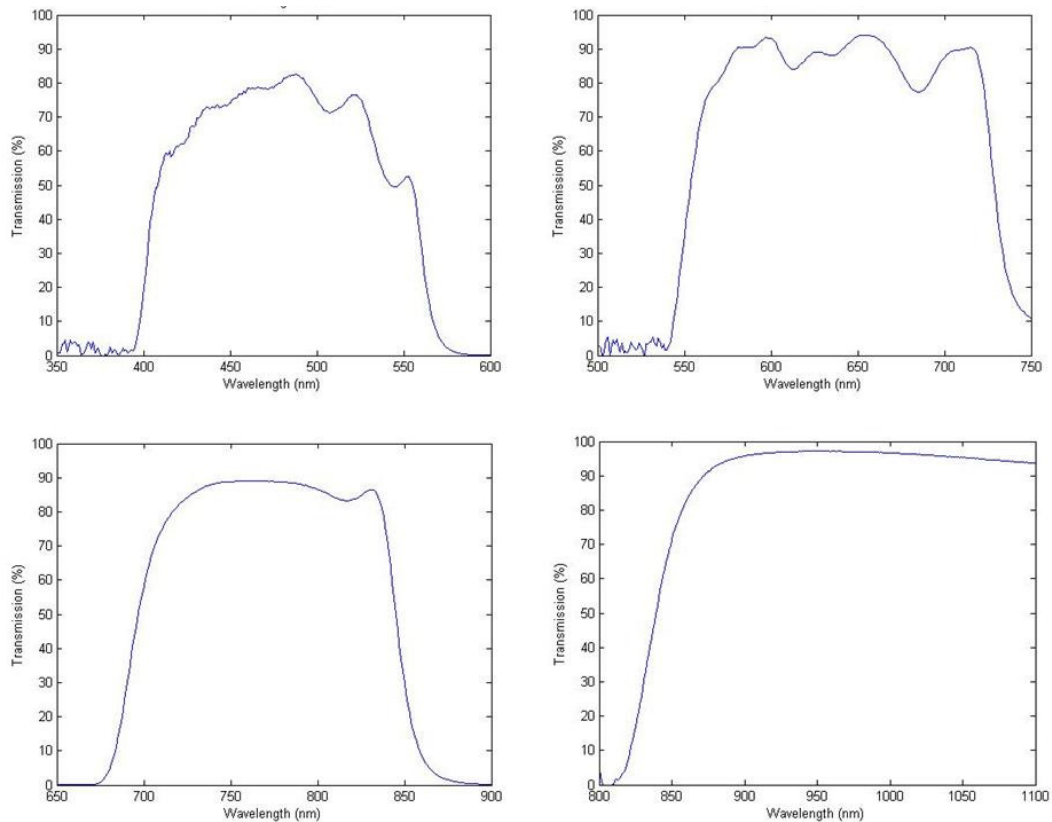


Figure 2.1.- From left to right and top to bottom: measured central spectral response of g', r, i', and z' filters, respectively, with normal incidence.

2.1.1.1 Zeropoints

From the observation of standard stars the following average zeropoints (1 ADU/s at AM=0) and extinction coefficients have been measured (those average values correspond to the period March 2010 – December 2013):

Filter	Zero point (mag)	Extinction (mag/airmass)
u'	25.79 (± 0.09)	0.47 (± 0.01)
g'	28.82 (± 0.07)	0.16 (± 0.01)
r'	29.29 (± 0.07)	0.10 (± 0.01)
i'	28.85 (± 0.05)	0.06 (± 0.01)
z'	28.23 (± 0.07)	0.03 (± 0.02)

With those zeropoints, instrumental magnitudes can be obtained directly using the formula:

$$m = Z - 2.5 \log_{10} [\text{Flux (ADUs/s)}] - k X$$

where standard extinction coefficients for the ORM can be found at:

http://www.ing.iac.es/Astronomy/observing/manuals/ps/tech_notes/tn031.pdf

The zeropoints have been measured at the standard GTC pointing for Broad Band imaging (that is placed at OSIRIS CCD2). Zeropoint values for CCD1 are on average 0.1-0.12 mag smaller in each filter.

The zeropoints are measured during photometric sky conditions. Clouds or dust in the atmosphere will reduce the limiting magnitudes (on average, in spectroscopic nights we measure up to 0.3-0.5 mags of extra extinction). Likewise, changes in the cleanliness and transmission of all optical components will affect the zero points.

An updated version of the daily zeropoint values can be found at:

<http://www.gtc.iac.es/instruments/osiris/media/zeropoints.html>

2.1.1.2 Sky background

Estimates of the sky brightness (ADUs /s/ pix) measured at a Elevation 55 deg in the standard OSIRIS Broad Band imaging mode (200 kHz / 9.5 - binning 2 x 2) are:

Filter	Sky Brightness (BRIGHT)	Sky Brightness (GRAY)	Sky Brightness (DARK)
u'	15	10	1
g'	250	150	25
r'	350	300	90
i'	290	265	160
z'	400	350	325

Although ETC predictions for sky brightness at the ORM are accurate enough, it is recommended to use the values from the table above for a quick estimation of the sky background counts in long exposed images to avoid possible sky saturation.

2.1.1.3 Colour corrections

Photometric transformations equations (with an arbitrary zeropoint of 25 magnitudes) are:

$$\begin{aligned} u' - u'_0 &= -0.797(\pm 0.053) - 0.071(\pm 0.023) (u_0 - g_0) \\ g' - g'_0 &= -3.823(\pm 0.040) - 0.078(\pm 0.013) (g_0 - r_0) \\ r' - r'_0 &= -4.291(\pm 0.017) - 0.114(\pm 0.028) (r_0 - i_0) \\ i' - i'_0 &= -3.857(\pm 0.015) - 0.079 (\pm 0.041) (i_0 - z_0) \\ z' - z'_0 &= -3.231(\pm 0.031) - 0.072 (\pm 0.052) (i_0 - z_0) \end{aligned}$$

2.1.1.4 OSIRIS/GTC Broad Band Imaging efficiency

The graph below shows the overall photon detection efficiency of GTC and OSIRIS in each of the Sloan filters (the plots include the contribution both of the telescope and instrument optics system).

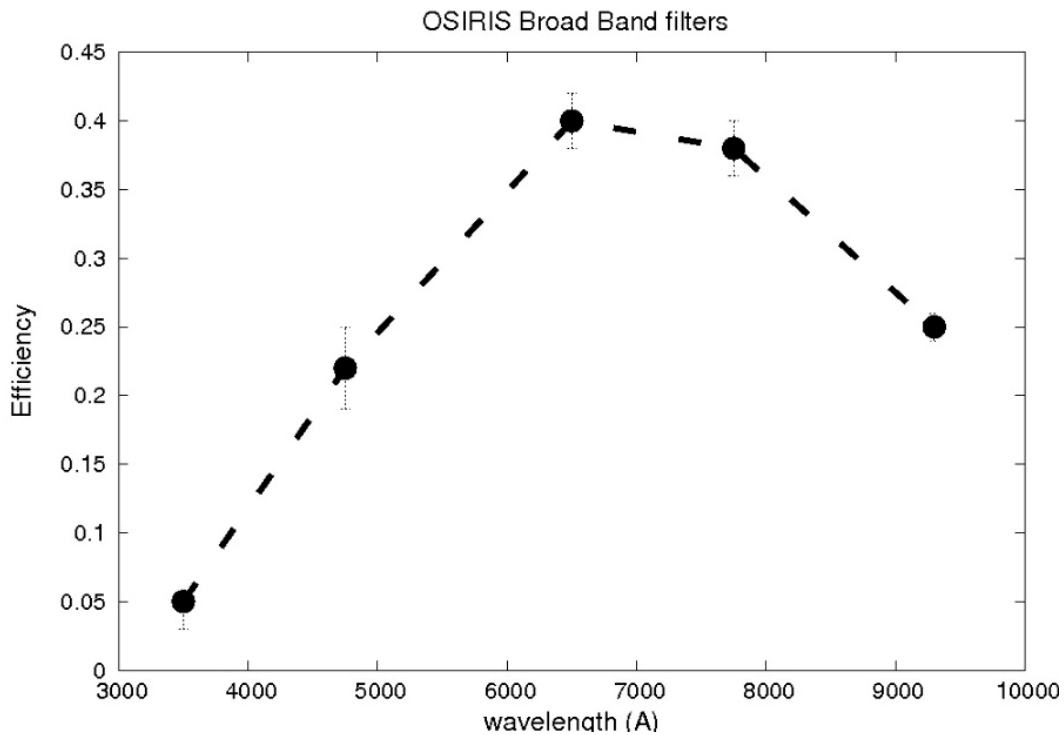


Figure 2.2.- Overall photon detection efficiency of GTC and OSIRIS in each of the Sloan filters.

Also, the following plots shows the limiting magnitudes with OSIRIS Sloan filters for getting $S/N=3$ as a function of the exposure time, assuming dark conditions, seeing = 1.0 arcsec, and airmass = 1.2.

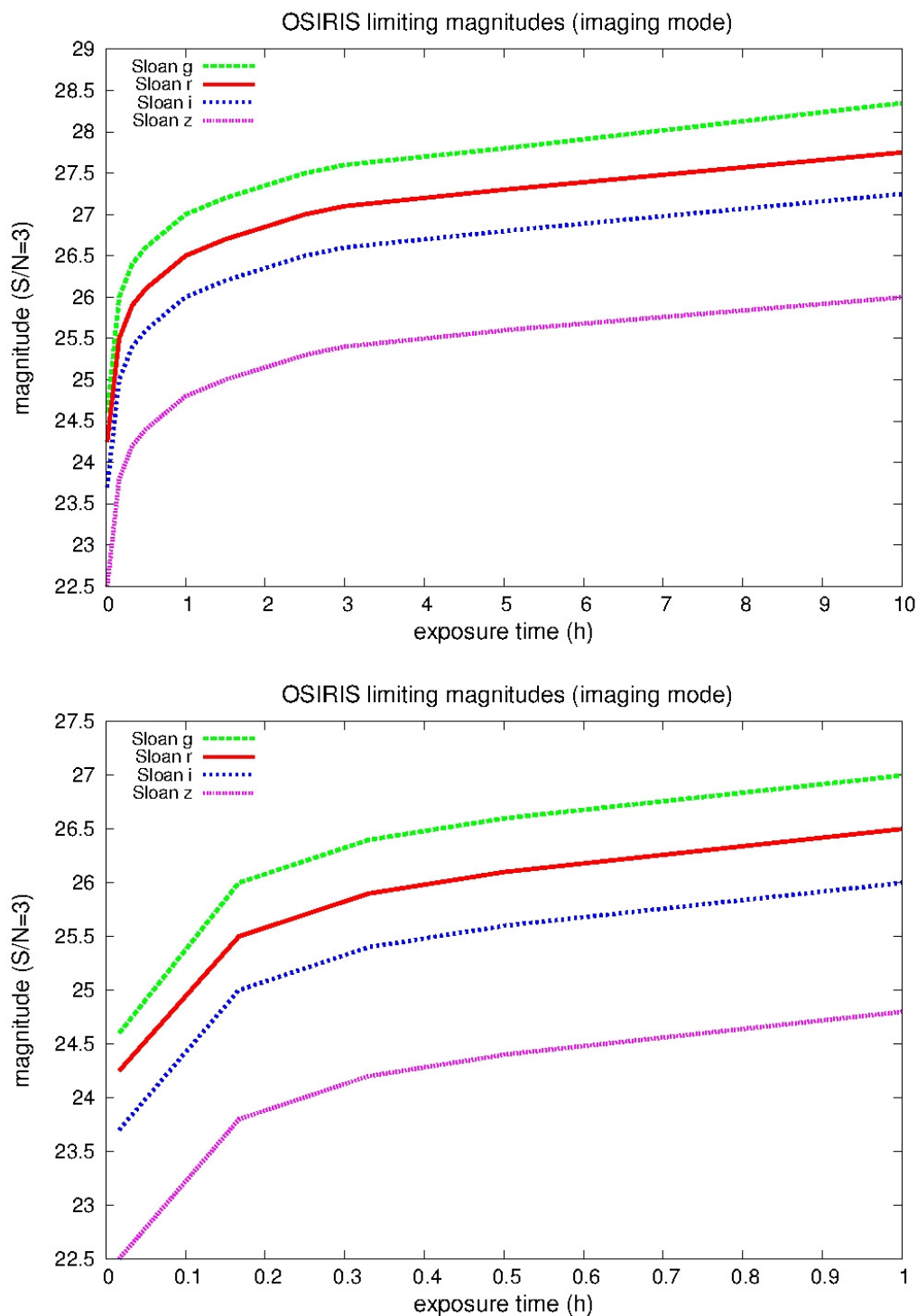


Figure 2.3.- Limiting magnitudes ($S/N=3$) achieved with OSIRIS broad band filters as a function of the exposure time. A detailed view for exposure times lower than 1.0 h is shown in the graph below.

2.2 Photometric uniformity

Given the structure and speed of OSIRIS shutter (of type moving screen) and that it is near collimated beam, exposures down to 0.1 seconds can be obtained with a uniformity of about 1% over the full field.

2.3 Sky Flat fields

The flat fielding homogeneity in each of the OSIRIS Sloan filters is better than 2.5% over the full unvignetted FOV of the instrument, except in Sloan u', where fluctuations up to 6% with respect to the mean value are found.

Day to day fluctuations in the flat fields are less than 0.05% , and less than 0.1% week to week. Hence, sky flat fields obtained with OSIRIS are well usable up to within a week before or after the observations.

Comparison twilight flat fields with those derived from scientific observations during bright time shows no variations in excess of 0.01%, hence they can be considered practically identical for scientific purposes. These percentage variations are measured globally, while of course locally, due to dust particles that can come and go, the variations may be larger. Moreover, differences between the night sky and the twilight spectrum may result in subtle flat fielding differences.

Comparisons between fky flat fields and dome flats show that the latter suffer from inhomogeneities in the dome illumination. Differences up to 10-15% are found in CCD2 and 2% in CCD1. Therefore dome flats are only recommended for obtaining reliable OSIRIS photometry in CCD1 and as last choice in CCD2.

As a product of the scientific operations with OSIRIS, a series of master flat fields frames can be retrieved from:

http://www.gtc.iac.es/instruments/osiris/osiris.php#BroadBand_Imaging

Flat fields were all obtained with exposure times larger than 1 s to minimize possible photometric effects due to OSIRIS shutter and a maximum exposure time of about 20 s (where the detection of stars becomes notable), with an average of 35,000-40,000 ADUs in each individual image. MasterFlats are available separately for each CCD of OSIRIS (as they have a slightly different gain and bias level). The latest master flats are available from the GTC web pages.

2.4 Sloan Photometric Standards

Photometric calibration for OSIRIS Broad Band imaging is done via a Sloan standard set taken from Smith et al. (2002, AJ, 123, 2121). The complete list of standards can be found in Section 13.

3. TUNABLE FILTER IMAGING

3.1 OSIRIS Tunable Filters description

A key aspect of OSIRIS is the use of tunable filters (TFs). OSIRIS TFs are a pair of tunable narrowband interference filters (FabryPerot etalons) covering 450–671 nm (blue ‘arm’) and 651–935 nm (red ‘arm’). They offer monochromatic imaging with an adjustable passband of between 0.45 and 2 nm. In addition, TF frequency switching can be synchronized with movement of charge (charge shuffling or frame transfer) on the OSIRIS CCDs, techniques that have important applications to many astrophysical problems.

3.1.1 Introduction to FabryPerot filters (FPFs)

In its simplest form, a FabryPerot filter (FPF) consists of two plane parallel transparent plates which are coated with films of high reflectivity and low absorption. The coated surfaces are separated by a small distance (typically μm to mm) to form a cavity which is resonant at specific wavelengths. Light entering the cavity undergoes multiple reflections (Figure 3.1) with the amplitude and phase of the resultant beams depending on the wavelength. At the resonant wavelengths, the resultant reflected beam interferes constructively with the light reflected from the first plate cavity boundary and all the incident energy, in the absence of absorption, is transmitted. At other wavelengths, the FPF reflects almost all of the incident energy.

3.1.1.1 Performance of an ideal FPF

The general equation for the intensity transmission coefficient of an ideal FPF (perfectly flat plates used in a parallel beam) as a function of wavelength is

$$\tau_r = \left(\frac{T}{1-R} \right)^2 \left[1 + \frac{4R}{(1-R)^2} \sin^2 \left(\frac{2\pi\mu d \cos \theta}{\lambda} \right) \right]^{-1}, \quad (3.1)$$

where T is the transmission coefficient of each coating (plate–cavity boundary), R is the reflection coefficient, d is the plate separation, μ is the refractive index of the medium in the cavity (usually air, $\mu = 1$) and θ is the angle of incident light. Thus, the FPF transmits a narrow spectral band at a series of wavelengths given by

$$m\lambda = 2\mu d \cos \theta \quad (3.2)$$

where m is an integer known as the order of interference. The peak transmission of each passband is

$$\tau_{r,max} = \left(\frac{T}{1-R} \right)^2 = \left(\frac{T}{T+A} \right)^2, \quad (3.3)$$

where A is the absorption and scattering coefficient of the coatings ($A = 1 - T - R$);

Therefore, the contrast between the maximum and minimum transmission intensities is

$$C_r = \frac{\tau_{r,max}}{\tau_{r,min}} = \left(\frac{1+R}{1-R} \right)^2. \quad (3.4)$$

For a FPF contrast greater than 100, the reflection coefficient R of the coatings needs to be greater than or about 0.82.

The wavelength spacing between passbands, known as the inter-order spacing or free spectral range (FSR), is about

$$\Delta\lambda = \frac{\lambda}{m} \quad (3.5)$$

which is obtained from Equation 3.2 by setting consecutive integral values of m . Each passband has a bandwidth ($\delta\lambda$), full width at halfpeak transmission, given by

$$\delta\lambda_r = \frac{\lambda(1-R)}{m\pi R^{1/2}} \quad (3.6)$$

derived from Equation 3.1. The ratio of inter-order spacing to bandwidth is called the finesse:

$$N = \frac{\Delta\lambda}{\delta\lambda}. \quad (3.7)$$

$$\tau_{r,min} = \left(\frac{T}{1+R} \right)^2. \quad (3.8)$$

For an ideal FPF, it is given by

$$N_r = \frac{\Delta\lambda}{\delta\lambda_r} = \frac{\pi R^{1/2}}{1-R}. \quad (3.9)$$

Thus, we can see that the resolving power of a FPF is equal to the product of the order and the finesse:

$$\frac{\lambda}{\delta\lambda} = mN. \quad (3.10)$$

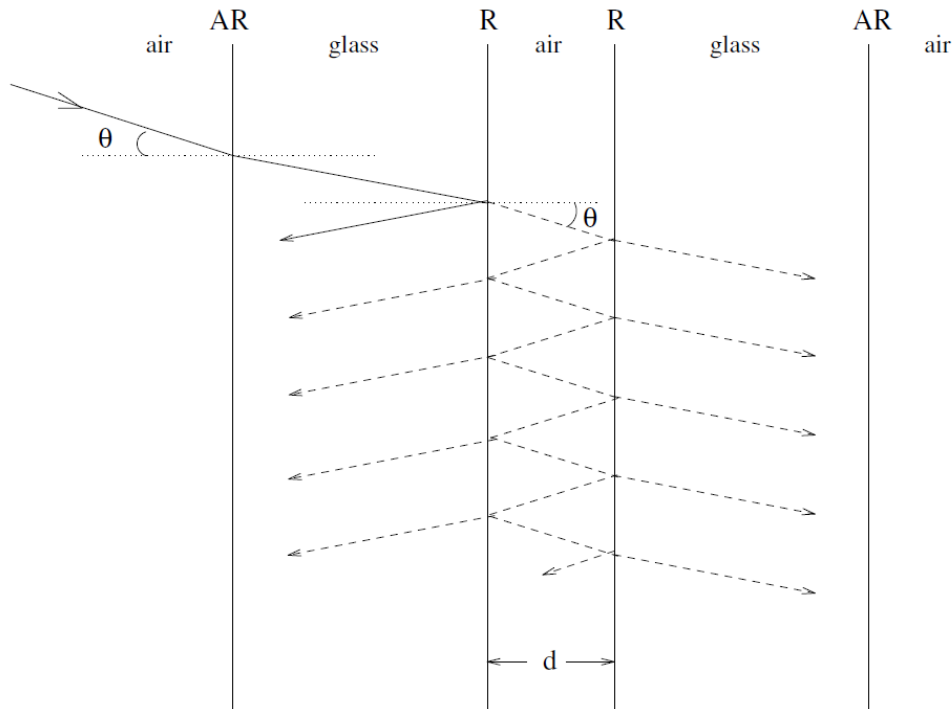


Figure 3.1.- Schematic diagram of interference with a FabryPerot filter. The outside surfaces of the glass are coated with antireflective (AR) coatings, while the inside surfaces are highly reflective (usually $R > 0.8$). The air cavity in the middle is not shown to scale (usually, d is about $10\ \mu\text{m}$ whereas the glass is over 20 mm thick on both sides). At resonant wavelengths, the first reflection (shown with a solid line) interferes destructively with light coming from the cavity in the same direction (dashed lines). The phase difference arises because the first reflection is 'internal', while all the other reflections are 'external' (with respect to glass). On the other side of the cavity, only constructive interference occurs. At nonresonant wavelengths, destructive interference occurs in the cavity and the first reflection dominates.

3.1.1.2 Limitations

It is apparent from the above equations that to obtain a higher resolution for a given order or to obtain a wider interorder spacing for a given resolution, the finesse needs to be increased. For a finesse greater than 100, a reflection coefficient R of greater than or about 0.97 is necessary (Equation 3.9). However, so far we have considered the ideal situation where the plates are flat and parallel, and the incoming light is parallel. In particular, Equations 3.1, 3.3–3.5, 3.7 and 3.9 refer to this situation using the subscript r to distinguish the results from a real filter. In practice, plate defects and the angular size of the beam limit the maximum finesse obtainable.

The effective finesse (N) is approximately given by:

$$\frac{1}{N^2} = \frac{1}{N_r^2} + \frac{1}{N_d^2} + \frac{1}{N_a^2}, \quad (3.11)$$

where N_r is the reflective finesse from Equation 3.9, N_d is the defect finesse (due to plate defects) and N_a is the aperture finesse (due to the solid angle of the beam).

The defect finesse is defined as:

$$N_d \sim \frac{2\pi}{2\delta l}, \quad (3.12)$$

where δl is a length scale related to deviations from flat parallel plates. The exact details depend on the type of deviations (Atherton et al. 1981). A FPF manufactured with $N_d \sim 80$ and a reflection coefficient of 0.97 ($N_r \sim 100$) performs with a finesse of about 60.

The aperture finesse is given by:

$$N_a \sim \frac{2\pi}{m\Omega}, \quad (3.13)$$

where Ω is the solid angle of the cone of rays passing through the FPF. This equation is related to the λ dependence on θ in Equation 3.2. In terms of astronomical imaging, the effect of aperture finesse is negligible for most objects in the field of view of a telescope. For example, an object which is one degree across (in the collimated beam) imaged with $m = 50$ has $N_a \sim 500$ according to Equation 3.13. A more relevant analysis to consider the change in central wavelength of the filter as the ray angle θ is varied in Equation 3.2. For example, a change in ray angle from 1° to 3° produces a change of 0.1% in the central wavelength of the filter at any given order. Therefore, at high resolving powers (~ 1000), a FPF may not be truly monochromatic across a desired field of view.

3.1.1.3 Gap-scanning etalons

In order to manufacture a tunable FPF, which can change the central wavelength for a given order, it is necessary to be able to adjust either the refractive index of the cavity μ , the plate separation d or the angle θ (as can clearly be seen from Equation 3.2). In a gap-scanning etalon, the plate separation can be controlled to extremely high accuracy.

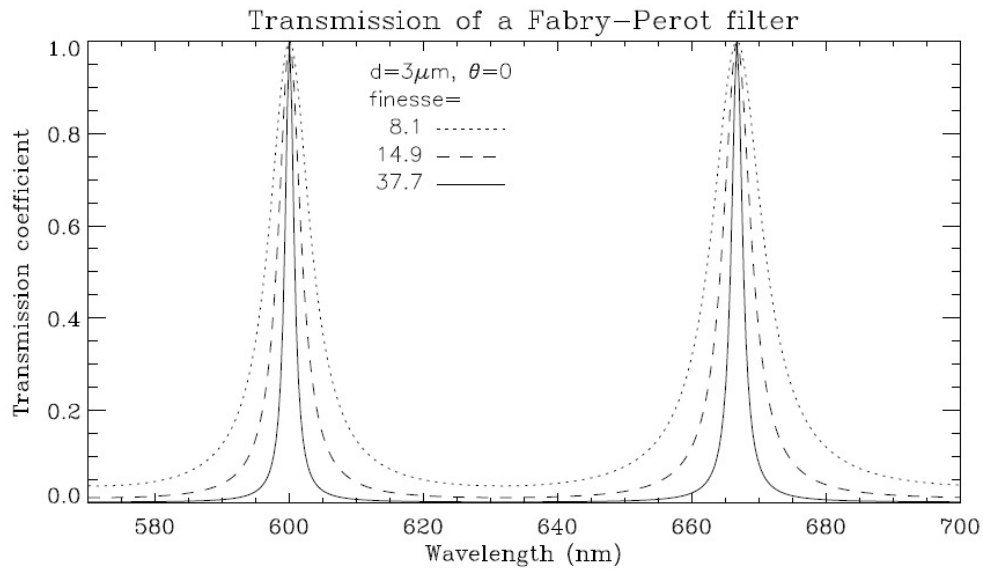


Figure 3.2.-: Variation of the transmission profile of a FPF with finesse. The profiles were determined for an ideal FPF (Equation 2.25) with $R = 0.68, 0.81$ and 0.92 ($A = 0$). Orders $m = 10$ and $m = 9$ are shown.

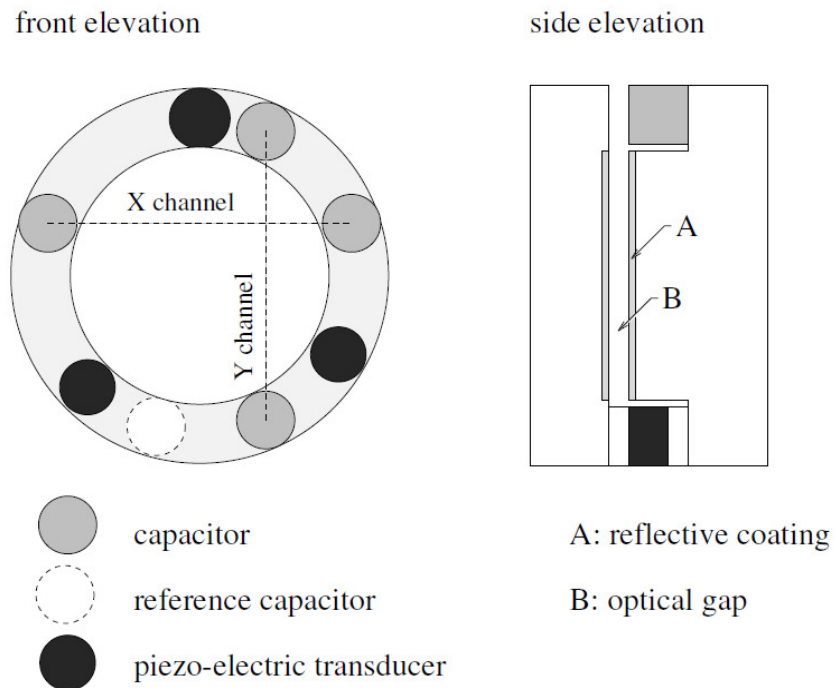


Figure 3.3: Front elevation and side elevation of a *Queensgate Instruments* etalon. Note that the thickness of the optical gap is exaggerated.

In Figure 3.3, we show the structure of a gap-scanning etalon manufactured by *Queensgate Instruments Ltd.* (now *IC Optical Systems*). In recent years, these etalons have undergone considerable improvements. It is now possible to move the plates between any two discrete spacings at very high frequencies (200 Hz or better) with no hysteresis effects while maintaining $\lambda/2000$ parallelism (measured at 633 nm). The etalon spacing is maintained by three piezoelectric transducers.

3.1.2 Charge shuffling

Central to almost all modes of OSIRIS use is charge shuffling. Charge shuffling is movement of charge along the CCD between multiple exposures of the same frame, before the image is read out. For shuffled TF imaging an aperture mask ensures that only a section of the CCD frame is exposed at a time. For each exposure, the tunable filter is systematically moved to different gap spacings in a process called frequency switching. This way, a region of sky can be captured at several different wavelengths on a single image. Alternatively, the TF can be kept at fixed frequency and charge shuffling performed to produce timeseries exposures.

The TF plates can be switched anywhere over the physical range at rates in excess of 100 Hz, although in most applications, these rates rarely exceed 0.1 Hz. If a shutter is used, this limits the switching rate to about 1 Hz. Charge on OSIRIS CCDs can be moved over the full area at rates of 30-50 $\mu\text{s}/\text{line}$: it is only when the charge is read out through the amplifiers that this rate is greatly slowed down to the selected readout speed. The high cosmetic quality of OSIRIS CCD allows moving charge up and down many times before significant signal degradation occurs. In this way, it is possible to form discrete images taken at different frequencies where each area of the detector may have been shuffled into view many times to average out temporal effects in the atmosphere.

3.1.3 Order sorters

A Fabry Perot Filter clearly gives a periodic series of narrow passbands. To use a FPF with a single passband, it is necessary to suppress the transmission from all the other bands that are potentially detectable. This is done by using conventional filters, called order sorters because they are used to select the required FPF order (see Section 3.4).

3.1.4 OSIRIS TF Characteristics and Features

The OSIRIS TF, manufactured by *IC Optical Systems*, with plate separations accurately controlled by means of capacitance micrometry, has the appearance of a conventional Fabry-Perot etalon in that it comprises two highly polished glass plates (Figure 3.4). Unlike conventional *ICOS* etalons, it also incorporates very large piezoelectric stacks (which determine the plate separation) and high performance coatings over half the optical wavelength range. The plate separation can be varied between about 3-4 μm to 10 μm .

The highly polished plates are coated for optimal performance over 370–960 nm using two separate etalons, one optimized for short wavelengths and one for longer wavelengths. The coating reflectivity determines the shape and degree of order separation of the instrumental profile. This is fully specified by the coating finesse, N , which has a quadratic dependence on the coating reflectivity. The OSIRIS TF was coated to a finesse specification of $N = 50$ (red) -100 (blue) which means that the separation between periodic profiles is, respectively, fifty-one hundred times the width of the instrumental profile. At such high values, the profile is Lorentzian to a good approximation. For a given wavelength, changes in plate spacing, d , correspond to different orders of interference, m . This in turn, dictates the resolving power (mN) according to the finesse.

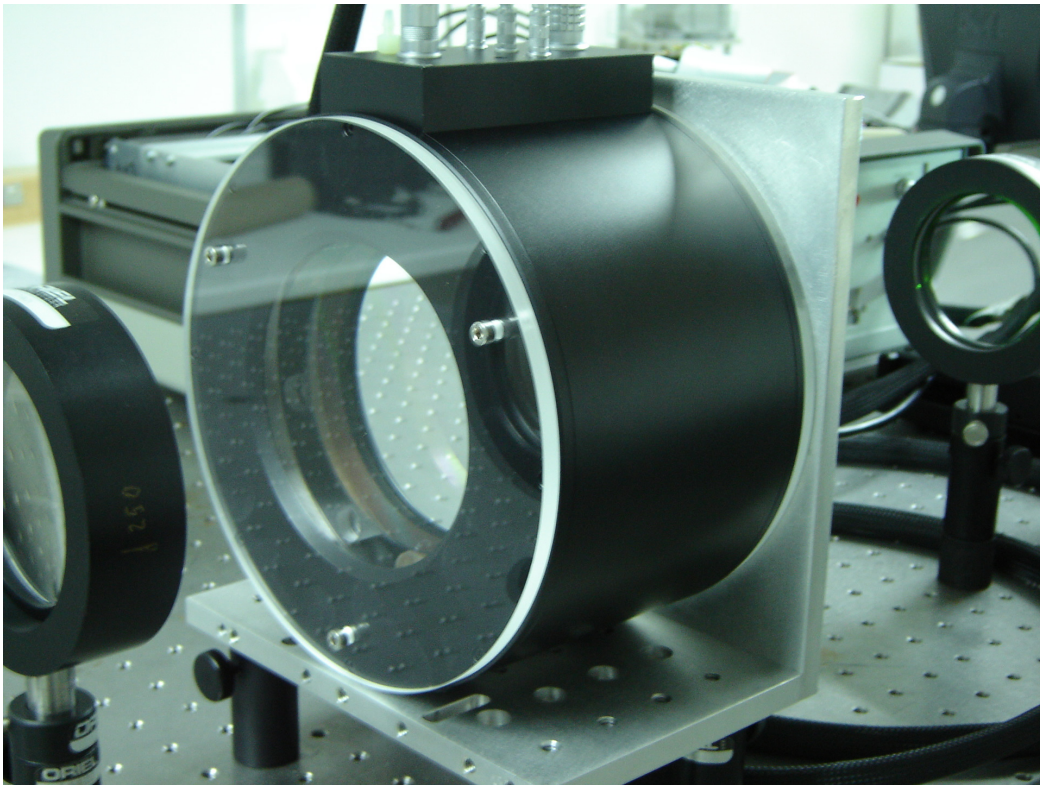


Figure 3.4.- OSIRIS red etalon at the IAC Optical Lab, while undergoing calibration tests.

In general, as can be appreciated in Eq. 3.2, for a given order, small changes in d change slightly the wavelength, while for a given wavelength the change of order requires a larger change in d . This is important to keep in mind.

With very good approximation, the spectral response of a TF, given by eq. (3.1) can be expressed by,

$$T = \left\{ 1 + \left[\frac{2(\lambda - \lambda_0)}{\delta\lambda} \right]^2 \right\}^{-1}, \quad (3.14)$$

where λ_0 is the wavelength at maximum transmission.

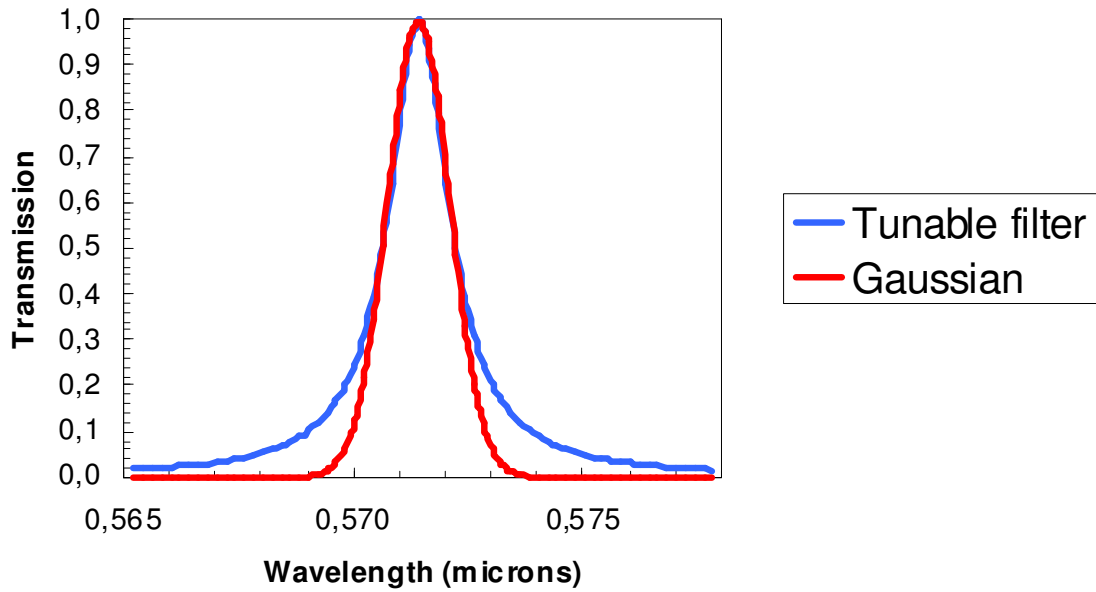


Figure 3.5.- Spectral response of a TF wrt. a Gaussian. The TF response can be considered Gaussian with a good approximation above FWHM, but is more winged below FWHM. This has to be taken into account when selecting the on and off frequencies.

3.1.4.1 Dimensions

The OSIRIS TF are model ET-100. Then the clear aperture is 100 mm diameter. The units are approximately 170 mm diameter by 100 mm of thickness and have a weight of approximately 8 kg.

3.1.4.2 Coatings

This is a critical aspect of TF performance as shown in section 3.1.1. For the OSIRIS TF the main difficulty is achieving a relatively constant reflectivity for a wide spectral range: from 370 to 670nm for the blue TF and from 650 through 1000nm for the red TF. This implies multilayered coatings, i.e.: thick coatings. Then the minimum distance (widest FWHM) between plates is driven by the minimum distances between the coating surfaces, not the plate surfaces.

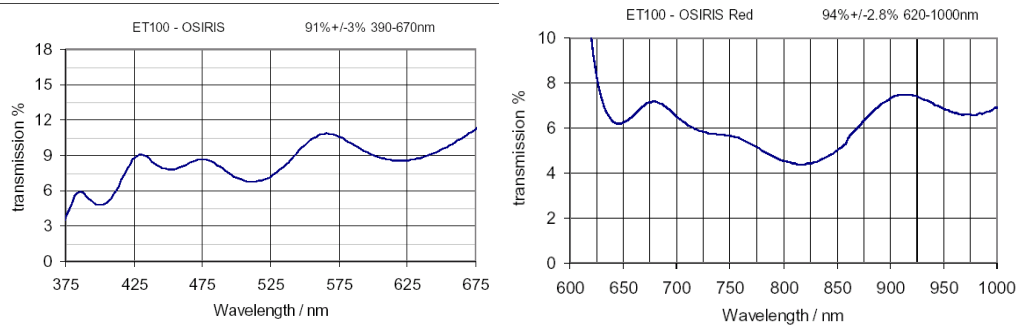


Figure 3.6.- Mean transmissions T for the blue (left) and red (right) OSIRIS TF. The mean reflectivity $R = 100 - T \%$ with a very good approximation. This results in a mean $R = 91\%$ for the blue TF and 94% for the red TF.

The wavelength dependence of the reflectivity R translates into a wavelength dependence of the FWHM range. Also, please note that the R is well behaved above 425 nm for the blue TF and above 650 nm for the red TF. Hence deviations are expected at lower wavelengths.

3.2 OSIRIS FOV for Tunable Filter Imaging

OSIRIS TF provides a circular FOV of 4 arcmin radius, where is assured that the observations will not have any contamination of other interference orders in the filter. The TF, as any interference filter, changes its response with the incident angle θ according to the formula,

$$\lambda_{\theta} = \frac{\lambda_0 \sqrt{n^2 - \sin^2 \theta}}{n} \quad (3.15)$$

where λ_0 is the central wavelength for normal incidence, λ_{θ} for the incident angle θ and n the refraction index.

As a consequence, for filters in a collimated beam (OSIRIS case), beams from different points of the GTC focal plane reach the TF at increasing incident angles, with symmetry with respect to the optical centre. Then there is a progressively increasing shift to the blue of the central wavelength as the distances r to the optical centre increase, according to Eq. 3.15. However, since the beams coming from the same point of the FOV are parallel, the FWHM is nearly the same. This is the case of OSIRIS, since OSIRIS TF are located in the pupil of the collimated beam. Since this is a pure geometric effect, the wavelength variation is completely fixed and predictable because it depends only on the incident angle, that is completely determined by the ratio between the telescope (f_{GTC}) and the instrument collimator mirror (f_{Coll}) focal lengths:

$$\tan \theta = \frac{f_{GTC}}{f_{Coll}} \tan r = 136.91 \tan r, \quad (3.16)$$

since the measured focal lengths are $f_{\text{GTC}} = 169888 \pm 2 \text{mm}$ (Castro et al. 2007) and $f_{\text{Coll}} = 1240.90 \pm 0.05 \text{mm}$ (SESO 2006). The distance r to the OSIRIS TF optical centre can be obtained from the OSIRIS mean plate scale of 0.127 arcsec/pixel. Wavelength or temperature variations can be neglected, since the OSIRIS collimator is made of Zerodur, and the camera has demonstrated to be very achromatic during commissioning.

However, as already stated in Section 3.1.1.1, Equation 3.2 apply to ideal FPFs. Really, the full expression of Equation 3.2 is:

$$m\lambda = 2\mu d \cos\theta + 2\mu_c d_c \cos\theta, \quad (3.17)$$

This additional term in Equation 3.17 can be neglected when $d \gg d_c$, as is the case for high resolution FPs, since d is of the order of hundreds of microns, while d_c is of the order of microns, but not in FPF, where both are of the same order of magnitude. The contribution is more severe when the coatings are thick, in other words, when the wavelength range covered is wide, as is the case of most FPF, and certainly of OSIRIS TFs. Also, the additional term depends on wavelength, since both refractive index and coating thickness depend on wavelength, and this dependence is non-linear. The effect can be noticed even for normal incidence ($\theta = 0$), producing effective etalon gaps that are wider than expected, and hence FWHMs that are narrower than expected, and that depend on wavelength. This has been observed mainly in the OSIRIS Blue TF, specially between ~ 490 and $\sim 590 \text{nm}$. The FWHMs can, however, be considered nearly constant within the whole OSIRIS TFs FOV.

For this reason, the wavelength variation of a FPF across the FOV does not follow a pure geometrical dependence as that given by the combination of Equations 3.2 and 3.16. This effect was first reported by Veilleux et al. (2010) for the TF of the Magellan-Baade 6.5m telescope. These authors detected variations of the wavelength dependence across the FOV, that depended non linearly on etalon gap and wavelength, and that they attributed to variations of the focal distance of the camera, although clearly this cannot be the origin of this effect.

3.2.1 Red Tunable Filter

For calibrating the wavelength dependence across the FOV for the OSIRIS red TF, images of different emission lines at different wavelengths, covering the full OSIRIS RTF wavelength range, were obtained. For each emission line, the red TF was tuned at different wavelengths. The results were checked against OSIRIS TF data of cluster galaxies covering the whole OSIRIS FOV, with spectroscopy available from the literature. From these data, the following wavelength dependence across the OSIRIS FOV is derived:

$$\lambda = \lambda_0 - 5.04 r^2 \quad (3.18)$$

where λ_0 is the central wavelength tuned, and r is the distance in arcminutes to the optical centre of the TF.

Within the inner ~ 2 arcmin, this expression is very accurate for any wavelength (Figure 3.7). Even at the edge of the 4 arcmin radius OSIRIS TF FOV, the maximum error is of the order of the tuning accuracy ($\sim 1-2 \text{\AA}$) for most wavelengths, and always within $\pm 6 \text{\AA}$ in the worse

cases (Figure 3.7). This accuracy is enough for most applications, given the TF tuning accuracy already mentioned, and that if images are dithered, an additional wavelength shift depending on the distance to the optical centre is produced. For example, at the edge of the 8 arcmin diameter TF FOV, the shift is of $\sim 7\text{\AA}$ for a dithering of 10 arcsec.

For those specific projects requiring more accuracy, that use no dithering, an additional chromatic term $a_3(\lambda)$,

$$\lambda = \lambda_0 - 5.04r^2 + a_3(\lambda)r^3, \quad (3.19)$$

with $a_3 = 6.1781 - 1.6024 \cdot 10^{-3} \lambda + 1.0215 \cdot 10^{-7} \lambda^2$, where λ is in \AA , allows obtaining accuracies of the order of the tuning error ($\pm 1\text{\AA}$) within the whole OSIRIS TF FOV.

In the above expressions the distances r are not corrected for distortion (i.e.: are before applying astrometric corrections).

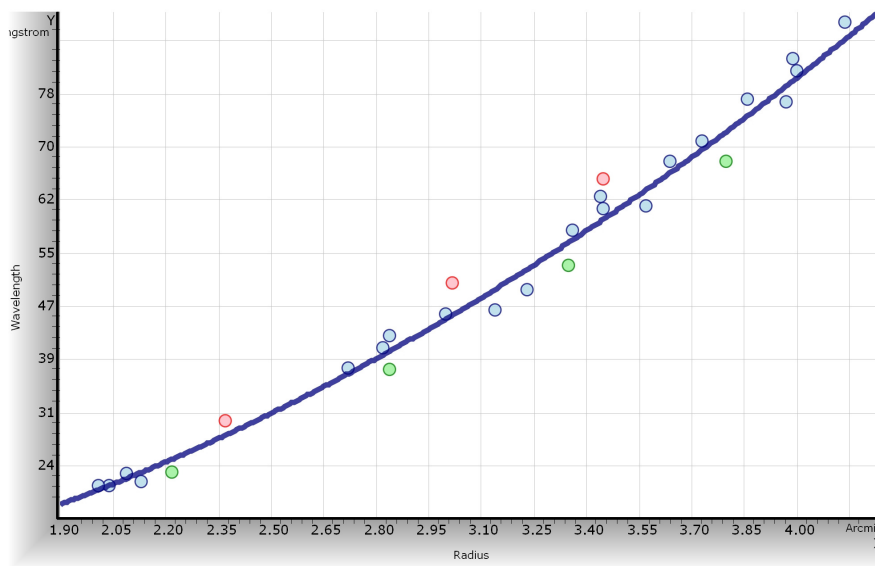


Figure 3.7.- $(\lambda_0 - \lambda)$ vs. radius for different emission lines from the ICM spectra lamps covering the whole OSIRIS red TF wavelength range. The curve is the equation (3.19). In red and green are the points that depart most from (3.19), corresponding to Hg(Ar) 7635 \AA and Xe 9162 \AA , respectively.

3.2.2 Blue Tunable Filter

In the same sense, for calibrating the wavelength dependence across the FOV for the OSIRIS blue TF, images of different emission lines at different wavelengths, covering the full OSIRIS BTF wavelength range, were obtained. For each emission line, the blue TF was tuned at different wavelengths. From these data, the following wavelength dependence across the OSIRIS FOV is derived:

$$\lambda = \lambda_0 - 3.8 \ r^2 \quad (3.20)$$

where λ_0 is the central wavelength tuned, and r is the distance in arcminutes to the optical centre of the TF.

The expression for BTF is extremely accurate for any wavelength and radius (Figure 3.8). Even at the edge of the 4 arcmin radius OSIRIS TF FOV, the maximum error is of the order of the tuning accuracy ($\sim 1\text{-}2\text{\AA}$) for all the wavelengths observed within the full BTF wavelength range. For this reason, no additional chromatic term is needed for the BTF.

Of course, the two derived expressions for the BTF and RTF are different, as the coatings (and their thickness) are different for both etalons and they are also wavelength dependent.

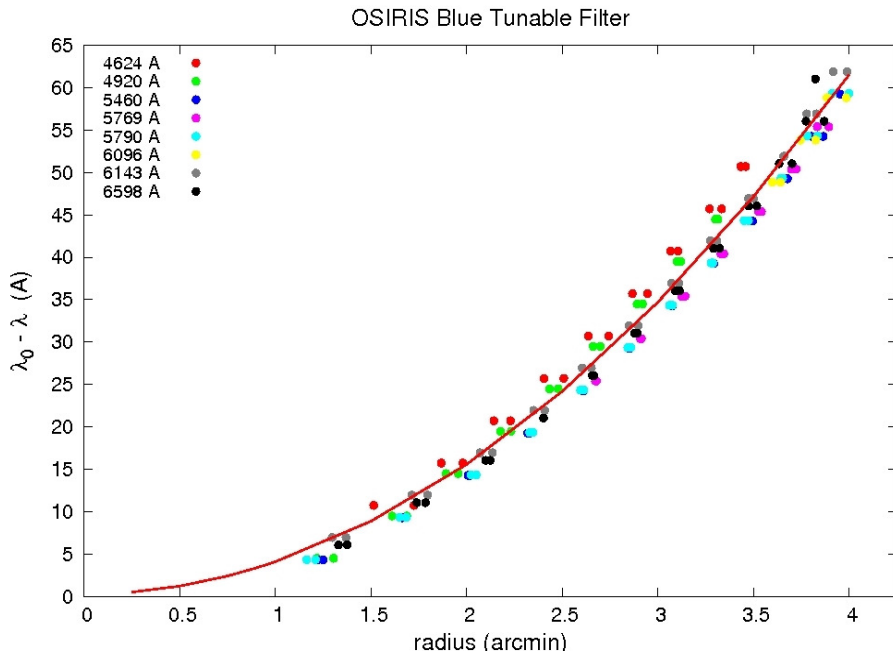


Figure 3.8.- $(\lambda_0 - \lambda)$ vs. radius for different emission lines from the ICM spectra lamps covering the whole OSIRIS blue TF wavelength range. The curve is the equation (3.20).

The optical center for both TFs is located at pixel (1051, 976) of CCD1 including the 25 pixels of overscan. That is, within the gap of the CCDs, and 2 pixels away from the right edge of the CCD1³, or equivalently, the center of the system lies at pixel (-10, 976) of CCD2. The wavelength observed with the TFs relative to this point changes following Equation 3.18 for the RTF, or Equation 3.20 for BTF.

Users should be aware that the wavelength tuning is not uniform over the full field of view of OSIRIS.

³ Note that those coordinates are binned coordinates, that is the standard operation mode of OSIRIS. When 1 x 1 binning is used, those values have to be doubled.

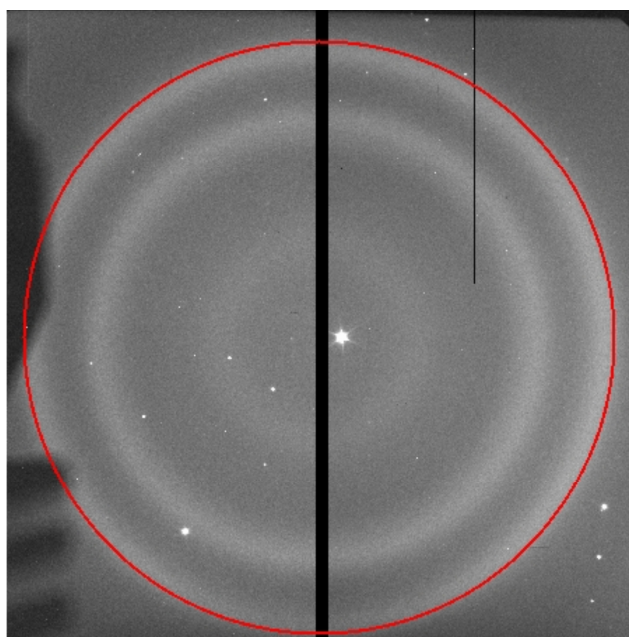


Figure 3.9.- Image with OSIRIS RTF tuned at 732.5 nm, showing the 4 arcmin radius where no contamination from other interference orders is assured. This is the operative FOV of the OSIRIS RTF.

The position of the objects in the Tunable Filter observing mode depends on the requirements of the PI since the value of the wavelength changes with the object's position in the FOV. The PI must indicate, in the Phase-2 form, the coordinates to which the telescope will be pointing and the CCD pixel position corresponding to these coordinates. By default, the pointing will be done at 15 arcsecs from the optical center of the system, in the pixel (50, 976) at the CCD2⁴.

3.3 OSIRIS Tunable Filter available widths

When working with the OSIRIS tunable filters the user needs to take into account two parameters: the observing wavelength and the required FWHM.

The range of operation of the OSIRIS Blue Tunable Filter is from 450 nm to 671 nm, while for the OSIRIS Red Tunable Filter (the only available at the telescope) is from 651 nm to 934.5 nm (both ranges will be increased in future upgrades of the instrument).

It should also be noted that the practical use of the Tunable Filters is more restrictive than was originally anticipated. For the **Red Tunable Filter (RTF)**, the minimum achievable width (that is imposed by the design of the order-sorting filters, in order to avoid contamination by other interference orders within the FOV) is 1.2 nm for most wavelengths, except for the longest wavelengths where even narrower pass bands can be tuned. There is

⁴ Note that those coordinates are binned coordinates, that is the standard operation mode of OSIRIS. When 1 x 1 binning is used, those values have to be doubled.

also a maximum width, depending on the wavelength range. Next Table shows a summary of the available FWHM ranges when using the RTF:

RTF range (nm)	RTF available FWHMs (nm)
$651.0 < \lambda < 800.0$	$1.2 < \Delta\lambda < 2.0$
$800.0 < \lambda < 820.0$	$1.0 < \Delta\lambda < 1.5$
$820.0 < \lambda < 840.0$	$0.9 < \Delta\lambda < 1.4$
$840.0 < \lambda < 880.0$	$0.8 < \Delta\lambda < 1.3$
$880.0 < \lambda < 910.0$	$0.85 < \Delta\lambda < 1.2$
$910.0 < \lambda < 934.5$	$0.9 < \Delta\lambda < 1.2$

In addition to the information of the maximum tunable widths with the TFs as a function of wavelength (see table above). Figure 3.10 shows the available range of widths as a function of wavelength. The minimum width is 1.2 nm for most wavelengths to avoid contamination due to other orders in a circular FOV of 4 arcmin radius. For the longest wavelengths ($\lambda > 800.0$ nm) even narrower pass bands can be tuned thanks to an upgrade in the RTF Order Sorters definition produced on September 2012.

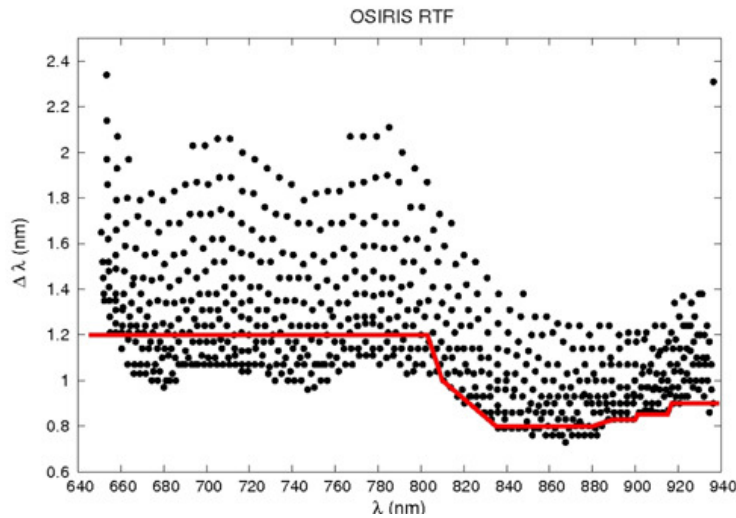


Figure 3.10.- Available RTF widths vs wavelength for all the operative range of OSIRIS RTF. The minimum width achievable is shown as a red line, that is also the maximum width for $\lambda > 850$ nm.

For the **Blue Tunable Filter (BTF)** the possible achievable pass bands are narrower than the ones provided by the RFT. Due to the particularities of the BTF only a single pass band is available for each wavelength that avoids contamination from other interference orders over the circular 4 arcmin radius field-of-view. In other words, for each wavelength only one passband FWHM is available. The following table shows the available FWHM for the BTF.

TF range (nm)	BTF available FWHMs (nm)
$448 < \lambda < 464$	0.80
$464 < \lambda < 481$	0.85
$481 < \lambda < 503$	0.80
$503 < \lambda < 522$	0.50
$522 < \lambda < 543$	0.45
$543 < \lambda < 584$	0.50
$584 < \lambda < 610$	0.70
$610 < \lambda < 638$	0.90
$638 < \lambda < 671$ (*)	1.10

(*) Note that redwards of 65.1nm the RTF can be used with higher efficiency and higher bandwidths.

When preparing TF observations it is highly recommended to use the TF Setup Tool available within ETC section at:

<http://gtc-phase2.gtc.iac.es/science/OsirisETC/html/TFSetupTool.html>

This tool allows to obtain the available widths for our wavelength of interest, as well as to define the corresponding Order Sorter Filter that has to be used for the observation (see Section 10).

3.4 Order Sorter Filters

The use of the tunable filters implies the utilization of order sorter filters (OS) in order to select the wavelength band that avoids confusion between different orders of interference of the Fabry-Perot. The observing wavelength defines which order sorter filter should be selected.

The available set of order sorter filters provides for a suitable filter for all wavelengths. Order sorter filters overlap in wavelength, but their working range ensures suppression of other orders. The OS are tilted 10.5 degrees with respect to TF and grisms, to avoid ghosts due to backwards reflections from the detector (the TF is not tilted and therefore suffers reflections). The description and characteristics for the complete OS filter set can be found in Section 10.

3.5 Calibrating the TF and Tuning accuracy

3.5.1 Parallelism

3.5.1.1 General considerations

TF parallelization consist in determining the X and Y values that keep plates parallel, and depends on Z and λ . OSIRIS TF Parallelism is very robust, and does not vary with time even when switching off and on again the TF controller. Hence, once the XY values for a certain Z

and λ range are determined, they can be used around these Z and λ values from then on. Checking parallelism values from time to time is recommendable.

3.5.1.2 TF parallelization procedure

This parallelisation procedure for the TF is a task to be done during the day. The basis consists of maximizing the intensity of the light in the optical centre of the TF, when tuned to the wavelength of an emission line from a calibration lamp, while varying X and Y. This is the same procedure to be employed for wavelength calibration, but then varying Z. A lack of parallelism (XY) or a poor of wavelength tuning (Z) will reduce the intensity measured. This procedure is achieved by inserting a wide centred long slit, and stepping the charge on the CCD while varying X, Y or Z in a systematic fashion. The TF must be tuned to the wavelength of an emission line (i.e.: the Z must be the one corresponding to the emission line)

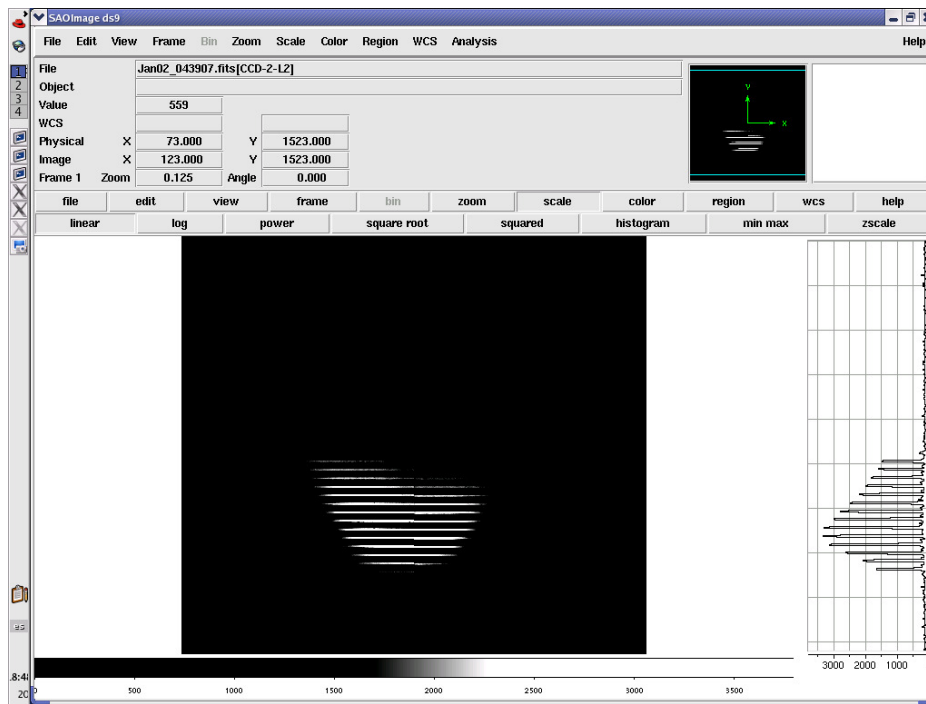


Figure 3.11.- Example of a X calibration image of 14 steps of 50 bits. Seen in the image is a slit illuminated by an arc lamp. The slit is centered on the field. After each exposure the charge is shifted downwards, the X setting of the TF changed, and a new image of the slit is taken. After a sequence of several steps the CCD is read out, which results in a series of slit images as is shown here. N note that in the X calibration, the slit image intensities are not symmetric.

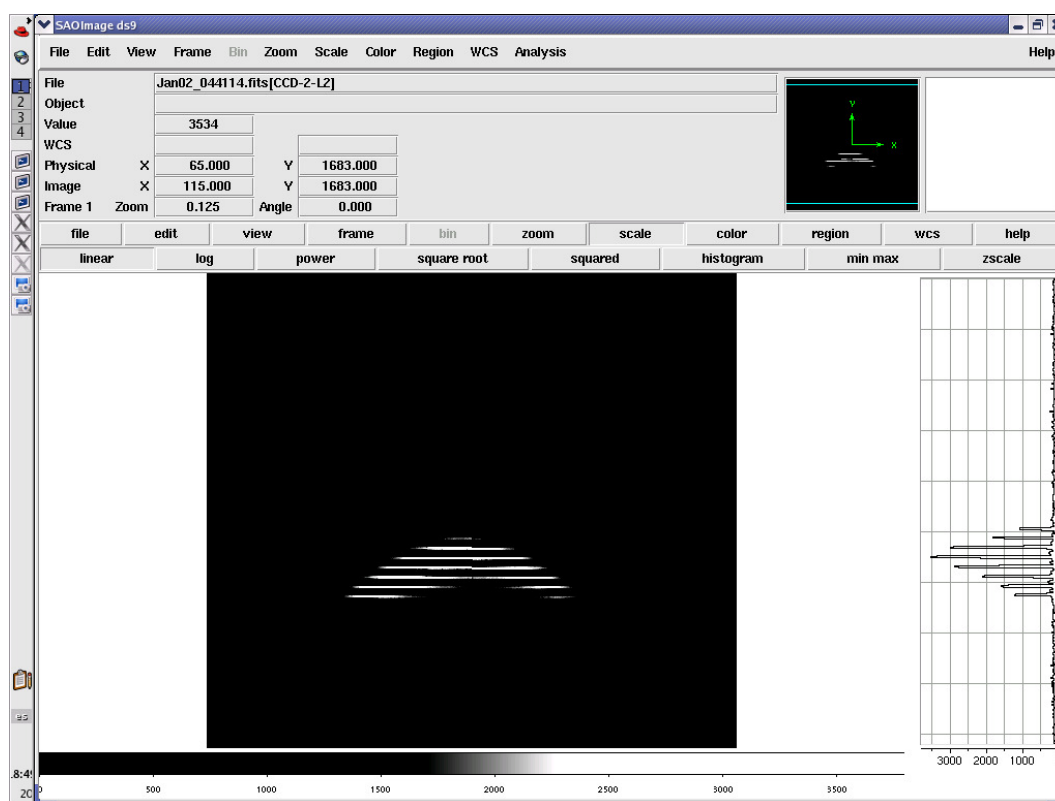


Figure 3.12.- Example of a Y calibration image of 8 steps of 25 bits.. Note that in the Y calibration, the slit image intensities are not symmetric.

3.5.1.3 Lack of parallelism

If the TF plates are not parallel the result will be:

- Distorted rings of the night sky emission lines and of calibration lamp lines.
- Asymmetric wavelength calibration (Z) scans, that are in opposite directions depending whether there is an excess or lack in X or Y values (see Figure 3.13)
- Lower intensities of slit images in wavelength calibration (Z) scans
- Wavelength shifts

The main consequences for the data are:

- Transmission losses
- Wider FWHM and distorted spectral response

The XY resolutions used for parallelism calibration, 50 and 25 bits, respectively, have been chosen as the most convenient. Larger steps are not accurate enough and the XY errors affect wavelength and transmission as shown in the following table (approximate values to serve as example only) for the red TF.

\pm errors Red TF	λ shift (nm)	$\delta T/T$ (%)
$\Delta X = \pm 50$	0.1	4
	0.1	4
$\Delta Y = \pm 25$	0.3	3
	0.2	0

It is important to keep a good parallelism better than 50 bits in X and 25 in Y. Again, note that Y is more sensitive.

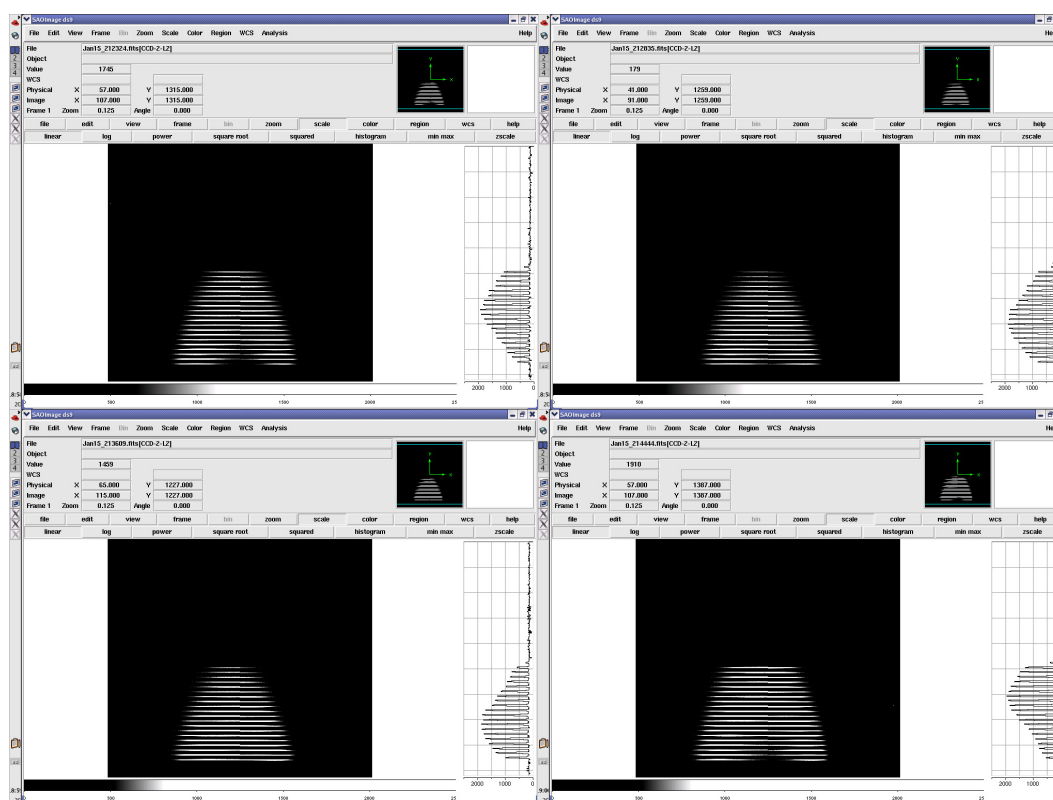


Figure 3.13.- Example of intensity losses and resulting asymmetric slit image intensity profiles obtained for the same Z calibration scan, in the following situations: top-left using Xbest+50 the Z scan is asymmetric and concave **below** the maximum intensity. Top-right using Xbest-50 the Z scan is asymmetric and concave **above** the maximum intensity. Bottom-left using Ybest+25 the Z scan is asymmetric and concave **above** the maximum intensity. Bottom-right using Ybest-25 the Z scan is asymmetric and concave **below** the maximum intensity.

3.5.2 Wavelength calibration

3.5.2.1 General considerations

Parallelization is a day-time procedure, because it is very stable in time and even with temperature changes and instrument rotation. Wavelength calibration, on the other hand, is a nightly procedure, since the Z - λ calibration depends upon many factors, and the calibration must be checked during the night, even for the same wavelength and order.

The wavelength calibration consists of establishing the relation between Z values in bits and the wavelength. This relation is non-linear enough, so that a linear approximation can be deemed valid only locally. Through tests of the TF carried out under controlled environmental conditions the relation between Z and wavelength has been derived for every order and through the full wavelength range that each TF can cover.

Extensive tests show that The λ - Z curve may be offset in Z by a constant factor, depending on the environmental conditions with a precision of 5 bits in Z (i.e.: better than 0.1nm). However, it is necessary to determine the offset for Z mimicking as closely as possible the true observing conditions. So in essence, wavelength calibrating the TF consists of determining this offset. This is done at the telescope by using a calibration lamp of the ICM.

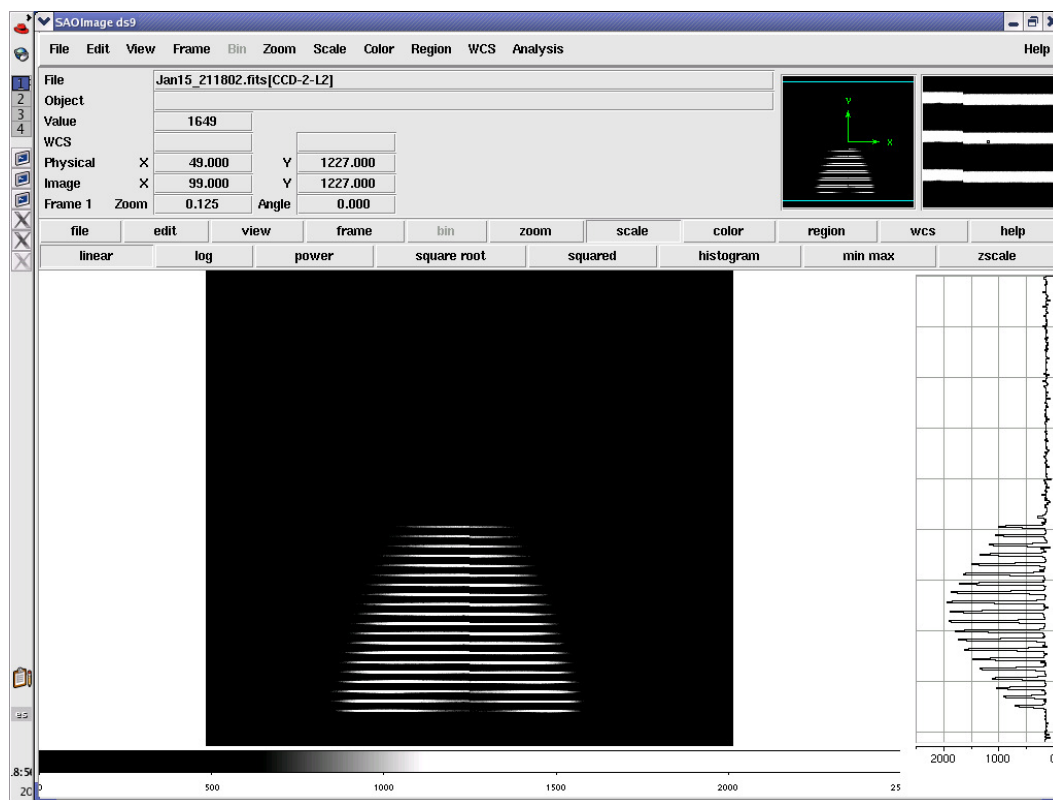


Figure 3.14.- Z calibration scan. 20 slit images can be seen. The first one is the bottom one. The tuning lies between image 11 and 12 as can be appreciated both from the maximum intensity and symmetry. Non symmetric intensities are suspicious of lack of parallelism.

3.5.2.2 Calibration using the ICM

The calibration procedure using the ICM has already been described within the parallelization procedure of the previous section. An accurate wavelength calibration can be obtained only after parallelization, i.e.: determining the best XY values for the given range of Z and wavelength.

Wavelength calibration depends, at least, of the following:

- Humidity. This is potentially an important factor, but since the instrument is flushed with dry air⁵ its effect is for practical purposes insignificant.
- Temperature. This produces a highly non-linear effect where the etalon undergoes several phases of different variations. ET100 are quite large and take up to three hours to stabilize versus temperature changes. However this is not as serious as it seems, since implies only calibrating more frequently, depending on the history and the temperature gradient. It has been demonstrated to be safe operating with TF temperature gradients of at least 0.6°C/hour, produced by temperature differences between TF and telescope of several degrees, as long as calibration is checked every 20 or 30 minutes. When the temperature gradient is of the order of 0.1-0.2 °C/hour the tuning can be considered stable for at least one hour. Telescope gradients are normally far smaller. In the future the instrument control system will take care of this effect at user's request.
- Instrument rotator angle. The calibration of the TFs is highly dependent on the angle of the rotator, and hence on the orientation of the TFs. We can find differences of up to 40 bits (~8Å) between two rotator positions (see Figure 3.15). In order to avoid this we define for TF operation the following useful range $(-160^\circ < \theta < -40^\circ \text{ and } 50^\circ < \theta < 160^\circ)$. This range ensures a stable calibration accuracy of $\pm 0.1\text{nm}$ and, if the rotator is moving less than 10° , the calibration can be considered virtually unchanged, with the precision given by the self-calibration ($\pm 0.02\text{nm} = 1 \text{ bit}$).

The global variation is the blue tunable filter is roughly inverse of the behavior of the red tunable filter, as gravity-induced flexure in the reference capacitors is opposite given their opposite location in the filter wheel (see Figure 3.15).

During the normal operation the observer predicts in advance, using the coordinates of the object and its instrument position angle, the position of the rotator to a specific time in order to ensure that the observations are performed in the optimal range.

This variation is independent both of wavelength and distance between plates (Z).

- TF history: if plates collide, the TF calibration might change. This is unlikely to happen since the Z range has been limited to safe values.

⁵ However, caution must be taken when opening the instrument for changing filters or masks shortly before observations. See environmental conditions in user manual.

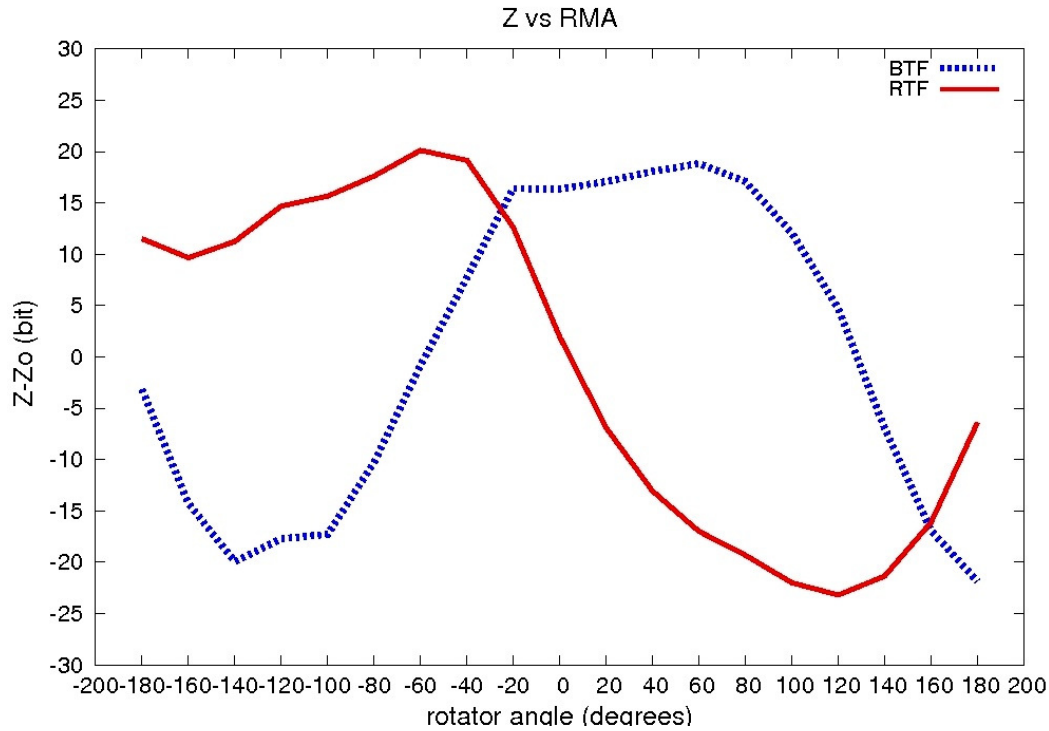


Figure 3.15.- Variation of the TF tuning (Z) with the rotator angle.

All those factors produce day to day variations in the TFs calibration. For this reason **the TFs have to be calibrated before every observing block**. The time needed for this procedure causes the relatively large overheads assumed in Phase 2 tool for TF observations.

3.5.3 Checking the calibration by using night sky emission lines

The OH group produce relatively strong emission lines, specially redwards of 700nm. These are a nuisance in broad-band and narrow-band imaging as they are for long-slit spectroscopy. However, they happens at precise wavelengths and with definite relative intensities and can be used for calibrating spectra or, as in this case, the tunable filter. Since the FOV is fully illuminated by these emission lines, rings are produced. Knowing the wavelength of the emission line, the radius of the ring, that can be obtained using ds9, the tuned central wavelength can be derived.

As a rule of thumb, for a wavelength drift lower than 0.1nm, the variation Δr of the ring radius r should be, in the worst case:

$$\frac{\Delta r}{r} \leq 0.02 \quad (3.21)$$

For better accuracy,

$$\frac{\Delta r}{r} \leq \frac{n}{2\Delta\lambda}, \quad (3.22)$$

where n is the number of nm of the allowed drift, and $\Delta\lambda$ is the wavelength variation in nm from the centre of the TF (λ_c) to the ring (Eq. 3.18 and 3.20),

$$\Delta\lambda = -5.04\lambda_c^{-1}r^2, \quad \text{for RTF} \quad (3.23)$$

$$\Delta\lambda = -3.8\lambda_c^{-1}r^2, \quad \text{for BTF} \quad (3.24)$$

with the radius r in arcminutes.

If the ring radius varies in more than the tolerated value, the Z must be changed. If r increases, the Z must decrease and vice versa. This

The above expressions can be used for an external check of fast recalibration without using the calibration lamps. However, it is advisable to use the calibration lamps to avoid errors from a tired and sleepy user.

For a good sky line map, the reader is referred either to Hanuschik (2003), that can be found on-line at http://www.eso.org/observing/dfo/quality/UVES/pipeline/sky_spectrum.html, or to use directly OSIRIS low-resolution sky spectra that are available at: <http://www.gtc.iac.es/instruments/osiris/media/sky/>

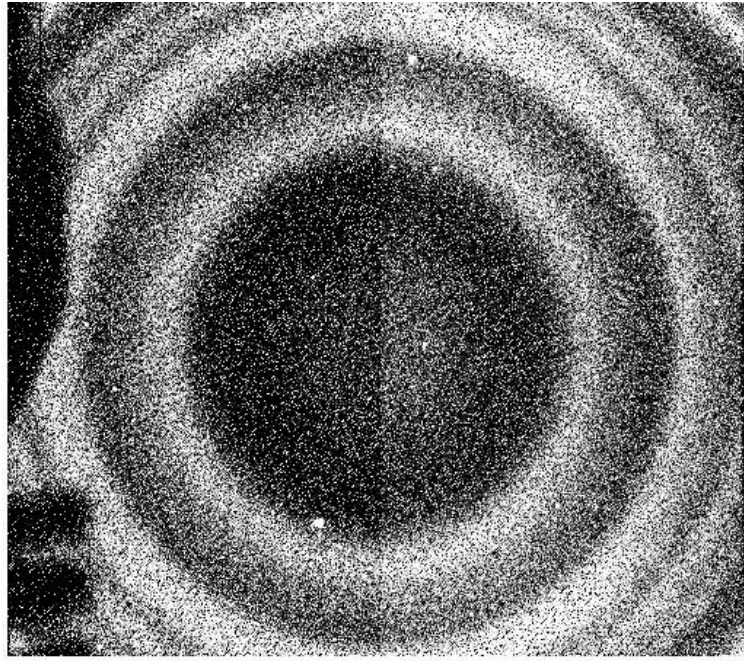


Figure 3.16.- Sky ring at 894.35 nm with the OS 878/59 with FWHM 1.21 nm, tuning the TF at 898.2nm for obtaining a ring radius of ~1100 pixels. The exposure time is of 120 s.

3.5.4 Tuning accuracy

The theoretical tuning accuracy is 0.02 nm in wavelength and FWHM as provided by the CS-100 etalon controller (in most cases this is the typical value of 1 bit in Z). The real accuracy in practical terms is driven by the wavelength calibration accuracy, that can be of the order of 0.1-0.2 nm.

3.5.5 Tuning speed

The tuning can be changed in an interval between 10 to 100 ms, depending on the change in Z. For large Z differences, the TF control system automatically moves the etalon in steps to avoid “out of range” failures. For fast modes it is advisable limiting the range of Z movement to the minimum (hundreds).

3.6 Observing with OSIRIS Tunable Filters

3.6.1 Tunable Filter vs. Spectroscopy

For a complex instrument such as OSIRIS, with a wide variety of observing modes and sub modes, one of the concerns of the user is whether the chosen mode is the most appropriate for the observing program. Since tunable filter imaging is a relatively new, and not widespread mode, most confusions arise between the convenience of the use of this mode versus spectroscopy.

In brief, the main advantages of TF versus spectroscopy is the ability to flux calibrate the emission (a tricky issue in MOS and even in long slit spectroscopy: slit slicing the image, differential refraction, centring errors,...), and of obtaining 2D emission line maps for targets over the FOV, either extended or of small size. The main disadvantage is that only one wavelength can be observed at a time. The following table and the flux diagram below help deciding the most appropriate mode.

Tunable imaging	Spectroscopy
1 or few spectral lines	Wide spectral range (at low R)
2D spectral features	1D (long slit) or very small area (IFU)
All targets in FOV (high ρ fields)	Number of spectra per mask limited
Reliable flux calibration	Uncertain (LS, IFU), unreliable (MOS) flux calibration
Low spectral resolution	Velocity fields & line profiles (at high R)
Approximate redshift should be known	Redshift knowledge not required
Position not required (survey)	Position required (pre-imaging. This introduce biases)
On-the-fly observations enabled. For ex: Galaxy clusters	Drilling masks overheads
TF pre-imaging avoid IFU mosaic	

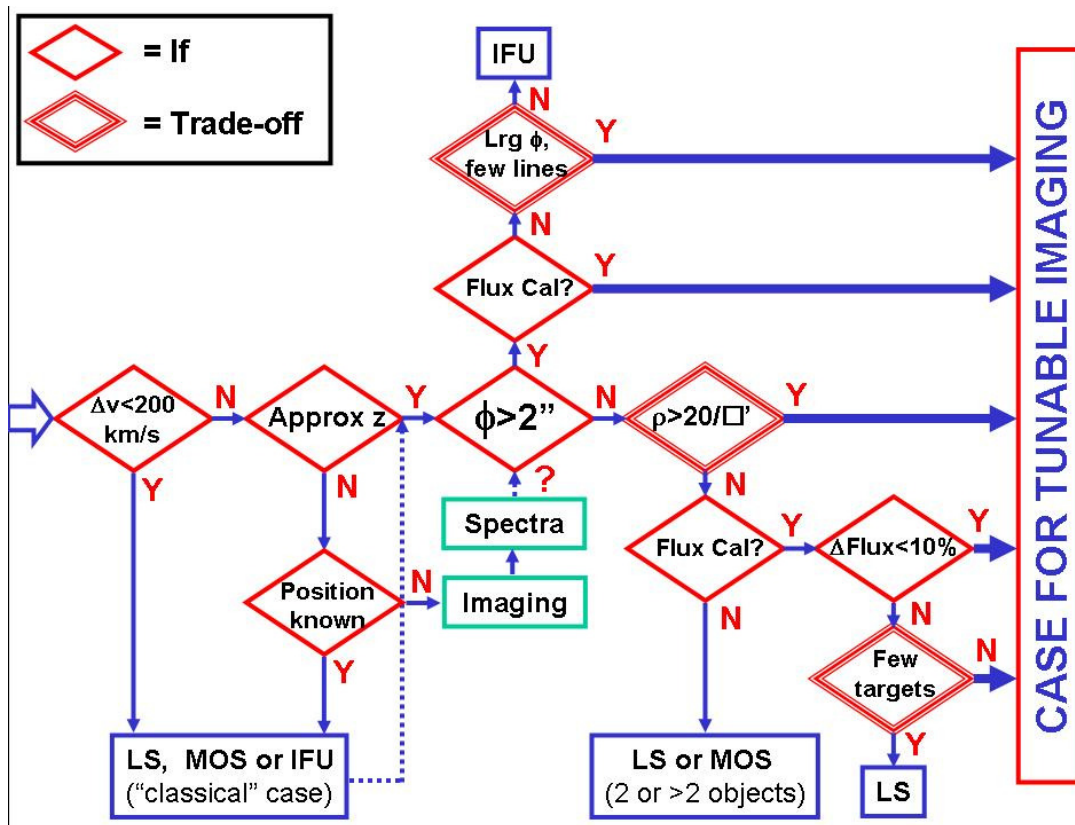


Figure 3.17.- Tree for deciding the most appropriate mode: TF versus spectroscopy. Δv is the line width or velocity dispersion, ϕ the target diameter, ρ the density of targets, and ΔFlux the error flux required.

3.6.2 Observing Strategies

The observing strategies for a TF are driven by the following instrumental effects:

1. The spectral response of the TF: more peaked and with more wings than a Gaussian or a squared 5-layer interference filter (Figure 3.5).
2. The diametric ghosts.
3. The centre to edge wavelength variation.

and affects the way to design an observation depending on the characteristics of the sources:

- Photometric accuracy requested. (**please note that from now on we will refer to photometric accuracy of instrumental origin, not due to readout or photon noise**).
- Possible neighbouring lines to the one studied.
- Velocity field or line width of the target.

- Size of the target.
- Redshift of the target.

playing with the possible variables:

- TF central wavelength for your ON and OFF images.
- TF FWHM.
- Position of the source in the FOV.
- Rotator position.

These points mark the difference with respect to direct imaging with conventional filters. In other words, **in tunable imaging the design of an observation is extremely important, as well as the observing procedure**, otherwise it can easily result on useless data..

In the following sections we provide derive recommended observing strategies depending on the type of sources, and the scientific aims, by explaining the impact of the previous parameters.

3.6.2.1 Selecting off-band wavelengths

3.6.2.1.1 Continuum subtraction

In line imaging, two images are usually required: the on-line image and the off-line (or continuum) image. The on-line image has line plus continuum photons and the off-line only continuum photons, to be subtracted from the on-line image to give the emission line (continuum free) image.

This can be done in two ways:

1. Using the TF for line and continuum has the advantage that the spectral response and FWHM are identical, and that you can select the continuum as nearby as desired from your line, thus alleviating possible continuum variations with wavelength. It is even possible, using the technique of shuffled exposures to on-line averaging continuum on both sides (blue and red) of the line and averaging possible seeing and atmospheric variation. In this way it is possible to achieve a very good continuum and sky subtraction with a direct pixel-to-pixel difference between your on-line and your continuum image. However, TF have quite narrow FWHM and hence the exposure times are quite large.
2. Using a medium band (and OS) or broad band filter (Sloan-SDSS). In this case continuum subtraction is not as good, and certainly not as direct, and must be faced with caution. Since the continuum filter is tens of times wider than TF, the exposure times required are reduced accordingly.

If the TF is to be used for continuum subtraction, the TF tuning of the off-band has to be chosen so that no or few emission enter into the continuum filter. This is driven by the photometric accuracy required via the following expression, derived from Eq. (3.14),

$$\frac{|\lambda - \lambda_0|}{\delta\lambda} = \frac{1}{2} \sqrt{\frac{1-T}{T}} \quad (3.25)$$

This equation can be interpreted, in this case, as providing the transmission T , normalized to unity, of your continuum filter, tuned at λ_0 and of FWHM $\delta\lambda$, at the wavelength λ of the on-line tuning.

For example, let assume that the continuum must be chosen with a contribution from the emission line lower than 5%. Then, for a given FWHM of say 1.8 nm, the tuning of the continuum must be placed 4nm away from the line tuning. Of course wider FWHM require increasing the wavelength difference between on and off-line tunings.

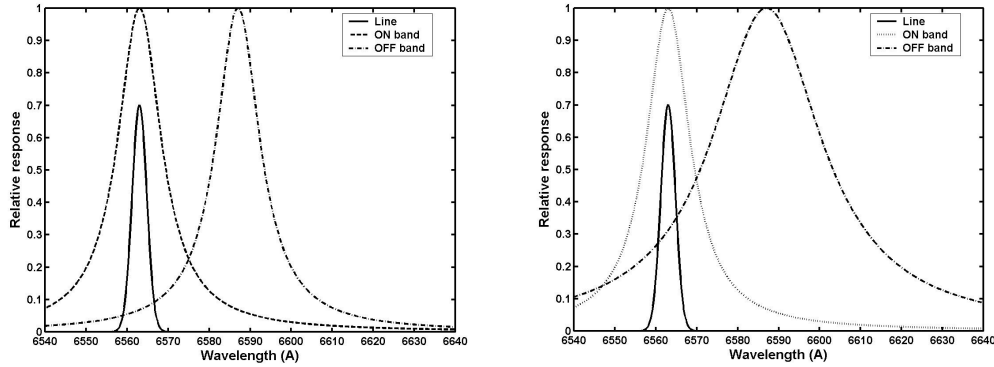


Figure 3.17.- Left: A proper tuning of the off-line wavelength minimizes contribution from your line to the continuum according to Equation 3.18. Right: Increasing the FWHM of the off-line tuning will require increasing the wavelength difference between on and off-line wavelength tunings. The distances are larger than expected since the TF spectral response has more wings than a standard interference filter.

3.6.2.2 Deblending lines

Equation 3.25 can also be used for deblending lines. Known the redshift, one tuning for each line can be observed. From the line separation and the FWHMs of the tunings, the contribution of the other lines to each tuning can be estimated, and corrected simply via simultaneous equations system.

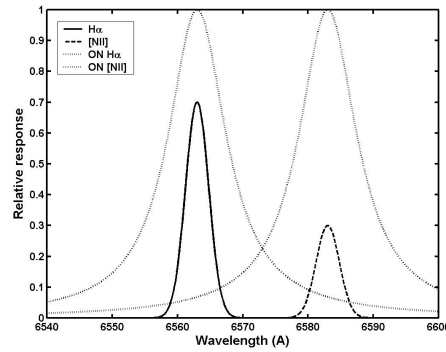


Figure 3.19.- H α can be deblended from [NII]658.4nm if the redshift or Doppler shift is known, via defining a simultaneous equation system with TF transmissions derived from the TF FWHM and line relative positions.

3.6.2.3 On-line FWHM selection

The TF FWHMs are quite narrow, and nearly Gaussian from peak to half transmission. Then the line width must be quite narrower than the TF FWHM or otherwise some flux will be lost. It can be easily demonstrated that, assuming Gaussian line profiles, the flux error can be approximated by,

$$\text{Flux error}(\%) = \frac{1}{2 \ln 2} \left(\frac{\delta}{\delta \lambda} \right)^2 \quad (3.26)$$

where $\delta \lambda$ is the TF FWHM and δ is the line width. For example, observing a line with the same width than the TF result in loosing ~28% of the flux (a more precise calculation gives 36%).

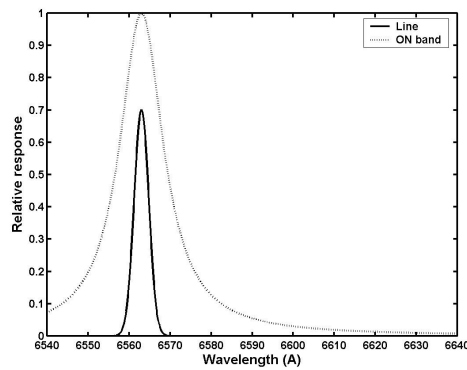


Figure 3.20.- Comparison of TF and line profiles.

The following table can be used for selecting to most suitable FWHM according to the expected line width. Please note that they are approximate values.

$\delta\lambda/\delta$	Flux error (%)
1.0	36
1.5	22
2.0	14
2.5	10
3.0	7
3.5	5
4.0	4

Table 3.1.- Approximate error fluxes depending on line width ($\delta\lambda$) and TF FWHM ($\delta\lambda$).

For example, the typical velocity field of a spiral galaxy (250 km/s) at zero redshift, would require TF FWHM of at least 1nm at H α , for an error smaller than 5%⁶, and the minimum FWHM recommended for the red TF at H α is of 1.2 nm. Hence this is not a problem in this case, but it might be for [OII]372.7nm (blue TF) or when observing objects at significant redshifts where the line widths are expanded⁷ by the factor (1+z). Since the range of available FWHM are quite limited, if a certain photometric accuracy is required and the needed FWHM cannot be obtained, it is possible to synthesize a wider FWHM by summing images of a scan (see Section 3.6.2.7).

3.6.2.4 Deciding target position and orientation

The presence of ghosts and the centre to edge wavelength variation drive target position on the OSIRIS FOV.

To avoid excessive wavelength variation, the target should be as centred as possible, but it cannot be placed right in the centre because, aside of falling into the gap between detectors, a mirrored ghost image of the source will overlap with the real image. This might be acceptable in some cases, for example if the user is interested in radial dependences only. However, in general, the target should be placed near the optical centre of the TF, but fully off it. Near the TF centre but on CCD2 (the rightmost) is a convenient location.

If the object is elongated, the wavelength variation can be minimized by turning the GTC rotator to align the major axis of the target perpendicular to the radial direction for the TF optical centre (Figure 3.21).

However, since the target is not at the centre of the TF, the TF must be tuned to the red of the line, so that the target is observed at the wavelength of the line required. This can be evaluated using Equations. 3.18 or 3.20. For example, a target of a diameter of 2 arcminutes should be placed somewhat more than 1 arcminute from the centre. Then the wavelength corresponding to the zero redshift H α at this position is not 656.3 nm but 656.8 nm.

⁶ Please note that 250km/s is the FULL velocity field, not the velocity field at FWHM.

⁷ Please do not forget this “detail”.

Even with the above strategy, and unless the target is very small, the wavelength dependence across the FOV will produce that some parts of the target are observed at different wavelengths. The induced photometric error can be evaluated using Equations 3.18/3.20 and 3.25. For example, for the same example above, the wavelength of the edge of the target near the TF centre is 656.8 nm and the wavelength at the edge of the target in opposite direction is 654.7 nm. The photometric errors induced by this line decentring are, respectively, 7% and 45% (from Equation 3.25) if a FWHM of 3.5 nm is assumed. Then, it is possible to choose a TF tuning wavelength that minimizes this variation: when the wavelength difference at both edges of the target is the same. For example, tuning at 657.3 nm gives a photometric error equal at both edges of the target and of the order of 25%. Of course **the velocity field of the target must be taken into account in this procedure** since it increase the photometric errors (if the velocity field is known, it is possible to adjust the target and rotator position to minimize it).

Were this photometric error too much, it is possible to synthesize a wider FWHM by adding TF scans (see 3.6.2.7).

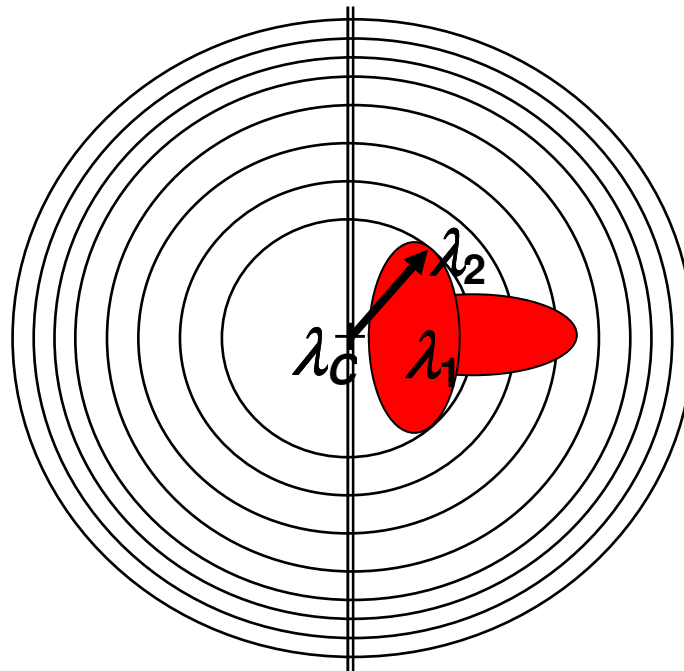


Figure 3.21.- Changing rotator angle is useful for minimizing the wavelength variation across the target.

3.6.2.5 Removing ghosts, cosmic rays and cosmetics

One feature of etalons is that they produce ghosts. In any astronomical instrument, the detector is a source of light: any light that is not detected or absorbed is reflected. This light reflected by the detector follows the same optical path in opposite direction, entering the etalon and reflecting in the most reflective surface, i.e.: that of the reflective coating of the etalon cavity, going back and hitting the detector in a place symmetric with respect to the optical centre of the etalon. This has three important implications for the observer:

1. Diametric ghosts are symmetric with respect to the centre of the etalon (Figure 3.22), that in the case of OSIRIS is almost the centre of the OSIRIS field, in the gap between detectors at the line ~ 976 (binned coordinates).
2. Diametric ghosts can be easily removed by the classical dithering procedure since moving the image in one direction shifts its ghost in the opposite direction with respect to the TF optical centre. When stacking up the images taking as reference the image of the target, all ghosts fall in different pixels and can be removed with average sigma clipping of similar algorithms
3. Only very bright, usually saturated sources, generate ghosts (Figure 3.22). For OSIRIS RTF, the integrated flux of the ghost images is less than 1.7% of the integrated flux of the main source. Hence, for RTF observations, unless very bright sources are in the FOV and their ghosts could spoil the image of the target, there are no need to worry about it. However, for OSIRIS BTF, as a result of a larger thickness of the internal reflective coating, the integrated flux of the ghost image can be up to 15% of the integrated flux of the main source for $\lambda < 610$ nm. Hence, for BTF observations dithering procedure is mandatory to remove these ghosts.

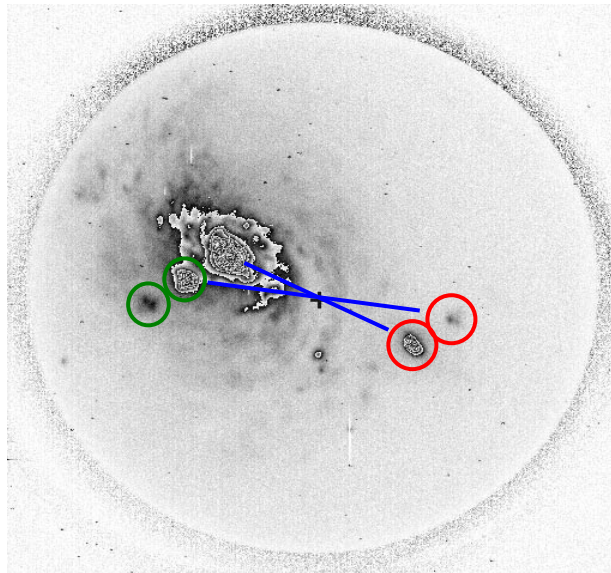


Figure 3.22.- Example of ghosts in a TF. The cross marks the optical centre. The red circles mark the diametric ghosts of the centre of the galaxy and that of an exponential ghost, while the green ones marks the exponential ghosts. The second exponential ghost does not produce a noticeable diametric ghost.

Exponential ghosts cannot be removed by dithering. Luckily OSIRIS TF does not have this kind of ghosts.

Of course ghosts drive the location of the target in the FOV, as is dealt in this document in Section 3.6.2.4. As stated above, ghosts can be removed using the same dithering method that removes for instance detector cosmetics. However dithering move the target in the TF FOV, i.e. it changes the wavelength at which the target is observed. This is specifically severe at the edges of the FOV, where the wavelength dependence with location is larger. There are several ways to alleviate this problem that will be described in the following

subsections. But note that in many cases ghosts do not required to be removed since they can be seen only for very bright sources.

3.6.2.5.1 Field masking

Inserting a focal-plane mask that covers half the field and hides detector CCD1 avoids ghosts coming from that part of the field. In this case dithering is not necessary to detect ghosts. But obviously in this case only half the field can be used and therefore normally not an attractive option.

3.6.2.5.2 Azimuthal dithering pattern

When only one relatively small source is of interest, the dithering can be done following the circle of equal wavelength.

3.6.2.5.3 TF tuning dithering pattern

If several relatively small targets spread on the FOV are to be observed, it is possible to do a three point dithering where the TF tuning is changed to minimize wavelength variations at the edge of the TF FOV in **one direction**. Then different sections of different images can be combined. This is valid only when using tunable tomography.

3.6.2.6 Tunable tomography

3.6.2.6.1 Technique

Tunable tomography or TF scanning consists of obtaining a set of images of the same pointing at different consecutive wavelengths (Figure 3.23). The characteristic parameters are:

- Initial and final wavelength (or Z)
- Step in wavelength $\Delta\lambda$ (not equivalent to a constant ΔZ since the λ -Z relation is in general not exactly linear)⁸

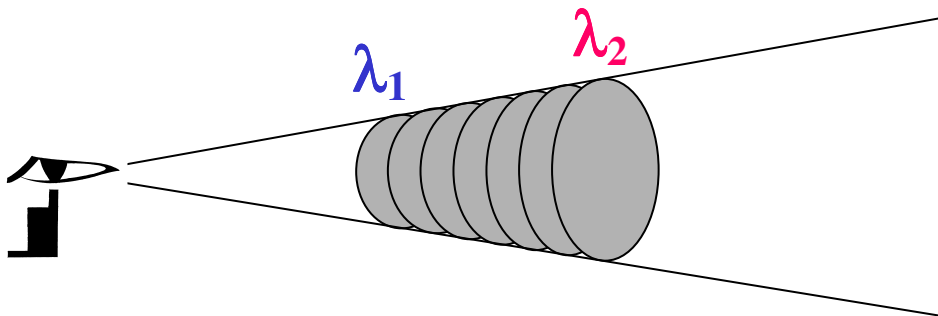


Figure 3.23.- Tunable tomography consists in scanning a wavelength range using the TF. For the same telescope pointing, a set of images at different wavelengths are taken.

⁸ Please note that further on this document $\Delta\lambda$ is NOT the FSR of Equations 3.5 and 3.7, but the scan step or wavelength step between consecutive exposures in tunable tomography.

The step must be carefully chosen since for a given wavelength range to be scanned, a step too fine will increase the observing time and overheads required, but a step too coarse would introduce larger photometric errors, that can be evaluated using Equation 3.25, but now considering that the maximum error will be half the scan step (i.e.: in the worst situation an emission line would be located in the middle of a step),

$$\frac{\Delta\lambda}{\delta\lambda} = \sqrt{\frac{1-T}{T}}. \quad (3.27)$$

In this observing mode, the different images are not combined, but analyzed separately. Usually aperture photometry of the sources of each image provide “pseudo-spectra” that are used for identifying emission lines and determining its fluxes and Doppler shifts or redshifts.

In the case that the TF images are going to be used for continuum subtraction, the images of the same scan (or several of them added together) can be used for this purpose, as long as they are separated enough to achieve the required photometric accuracy based on TF FWHM, scan step and the number of images. This might require obtaining some additional images at the end and/or the beginning of the scan (at the end and beginning would allow averaging possible continuum variations).

Examples of applications of this method are:

- Scanning a spectral region for de-blending neighbouring lines.
- Scanning a target looking for systems of high velocity faint or diffuse ionized gas.
- Scanning blank fields searching for serendipitous emission line targets in a certain volume of universe determined by the FOV and the initial and final wavelength for every emission line detected.
- Scanning the velocity field of galaxy clusters allows determining emission line objects and even the cluster velocity dispersion.
- Scanning a certain emission line of a target of inaccurate redshift.

3.6.2.7 Band synthesis technique

3.6.2.7.1 Technique

As before, but in this case the final destination is not analyzing images separately but adding them together providing a “wider” synthetic filter (Figure 3.24).

The main difference is that in this case one additional image must be obtained at the beginning and at the end of the scan (in a conventional filter equivalence this would be similar to the zone where the spectral response is varying and the flat zone has not been reached yet), and that the photometric accuracy refers to the wiggles generated when adding

the images (Figure 3.24). Alternatively instead of obtaining this “extra” images, it is possible to correct them by multiplying by the appropriate factor > 1 that can be easily calculated.

As a guideline, the photometric accuracy that can be achieved as a function of the scan step is summarized in the table below (Figure 3.24).

$\Delta\lambda/\delta\lambda$	$\delta I/I$ (%)
1	20
2/3	5
1/2	2

Table 3.2.- Approximate accuracy achieved as a function of the scan step.

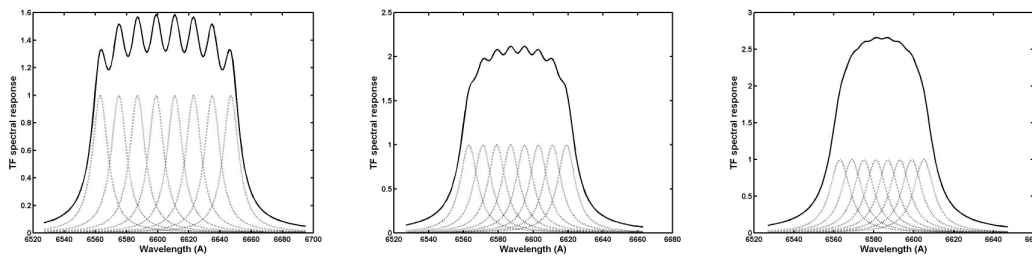


Figure 3.24.- Theoretical examples of the band synthesis technique. Left: a scan step equal to the TF FWHM gives photometric uncertainties of $\sim 20\%$. Middle: a scan step $2/3$ of the TF FWHM gives photometric uncertainties of $\sim 5\%$. Right: a scan step equal to half the TF FWHM gives photometric uncertainties of $\sim 2\%$. The first and last images are either not used or corrected via the corresponding multiplicative factor.

Of course the images obtained can be used both for Tunable tomography and band synthesis. For example: in tunable tomography, images can be combined in, for example, pairs or terns to increase S/N in the case of faint targets (depending on line widths and TF FWHM), or all added together to serve as pseudo-broad band image for target detection.

Examples of applications of this method are:

- Scanning the velocity curve of a large spiral galaxy compensating for the centre to edge wavelength variation.
- Scanning a wide spectral line (i.e.: that of a high redshift galaxy or a QSO).

3.6.2.8 Summary

3.6.2.8.1 Sources of instrumental photometric errors.

The sources of photometric errors of instrumental origin (again, please note that contributions of readout or photon noises must be considered aside) are:

- The FWHM of the TF, depending on line width (driven by velocity dispersion, velocity field, peculiar velocities, and redshift). This can be evaluated using Equations. 3.25 or Table 3.1, and if appropriate can be corrected using the method of band synthesis (Sec. 3.6.2.7).
- The contribution of the line to the off-band or to other lines to the on-line image. Can be evaluated using Equation 3.25.
- The wavelength variation across the target. Depends on the size and the velocity field. Can be evaluated using Equations. 3.18/3.20 and 3.25. If required can be corrected using the method of band synthesis (Sec. 3.6.2.7).
- Dithering that varies the wavelength of pixels of the source from one image to a dithered one. Can be evaluated using Equations. 3.18/3.20 and 3.25. If required can be corrected using the method of band synthesis (Sec. 3.6.2.7) or choosing a suitable dithering pattern combined with TF tuning (Sec. 3.6.2.5.2 and 3.6.2.5.3).

3.6.2.8.2 Preparing an observation: a checklist.

According to the previous sections, depending on the scientific program, the line to be observed, the type of target, its size, velocity field or velocity dispersion, redshift of Doppler shift, accuracy of this shift, and the number of targets, it is necessary to determine:

- Position of the target(s) in the FOV.
- Orientation of the detector on the sky.
- Wavelength to be tuned (in the centre of the TF).
- Dithering pattern to be used.
- Technique to be used: single exposures, shuffled images, fast photometry, TF tomography or band synthesis.
- FWHM to be used. Use calculator for exploring possibilities. This might drive reconsidering the technique to be used if FWHM is too narrow.
- Wavelength range to be scanned (for TF tomography or band synthesis).
- Exposure time.
- Use of TF, OS or broad-band filters for continuum subtraction.

3.7 Spectrophotometric standards for TF flux calibration

The TF flux calibration is done using standard spectrophotometric stars as usual, using the same settings as for obtaining the science data, that is, an image from the standard star at each of the wavelengths and with the same TF FWHM used for obtaining the science images. The TF spectrophotometric standard is observed only under user request, and a corresponding Observing Block has to be completed for this purpose.

The complete list of spectrophotometric standard stars for TF flux calibration can be found in Section 14. They are the same that are used in Long Slit Spectroscopic and MOS observing modes.

3.8 OSIRIS Tunable Filters global efficiency

The graph below shows the overall photon detection efficiency of OSIRIS Tunable Filters at GTC, including the contribution both of the telescope and instrument optics system.

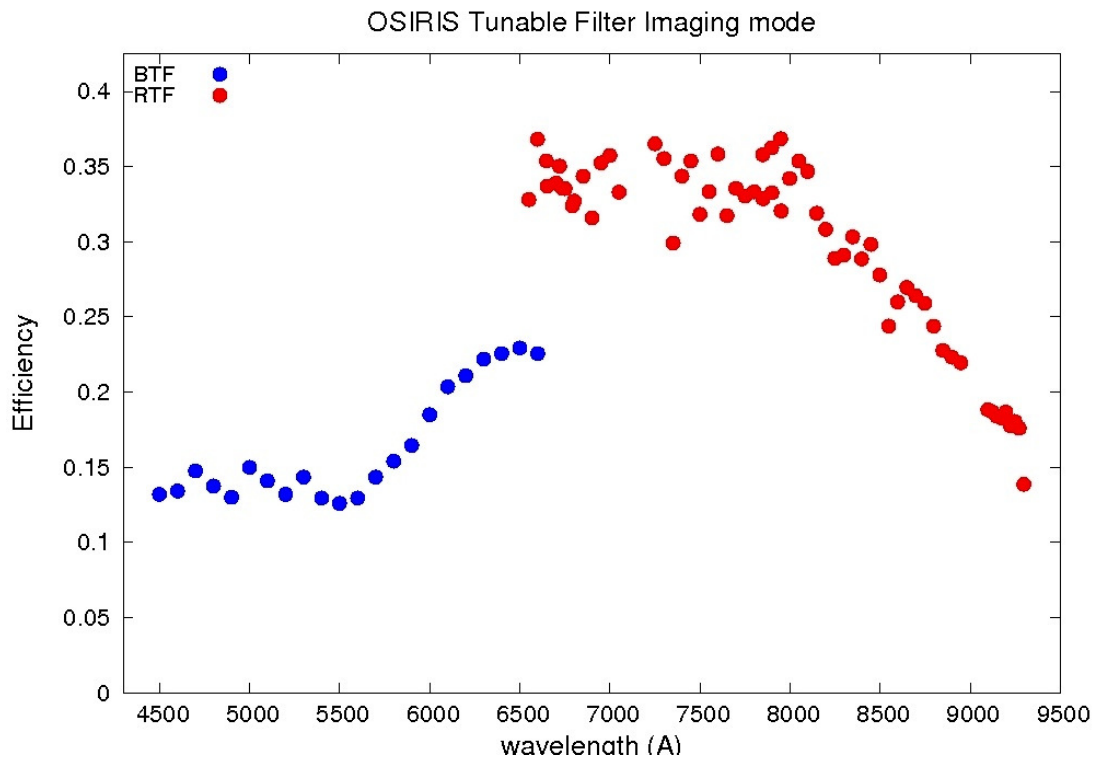


Figure 3.25.- Overall photon detection efficiency of GTC and OSIRIS with the Tunable Filters.

3.9 Post-processing TF data

The TF data reduction procedure is like that of narrow-band direct imaging: requires de-biasing, flat fielding, combining dithered images (if required), flux calibration using aperture or PSF photometry of spectrophotometric standard stars, and continuum subtraction (if required).

The main differences with narrow-band direct imaging are:

- For removing cosmic rays, cosmetics or sky rings, only dithered images at the same tuning (Z) can be combined⁹, taking care of the possible wavelength shift of the dithered images, specially at the edges of the TF FOV (see Sec. 3.6.2.5 for some hints on alleviating this problem).
- Depending on the type of sources, subtracting continuum images might be unnecessary if a pseudo-spectra is obtained by aperture photometry of the sources observed at different contiguous wavelengths (Sec. 3.6.2.6).
- Images of the same field at different contiguous wavelengths can be combined in the band synthesis technique (Sec. 3.6.2.7).
- In the red spectral domain sky rings appear (see Sec. 3.9.2).

3.9.1 Calibration images

3.9.1.1 Bias

Images to correct for the electronic bias of the CCDs should be obtained and applied as usual. These same readout speed and binning must be selected.

3.9.1.2 Flat fields

During the normal operation of OSIRIS at GTC, flat fields for the TF observations are obtained using dome flat fields, with the TF tuned to the same wavelengths of the science observations. It is practically impossible to get a series of enough sky flat fields at all the wavelengths requested for a typical program due to time limitations.

Some features that can be observed at some wavelengths in the TF dome flats are also present in sky flat images, hence they are not due to particularities of the dome illumination. We consider that the dome flat fields are adequate for their purpose and little is gained from using TF sky flat fields. The main features in the illumination pattern seen in the dome flats are also noted in the science images.

⁹ As images obtained using different conventional filters would not be combined for this purpose either.

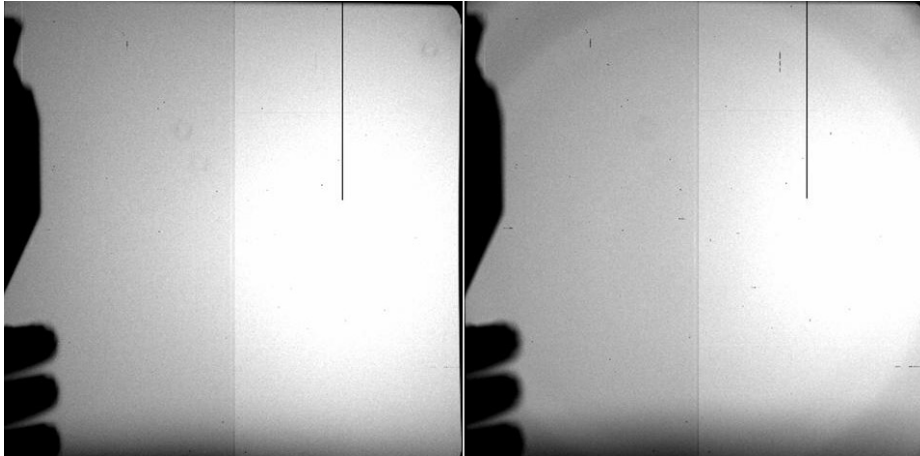


Figure 3.26.- TF dome and sky flat at 715.0 nm, where the same features can be observed.

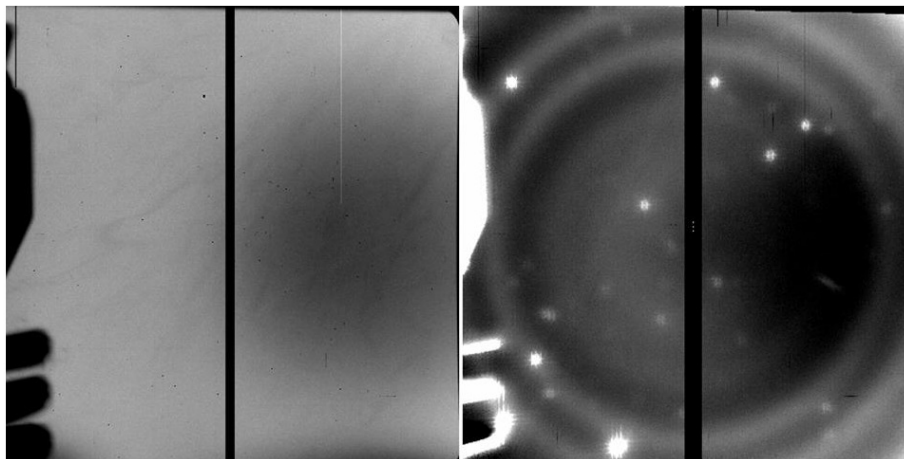


Figure 3.27.- TF dome flat at 660 nm (left), and a sky image at 660 nm (right) obtained from an artificially dithered raw science image

3.9.2 Night-sky emission line rings

The OH atmospheric emission lines are observed through the TF as rings (Figure 3.16), due to its centre-to-edge wavelength variation. They are equivalent to the fringing observed in direct broad band imaging and, like it, are an **additive** effect. They increase the background photon noise in the zones affected by the ring, thus reducing the S/N in these zones.

Sky rings not necessarily require correcting as long as the ring is not on the target, and the target is not too faint. Nevertheless, if a correction is required, there are several ways to proceed:

- If the targets are not very large, a superflat with the sky ring pattern can be obtained by combination of dithered and smoothed images, even of different pointings: (i) smoothing the dithered images to be corrected using a kernel that wipes small-scale structures (sources) but keeps large-scale structures (the rings), (ii) obtain the media of the combined smoothed **unmatched** dithered images using a rejection algorithm (the sources are not in the same position due to the dithering, but the rings does since their position

depend on the wavelength tuned only). Even images of different pointings can be used as long as the wavelength tuned is the same. (iii) Subtracting the resulting superflat from the original images.

- Running, for example, SExtractor to remove sources thus creating again a superflat.
- Using specially devised programs for creating a synthetic ring image by fitting an azimuthal average of the image, and subtracting it.
- Fitting a 2D surface to the ring, creating a synthetic ring image, and subtracting it.

Synthetic ring images do not introduce photon noise in the final image, as the other methods does.

3.10 Medium Band Imaging with TF Order Sorters

The TF Order Sorter filters can also be used for direct image observations. Measurements made during the commissioning of OSIRIS (January 2010) have provided zeropoint values for some of the most significant OS for the RTF. These values are given in absolute magnitudes (m_{AB}) at airmass = 1, using these measures of spectrophotometric standard stars.

OS	$m_{AB}(\text{standard})$	Zeropoint
OS657	15.25 ± 0.05	27.86 ± 0.09
OS666	15.27 ± 0.05	27.72 ± 0.02
OS709	15.35 ± 0.05	27.89 ± 0.05
OS770	15.45 ± 0.10	27.73 ± 0.02
OS858	14.35 ± 0.05	27.58 ± 0.03
OS902	14.48 ± 0.05	27.07 ± 0.09

Please note that the OS are tilted 10.5 degrees to avoid ghosts due to backwards reflections from the detector, therefore, their central wavelength is shifted with respect to the nominal central wavelength with a drift in wavelength along the FOV following the tilting axis, that is approximately the detector gap. This is the same effect that was discussed in Section 2.1.2 for OSIRIS Sloan broad-band filters, but in this case the effect is more noticeable as the filters are narrower.

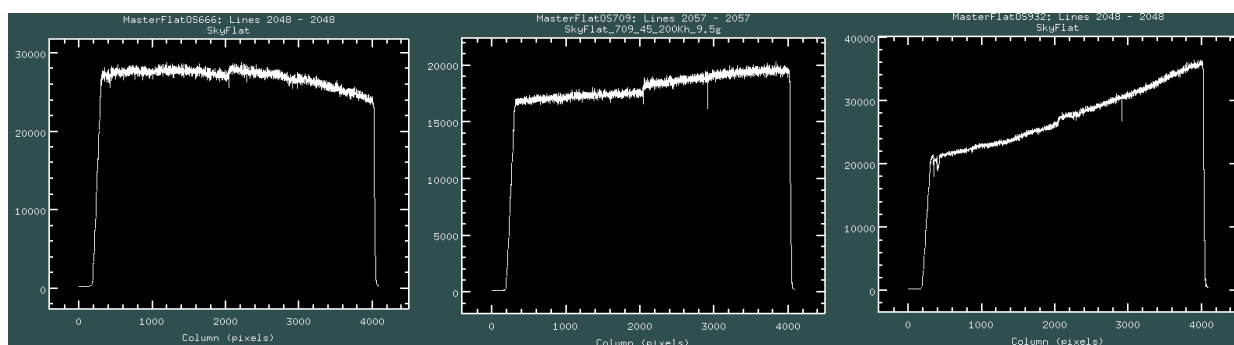


Figure 3.28.- Horizontal cut for three Sky Flat images taken with OS666 (left.), OS709 (center) y OS932 (right.). The intensity gradient observed is due to the combination of a different contribution of the Sky lines and a different sensitivity of the CCDs (from redder to bluer wavelengths)

For calibrating the data obtained with the OS filters when used in imaging mode, the spectrophotometric standards for both tunable filter imaging and long-slit spectroscopy observations can be used (see Table in Section 14). The spectral responses of each of the OS filters are available at:

http://www.gtc.iac.es/instruments/osiris/osiris.php#Blue_OS

http://www.gtc.iac.es/instruments/osiris/osiris.php#Red_OS

The graph below shows the overall photon detection efficiency of OSIRIS TF Order Sorters at GTC, including the contribution both of the telescope and instrument optics system.

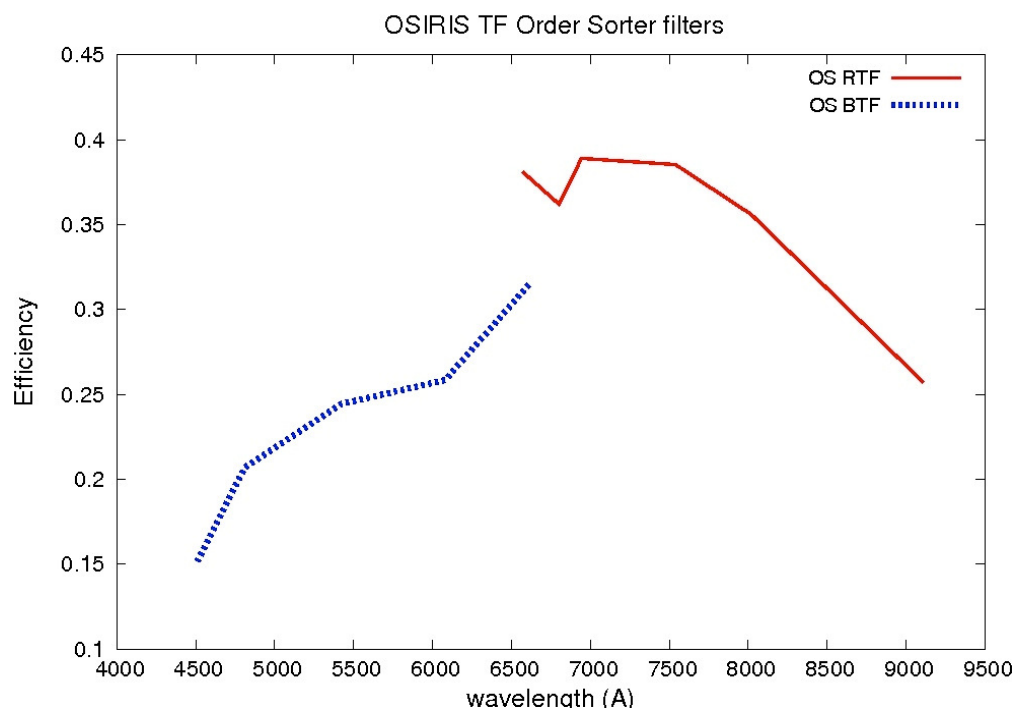


Figure 3.29.- Overall photon detection efficiency of GTC and OSIRIS with the TF Order Sorter Filters.

The OS high inclination also makes impossible to use two contiguous OS to produce a single narrower filter. This is due to internal reflections occurring in different layers of the filters that lead to the formation of ghosts. Their intensity and position in the field vary depending on the combination of filters that is, the position of the rotator, etc. This mode of operation is not offered.

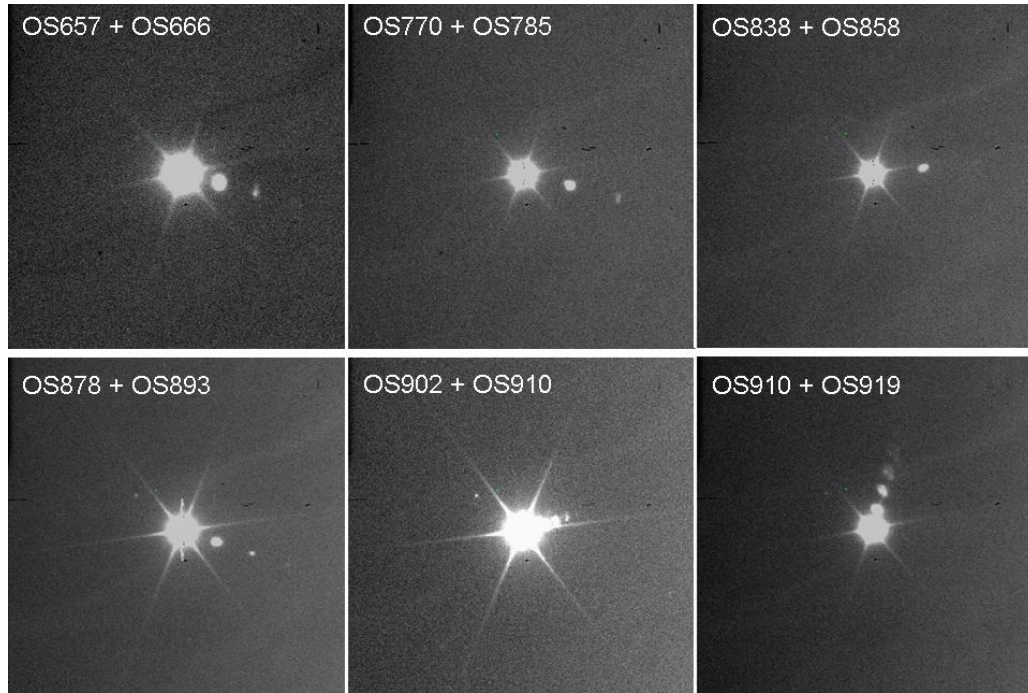


Figure 3.29.- Some examples of ghosts observed when using a combination of two contiguous OS.

4. MEDIUM BAND IMAGING (SHARDS FILTERS)

From June 2012, the number of filters available for general use with the OSIRIS instrument has been drastically extended thanks to a generous gesture by Dr. Pablo Pérez González from the Universidad Complutense de Madrid to make available his private optical filters. Dr. Pérez González designed and purchased (using funding from the Spanish Government through projects CSD2006-00070 and AYA2009-07723E) a set of medium-band filters for the SHARDS science program has been successfully executed on the GTC (for further details on this program, see <http://guaix.fis.ucm.es/~pgperez/SHARDS/>).

This set consists of no less than 25 filters spanning the wavelength range from 500 to 940 nm with bandwidths from 14 to 34 nm. Interested parties who would like to use of any of these filters should contact Dr Pérez González and GTC to request their use, and write the appropriate credits in any paper that may result from the use of these filters. The main characteristics of these filters are summarized in the following table:

Filter ID	λ (nm)	FWHM (nm)	A (nm)	B ($\times 10^{-6}$ pix $^{-2}$)	X (pix)	Y (pix)	Sky (ADUs/s/pix)
U500/17	500	15	503.37	-1.323	-315.7	1003.7	< 5
U517/17	520	16	520.31	-1.304	-430.5	991.6	< 5
U534/17	536	17	538.51	-1.379	-421.0	1055.2	< 5
U551/17	552	14	555.01	-2.060	-255.8	988.1	< 10
U568/17	569	14	572.11	-2.117	-289.8	1008.8	< 10
U585/17	586	15	588.69	-2.327	-86.2	1021.2	< 10
U602/17	603	16	605.75	-2.277	-212.5	1001.2	< 10
U619/17	619	16	623.14	-2.404	-202.3	984.8	< 10
U636/17	636	16	641.37	-2.589	-116.3	985.8	< 10
U653/17	653	16	656.01	-2.636	-151.1	998.6	< 10
U670/17	668	16	671.86	-2.602	-183.3	1037.2	< 10
U687/17	688	17	691.22	-2.366	-383.2	946.8	< 10
U704/17	704	18	707.78	-2.725	-209.3	1027.1	< 10
U721/17	720	19	723.12	-2.972	-94.5	960.0	20
U738/17	738	15	741.80	-2.413	-328.0	1050.3	15
U755/17	754	15	758.12	-2.662	-237.9	1032.1	15
U772/17	771	16	774.62	-2.931	-122.0	1026.0	20
U789/17	789	16	791.22	-3.089	-123.4	994.3	20
U806/17	806	16	809.42	-2.941	-200.1	932.8	15
U823/17	825	15	829.15	-2.058	-152.7	888.0	20
U840/17	840	16	843.57	-3.104	-150.0	992.2	35
U857/17	856	16	859.97	-2.895	-249.3	1002.1	25
U883/35	880	34	885.33	-2.892	-285.2	977.5	65
U913/25	910	28	913.64	-4.055	-60.4	975.4	50
U941/33	941	34	944.04	-3.406	-165.0	1067.1	70

As in the rest of filters used in OSIRIS, the SHARDS filters are placed in the collimated beam and close to the pupil of the instrument, at an angle of 10.5° with respect to the optical axis of the instrument. This causes that the central wavelength depend on the position in the field, with a center of symmetry corresponding to the center of rotation of the instrument, located on CCD1 towards the left side of the field (see Figure 1.4).

This effect is small for the standard Broad Band Sloan filters but has a stronger impact in the operation of the SHARDS filters, as the filter widths are notably narrower than in the case of Sloan filters. Hence this is not a defect of the filters, but due to the design of the OSIRIS instrument that becomes more prominent as filter pass band gets narrower. The central wavelength variation effect is more relevant in the case of medium-band filters such as SHARDS' (and also for the order sorter filters) given that the central wavelength shift from edge to edge of the OSIRIS FOV is of the same order of the width of the filter. Note that the typical shift (14-15 nm) would be 10%-20% for broad-band filters. Summarizing, potentially users of the SHARDS filters set have to take two main aspects into account when using these filters:

- The central wavelength in the rotation center of the instrument, (approximately pixel 462.5,995 in CCD1), is different from the central wavelength at the standard pointing position for OSIRIS Broad Band imaging (pixel 250,1024 in CCD2). This latter can be as much as 5-6 nm bluer than the central wavelength at CCD1, reaching differences up to 12-14 nm at the extremes of the FOV. Taking into account that most SHARDS filters have a bandwidth as narrow as 17 nm (except in two cases), this produces that the wavelength range observed in OSIRIS CCD1 can be notably different than the one observed in OSIRIS CCD2. Hence, for instance when making use of the whole FOV of OSIRIS for mapping a single emission line probably more than one filter has to be used.

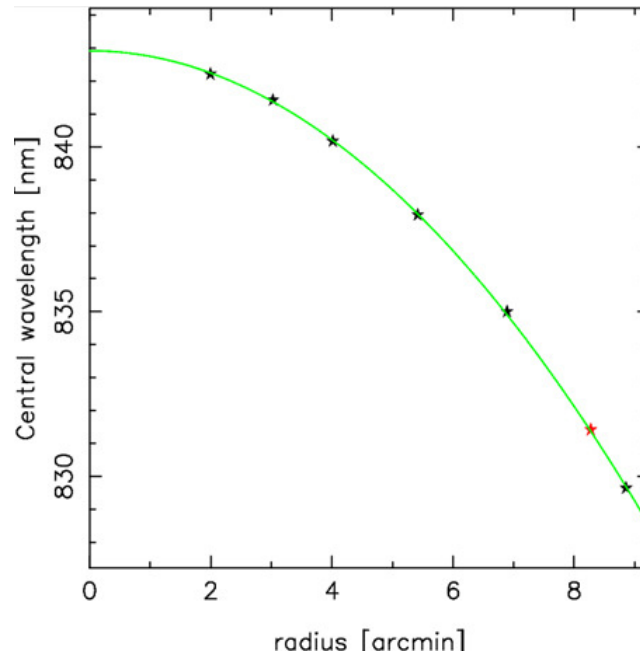


Figure 4.1.- Central wavelength variation along the OSIRIS FOV for SHARD filter U840/17.

An example of this effect is shown in Figure 4.1 for filter U840/17 filter. The central wavelength in CCD1 is 843 nm, while the nominal wavelength for an angle of incidence of 10.5° is 840 nm (approximately at the central gap between CCDs). For CCD2, the central wavelength changes drastically, from 840 nm to 830 nm at the edge of OSIRIS FOV, a value that is 13 nm bluer than the central wavelength in CCD1.

The central wavelength variation has been calibrated for each filter, and can be represented by the following function:

$$CWL(X,Y) = A + B \times \left[(X - X_0)^2 + (Y - Y_0)^2 \right]^2 \quad (4.1)$$

where X, Y are the positions in (standard binned) pixels in the OSIRIS FOV, and (X_0, Y_0) are the positions of the optical axis (also in binned pixels). The values for X_0, Y_0 , as well as the A, B coefficients for each SHARDS filter are shown in the previous Table. With those, it can be possible to predict the expected wavelength observed with a SHARDS filter at any position in OSIRIS FOV (Figure 4.2).

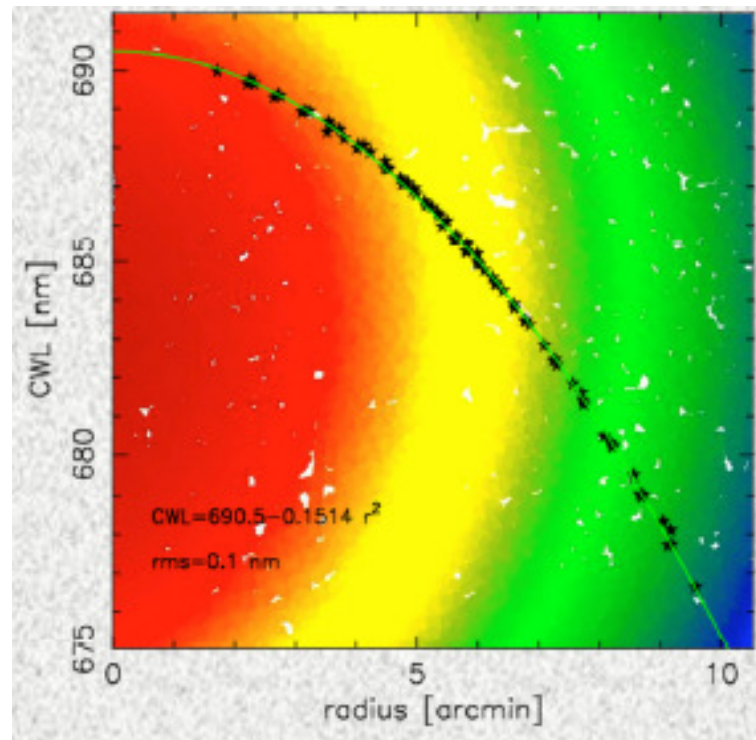


Figure 4.2.- Central wavelength variation along the OSIRIS FOV for SHARD filter U687/17, showing the radial variation along the optical centre (X_0, Y_0) for this filter that can be fitted by Equation 4.1.

- The wavelength variation over the FOV also results in that the sky background is inhomogeneous. This is in particular pronounced when strong sky lines fall within the band. This makes that the sky background subtraction is a critical step in the reduction of data taken using SHARDS filters.

The following figures demonstrate this effect. In Figure 4.3 (left), we have the wavelength variation for U687/17 filter, in combination with a sky emission spectrum. As it can be seen, the stronger emission lines fall at the reddest wavelengths, -the ones that are observed in CCD1-, while these same lines are nearly undetected at the bluer wavelengths, that are the ones observed in CCD2. This produces that the sky background will be notable different from one CCD to other, being stronger at CCD1 than in CCD2.

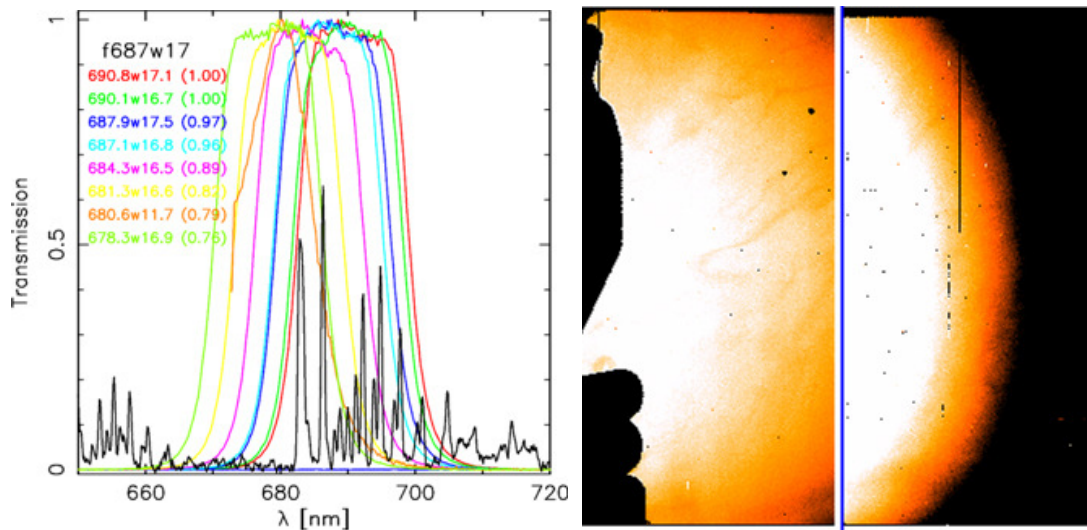


Figure 4.3.- *Left:* Change in the Sky lines coverage with SHARD filter U687/17 as the central wavelength moves bluewards along the OSIRIS FOV. *Right:* Sky image with the same filter, showing the radial differences in background level from both CCDs.

This effect can be clearly also seen in Figure 4.3 (right), where a sky image with U687/17 filter is shown. Note the strong gradient observed in the background level, and how this follows a radial geometry from CCD1 to CCD2. This effect should be taken into account when using the sky flat frames that can show some variability as sky emission itself changes (in any case, this can be properly corrected during the data reduction process).

As it is shown, the sky background correction plays a very important role in the data reduction for observations obtained with SHARDS filters. In order to have initial estimates of the background levels with SHARDS filters, average values for the sky background counts are shown in the previous Table.

For a detailed description on the full characteristics of the SHARDS filters, as well as complete details on the calibration process, data reduction, etc.. see Pérez-Gonzalez et al. (2013).

4.1 Photon detection efficiency with SHARDS filters

The graphs below shows the overall photon detection efficiency of GTC and OSIRIS with the SHARDS filter set, and the overall system efficiency of OSIRIS in imaging mode, as a function of wavelength. Note that the curves for the tunable filter order sorters, the efficiency of the tunable filter itself is not included in the curve.

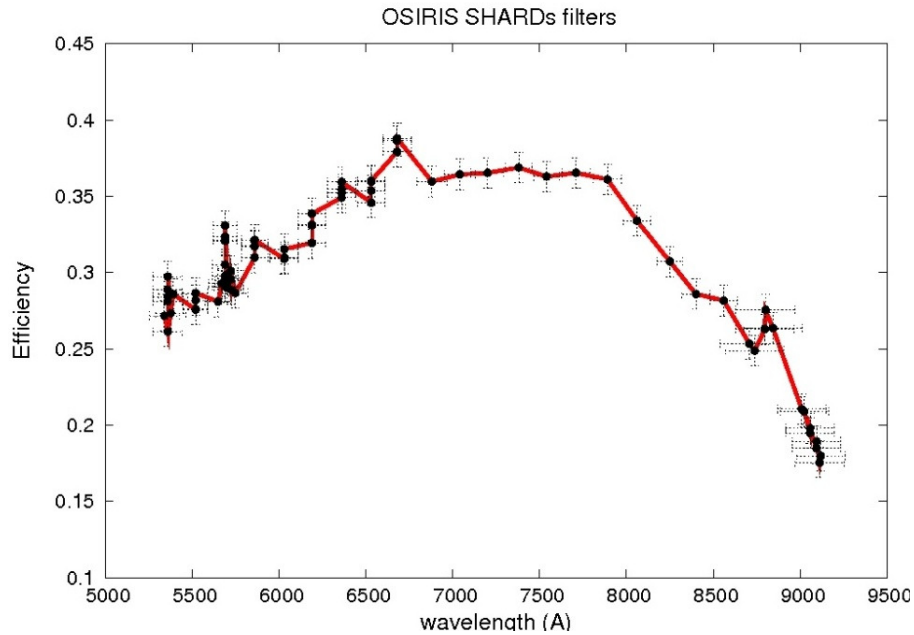


Figure 4.4.- SHARDS filters efficiency curve.

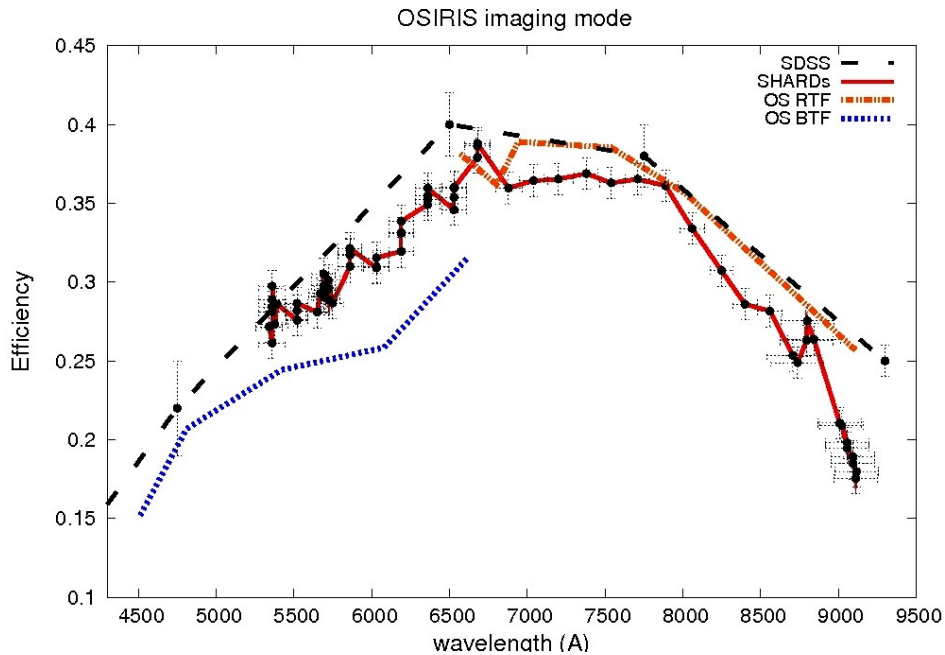


Figure 4.5.- Overall efficiency of OSIRIS in all the available imaging modes with medium and broad band filters.

5. FAST IMAGING MODES

5.1 Fast Photometry

For fast photometry with OSIRIS, a mask with a 7' x 3" slit is used; the fast photometry mask. This slit is placed in one of the detector edges. The images are obtained while the shutter remains open, and after each exposure the charge is shifted a number of lines, at least the equivalent to the width of the slit (12 pix approximately in standard 2 x 2 binning mode). The minimum exposure time and photometric accuracy is determined by the time needed for the vertical displacement of the charge on the CCD (typically by 50 μ s/row). For example, to displace 12 binned pixels requires 0.0012 s (this will be the minimum exposure time allowed in this configuration), hence for exposure times larger than 0.1 s the photometric accuracy will be better than 1%. For larger pixel shifts, the minimum exposure times required will increase accordingly.

Standard configurations for this mode allows obtaining up to 147 consecutive images before readout (see Figure below as an example). However, more conservative numbers are recommended (70-90 consecutive images per frame) in order to avoid possible flux contamination from the previous images along the series. The fast photometry standard mode means using the same broad-band (Sloan) or medium-band (SHARDS) filter throughout the observation, or a tunable filter adjusted to a fixed wavelength, as no delays due to filters exchanging or TF tuning are possible as this is a shutterless mode.



Figure 5.1.- Example image taken in fast readout mode, where many individual narrow-strip images are combined in a single detector readout.

The only delay in the series would be imposed by the readout time once the detector is filled with the individual images, plus the 4 s delay needed for clearing/configuring the detector. In standard readout mode (200 kHz) this time will be 25 s. However, this time can be reduced by defining a single readout window limiting the extent of the readout area along the slit. Also the higher readout of 500 kHz can be used to reduce the readout time to 12 s (and even

less with windowing). However, this readout speed is a non-standard operation mode in OSIRIS and its performance is not guaranteed.

As the fast photometry mask is restricted to a 3" size in the vertical direction, good seeing conditions are required for its use. It is also possible to use the longslit masks as fast photometry masks, allowing up to 10" of vertical aperture. However, in this case, only half of the detector will be completed before readout since the position of the long slit is centered in the FOV.

Due to the high flexibility and the multiple possible combinations in using this observing mode, fast photometry with OSIRIS is only offered in visitor mode. Prior to defining your observing proposal it is strongly recommended to contact GTC staff astronomers to evaluate the optimum mode of operation.

5.2 Frame Transfer

Frame transfer capability in OSIRIS uses a half-field mask (see Figure 5.2.) with an accessible FOV of 7' x 3.5', approximately. In this operation mode, only half of the detector is exposed while the other half of the detector is being read out. The minimum exposure time allowed is now imposed by the time required to displace the charge over half the number of the detector lines (0.1 s) plus the readout time of this area. In standard readout mode (200 kHz) this time will be 8.25 s, which can be decreased to 4.3 s using 500 kHz readout mode. However, using this higher readout speed is a non-standard operation mode in OSIRIS and its performance is not guaranteed.

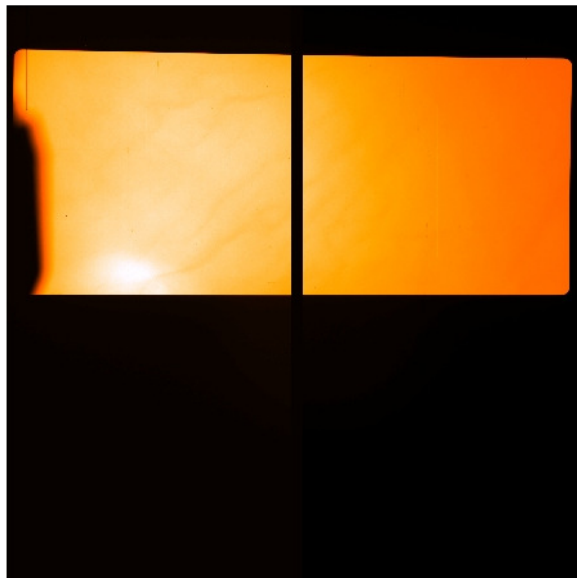


Figure 5.2.- Example image taken through the frame-transfer mask, showing half the field blocked.

Frame transfer standard mode means using the same broad-band (Sloan) or medium-band (SHARDS) filter throughout the observation, or a tunable filter adjusted to a fixed wavelength, as no delays due to filters exchanging or TF tuning are possible since the shutter remains opened. The difference of this mode with respect to the fast photometry is that the

sampling interval between exposures is smaller since it is possible to expose while reading out, obtaining a continuous series of temporal data.

A possibility for decreasing the minimum exposure time is to use a single readout window. In this case, the minimum exposure time will be determined by the size of the window combined with the readout time and the time used for skipping the remaining pixels. This is independent on the window placement, hence by knowing the desired window size and the readout speed, the final minimum exposure time can be determined.

The following Table shows an estimates of the minimum exposure times allowed depending on both the readout speed and window size. It can be noted that for decreasing a window by half of the size of a previous one the exposure time is not decreased exactly in the same proportion, as the time for skipping the rest of the pixels increases. Also, for very small windows, the skipping time dominates and the minimum exposure times are nearly the same for both readout speeds (as the skipping time is the same, independent of the readout speed).

Detector Area	Readout Speed	
	200 kHz	500 kHz
Full (3.5' x 3.5')	8.25 s	4.3 s
3' x 3'	4.45 s	2.6 s
2' x 2'	2.43 s	1.6 s
1' x 1'	1.02 s	0.8 s
0.5' x 0.5'	0.55 s	0.5 s

There are a lot of possible combinations depending on the desired FOV and sampling requested. Due to the high flexibility and the multiple possible combinations in using this observing mode, Frame Transfer in OSIRIS is only offered in visitor mode. Prior to defining your observing proposal it is strongly recommended to contact GTC staff astronomers to evaluate the optimum mode of operation.

6. LONG SLIT SPECTROSCOPY

OSIRIS facilitates long-slit spectroscopic observations. A selection of 7.4' long slits of different widths are available, which, in combination with a selection of dispersive elements in the collimated beam provides for efficient low to medium-resolution spectroscopy. Available slit widths are: 0.4", 0.6", 0.8", 1.0", 1.2", 1.5", 1.8", 2.5", 3.0", 5.0", 10.0".

OSIRIS has a wide variety of grisms and volume-phased holographic gratings (VPHs) covering low to intermediate resolutions, from $R=300$ up to $R=2500$. The following table summarises the resolutions and spectral ranges available. For the end-to-end efficiencies including telescope, instrument and detector, the measured transmissions measured so far are in Section 11.

Resolutions and dispersions are measured at $\lambda_c(\text{\AA})$ for a slit with of 0.6". Dispersions correspond to binned pixels, that is the standard operation mode, while the physical pixels (unbinned) dispersions are half of those listed in the table.

ID	$\lambda_c(\text{\AA})$	λ Range (Å)	D (Å/pix)	R ($\lambda/\Delta\lambda$)	Peak Efficiency	Type
R300B	4405	3600-7200	4.96	360	70%	Grism
R300R	6635	4800-10000	7.74	348	70%	Grism
R500B	4745	3600-7200	3.54	537	68%	Grism
R500R	7165	4800-10000	4.88	587	67%	Grism
R1000B	5455	3630-7500	2.12	1018	65%	Grism
R1000R	7430	5100-10000	2.62	1122	65%	Grism
R2000B	4755	3950-5700	0.86	2165	87%	VPH
R2500U	3975	3440-4610	0.62	2555	70%	VPH
R2500V	5185	4500-6000	0.80	2515	80%	VPH
R2500R	6560	5575-7685	1.04	2475	80%	VPH
R2500I	8650	7330-10000	1.36	2503	80%	VPH

For $R \geq 1000$, the spectral range covered is limited by detector size. Lower resolutions are limited by second order light.

Red-optimized dispersers require the use of an order sorter filter (GR, see Figure 6.1) to suppress the second-order light.

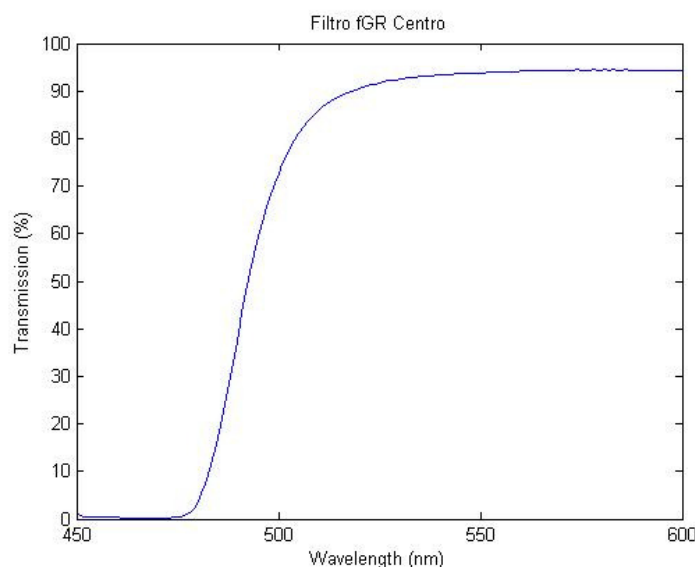


Figure 6.1.- Measured central spectral response of spectroscopic OS.

The spectral direction in OSIRIS coincides with the vertical direction on the detector, hence spectra are not affected by the gap between both CCDs.

6.1 Acquisition in Long-Slit Spectroscopic mode

In long-slit spectroscopy mode, point sources are centered on the slit at the coordinates (X,Y) = (250,994) of the CCD2 (binned pixels). This position minimize the amount of cosmetic effects of the CCD2 compared to those on the CCD1. On this area the distortion of the spectra is very low and this location is sufficiently far from the central gap in order to allow a good sky subtraction.

To ensure accurate centering on the slit an acquisition image and a through-slit images are normally taken. During the observation, after the acquisition image is obtained with the target placed at the pixel (250,994) in CCD2 an iterative process for slit alignment is employed until the object is well centered. This is verified by taking through-slit images. For this reason the coordinates for the target in the acquisition and through-slit images can be slightly different.

Due to the obscuration present in one of the edges of OSIRIS FOV, and the manufacture process in producing the slits, the maximum distance allowed for placing two targets in the same slit configuration is 7.4 arcmin. For a proper sky subtraction, however, no distances larger than 7.0 arcmin are recommended in order to get enough pixels for the background estimation on both sides of the targets. Likewise, if offseting is required during the observation, the maximum distance to the targets has to be estimated accordingly (for example, a maximum distance of 6.5-6.7 arcmin between the targets is a good approximation for this kind of observations).

6.2 Flexure

OSIRIS allows a very stable spectral calibration, with no significant drifts with rotator position (< 1 pix) thanks to its active collimator. Therefore, the calibrations for each observation can be taken at the beginning or at the end of the night regardless of the orientation of the instrument when the science observation is carried out. Figure 6.2 shows an example of the wavelength shift as a function of rotator angle, for two spectral resolutions.

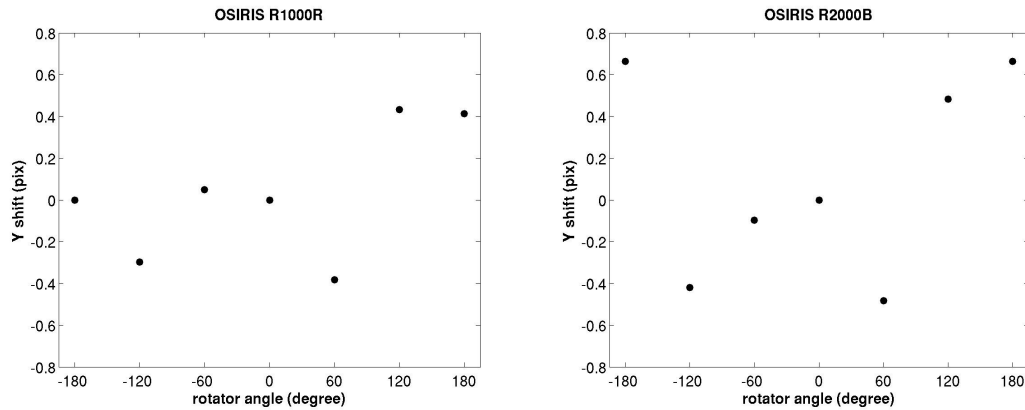


Figure 6.2.- Shift in the spectral direction (Y) for the arcs emission lines with rotator position for OSIRIS R1000R (left) and R2000B (right). The more extreme variations are lower than 1 pix (binned).

6.3 Fringing

The measured value of fringing in the OSIRIS CCD is $<1\%$ for $\lambda < 9000$ Å and 5% for $\lambda > 9300$ Å (with a slightly increase to 7% at higher resolutions, $R=2500$), so it is relevant only at higher wavelengths (and in the range z' in imaging mode). Figure 6.3. shows an example of fringing vs. wavelength obtained with OSIRIS R500R.

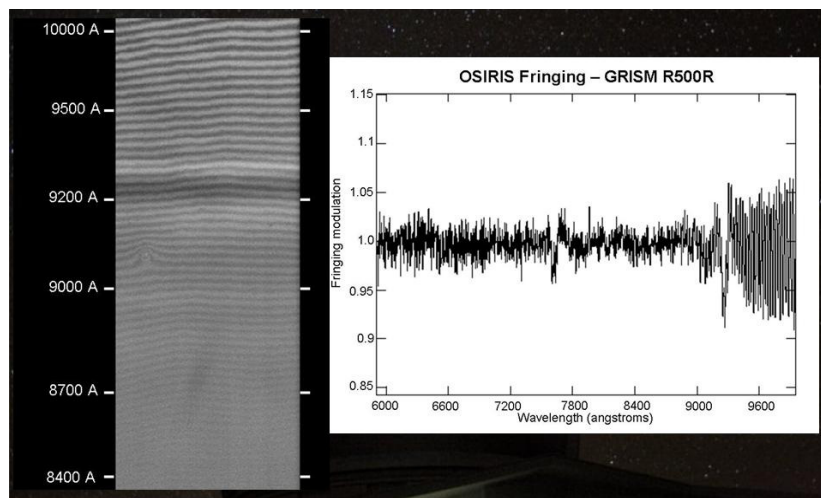


Figure 6.3.- OSIRIS fringing vs wavelength, obtained with the R500R grism.

The effect of possible wavelength drifts due to flexures in OSIRIS has been measured in order to evaluate its influence on the fringe pattern. As a practical example, for VPH R2500I (which is the VPH most affected by fringing), the fringing is doubled when a shift of 6 pixels is produced in the spectra, while no noticeable effects are shown for shifts up to 3 pixels. As instrument flexures causes displacements no larger than 1 pixel in the wavelength calibrations (see section 6.2), the fringing in OSIRIS will not be affected by this. Hence, there is no need to obtain a spectral flat calibration taken with the same orientation as the science images.

In case fringing is of critical importance, to reduce the fringing effect it is recommended to the user to use an offsetting pattern (ABBA, ABAB, AB, etc..) when observing at wavelengths larger than 9000 Å, and also for getting a better sky subtraction. This strategy strongly recommended at higher resolutions (VPHs R2500R and R2500I).

6.4 Spatial displacement

Upon inserting a VPH dispersing element into the optical train a small displacement between the target position in the acquisition image and the spectrum position in the spatial direction can be observed. In OSIRIS, only VPH R2500I shows a notable displacement (larger than 1 arcsec) while in the rest of VPHs this effect is negligible.

The next table shows those spatial displacements for all the grisms/VPHs set in OSIRIS. Please take this into account when observing extended objects or crowded regions with VPH R2500I, to avoid confusion between different spectra:

Grism / VPH	ΔX (pix)	Grism / VPH	ΔX (pix)
R300B	-0.5	R2000B	-2.0
R300R	0.0	R2500U	5.0
R1000B	0.5	R2500V	1.5
R1000R	0.5	R2500R	0.5
---	---	R2500I	15.0

6.5 Arc line maps

Instrument Calibration Module (ICM) at GTC has three different calibration lamps: HgAr, Ne and Xe. In this subsection, the arc lines for the OSIRIS grisms/VPH are shown, together with the exposure times used to produce these, for reference. The following table summarises the optimal exposure times for each lamp when powering on two lamps for each type using the standard spectroscopic configuration (200 kHz readout speed, binning 2×2)

Grism/VPH	HgAr	Ne	Xe
R300B	5.2 s	3.2 s	13.0 s
R300R + GR	6.5 s	1.6 s	5.8 s
R500B	5.2 s	3.6 s	---
R500R + GR	7.8 s	2.3 s	6.5 s
R1000B	6.0 s	3.5 s	---
R1000R + GR	7.8 s	2.9 s	10.1 s
R2000B	8.0 s	600 s (*)	1200 s (*)
R2500U	20.0 s	---	1200 s (*)
R2500V	9.0 s	25.0 s	1200 s (*)
R2500R + GR	42.0 s	2.5 s	---
R2500I + GR	50.0 s	12.0 s	5.0 s

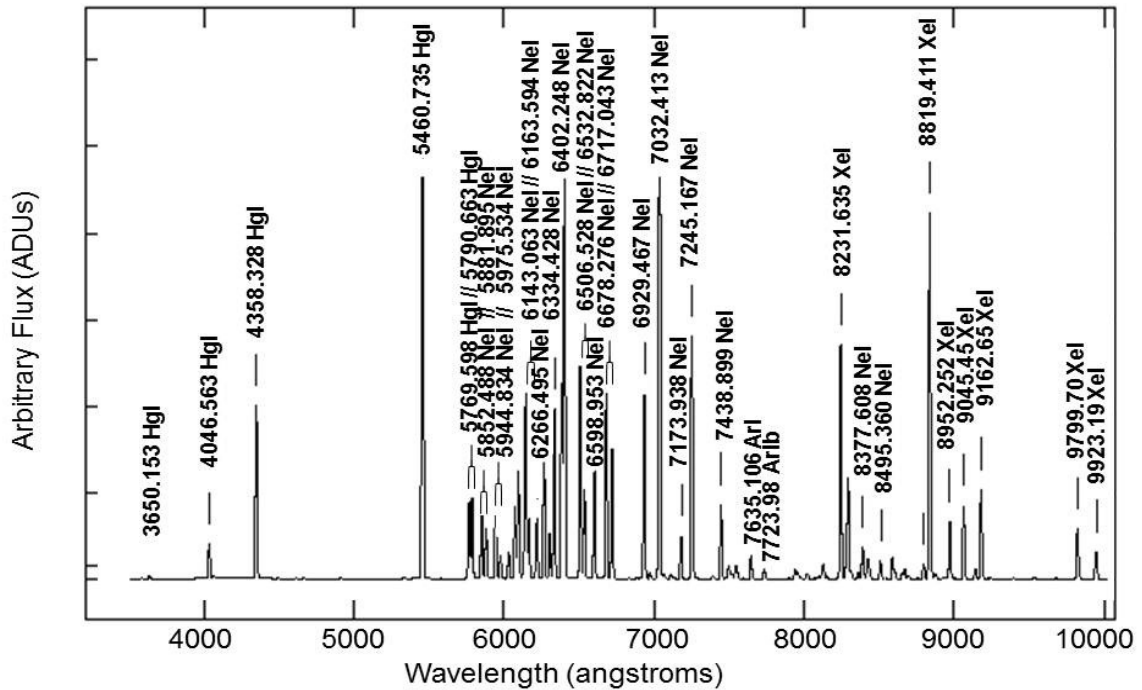
(*) For some of the OSIRIS R2000/2500 VPHs long exposed lamp images are required to obtain enough signal which allows a good line identification. For this reason, a master arc collection with the arc lamps images obtained with OSIRIS R2000/2500 VPHs with the 0.6'' slit can be retrieved from:

http://www.gtc.iac.es/instruments/osiris/osiris.php#Longslit_Spectroscopy

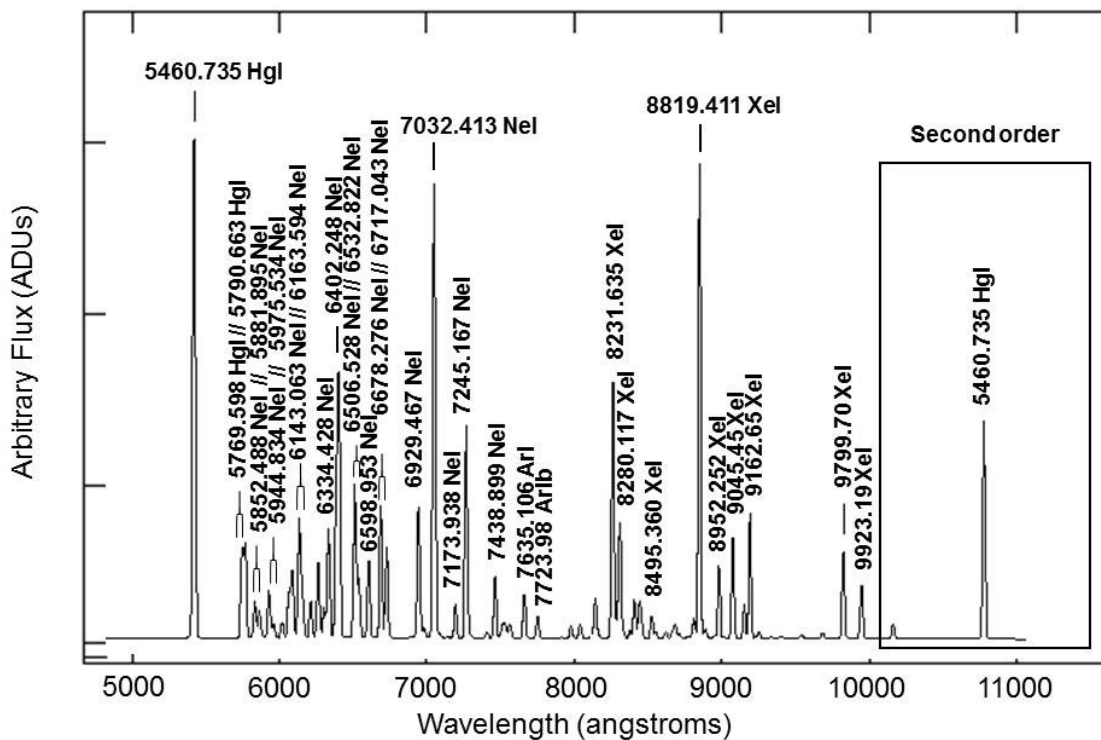
Note that this master arc collection was obtained using a 0.6'' slit. If the scientific program use another slit, a possible small drift in the lines could be observed due to the different position of the slit in the OSIRIS focal plane. To use the master arc it is necessary to correct for a possible drift in the lines by correlating the short exposure lamp frame with the master frame.

For OSIRIS low resolution grisms (R=300, 500 and 1000) there are also individual arc line maps available for each of the calibration lamps used, that are shown in Section 12. Note that in the HgAr lamp, there are a series of high excited Argon lines that appear only during the first few seconds of the exposure. Those usually are not provided when calibrating the scientific data, but in case that they contribute noticeably in the final HgAr arc image, an additional Ar line map has been also produced for each grism.

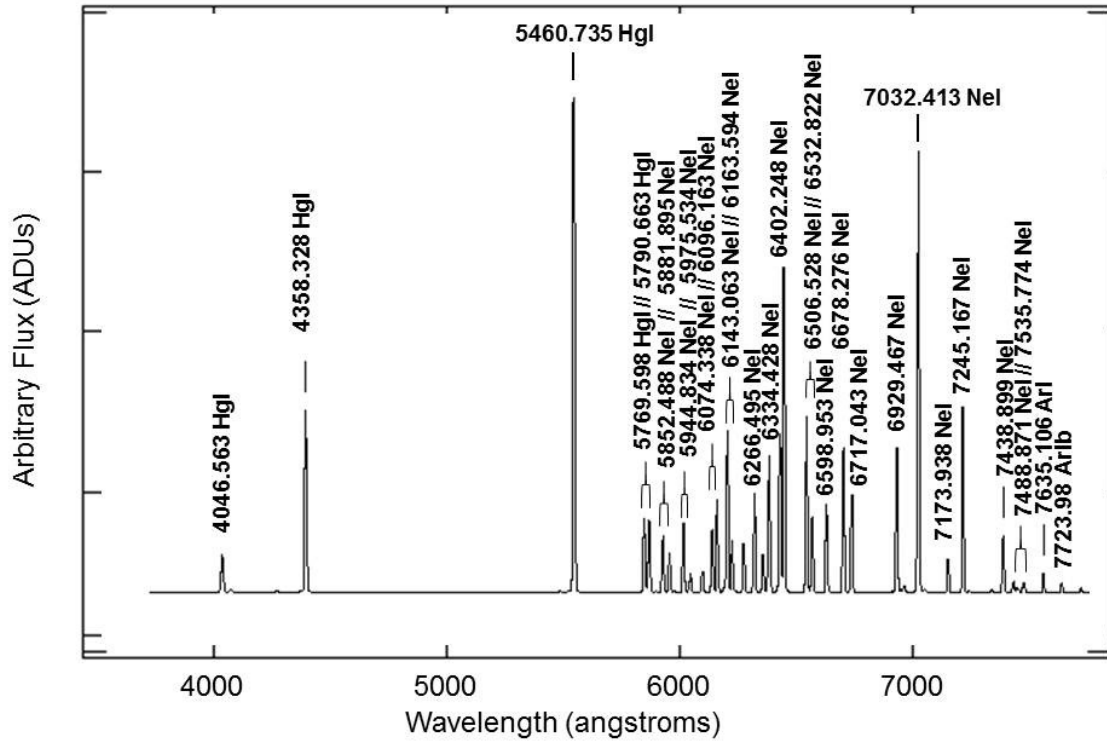
OSIRIS R300B: HgAr + Xe + Ne calibration lamps



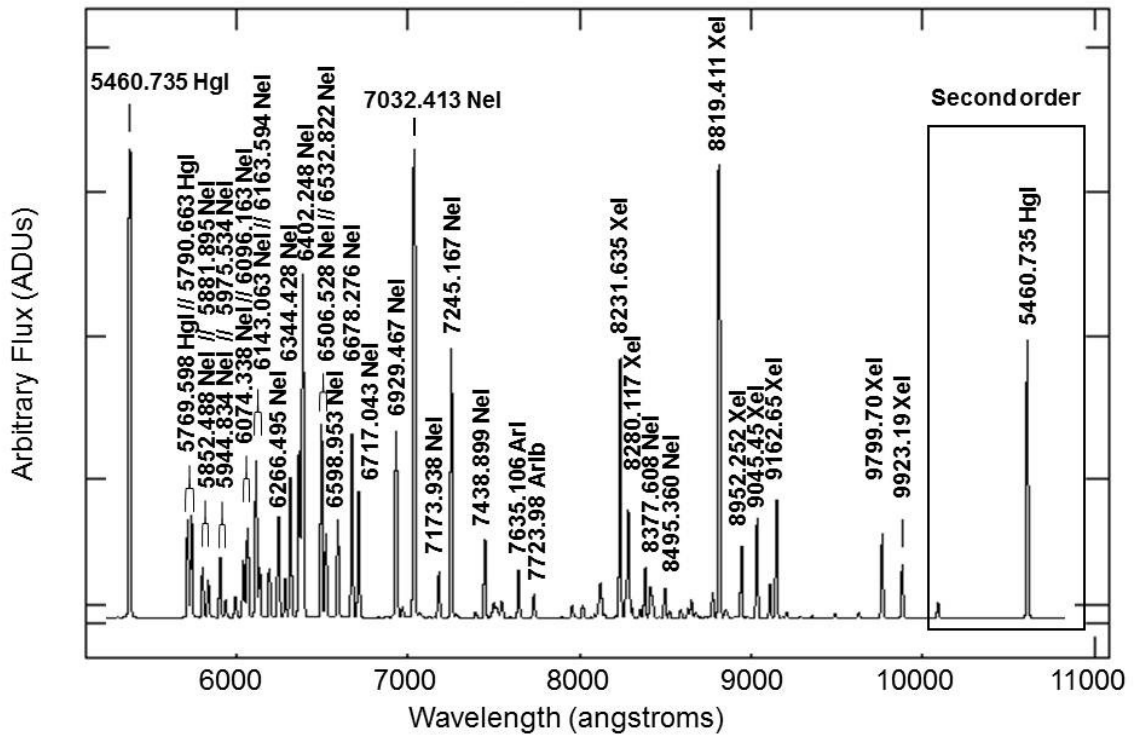
OSIRIS R300R: HgAr + Xe + Ne calibration lamps

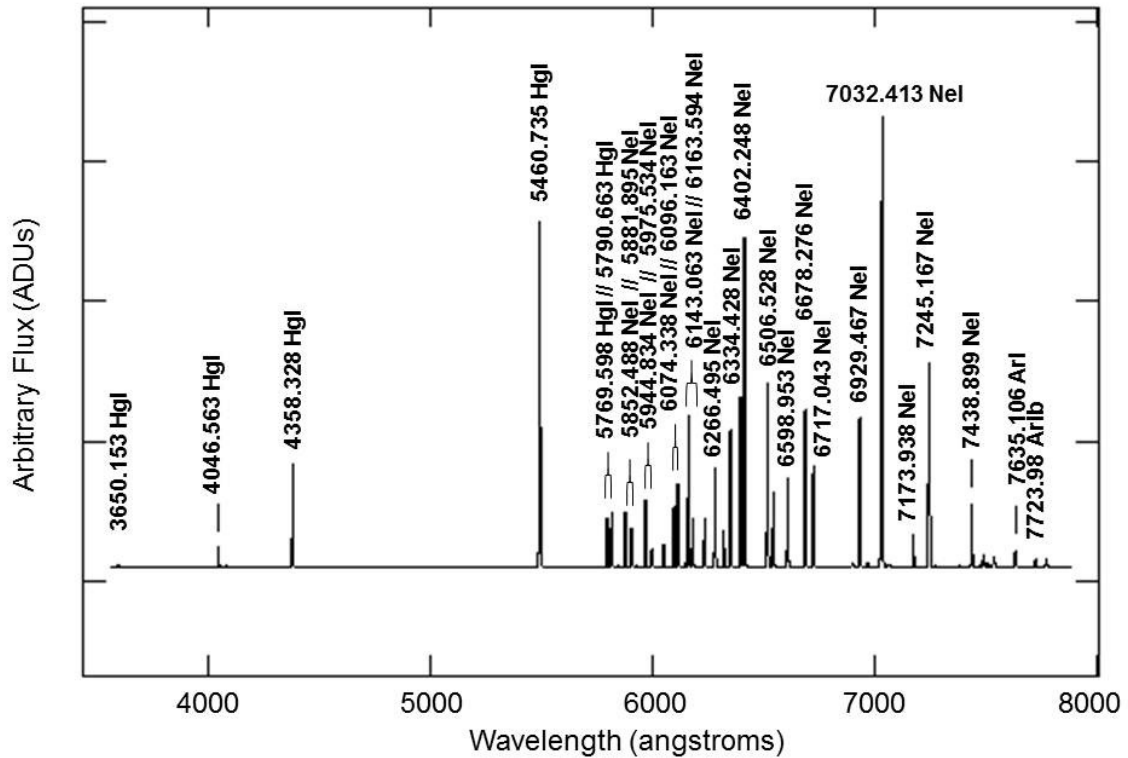
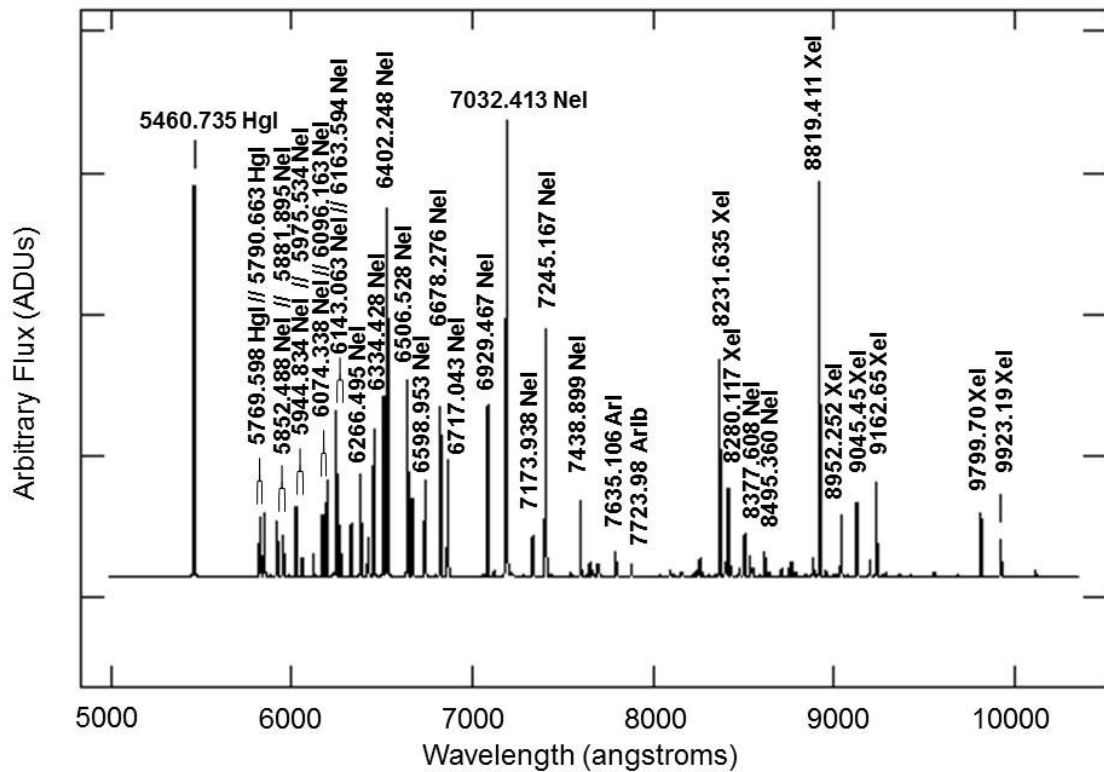


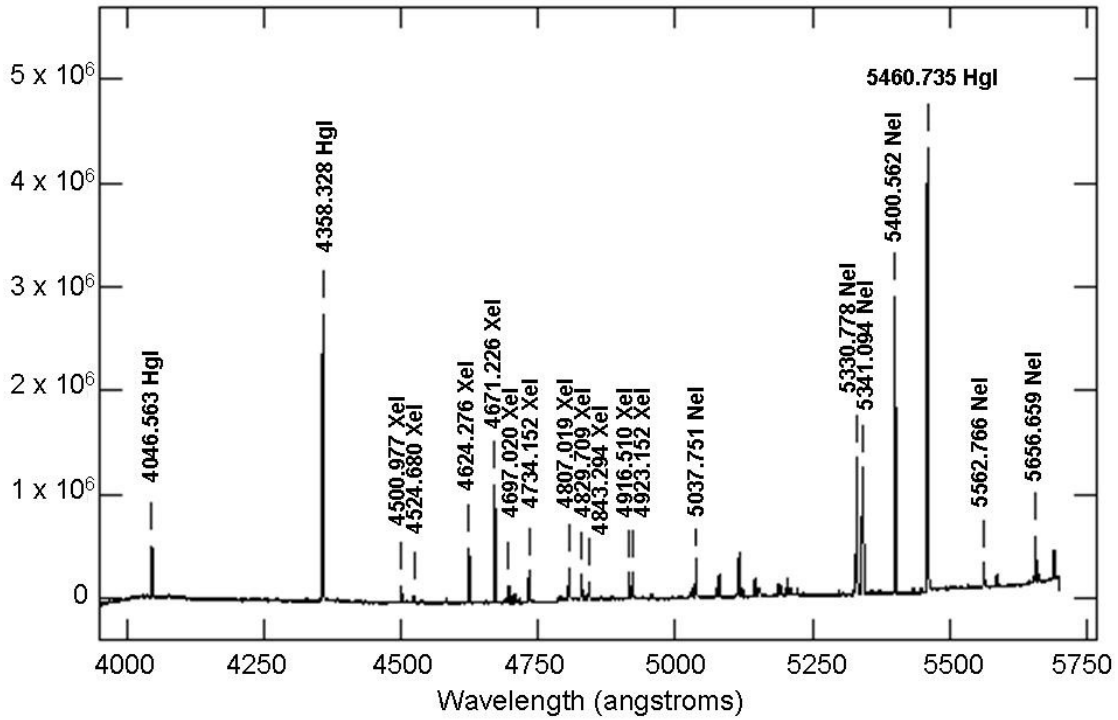
OSIRIS R500B: HgAr + Ne calibration lamps



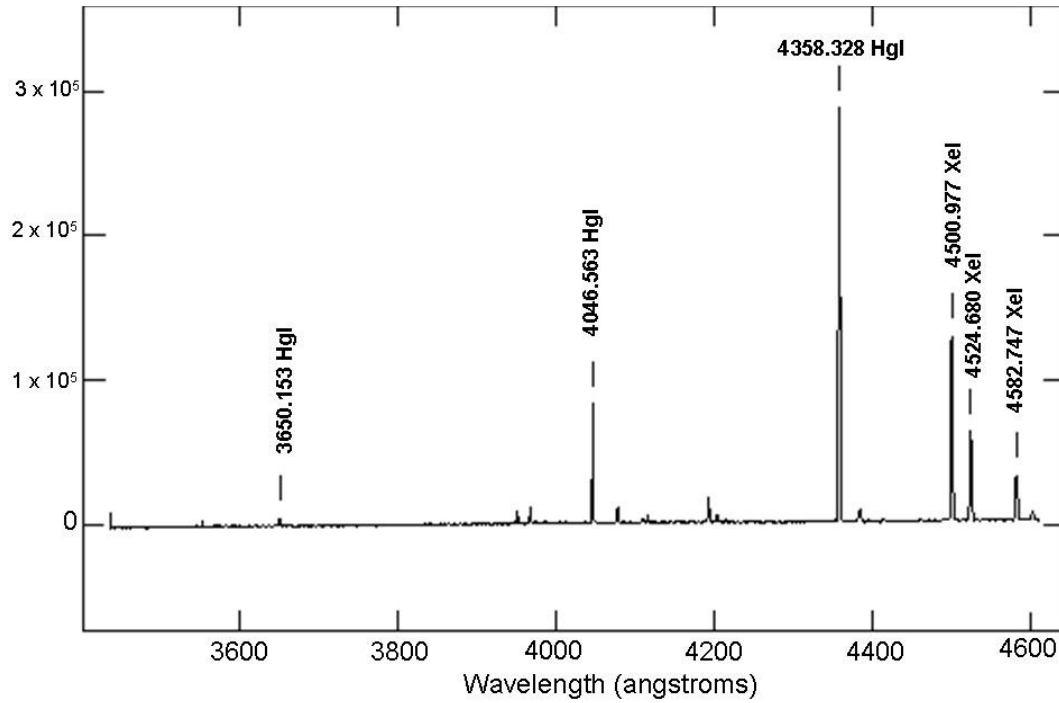
OSIRIS R500R: HgAr + Xe + Ne calibration lamps



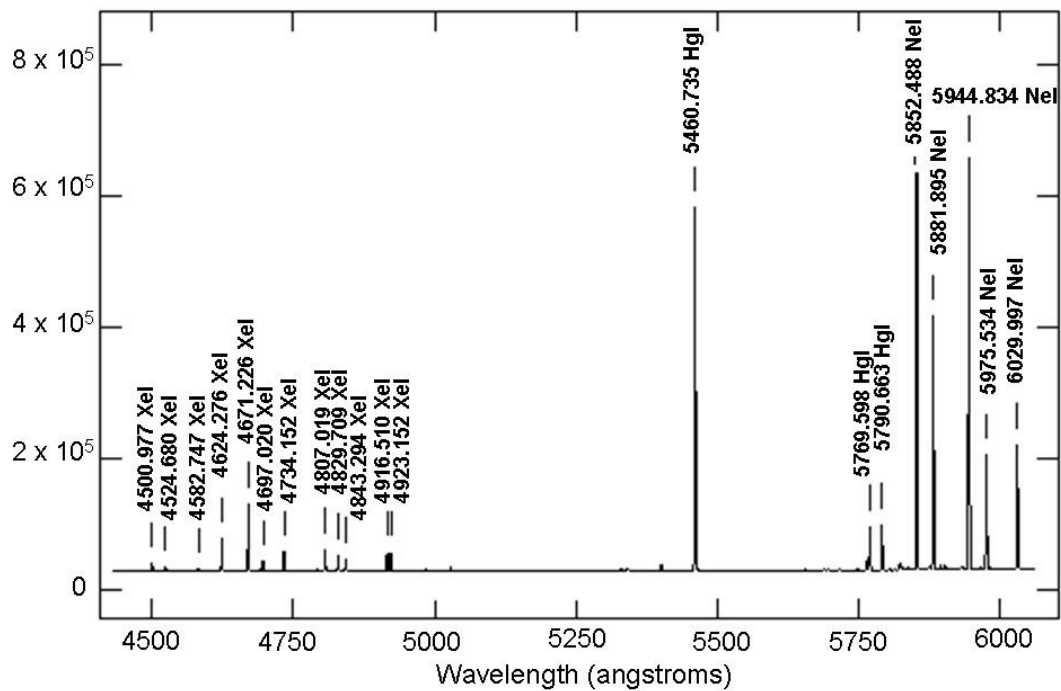
OSIRIS R1000B: HgAr + Ne calibration lamps**OSIRIS R1000R: HgAr + Xe + Ne calibration lamps**

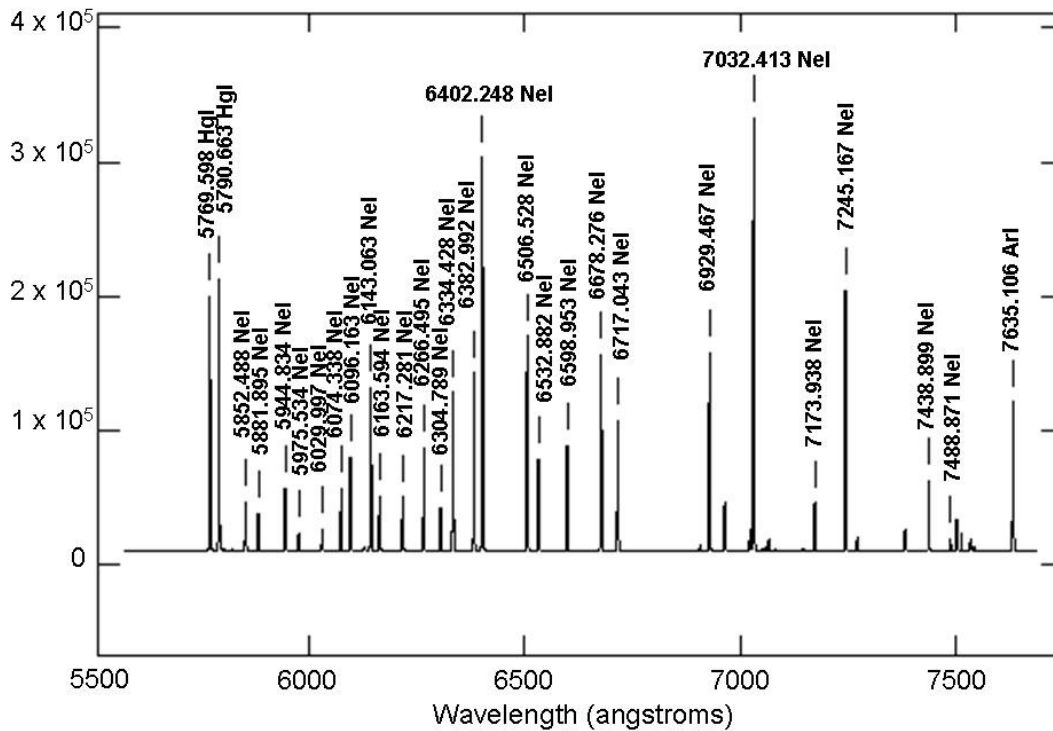
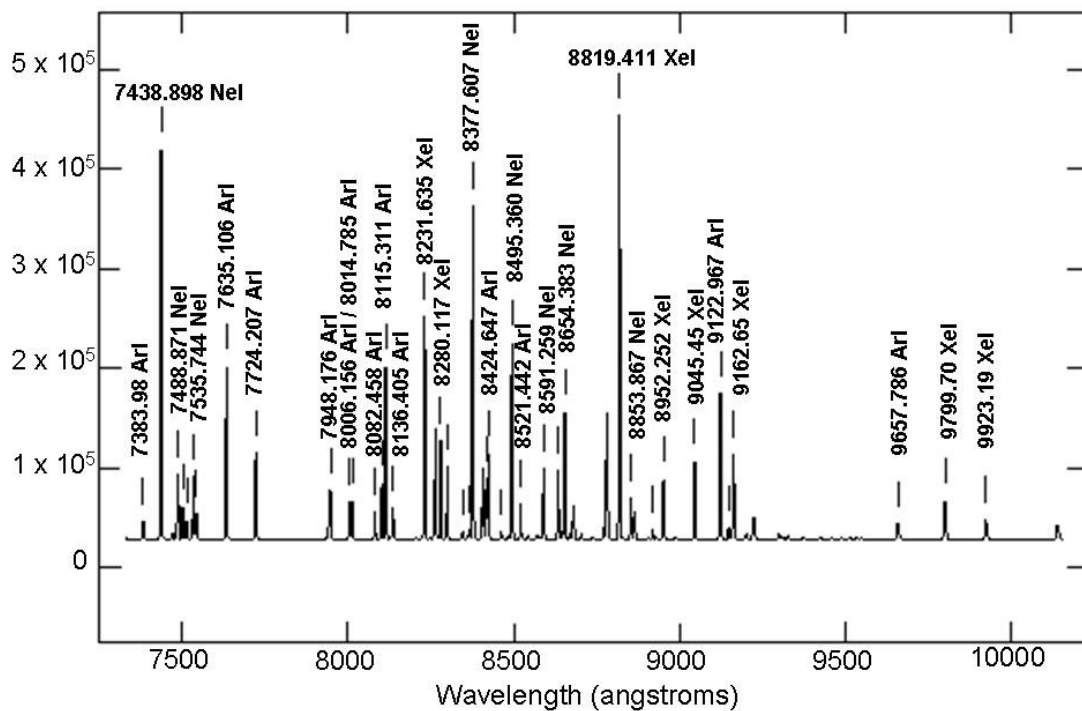
OSIRIS R2000B: HgAr + Xe + Ne calibration lamps

OSIRIS R2500U: HgAr + Xe calibration lamps



OSIRIS R2500V: HgAr + Ne + Xe calibration lamps



OSIRIS R2500R: HgAr + Ne calibration lamps**OSIRIS R2500I: HgAr + Ne + Xe calibration lamps**

6.5.1 Arc-line ghosts

All the OSIRIS grisms show some minor ghost effects in the arc-line images. Those ghosts are due to internal reflections within the grisms, and can be identified as the curvature in these spectra differs from those of the main arc lines. The intensity of these ghosts is negligible and they do not affect the line identification or the science images.

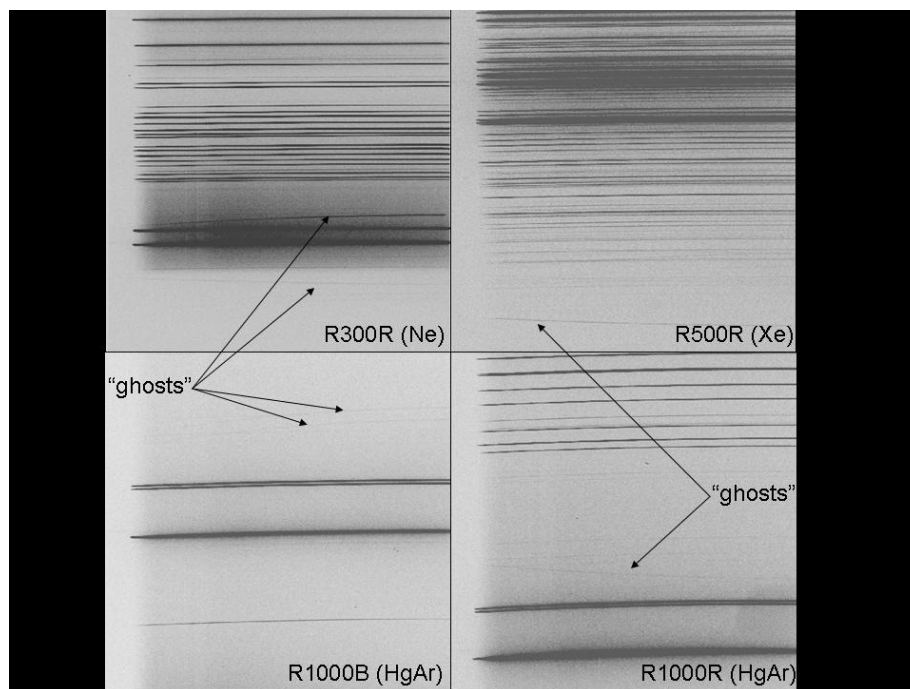


Figure 6.4.- OSIRIS grisms ghost effects shown in the arc images.

6.5.2 Spectral solutions

The following table shows the example solutions obtained with the IRAF routine IDENTIFY corresponding to the standard pointing in Long Slit Spectroscopy mode (X=250 in CCD2), as a guideline for the image reduction.

Grism/VPH	Lamps	# features	R.M.S	Function (order)
R300B	Ne + HgAr + Xe	31	0.1165	spline3 (5)
R300R	Ne + HgAr + Xe	30	0.2478	spline3 (5)
R500B	Ne + HgAr	42	0.0931	spline3 (5)
R500R	Ne + HgAr + Xe	43	0.1273	legendre (5)
R1000B	Ne + HgAr	34	0.0425	spline3 (3)
R1000R	Ne + HgAr + Xe	49	0.0651	spline3 (3)
R2000B	Ne + HgAr + Xe	20	0.0162	spline3 (3)
R2500U	HgAr + Xe	6	0.0178	spline3 (1)
R2500V	Ne + HgAr + Xe	20	0.0118	spline3 (3)
R2500R	Ne + HgAr	34	0.0151	spline3 (3)
R2500I	Ne + HgAr	41	0.0330	spline3 (3)

6.5.3 Spectral flat fields

Spectral flats can be obtained either by using dome lights or using the incandescent lamp of the instrument calibration module (ICM).

ICM spectral illumination is rather inhomogeneous and has a strong gradient from CCD1 to CCD2. For this reason, spectral flats obtained with the calibration unit are only recommended for targets placed in CCD2.

There are no significant dependences in the spectral flats with instrument rotator angle. Therefore, as with the arc lamps, the spectral flats for each observation can be taken at the beginning or at the end of the night regardless of the position of the rotator.

6.6 VPHs R2000/R2500 ghosting

The R2000 and R2500 VPHs suffer from a faint ghost image of the spectrograph slit that normally will have a negligible impact on the quality of the spectra. The ghost is negligible in the R2500I and R2500R VPHs, while in R2000B, R2500U, and R2500V the ghost is only noted in the spectral flat-field images and arc lamp frames, where a very faint slit image can be observed superimposed on the spectral flat / lamp arcs. The approximated position for those ghost images are: R2000B : from pixels Y = 988 to 996; R2500U : from pixels Y = 980 to 988; R2500V: from pixels Y = 992 to 1000 (all binned coordinates).

There are no problems for the line identification as the intensity of the ghost is far below the average of the counts for the spectral lines. However, users must be aware when obtaining the flat-fielding correction in the pixels range described above, and only for R2000B, R2500U and R2500V. In the science images the effect is irrelevant for the complete set of VPHs (the average ratio between the ghost intensity and the integrated flux from the target that causes the ghost is on the order of 10^{-5}). The ghost in science images can be noted as a focused image from the target in the other CCD. (see Figure 6.5).

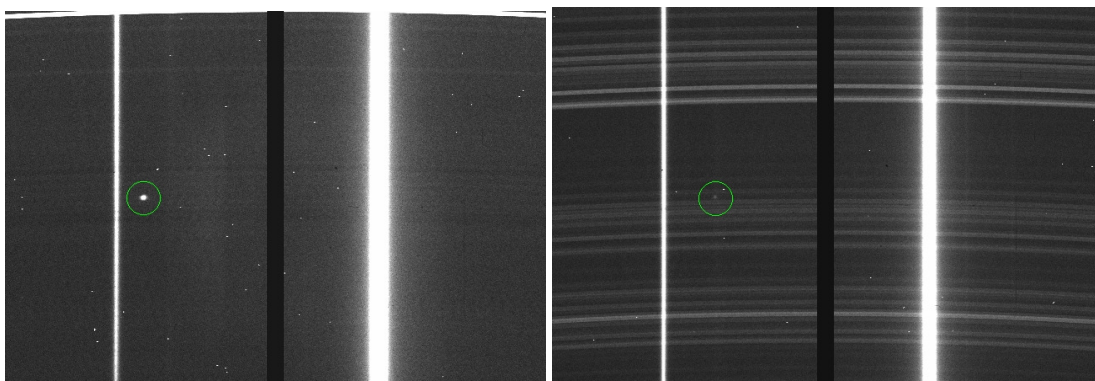


Figure 6.5.- Two examples of OSIRIS VPHs R2000/2500 ghosting, corresponding to R2500V (left) and R2500R (right). The focused image from the target (a bright standard star) can be observed in the opposite CCD respect to the spectra location, being much more fainter in the case of R2500R.

6.7 Second order contamination

All the OSIRIS red grisms/VPHs (R300R, R500R, R1000R, R2500R, and R2500I) are used in combination with an spectral order shorter filter (GR), which cuts out the light blueward from ~495 nm. However, there is a slight contamination in the spectrum due to the second order, as the spectral order shorter filter doesn't block completely the contribution for wavelengths lower than the defined cut level (see Figure 6.1). Hence, there is a distinguishable contribution for wavelengths at 480 – 490 nm, whose second order may contribute somewhat at 960 nm – 980 nm, depending of the source spectral distribution.

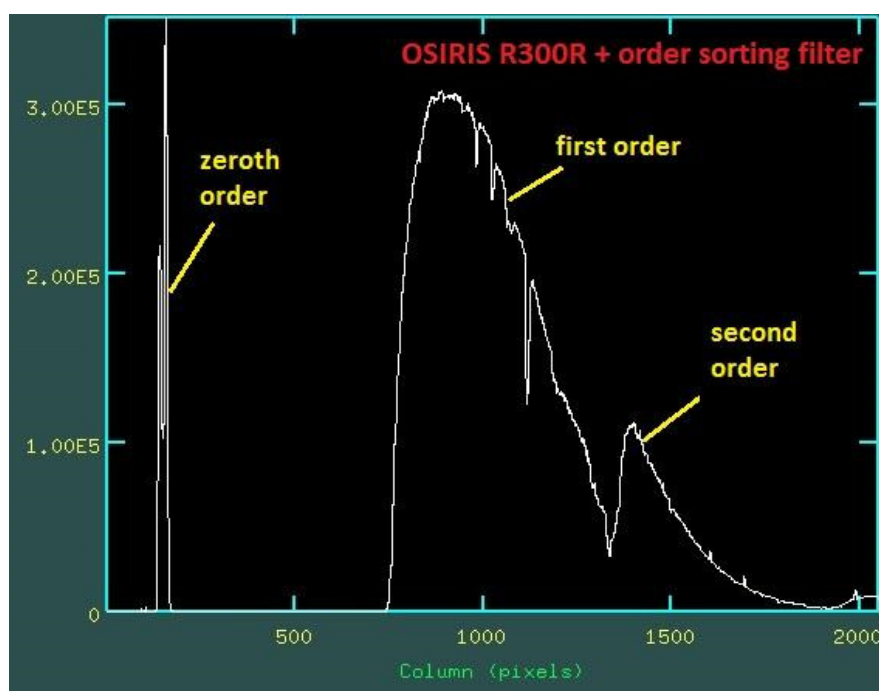


Figure 6.6.- Example spectrum of the flux standard star PG1545+035 taken with a 2.5 arcsec slit and 300 secs exposure time. The low-resolution spectrum with the R300R grism shows the first order of dispersion well centered on the CCD. Also visible is the zeroth order on the left, and the second order spectrum on the right-hand side of the graph. The effect is present in all the red grisms/VPHs but it's more noticeable at lower resolutions.

6.8 Spectrophotometric standards

The complete list of spectrophotometric standard stars for flux calibration can be found in Section 14.

6.9 Spectroscopic photon detection efficiency

The overall photon detection efficiency in spectroscopic mode was obtained using spectra from spectrophotometric standards stars on photometric nights through a wide slit. The results are displayed in the following two graphs. This first plot shows the end-to-end overall percentage detection efficiency in spectroscopic mode (individual plots for each grism/VPH can be found in Section 11), and the second one shows the limiting magnitudes (AB) for obtaining $S/N=5$ in 1 h of integration time with OSIRIS@GTC.

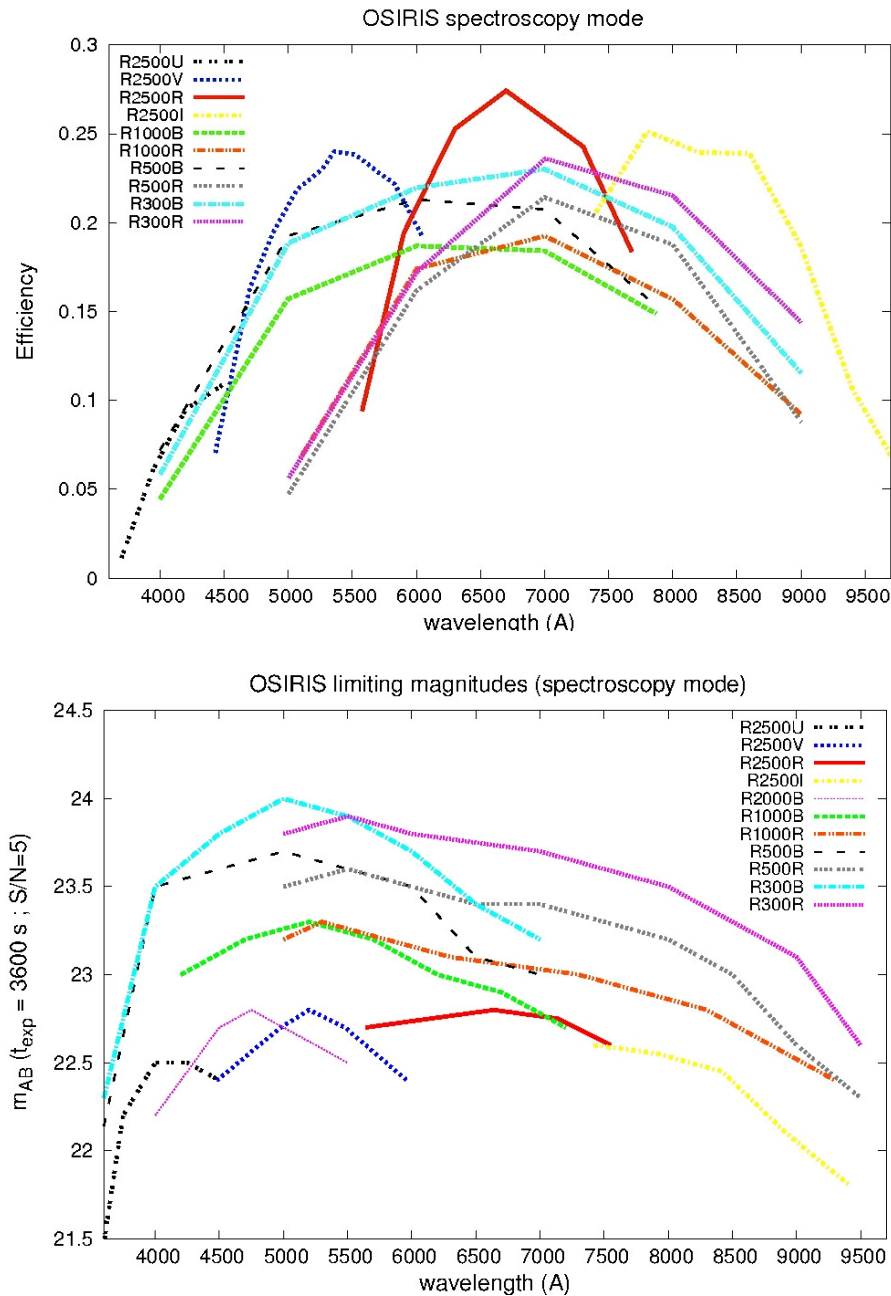


Figure 6.9.- Overall photon detection efficiency of GTC and OSIRIS in spectroscopic mode (above) and limiting magnitudes ($S/N=5$ in 3600s exposure time) achieved in OSIRIS spectroscopic mode, assuming dark conditions, seeing = 1.0 arcsec, and airmass = 1.2 (below).

7 MULTI-OBJECT SPECTROSCOPY

7.1 General description

OSIRIS possesses significant spectroscopic multiplexing capability through the use of focal-plane multi-slit masks instead of a single long slit. Hence observing in MOS mode requires the design and construction of a physical mask that contains a number of small slits, or slitlets, where each slitlet produces the spectrum of a source in the field. By placing a mask with carefully designed and manufactured slits in the focal plane, spectra of several, including tens of objects can be observed at the same time.

The effective available field for placing slitlets is about 7.5 by 6 arcmin. At lower Resolutions (R=300, R=500) the spectrum fits well within the available detector area and hence it is possible to observe the complete spectral coverage, but within in a restricted region. Users can place their slitlets in this restricted FOV where all the spectra will provide the complete spectral coverage of the grism (see Table below). At higher resolutions (R=1000, 2000, and 2500), a spectrum will cover the whole detector length. Therefore, the spectral coverage is dependent on the position of the slit in the FOV, and users should be aware of this when defining the observations. In any case, The Mask Designer Tool (see Section 7.6.) will provide information about the spectral coverage associated with each defined slit for higher resolution grisms/VPHs.

	R300B	R300R	R500B	R500R
Effective FOV	7.5' x 2.8'	7.5' x 3.4'	7.5' x 1.3'	7.5' x 1.6'
(for complete spectral coverage)				

Apart from the focal plane slit mask, spectral observations in MOS mode are no different from normal long-slit observations. In principle MOS mode can be used with all grisms. However, the projection of the spectrum onto the detector is displaced in the dispersion direction in accordance with the position of each specific slitlet. This implies that for slits close to the upper or lower boundary of the field part of the spectrum may be lost, and in the case of higher resolution grisms the spectral window that falls onto the detector is directly related to the slit position in the field. The Mask Designer tool that is described in detail further on assists the user in optimizing the design and produces a design file that is used for producing the mask.

The success of MOS observations depends critically on having accurate coordinates of the sources of interest, together with those of a number of appropriate stars in the field specially selected for alignment purposes: the fiducial stars. Intrinsic errors in coordinates, effects of proper motion, systematic differences between catalogues, and effects due to differential refraction by the atmosphere must be controlled for MOS observations to be successful. Users of MOS mode must pay special care to these aspects.

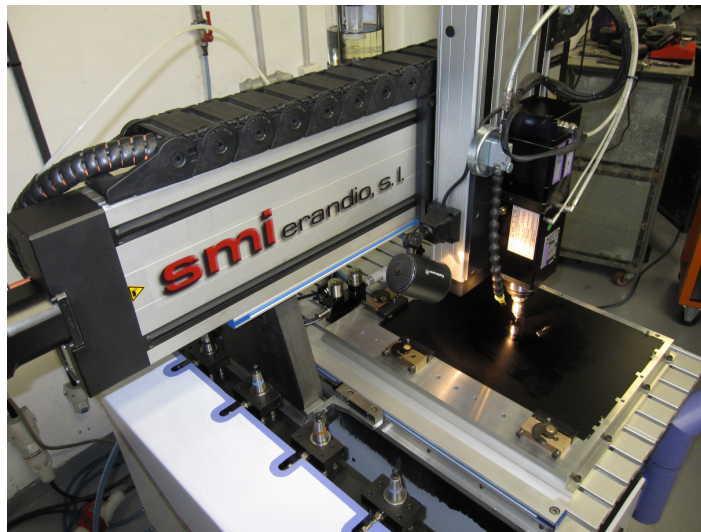


Figure 7.1.- Mask driller machine available at the GTC for MOS observations.

If the fiducial stars work well, alignment of a slit mask on the sky takes a similar amount of time as aligning a long-slit mask. Hence the overheads in MOS mode are similar to those for normal long-slit spectroscopy with OSIRIS.

For the design of slit masks a special software tool, the OSIRIS Mask Designer (MD), must be used. This tool allows the user to input a coordinate list (either equatorial coordinates or coordinates on the CCD pixel scale of OSIRIS) and to optimize the position of the slits. The Mask Designer shows where the spectrum will be projected onto the detector. It also avoids that spectra will overlap. This tool takes automatically care of field distortions when mapping coordinates into the focal plane of the telescope. More details are provided in Section 7.6.

7.2 MOS life cycle

The complete process of planning and executing MOS observations becomes quite involved. In order to design a mask the PI must have a list of target coordinates, either from an existing catalogue with equatorial coordinates, or based on pixel coordinates from a Sloan r' band image taken previously with OSIRIS. Hence it may be necessary to first obtain this pre-image before the MOS observations can be planned. In the case of using external, non-OSIRIS, images it is strongly advised to check that the astrometric solution of such images is of sufficient accuracy (typically for good results one needs astrometry better than 0.2 arcseconds).

Once completed the design of a mask, or set of masks, the resulting design file(s) may be sent to the observatory where the masks will be produced on a dedicated machine. The observatory requires at least one full month to guarantee that the mask will be available in time. The produced masks, used or unused, will remain in the possession of the observatory and are available for later (re-)use.

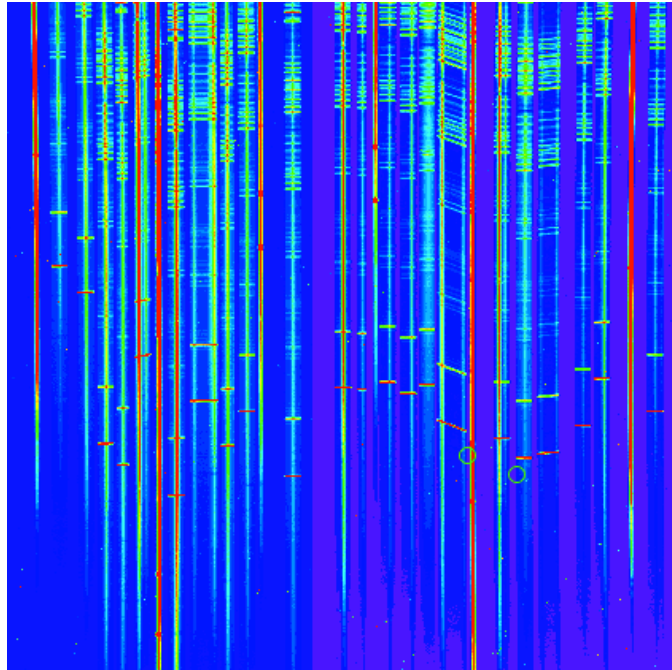


Figure 7.2.- Example of a series of spectra taken with OSIRIS using a MOS mask.

At the time of taking the observations the mask(s) are installed in OSIRIS. Only a small number of masks can be installed at any one time. When the field is being acquired, the fiducial stars have the function of correctly aligning the mask with the projected star field. This alignment process again relies on information provided in the mask design file. When a good alignment is obtained, then the exposure can start.

7.3 MOS mode practical limitations

As was indicated before, the successful use of MOS masks stands or falls with having accurate coordinates of a number of stars for aligning the mask on the sky, and of the science targets. Especially the positions of the fiducial stars are crucial, as any error in these stars will translate to a poor positioning of the whole mask. For the fiducial stars circular holes must be used on which the mask can be centered. At least three fiducial stars are needed, but we strongly advice users to allow for more stars, for instance six.

Special care should be taken with the proper motion of these stars, although often this is not known. This is one of the key reasons to define several fiducial stars so that one or two stars that happen to have a high proper motion can be identified and omitted when aligning the mask. Of course when the target pixel coordinates are used directly from an OSIRIS image, proper motion should not be a concern.

Holes for the fiducial stars should have a diameter of no less than 4 arc seconds. Also the brightness of fiducial stars is crucial. These stars should of course not be so bright that they saturate, and they should all have a similar brightness. A good choice is to have stars of about magnitude 18 in the r' band, but certainly not brighter than 17 as there will be a risk of saturation even with short exposure times. They should not differ by more than 2 magnitudes in brightness. Fainter stars can be used, but exposure times will increase and hence also the overheads in aligning the mask.

Furthermore, the fiducial stars should be well spread over the field and cover both CCDs. We advise to have alignment stars covering both CCDs and span a distance of at least 4 arc minutes.

Slitlets for the science targets must not be narrower than 1.2 arc seconds, and we advise users to design wider slits as this reduces the impact of any alignment error on the final signal-to-noise ratio of the spectra. Having wider slits gives also more flexibility with respect to the seeing conditions, and we strongly advise potential applicants to request reasonable seeing limits for their observation. For reasons of efficiency and cost, the observatory will not produce multiple masks for the same target fields (for instance identical masks but with different slit widths).

Slits can be of any sensible length up to 24 arc seconds and may be tilted relative to each other (for instance to position a slitlet along a certain orientation of a galaxy, or to get two nearby targets into one slitlet). Curved slits, however, are not (yet) admitted.

As described before, the instrument field orientation must be such that the general slit orientation is either North-South, or East-West.

When designing masks based on OSIRIS images, only images taken in the Sloan r' band and with standard binning 2×2 may be used.

Users may consider doing MOS spectroscopy with a grism in combination with a medium-band filter so that only a part of the spectrum will be shown. In that way more objects can be packed into a single mask. However, for the moment this way of operation is not yet supported.

7.4 Calibrating MOS observations

Standard calibrations provided by the observatory for MOS data will be identical to those for normal spectroscopy (i.e. including a spectro-photometric standard star observed with the correct grism and a normal wide longslit). Any special night-time calibrations need to be defined in the Phase-2 tool as observing blocks and the time will be charged to the observing program.

Accurate absolute flux calibration in MOS mode can be a difficult matter and must be planned with care. For specific calibrations each PI will have to define observing block specifically for the purpose of calibrating her/his science data.

7.5 Designing MOS masks: a summary

Designing OSIRIS MOS masks is not a very complex process in itself, thanks to the *Mask Designer* tool that helps the user in making the right choices. The process can however, be time consuming depending on the quality of information that one has available at the outset. There are a number of aspects in the design that require special attention.

From the outset one has to have clear whether the mask will be designed based on a set of accurate equatorial coordinates (coordinate design method), or on the basis of pixel coordinates taken from an OSIRIS image (pre-image design method). The necessary steps for both design methods will be described in detail in Section 7.6.

When designing masks based on equatorial coordinates great care has to be taken with the quality of the coordinates, which is all-important for a correct design. The user should be aware of effects like intrinsic uncertainty of the coordinates, proper motions, and systematic differences between catalogues. Note also that only J2000 coordinates should be used.

In the case of designing a mask based on an image taken with OSIRIS (pre-imaging mode), one must have access to a suitable image of OSIRS taken in the Sloan r' filter. Other filters may introduce unexpected field distortions. Images taken with the tunable filter, for instance, are not valid as input for designing MOS masks. The raw pre-image containing the two CCDs must first be converted into a single mosaic that contains the images of both CCDs, correctly positioned so that the pixel coordinates are continuous and geometrically correct. Also this step is described in detail in the following section.

When using a pre-image for the mask design, the OSIRIS image should be taken with the correct orientation and elevation, so that the design based on this image will reflect the reality at the moment of observing with the mask.

Before designing a mask, the user should consider the right orientation of the field in order to take into account the optimal angle of the slits projected onto the sky. This is important to reduce the effects of differential atmospheric refraction that may introduce important slit losses. This problem is exacerbated by the fact that currently the dome shutter cannot be fully opened and hence objects passing through the dome blind-spot cannot be observed in their optimal position. Moreover, although a mask design may be optimized for a certain hour angle of observation, there is no guarantee that the observation can be scheduled at exactly that hour angle.

Here follow some simple guidelines that will probably work well for most cases: For fields that are to be observed close to the meridian without being affected by the dome shutter limitation (vignetting for elevations above 72 degrees) the slits are best oriented in the North-South direction. However, fields that pass close to the zenith and will be affected by the dome shutter, i.e. declinations between approximately 10 and 47 degrees, the slit orientation is best placed East-West, so that the field can be observed with the same mask both when the field is rising and when it is setting, since the slits will remain reasonably close to the parallactic angle, while when crossing the meridian atmospheric refraction is at its minimum and deviations from the parallactic angle will have little impact. Although other angles are in principle possible, for the time being only slit orientations N-S or E-W will be accepted.

A simple calculator for atmospheric refraction and parallactic angles is available at:

<http://gtc-phase2.gtc.iac.es/science/astroweb/atmosRefraction.php>.

For a more detailed description of the issue of the choice of slit angle we refer to a paper by Szokoly (2005, A&A, 443, 703). And a detailed study on atmospheric refraction and its effects on spectroscopy can be found in Filippenko (1982, PASP, 94, 715).

7.6 The Mask Designer tool

Here follows a practical description of how the OSIRIS Mask Designer tool is used. In what follows we refer to MaskDesigner (MD) Version 3.25 (released November 2013). The MD was developed by Txinto Vaz Cedillo, based on previous work by J.I. González-Serrano and

co-workers (2004, *Experimental Astronomy* 18, 65), with important input and invaluable assistance from Ángel Bongiovanni.

7.6.1. Starting up

The MD software is written in JAVA and uses elements of the JSky project (see <http://archive.eso.org/cms/tools-documentation/jsky.html>). The MD tool runs locally on your machine and hence needs to be installed. You need to have the JAVA Runtime Environment Version 1.5.0 or later installed (see <http://java.com/en/download/index.jsp>).

First download the latest version from the GTC web site:

<http://www.gtc.iac.es/instruments/osiris/osirisMOS.php#Downloads>

Then unpack the compressed file by typing:

```
$> unzip maskDesigner_v325.zip (the filename may be different, depending on the version).
```

Within the directory structure you will find the java program `MaskDesigner.jar`, that you can start by typing the command:

```
$> java -jar -Xmx256m MaskDesigner.jar
```

(or simply just double-clicking on the file in your directory might start the program).

To force the use of the latest version of java, in a typical linux platform, one may type:

```
$> /usr/java/latest/bin/java -jar -Xmx256m MaskDesigner.jar
```

If you wish to start up the MaskDesigner software directly loading a specific mask design file one may pass that file at startup as given in the following example:

```
$> java -jar -Xmx256m MaskDesigner.jar /projects/abell_2065_test.mdp
```

7.6.2. Getting to know the Mask Designer

Before starting work with the MaskDesigner (MD) it is useful to understand some basic principles of its function.

The main goal of the MD is to provide an interface and conversion between either the equatorial sky coordinate system (RA, DEC in J2000) or the OSIRIS detector pixel coordinate system (X,Y) and the coordinate system of the physical mask that must be produced. This requires a set of transformations and checks that the software takes care of in an automatic fashion based on the input given by the user. The abovementioned transformations include the geometric field distortions and corrections related to atmospheric refraction, the proper motions of objects, and precession. The software also ensures that there are no conflicts between slitlets (i.e. overlapping spectra, manufacturing limitations), that the slits fall onto the mask, and that the spectrum is correctly projected onto the detector.

When designing a configuration of slitlets on the mask, the MD avoids conflicts that may occur when spectra from different slitlets overlap. It also shows how the spectra will be projected onto the detector. The user is informed of any conflicts that may occur (in the log window, through a pop-up window, and in the graphical displays of the mask design). Moreover, the user can add priorities to slitlets so that the MD software can give priority to the highest-priority slitlet and adjust the design accordingly.

The MD tool can be used to optimize and manage several masks at the same time, which might be useful in large projects. In fact, the MD tool resolves conflicts by automatically demote slitlets that are in conflict to secondary masks. However, we advise users to start with designing individual masks in order not to complicate the designs when dealing with complex arrangements. Moreover, the observatory only will accept design files for a *single mask* that each is *associated with specific observing block*.

Before starting with the design of an OSIRIS MOS mask the user must either have a set of accurate equatorial J2000 coordinates prepared, or a set of accurate x, y pixel coordinates based on an OSIRIS Sloan r' band image (pre-image mode). When using an OSIRIS image, the MD can be used to interactively select the objects based on the image.

The MD allows the user to visualize the end result of the masks.

Mask designs can be stored and reloaded at a later moment. Slitlet details can be edited online for instance for making small adjustments. All details of a design are stored in an MDP file (Mask-Design-Project file). When a design is completed one must save the end result as a so-called MDF file (Mask-Design-File). This file will be used as input by the observatory to manufacture the mask according to the design.

7.6.3. The graphical user interface

After starting up the MD two windows appear: a log window and the main window that acts as the main interface with the user from where all actions are activated. The log file can be consulted at any time, but plays no active role during the design process.

The main window consists of the following areas indicated in Figure 7.3:

1. Pull-down menu options.
2. Box providing a listing of all the slitlets that have been defined.
3. Buttons for some specific actions.
4. Tick-boxes to select visualization options for the slit geometry.
5. Listing of the details of the slit size and orientations in three different coordinate systems: equatorial, pixel, and physical coordinates.
6. Box to set slit properties.
7. Box to define target details.

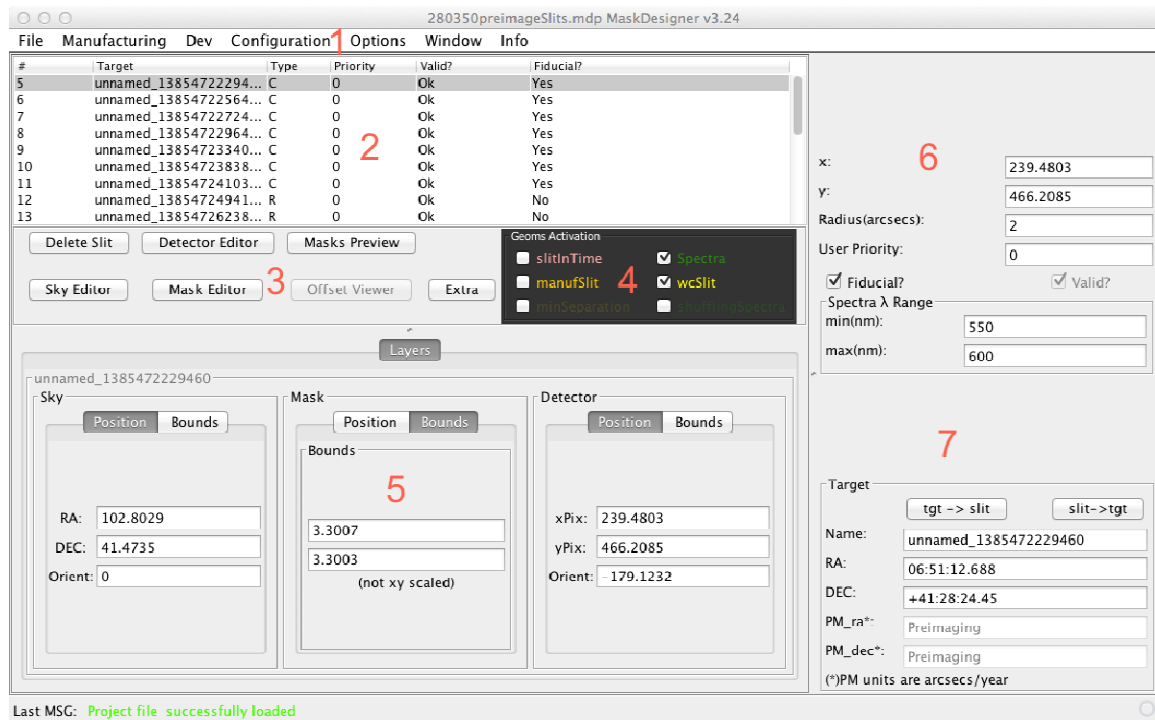


Figure 7.3.- The principal panel of the Mask Designer tool.

Next we describe each point in somewhat more detail:

Menu options

At the very top of the MD window one finds the usual pull-down menu options. Here one can save a project, load a previously defined project, configure the project, set default values for slits, or open specific windows etc. The configuration method is described later when specific examples are presented.

Slitlet Listing

The top-left section of the window provides an overview of all the slitlets that have been defined. Each slit is given a unique number. The target names are copied from the input target list as provided by the user (and may be edited through the target information box). The listing also indicates the type of slitlet (i.e. “R” for a rectangular slitlet and “C” for circular), its priority, whether its current position is valid and does not conflict with other slitlets, and whether the slitlet pertains to a fiducial star.

By clicking on an entry in this list, that entry is highlighted and the information of this slitlet is given in other information boxes, and this slitlet is highlighted in the graphical mask representations.

Action buttons

There are five action button. Three of them activate the main graphical representations of the current mask design: the *Detector Editor (DE)*, the *Mask Editor (ME)* and the *Sky Editor*

(SE), that allow the user to view the same slitlet configuration in the three different coordinate systems. The graphical display for these views employ the *JSky* tool. Figure 7.4. shows as an example of the *Detector Editor* view. The green rectangular outline shows the OSIRIS detector, while the yellow box indicates the mask area that is available for placing slitlets. Each of the visualization modes show these same outlines.

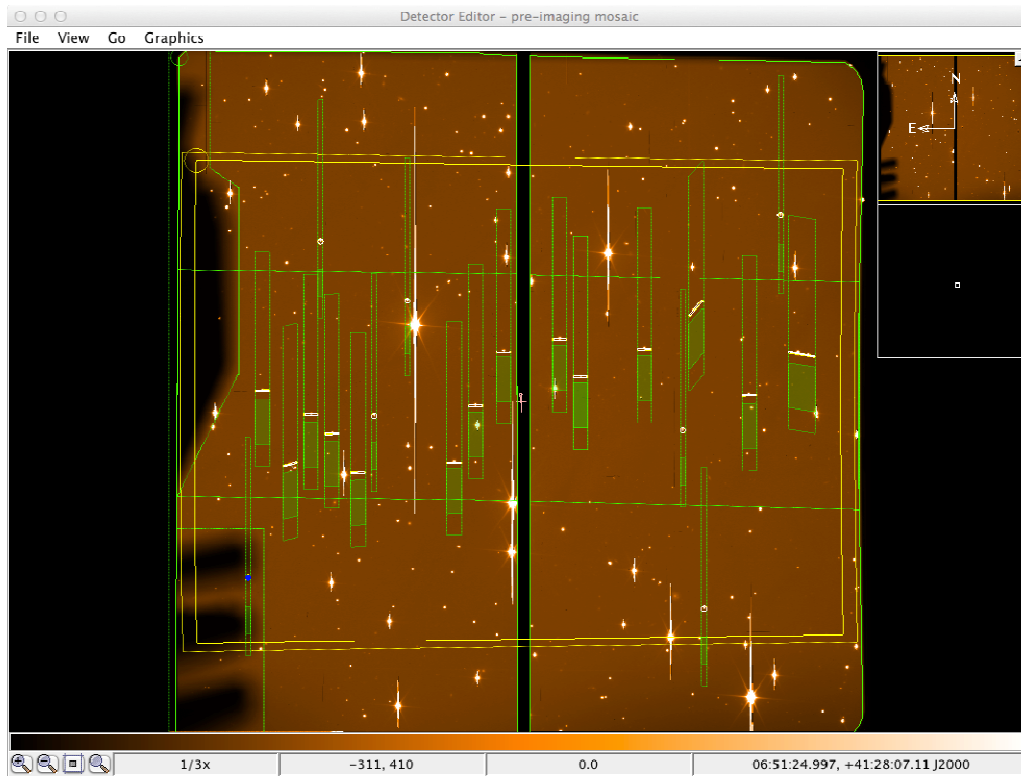


Figure 7.4.- Example of the Detector Editor view.

The visualization options maintain many of the facilities provided by *JSky*. For example, the *Sky Editor* may be used to load images or catalogues, either locally or remotely. The *Detector Editor* by default shows an engineering image that indicates the useful area of the OSIRIS field, but in case of designing a mask using an OSIRIS pre-image, this image will automatically be projected onto the *Detector Editor* view, as show in the Figure 7.4.

The *Mask Preview* button gives a view of what the physical mask will look like. The fifth button *Delete Slit* deletes the selected slitlet that is highlighted in the list of slits.

Slitlet geometry visualization

The abovementioned action buttons allow visualization of the geometry of the slitlets. The visualisation of different aspects of the geometry of the slitlets can be activated, or de-activated using a set of tick boxes labeled *Geoms Activation*.

- *spectra*: shows the projection of the spectra pertaining to the slitlets.
- *wcSlit*: shows possible errors that might occur in the production process of the slitlet according to the manufacturing tollerances of the cutting machine. It allows the user

to assess whether there is risk of contamination by nearby targets.

- *slitInTime*: this options show the geometry of the slitlet taking into account the proper motion and atmospheric refraction. This geometry is the basis for the fabrication definition of the slitlet.
- *manufSlit*: slitlets, at the level of the manufacturing machine, are defined as (sets of) rectangles. However, the various transformations imply that switching between coordinate systems the rectangles will become distorted. This options allows the user to see the effects of such distortions and what shape will be sent to the manufacturing machine.
- *minSeparationSlit*: (not activated by default) shows the manufacturing safety margin around the slits.
- *shufflingSpectra*: (not activated by default) in case of shuffling spectra over the detector spectra are displaced over the detector by a certain number of lines before taking another exposure. This option will show where the spectra will fall in order to avoid overlapping the displaced spectra with the actual slitlet spectra.

Slitlet details

Below the action buttons one finds a box that displays the details of the selected slitlet in three different coordinate systems: the equatorial “sky” coordinates, the physical “mask” coordinates, and the pixel “detector” coordinates. For each set of coordinates its position is shown, the orientation, as well as the range it spans. One can toggle between the two by selecting either “position” or “bounds”.

The position of each slitlet can be edited here in order to make small adjustments, but this should not normally be necessary.

Slit properties

In the upper-right-hand corner of the MD window one finds further details of the slitlet. Apart from the RA and DEC coordinates, one can select or de-select fiducial objects and set the wavelength range that is relevant to this specific slitlet. Setting this overrides the default values that have been defined in the configuration panel (but only within the physical possibilities of the grisms).

Target details

In this last box, at the bottom-right-hand corner of the window, one can edit details of the target that is associated with the slitlet. For instance, proper motion details can be entered here.

Mask editor and visualization windows

Three of the abovementioned action buttons open visualization windows where the mask design can be seen. Each slit that is defined is shown in these window, together with the associated band that will be occupied by the spectrum corresponding to the dispersive element and wavelength range chosen.

The three windows provide a view of the slits in equatorial sky coordinates for the *Sky*

Editor, in detector coordinates for the *Detector Editor*, and in physical mask coordinates for the *Mask Editor*. These windows are interactive to some extent. One can click on a slit upon which it will be highlighted as selected. At the same time on the main window that same slit will be selected and its properties can be selected. Changes in its properties are instantly reflected in the visualization windows. Conflicting slitlets that are rejected are shown in red.

Through the *Detector Editor*, the *Sky Editor*, and the *Mask Editor* one can also define new slits by double-clicking on the location where you want the slit to be. However, it is advisable to prepare the target list using other tools such as IRAF and importing such list into the MaskDesigner. When using the MaskDesigner visualisation windows to define slits, one must be aware that the definition will be on the basis of the coordinate system relevant for the window (i.e. pixels coordinates for the *Detector Editor*)

Log window

The log window essentially keeps a record of warnings and errors that might come up during the design of a MOS mask.

Configuring the MD

Once a mask design has been initiated, some configuration parameters can be set. Under [Options](#) menu one can activate the [Project Options](#) window where some details and defaults for the current design can be set. It is useful to keep the default values and to enter the PI name. It is not required to fill in the observation ID as this will be defined by the observatory after the design has been submitted for manufacturing.

Further specific details related to the mask design must be set under [Configuration](#) and then selecting [Config Obs](#). Here some basic configuration related to the OSIRIS instrument are set, such as the dispersing element, the detector binning factor, whether the mask design is based on an OSIRIS pre-image or uses a catalogue of equatorial coordinates, etcetera. Details on how this is used is explained in the examples that follow.

In the configuration panel the selected grism (and filter) combination set the spectral range of interest, while the date is used to calculate effects of precession and proper motion, while the hour angle is used to calculate the effects of atmospheric refraction. In the case of using a pre-image, the relevant details are taken from this image itself.

The Offset entry allows the user to introduce an offset to the pointing coordinates in order to ensure that in the case of making a sky observation for calibration purposes with the same mask, that no stars by coincidence enter the slits.

When having made changes one has to click the button *Commit changes* to activate them. This causes the program to re-calculate the current design.

Configuring the default slit shape

When designing a mask, the MD tool assumes a built-in default shape for the slitlets. This default is set in option [Config default slits](#) in section of [Configuration](#). In this configuration panel you can set the default type of slitlet being either rectangular, circular, or curved. In this same panel the sizes and relevant wavelength range can be set. These default settings can be overruled for individual slits in the main panel.

Configuring the spectral range

Each slitlet projects a spectrum onto the detector and obviously spectra from slitlets must not overlap or be projected outside the detector. The MaskDesigner tool is set up to detect and prevent overlapping spectra and allows the user to change the slit properties to avoid conflicts. The software also warns the user when spectra fall outside the detector. However, it could happen that the user is only interested in a limited part of the spectrum, in which case it may be acceptable when spectra partly overlap or are projected outside the detector, as long as the interested part remains detectable. Therefore the MD allows the user to specify for each slitlet the wavelength range of interest that the MD will use to detect any conflicts. This information can be set in the section labeled *Spectral Range*. If a same limited range is to be used for all slitlets, it is recommended to first set these default values for the whole project in the *Default slit configuration* window before importing coordinates or otherwise defining slitlets.

7.6.4. Designing MOS masks step-by-step

There are two distinct starting points when designing an OSIRIS MOS mask: (i) using target coordinates based on pixels of an OSIRIS *r'* band image, or (ii) using target coordinates based on equatorial J2000 coordinates. The two options have a distinct treatment and are therefore described separately following specific examples:

7.6.4.1. Example #1: Using an OSIRIS pre-image

Using an image taken with OSIRIS as the basis for designing a mask is the easiest and hence preferred method to successfully obtain multiple-object spectra with OSIRIS. This so-called *pre-imaging mode* requires you to have access of an OSIRIS image of the field taken in the Sloan *r'* filter and on which your targets can be identified. This image must have exactly the same position and orientation as will be used for the spectroscopic observations; this is essential since the field distortions for OSIRIS are significant and non-symmetric.

An OSIRIS image consists of a mosaic of two CCDs with a gap and a slight shift and rotation between them. In order to measure pixel coordinates first the two CCD images must be combined into a single frame where the pixel coordinates are continuous and geometrically correct by creating an image mosaic. This is accomplished using an IRAF task *mosaic_2x2_v2.cl* that has been written for this purpose and that is made available on the GTC web site:

<http://www.gtc.iac.es/instruments/osiris/osirisMOS.php#Downloads>

It is used in the following way:

- Place the script *mosaic_2x2_v2.cl* into your data directory. Then open IRAF and go to the data directory.
- Load the task into IRAF by typing the following at the IRAF prompt:
`task $mosaic=mosaic_2x2_v2.cl`
- Run the task on your raw image by typing at the IRAF prompt: `mosaic 12345.fits` where of course the FITS file name must indicate the filename of the input OSIRIS image.

The output file is called *OsirisMosaic.fits* and has a single layer containing the image of both CCDs. This is the FITS file you will be using to determine pixel coordinates of your targets. You can rename this file to anything you like.

From this mosaic FITS image use IRAF or any other tool to identify your targets and measure the targets centroid positions, for instance using the IRAF *imexam* routine with option “r”. (As an alternative, one can use the MaskDesigner tool itself to directly identify targets. This is described further down. However, the preferred and most secure method is what is described here).

Place these positions of all the targets in a text file (alternatively, you can use a spreadsheet tool such as EXCEL and save the file in CSV format) containing the following columns:

1. “img” to indicate pre-imaging-mode;
2. Centroid x-coordinate;
3. Centroid y-coordinate;
4. Proper motion in RA in arcsec/year (no effect in pre-imaging mode);
5. Proper motion in DEC in arcsec/year (no effect in pre-imaging mode);
6. Slit type “R” for rectangular and “C” for circular holes;
7. Angle of the slitlet in degrees;
8. “N” for normal slitlets and “F” for a fiducial alignment target;
9. Priority indication; integer value;
10. A target name (or any other relevant information).

Make sure that you have **at least 3 fiducials targets** (5 or 6 would be optimal), that the fiducials are not too bright nor too faint, as was described earlier, and that they are well distributed over the whole field of OSIRIS, as was described earlier in this document.

//			PMRA(XX.xxx arcsec/year)		SlitType(C/R/V)		Fiducial/Normal(F/N)		TargetName(string)
// ccd	xPix(XXXX.xx)	yPix(YYYY.yy)	PMDEC(XX.xxx arcsec/year)		Angle(DD.ddd)		Priority(int)		
ccd	112.49	396.889	00.00000	00.00000	R	90.000	N	0	tgtUnolnCCD
ccd	873.718	436.525	00.00000	00.00000	R	90.000	N	0	tgtDoslnCCD
ccd	899.417	483.438	00.00000	00.00000	R	90.000	Fiducial/Nor	0	tgtTreslnCCD

Figure 7.5.- Example of a target input list based on detector pixel coordinates.

Now you are ready to start using the Mask Designer tool.

- To start the design, begin with opening a new project by selecting from the [File → New MDP](#).

- Setup the global parameters for the project by going to [File → Configuration → Config Obs](#). Select the standard MOS mode, no filter, select the grism you want to use, and set binning to the standard 2x2 pixels (binning 1x1 is not accepted). In the observation details box you select below the question *Use Pre-imaging?*, the option *Use a pre-image file* and you identify the FITS file that must contain the mosaic image that you prepared earlier. Ignore the *Telescope Offset* boxes. When you're done, select [Commit changes](#) and save the MDP file.

- Next step is to set up the default slits and fiducial star holes. For that, go to [File → Configuration → Config Default Slits](#) where you can proceed to define rectangular slits,

circular holes (used for the fiducial alignment stars), and curved slit. (Note that curved slits are not yet supported). For the rectangular holes you can specify the generic size, as well as the typical wavelength range of interest and their generic orientation. Note that in case the field orientation is set at 0 degrees, then the slit angle would normally be set at 90 degrees. These geometric details can later be tuned per slitlet, if necessary. The minimum supported slit width is 1.2 arcsec. Similarly, for circular apertures the diameter can be set. Normally circular apertures are used for the fiducial alignment stars in the field, and hence the tickbox *fiducial* should be activated. The minimum radius for fiducial holes is 2 arcsec. Just close the window after having edited your default values.

All the slits that will be defined now will take as default values of the parameters that you last selected. When you are interactively defining slitlets, to change, for instance, from defining fiducial holes to rectangular slitlets, you need to go back to the configuration panel and change the default to *rectangular*, with the appropriate sizes.

When having configured the setup, it is advised to save the project by selecting *File → Save MDP* and giving it an appropriate file name.

- Now it's time to load the list of coordinates by selecting *File → Import targets* and selecting the file you prepared. If the software has accepted your file you should see your list of slitlets appear in the table in the MaskDesigner window. The list will show which slitlets refer to fiducial objects or normal targets, and whether the MD software encounters any problems with the design (see the column labeled *valid*). The slitlets that are not considered valid will require further attention. Typical problems that are encountered are overlapping spectra with other slitlets, that the slitlet falls outside the mask, or that its spectral range falls outside the detector. The design can be tuned in order to reduce the conflicts, as will be shown in the next points. When you click on an entry in the list then the numbers in the other panels will display the details referring to the selected slitlet.

- The *Detector Editor* is the most suitable visualisation tool to verify and possibly change the design of the mask made in pre-imaging mode. The *Detector Editor* panel shows the layout of the mask design superimposed on the pre-image mosaic itself, in the pixel coordinate frame. Obviously the targets on the image should align well with the slitlets. Slitlets that for some reason are rejected by the MD tool show up in red.

When clicking on a slitlet in the image, that slitlet entry will be highlighted in the image, and it will be selected in the list of slitlets. Slitlets can also be identified by their pixel coordinates.

The description of target selection so far has been based on the user having generated a target list prior to using the MaskDesigner tool. As an alternative, object coordinates can also be generated within the MaskDesigner software itself by going to the *Detector Editor* panel and double-clicking on the targets. This automatically centroids the target seen in the image and adds that target to the list with the attributes (slit size and shape, wavelength range, fiducial etc.) as they are set at that moment. This is a very quick and easy method. However, we advise users to generate their coordinate list with trusted and well-known tools such as IRAF.

- Editing the properties of a specific slitlet can simply be accomplished by changing any of the input boxes. First select a slitlet in the list so that its properties will show up and can be edited. For instance, the pixel coordinates may be altered, the slitlet might be given an angle, its size changed, or the wavelength range of interest adapted.

Slitlets may also be deleted from the list by activating the *Delete Slit* button. Or the priority of a slit may be altered so that it is given the appropriate weight when the MD tool optimizes the mask design.

Priorities of slitlets are treated by the MD program in the following fashion: in case of conflict between slitlets, the slit with the lowest number remains in the primary mask design, while slits with a high priority index are automatically translated to a secondary mask.

- When you are done with your design, just save the Mask Design Project file by selecting *File → Save MDP* and giving it an appropriate file name. At a later stage you can reload this file and continue work where you left off.

It is important to note that since the pre-image design essentially deals with translating detector pixel coordinates to mask coordinates, no account is made for atmospheric refraction. Nor is proper motion of the objects accounted for; the image is assumed to correctly represent the actual sky.

7.6.4.2. Example #2: Using equatorial coordinates

This second example has much in common with the previous one, except for the initial coordinates provided for the slitlets. When you possess a set of accurate J2000 equatorial coordinates of your targets and fiducial stars you can input this list directly into the MaskDesigner tool and from there work to refine your mask design. The MD allows you, with its *Sky Editor* view to overlay your mask design on an image which has its astrometry well calibrated.

An important difference when working with equatorial coordinates as opposed to using a pre-image is that in translating the J2000 input coordinates on the sky to the mask coordinates, precession, atmospheric refraction and proper motion are taken into account.

Before starting the design of a mask one has to prepare a target list with accurate coordinates. This target list should include not only the science targets, but also the fiducial stars. Make sure that you have **at least 3 fiducials** (5 or 6 would be optimal), that the fiducials are not too bright nor too faint, as was described earlier, and that they are well distributed over the whole field of OSIRIS.

Place the coordinates of all the targets in a text file (alternatively, you can use a spreadsheet tool such as EXCEL and save the file in CSV format) containing the following columns:

1. “sky” or “skyDeg”, depending on the format of the coordinates (see next points);
2. Centroid RA coordinate (J2000). The format is either in hours HH:MM:SS.ssss or DDD.ddddddd, respectively, depending on the entry in the first point;
3. Centroid DEC coordinate (J2000). The format is either in hours +/-DD:MM:SS.sss or +/-DD.ddddddd, respectively, depending on the entry in the first point;
4. Proper motion in RA in arcsec/year;
5. Proper motion in DEC in arcsec/year;
6. Slit type “R” for rectangular and “C” for circular holes;
7. Angle of the slitlet in degrees;
8. “N” for normal slitlets and “F” for a fiducial alignment target;
9. Priority indication; integer value;

10. A target name (or any other relevant information).

//	PMRA(XX.xxx arcsec/year)			SlitType(C/R/V)		Fiducial/Normal(F/N)		TargetName(string)	
// sky	RA(HH:MM:SS.sss)	DEC(+/-DD:MM:SS.sss)	PMDEC(XX.xxx arcsec/year)	Angle(DD.ddd)	Priority(int)				
sky	16:59:31.80336	-12:57:55.01160	00.00000	00.00000	C	00.000	F	0	tgtUno
sky	16:59:28.29600	-12:56:21.57000	00.00000	00.00000	C	00.000	F	0	tgtDos
sky	16:59:26.33688	-12:55:05.42280	00.00000	00.00000	C	00.000	N	0	tgtTres
sky	16:59:27.45552	-12:52:01.35120	00.00000	00.00000	C	00.000	N	0	tgtCuatro

Figure 7.6.- Example of a target input list based on equatorial coordinates.

In what follows the basic steps are described about what one needs to do with the MaskDesigner tool.

- To start the design, begin with opening a new project by selecting from the [File → New MDP](#).

- Setup the global parameters for the project by going to [File → Configuration → Config Obs](#). Select the standard MOS mode, no filter, select the grism you want to use, and set binning to the standard 2x2 pixels (binning 1x1 is not accepted). In the observation details box you select, below the question *Use Pre-imaging?*, the option *Don't use it (catalog)*.

Fill in the correct RA, DEC and orientation that must correspond with the center of the OSIRIS field of view, i.e. corresponding to the center of the mask. An orientation angle of zero degrees will imply that North is at the top and East is towards the left of the *Sky Editor* and the *Detector Editor* views.

Although the MaskDesigner tool allows for the design at any orientation, GRANTECAN only accepts mask that are either oriented N-S or E-W. Our advice is that for fields to be observed close to the meridian without being affected by the dome shutter limitation (vignetting for elevations above 72 degrees) the slits are best oriented in the North-South direction. However, fields that pass close to the zenith and will be affected by the dome shutter, i.e. declinations between approximately 10 and 47 degrees, the slit orientation is best placed East-West, so that the field can be observed with the same mask both when the field is rising and when it is setting, since the slits will remain reasonably close to the parallactic angle.

In the Box labeled *Date System* fill in the optimal date and hour angle for the observation. These details are relevant to correct for precession, proper motions, and atmospheric refraction. Hence the MaskDesigner automatically corrects for these effects and ensures that the physical location of the slitlets will be correct. In case of doubt, selecting and hour angle of 0 is normally a good choice. (Note that the slit angle is defined in sky coordinates, independent of the instrument orientation).

Ignore the *Telescope Offset* boxes. When you're done, hit [Commit changes](#) and save the MDP file.

- Next step is to set up the default slits and fiducial star holes. For that, go to [File → Configuration → Config Default Slits](#) where you can proceed to define rectangular slits, circular holes (used for the fiducial alignment stars), and curved slit. (Note that curved slits are not yet supported). For the rectangular holes you can specify the generic size, as well as the typical wavelength range of interest and their generic orientation. If the field orientation

is set at 0 degrees, then the slit angle would normally be set at 90 degrees. These geometric details can later be tuned per slitlet, if necessary. The minimum supported slit width is 1.2 arcsec. Similarly, for circular apertures the diameter can be set. Normally circular apertures are used for the fiducial alignment stars in the field, and hence the tickbox *fiducial* should be activated. The minimum radius for fiducial holes is 2 arcsec. Just close the window after having edited your default values.

- Now it's time to load the list of coordinates by selecting [File → Import targets](#) and selecting the file you prepared. If the software has accepted your file you should see your list of slitlets appear in the table in the MaskDesigner window. The list will show which slitlets refer to fiducial objects or normal targets, and whether the MD software encounters any problems with the design (see the column labeled *valid*). The slitlets that are not considered valid will require further attention. Typical problems that are encountered are overlapping spectra with other slitlets, that the slitlet falls outside the mask, or that the spectral range falls outside the detector. The design can be tuned in order to reduce the conflicts, as will be shown in the next points. If you click on an entry in the list then the numbers in the other panels will display the details referring to the selected slitlet.

- The *Sky Editor* is the most suitable visualisation tool to verify the mask design as it projects the slitlets in the same equatorial coordinate frame as was used to define your targets. Slits and the spectral projection might look curved and distorted, which is due to the projection of rectangular outlines on the equatorial coordinate grid. The *Sky Editor* allows you to load images and catalogues. For instance, to overlay an image of the Digital Sky Survey, in the *Sky Editor* panel go to [Catalog → Image Servers → Digitized Sky \(Version II\) at ESO](#) and select the appropriate field (of course for this example you need to be connected to the internet in order to access the on-line catalogues). The DSS image will appear together with your design and if all is well your slitlets should align well with the targets in the image. Slitlets that for some reason are rejected by the MD tool show up in red.

- Editing the properties of a specific slitlet can simply be accomplished by changing any of the input boxes. First select a slitlet in the list. Its properties will then show up and can be edited. For instance, the coordinates may be altered, the slitlet might be given an angle, its size changed, or the wavelength range of interest adapted.

In the box labeled "Target" the proper motion of the target may be set or altered. The MaskDesigner calculates the movement for the epoch 2000 coordinates to the observing date set in the configuration.

Slitlets may also be deleted from the list by activating the *Delete Slit* button. Or the priority of a slit may be altered so that it is given the appropriate weight when the MD tool optimizes the mask design.

- When you are done with your design, just save the Mask Design Project file by selecting [File → Save MDP](#) and giving it an appropriate file name. At a later stage you can reload this file and continue work where you left off.

8 OBSERVING WITH OSIRIS

8.1 Exposure time calculator (ETC)

For preparing observations estimating exposure times for the different modes, the OSIRIS ETC can be found in:

<http://gtc-phase2.gtc.iac.es/science/OsirisETC/html/Calculators.html>

Also, for Tunable-Filter observations it is highly recommended to use the TF Setup Tool, available at:

<http://gtc-phase2.gtc.iac.es/science/OsirisETC/html/TFSetupTool.html>

before using the ETC. The TF Setup Tool allows to perform very useful estimates for the TF operation, as:

- obtaining the available widths for our wavelength of interest, as well as to define the corresponding Order Sorter Filter that has to be used for the observation.
- calculating the change in wavelength along the OSIRIS FOV.
- estimating the effect of the sky lines in our tuned filter.

Estimates from the ETC are obtained by using the most recent data coming from the instrument and are well in agreement with the obtained results in the scientific operation of the telescope. In any case, there are also some useful information to take into account when using the OSIRIS ETC:

- If you were awarded with 'Spectroscopic' night conditions, it's advisable to add +0.5 mag to the target magnitude when obtaining S/N estimates (as it was observed by daily monitorizing of OSIRIS zeropoints, see Section 2.1.1.1).
- When using the R2500I VPH, increase the exposure times a factor 1.2 to obtain the S/N given by the ETC. This VPH suffers some internal fringing effects that slightly decrease the S/N in the scientific spectra.
- Blue Tunable Filter (BTF) calculations are still in progress, please contact with GTC SA staff for estimates for the BTF.

8.2 GTC Phase 2 tool

Observations with OSIRIS / GTC can be done both in queue or visitor mode, but in any case, observers must use the GTC Phase 2 tool in advance to prepare the observations. In queue mode, this is mandatory in order to provide to GTC SA staff with the instructions for completing the observing programmes; in visiting mode, this is highly recommended as the

Phase 2 tool allows to the GTC SA staff to generate automatized observing sequences at the telescope, hence notably increasing the nightly operating efficiency.

For a complete help in how to use and complete this GTC Phase 2 tool, users are referred to the on-line help document available at:

<http://gtc-phase2.gtc.iac.es/science/media/docs/phase2help.pdf>

Regarding other overall details in GTC queue observing mode please read carefully the section 'Observing with GTC' at GTC web pages:

<http://www.gtc.iac.es/observing/observing.php>

and for assistance of users of the GTC in planning and preparing their observations, it's strongly recommended to read the following section at GTC web pages:

<http://www.gtc.iac.es/observing/toolbox.php>

9 OSIRIS DATA PROCESSING

9.1 OSIRIS / GTC Keywords

Data files produced by OSIRIS on GTC have a standard FITS structure. In the standard operative mode of the instrument, both CCDs are read using a single amplifier. Data corresponding to each CCD are stored as independent subdimensions of the image.

The filenames have a structure which contains a unique run number, the date, instrument, and observing mode as follows: <number>-<date>-<instrument>-<mode>.fits

For example: 0000007448-20090703-OSIRIS-OsirisBroadBandImage.fits

Here is a complete list of available OSIRIS observing modes:

Calibration Modes	Science Modes
OsirisBias	OsirisBroadBandImage
OsirisDark	OsirisTunableFilterImage
OsirisDomeFlat	OsirisLongSlitSpectroscopy
OsirisSkyFlat	OsirisMOS
OsirisSpectralFlat	OsirisFastBroadBandImage
OsirisCalibrationLamp	OsirisFastTunableFilterImage
	OsirisFrameTransferBroadBandImage
	OsirisFrameTransferTunableFilterImage

The following table provides a listing and description of the OSIRIS FITS headers. Please note that the complete list will be upgraded, and the latest version can be found at:

<http://www.gtc.iac.es/instruments/osiris/media/osirisFitsDictionary.html>

Name	Value	Description	Units	Additional Description
AG1ARM	90.375	ASG arm position	degrees	AG1ARM=90 means the ARM is placed at the center of the focal plane

AG1FOCUS	43.17	ASG focus position	mm	AG1FOCUS=0 is the correct value at center of focal plane
AG1TURNT	37.123	ASG turn table position	degrees	Guide probe turn table position.
AIRMASS	1.2	AIRMASS	N/A	AIRMASS=1 means observation was started at zenith
AMPNAME	'CCD_1: Left'	Name of the amplifier used during readout	N/A	Name of the amplifier used during readout
AMPSEC	'[1:2048,1:4102]'	AMP Section	Pixels	Amplifier section in pixels
APPLYPRE	'true '	Reordering applied or not	N/A	Boolean
ARCHID	175464	File archive number	N/A	File archive number
ASGDEC	'+62:16:21.821'	ASG declination	DD:PP:SS	Useful to know which guide star was used during observation
ASGRA	'+12:37:36.550'	ASG right ascension	HH:MM:SS	Useful to know which guide star was used during observation
AZIMUTH	166.983854397316	Azimuth at start of observation	degrees	Telescope azimuth
BIASSEC	'[3:22,5:2051]'	BIAS section	Pixels	Bias section. Area where to measure bias.
BITPIX	16	Number of bits for data pixel	N/A	This means CCD saturates at 65563 ADU.
BSCALE	1	Default scaling factor	N/A	Scale factor applied to data values.
BZERO	32768	Offset data range to that of unsigned short	N/A	Offset applied to data values to avoid negative numbers.
CCDSUM	'2 2 '	First horizontal bin, then vertical bin	N/A	Indicates whether signal from 2 or more pixels have been summed.
CCDSEC	'[1:2048,1:4102]'	CCD Section	Pixels unbinned	Area of the ccd actually read out

CCDSIZE	'[1:2048,1:4102]'	CCDSIZE	Pixels unbinned	Size of ccd in pixels
CD1_1	6.1523E-05	WCS matrix element 1,1	degrees/pixels	World coordinate system matrix element 1,1.
CD1_2	-3.4749519E-05	WCS matrix element 1,2	degrees/pixels	World coordinate system matrix element 1,2.
CD2_1	-3.4749519E-05	WCS matrix element 2,1	degrees/pixels	World coordinate system matrix element 2,1.
CD2_2	-6.1519739E-05	WCS matrix element 2,2	degrees/pixels	World coordinate system matrix element 2,2.
CLOSTIME	'12:23:17.593'	Close Shutter Time	HH:MM:SS	Time the OSIRIS shutter close. Only appears if the shutter actually moved (e.g., does not appear in bias images)
COMMENT	This is a comment	None	N/A	Keyword used to include comments of whatever nature
CRPIX1	462.5	Ref pix of axis 1	pixel	Pixel in image corresponding to the RA given by CRVAL1
CRPIX2	995.23	Ref pix of axis 2	pixel	Pixel in image corresponding to the DEC given by CRVAL2
CRVAL1	1.55213538050385	RA at Ref pix in decimal degrees	degrees	This is the Right ascension of the pixel given in CRPIX1
CRVAL2	63.6936537290756	DEC at Ref pix in decimal degrees	degrees	This is the declination of the pixel given in CRPIX2
CSCXOFF	34680	TF Red Auto Adjustment X (encoder units)	Encoder units	Same as EKW16 (Default value of TF X position, set at starting time).
CSCYOFF	34680	TF Red Auto Adjustment Y (encoder units)	Encoder units	Same as EKW17 (Default value of TF Y position, set at starting time).
CSCZOFF	34680	TF Red Auto Adjustment Z (encoder units)	Encoder units	Same as EKW18 (Default value of TF Z position, set at starting time).
CTYPE1	'RA---TAN'	R.A. in tangent plane projection	N/A	System used for world coordinate projection. Must be written

				exactly as 'RA---TAN'.
CTYPE2	'DEC--TAN'	DEC. in tangent plane projection	N/A	System used for world coordinate projection. Must be written exactly as 'RA---TAN'.
DARK	'false '	Apply Dark	Boolean	Indicates whether the shutter open or not inspite of the value reported by EXPTIME. If "true", the shutter did not open.
DATASEC	'[26:1049,1:2051]'	Data Section	Pixels	Data section in binned pixels. Differ from AMPSEC because of overscan and binning. Disply use it to show only data pixels
DATE	'2012-02-14T16:12:52'	file creation date (YYYY-MM-DDThh:mm:ss UT)	N/A	Time stamp for fits file creation. This is not the time of observation.
DATE-OBS	2012-02-14T16:12:16.632	Time when starts the first exposure	N/A	Time stamp relative to the start of the exposure (for charge transfer mode this refers to the first exposure).
DEC	'+63:41:39.856'	Telescope declination (DD:PP:SS), d:m:s	DD:PP:SS	Declination the telescope is aiming to. In sessagesimal degrees.
DECDEG	63.6944043136059	Telescope declination in degrees, degrees	degrees	Declination the telescope is aiming to. In decimal degrees.
DEEP	2	Bytes per pixel	bytes	Number of bytes used to represent numbers.
DETECTOR	'E2V CCD44_82_BI'	Detectors Model	N/A	Detector identification model
DETSEC	'[1:2048,1:4102]'	Detector Section	Pixels	Area of the detector actually used in exposure.
DETSIZE	'[1:4096,1:4102]'	Maximum Imaging Pixel Area	pixels	Detector size in pixels.
DEWPOINT	-12.3	Ambient dew point in Celsius degrees	Degrees Celsius	Ambient dew point in Celsius degrees
EKW1	3	Filter Wheel 1	Integer	Filter Wheel 1 currentPosition.

		currentPosition.		
EKW2	5	Filter Wheel 2 currentPosition.	Integer	Filter Wheel 2 currentPosition.
EKW3	5	Filter Wheel 3 currentPosition.	Integer	Filter Wheel 3 currentPosition.
EKW4	7	Grism Wheel currentPosition.	Integer	Grism Wheel currentPosition.
EKW5	2	Mask positioner currentPosition	Integer	Mask positioner currentPosition
EKW6	37634	Red TF Displacement in Z (encoder units)	Encoder units	Tunable filter Red DisplacementZ
EKW7	69	Red TF offset (encoder units)	Encoder unites	Tunable filter Red currentOffset
EKW12	34680	Red TF position X (encoder units)	Encoder units	Tunable filter Red position X
EKW13	24680	Red TF position Y (encoder units)	Encoder units	Tunable filter Red position Y
EKW16	34680	Red TF auto adjustement X (encoder units)	Encoder units	Tunable filter Red position Auto Adjustment X
EKW17	32080	Red TF auto adjustement Y (encoder units)	Encoder units	Tunable filter Red position Auto Adjustment Y
EKW18	34350	Red TF auto adjustement Z (encoder units)	Encoder units	Tunable filter Red position Auto Adjustment Z
ELAPSED	'45.810 '	Total elapsed time from start to end (s)	Seconds	Time difference between End and start of observation.
ELAPSHUT	'6.966 '	Total elapsed time (seconds followed by ms)	Seconds	Time difference between CLOSETIME - OPENTIME, in seconds.
ELEVAT	47.3367634069994	Elevation at start of observation	Degrees	Telescope elevation at start of observations.

END			N/A	Marks end of image header
EQUINOX	2000.	Epoch of the mean equinox for WCS	Years	Equinox for world coordinate system.
EXPMODE	'UNIQUE '	ExposureMode	N/A	Exposure mode, could be UNIQUE, FORWARD_START, y FORWARD_RETURN.
EXPTIME	6.5	Exposure Time in seconds	Seconds	Exposure time. Differ form ELAPSHUT because of shutter flying time.
EXTEND		None	N/A	Mark end of fits header extention.
EXTNAME	'CCD_1_L1_1'	Extension Name	N/A	Extension name according to detector been read, readout mode, and readout channel.
FILSTAT	'COMMITTED'	None	N/A	Not Used.
FILTER1	'OPEN '	Filter identifier in wheel 1	N/A	Position of filter wheel 1
FILTER2	'OPEN '	Filter identifier in wheel 2	N/A	Position of filter wheel 2
FILTER3	'OPEN '	Filter identifier in wheel 3	N/A	Position of filter wheel 3
FILTER4	'R1000B '	Filter 4 device identifier	N/A	Position of Grism wheel
FRAMESI	8606008	Raw Data Size in bytes	Bytes	Size of data file
FRAMETY	1	Frame Type(1:RDI,2:RDS, 3:RDW)	N/A	Frame type. RDI=modo simple, RDS= modo shutterless, RDW= modo frame transfer.
GAIN	1.18	Gain (e-/adu)	Electrons/ADU	Gain in electrons per ADU
GAINTYPE	'GAIN_x4_75'	Gain requested by user	N/A	String identifying the gain mode.
GCOUNT	1	required keyword. must = 1		One data group.

GRISM	'R500B '	GRISM identifier	N/A	Grism identification name (duplicate value of FILTER4)
GTCOBID	'0001'	Observation Block	N/A	Observing block number
GTCPRGID	'GTC50-11B'	Program Identifier	N/A	Unique observing program ID.
HBIN	'true '	Horizontal Binning	Boolean	Whether binning was applied in the horizontal direction. See also VBIN.
HEIGHT	2348	Telescope height above sea level (m)	Meter	Telescope altitude above sea level in meter.
HUMIDITY	33.34	Ambient humidity in percent.	Percent	Ambient humidity in percent.
INHERIT	T	inherit keyword	Boolean	Either T or F. Whether extension inherits keywords from primary extension
INSMODE		Instrument Mode	N/A	not defined
INSTRUME	'OSIRIS '	Instrument Name	N/A	Unique instrument name
IPA	0.23	Instrument position angle in degrees, degrees	Degrees	Instrument position angle
LATITUDE	28762000	Telescope latitude (degrees), +28:45:43.2	Degrees	Telescope latitude
LONGITUD	17877639	Telescope longitude (degrees), +17:52:39.5	Degrees	Telescope longitude
LOOPSHIF			Integer	Times charge displacement is repeated, in charge transfer/shuffling mode.
LST	'+23:58:53.137'	Local sidereal time (HH:MM:SS)., h:m:s	HH:MM:SS	Local sidereal time.
M2RX	0.00024826789740	GTC secondary mirror RX position	Radians	GTC secondary mirror RX position

M2RY	-7.7156859333E-05	GTC secondary mirror RY position	Radians	GTC secondary mirror RY position
M2UX	-0.90281625366211	GTC secondary mirror UX position	mm	GTC secondary mirror UX position
M2UY	3.28916454315186	GTC secondary mirror UY position	mm	GTC secondary mirror UY position
M2UZ	-0.71310837604523	GTC secondary mirror UZ position	mm	GTC secondary mirror UZ position
MASKNAME	'NOMASK '	Mask name	N/A	Multi-object spectroscopy mask name.
MJD-OBS	55971.6491228745	Modified Julian day at observation start	Days	Modified Julian day at observation start
MOSAIC	'true '	Mosaic active or not	N/A	Whether CCD mosaic is active or not
MOVTYPE	'ONLYDOWN'	Direction of charge displacement	N/A	Direction of charge displacement: can be "ONLYDOWN", "ONLYUP", "ALT_START_UP", "ALT_START_DOWN"
NAMPS	2	Number of channels	Integer	Number of amplifier used during CCD readout
NAXIS	2	Number of data axis	Integer	Number of data axis, zero on primary fits header extension.
NAXIS1	1049	length of data axis 1	Pixels	Number of data pixel in axis 1
NAXIS2	2051	length of data axis 2	Pixels	Number of data pixel in axis 2
NSHIFTS	20	Number of lines charges are moved on the CCD	Integer	Number of lines charges are moved on the CCD in charge transfer/shuffling mode.
NUM_IMAG	1	Total number of images into the sequence	Integer	Sequence total number of images in frame transfer mode.
NUM_INDX	0	Image Index into sequence. Starts from 0.	Integer	Image Index within sequence in frame transfer mode. Starts from 0.

NUM_ROIS	1	Number of windows	integer	Number of CCD windows, maximum 5.
NUM_SHIF	2	Number of times charges are moved	Integer	Number of times charges are moved in charge transfer/shaffling mode
OBJECT	'NGC1234'	OSIRIS comment	N/A	Should be the user defined target name.
OBSCLASS	'science '	Observation class	N/A	This should be the observation class, like SCIENCE or CALIBRATION. Duplication of OBSTYPE
OBSERVAT	'ORM '	Observatory name	N/A	Perhaps the name of the observatory (Roque de los Muchachos).
OBSERVER	'SA '	Observer Name	N/A	Observer name (SA = support astronomer).
OBSMODE	'OsirisDark'	Observation Mode	N/A	Instrument observing mode (for data factory use).
OBSTYPE	'Calib '	Observation Type	N/A	Observation type, should be either SCIENCE or CALIB.
OPENTIME	'12:23:17.593'	Open Shutter Time	HH:MM:SS	Time the OSIRIS shutter did open. Only appears if the shutter actually moved (that is, does not appear in bias images).
OPTCENTX	1000.	OSIRIS Optical Center X	Pixels	Position of optical center in the X direction
OPTCENTY	1001.	OSIRIS Optical Center Y	Pixels	Position of optical center in the Y direction
ORIGFILE	'Jan14_050116.fits'	Filename	N/A	Original FITS file name
ORIGIN	'GRANTECAN'	Organization responsible for creating the FITS	N/A	
OSFILT	' '	Order Sort Filter identifier	N/A	Order Sort Filter identifier
OSISTAT	1	OSIRIS status:	N/A	Flag to indicate osiris status.

		l=ok		l=OK
OSIVERS	1.	OSIRIS software and hardware version	N/A	OSIRIS software and hardware version
OSWAV	4500.	Order Sort Filter central wavelength	Angstrom	Order Sort Filter central wavelength
OUTMODE	'TWOCCDS_A'	OutputMode	N/A	CCD readout output mode.
PCOUNT	0	required keyword. must = 0	N/A	Size of special data area.
PI	'mespinoza'	Personal Investigator	N/A	Principal investigator of the project for which the observation was taken.
PRESCAN	'true '	Prescan active or not	Boolean	Whether the prescan was active or not.
PRESSURE	777.289978027344	Ambient atmospheric pressure (hPascal)	hectoPascal	Ambient atmospheric pressure.
RA	'+9:35:13.247'	Telescope right ascension (HH:MM:SS) , h:m:s	HH:MM:SS.sss	Telescope right ascension.
RADEG	143.80519462267	Telescope right ascension in decimal degrees.	Degrees	Telescope right ascension in decimal degrees.
RADESYS	'FK5 '	Equatorial coordinate system	N/A	Reference system for World Coordinate System.
READTIME	'05:35:17.972'	Approximate time when read starts	HH:MM:SS	Approximate time when read starts!! NOT CLEAR
ROI_X	2098	X-Size of windows in pixels	Unbinned Pixels	X-Size of the CCD area actually readout, unaffected by binning. Equal to the whole CCD, except when using windows.
ROI_Y	4102	Y-Size of windows in pixels	Unbinned Pixels	Y-Size of the CCD area actually readout, unaffected by binning. Equal to the whole CCD, except when using windows.

ROI_1X	0	X-Origin of ROI-1 in RDI-RDW	Pixels	X of lower left corner position of the window. Unclear description, what is RDI-RDW?
ROI_1Y	0	Y-Origin of ROI-1 in RDI-RDW	Pixels	Y of lower left corner position of the window. Unclear description, what is RDI-RDW?
ROI_2X	0	X-Origin of ROI-1 in RDI-RDW	Pixels	If a second window is defined, this is its X of lower left corner position.
ROI_2Y	0	Y-Origin of ROI-1 in RDI-RDW	Pixels	If a second window is defined, this is its Y of lower left corner position.
ROTANG	-61.8845	Rotator position angle in degrees	Degrees	Rotator position angle in degrees.
RSPEED	100	Readout Speed Khz	kHz	CCD read out speed in kHz
SEQUENCE	'SIMPLE '	Basic sequence mode	N/A	CCD read out sequence mode
SIMPLE	T	file does conform to FITS standard	Boolean	Whether the file conform to fits standard.
SIMVAL	0	SimulateVal	N/A	Should be always 0. Data are never simulated!
SIMTYPE	0	SimulateType	N/A	Should be always 0. Data are never simulated!
SIMULATE	'false '	Simulate active or not	Boolean	Should be always false. Data are never simulated!
SLITPA	0.	Slit pa	Degrees	Slit position angle in degrees from North toward east
SLITW	1.	Slit width	Arcsec	Slit width in arcsec
TAMBIENT	0.23	Ambient temperature in Celsius degrees	Degrees Celsius	Ambient temperature in Celsius degrees
TELESCOP	'GTC '	Telescope	N/A	Telescope name
TFBANDW	14.93255615	filter bandwidth	Angstrom	Tunable filter band width.

		after z processing		
TFID	'TF_RED '	TF identifier	N/A	Tunable filter unique name.
TFTEMP	' '	TF temperature	Degrees Celsius	Tunable filter temperature.
TFWAVEL	8234.4411	filter wavelength after z processing	Angstrom	Tunable filter central wavelength.
TITLE	' '	Title given to the image	N/A	Image title. Duplicate OBJECT
TRIMSEC	'[280:1049,1:2000]'	TRIM section	Pixels	Trim section. Should indicate the ccd vignetted region.
VBIN	'true '	Vertical Binning	Boolean	Whether binning was applied in the vertical direction. See also HBIN.
WINDDIRE	177.	Wind direction (from) in degrees from N to E.	Degrees	Wind direction (from). In degrees from north toward east.
WINDSPEE	5.96	Wind speed in m/s	m/s	Wind speed in m/s

9.2 Astrometry with OSIRIS

This section of the User Manual is devoted to explain how to perform a sub-pixel precision astrometry of OSIRIS images from minimum header information. The instructions are given in an example-oriented fashion.

As mentioned in Section 1.1, the instrument contains a camera composed by a mosaic of two CCDs arranged along the largest dimension, with 4192 x 2098 physical pixels each (however, throughout this section of the Manual, any reference to pixel coordinates is given in the standard binned operation mode of OSIRIS). A `fits` image (extensions 1 and 2) with two headers plus a zero extension header is generated for each detector reading. Both non-zero extensions include information about the telescope pointing, expressed through the keywords `RA` and `DEC`. The projection of the telescope optical axis on detector 1 roughly coincides with the pixel (462.5, 995). If the position angle of rotator (header keyword `IPA`) is 150.54036 degrees, the images are oriented with North up, East left. At first order, the mean plate scale is 0.254 arcsec/pixel (binned) and the physical gap between CCDs is 12 pixel wide. Additionally, the CCD2 is shifted in 2 pixels with respect to the CCD1 in the positive Y-direction.

9.2.1 Input Data

As initial condition, individual extension frames to be astrometrically calibrated must be corrected for zero level (including overscan) and flat field.

- Construct an input source catalog with logical positions of astrometric sources (preferably point-like objects) by using the task `daofind` in IRAF `noao.digiphot.apphot` package, specifying input image, mean FWHM of image features to be detected, as well as the detection threshold and standard deviation of the background. Alternatively, the `SExtractor` software (Bertin & Arnouts, 1996) can be used for this purpose. The `Starlink GAIA` software has the `SExtractor` embedded: after loading any image, it is possible to obtain a catalog of sources invoking the task `Object Detection`, in the `Image-Analysis` menu. `GAIA` provides the facility to see the extracted sources on the image, pick on a specific source and edit the output list. You can also play with background parameters and re-do detection/extraction. In both cases, the required output is a list with x,y logical positions (here named `xy.cat`).
- Construct a catalog with the reference positions of astrometric stars in equatorial coordinates for a defined equinox (usually J2000.0) and epoch of observation (i.e. proper motion corrected coordinates). This catalog is simply an ASCII file with an ID (optional), right ascension and declination in degrees (here called `radec.cat`). It doesn't matter if the angular coverage of the catalog exceeds the OSIRIS field for a given detector.
- Match both files using IRAF `imcoords.ccxymatch`. The output file is `radecxy.cat`, an ASCII list with the matched coordinates in a suitable format to be used as input in the following task. An example of the line command is:

```
ccxymatch xy.cat radec.cat radecxy.cat toleranc=5 ptoleranc=40
xin=xxxx.x yin=yyyy.y xmag=0.254 ymag=0.254 xrotation=180.
yrotation=0. projection="tan" lngref=aaa.aaaaaa latref=+/-dd.ddddd
lngcolumn=2 latcolumn=3 xcolumn=2 ycolumn=3 lngunits="degrees"
latunits="degrees" matchin="triangles" nmatch=40
```

Some cautions should be taken before running `ccxymatch`: (i) it is necessary that a position on the detector (given by parameters `xin`, `yin`) corresponds to a previously known sky position (given by parameters `lngref`, `latref`); ideally, this position should be close to the image centre, (ii) `xrotation` and `yrotation` correspond to a image orientation with north up and east left, (iii) depending on the method used for generating input files, the parameters `lngcolumn`, `latcolumn`, `xcolumn` and `ycolumn` could change, and (iv) `nmatch` must be smaller than the number of lines in `xy.cat`. Possible redundancies in the output file will be naturally discarded in the following step. Use the command `help ccxymatch` at the IRAF prompt to obtain more information.

9.2.2 Astrometric Solution

To find the astrometric solution for each frame, the IRAF `imcoords.ccmmap` task should be used. Figure 9.1 below represents the mean distortion vectors (in the sense of deviation of positions from linear solution respect to the general -full precision- astrometric solution) in

pixels (5 times magnified), for each OSIRIS detector and without filter. For any broad-band filter, measured distortions are similar.

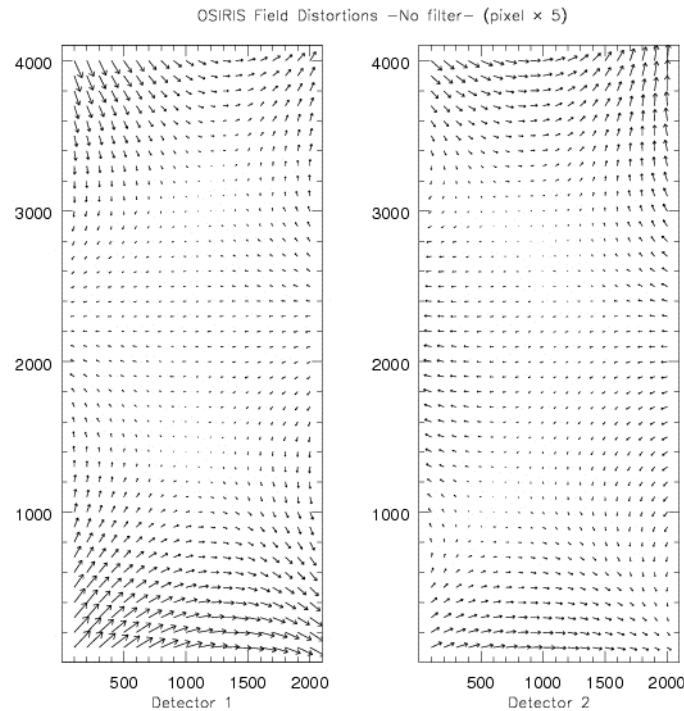


Figure 9.1.- OSIRIS field distortion without filters.

Obviously, the non-linear components of an astrometric solution for both detectors are not negligible. For this reason, a “general” scheme (linear terms plus distortion) must be chosen to find a solution with sub-pixel precision. An example of a `ccmap` task command could be the following:

```
ccmap radeccxy.cat image.db images="image" results=image.res xcol=3
ycol=4 lngcol=1 latcol=2 lngunits="degrees" latunits="degrees"
insystem="j2000" refsystem="j2000" projection="tnx"
fitgeometry="general" function="polynomial" xxorder=5 yyorder=5
yxorder=5 xyorder=5 xxterms="full" yxterms="full" maxiter=100
reject=3.0 update=yes pixsyst="logical"
```

It is desirable to execute the task in interactive mode. With this feature activated you can pick the outliers of the initial fit (e.g. encircled plus marks in figure below) and find a satisfying solution clicking on 'f' key:

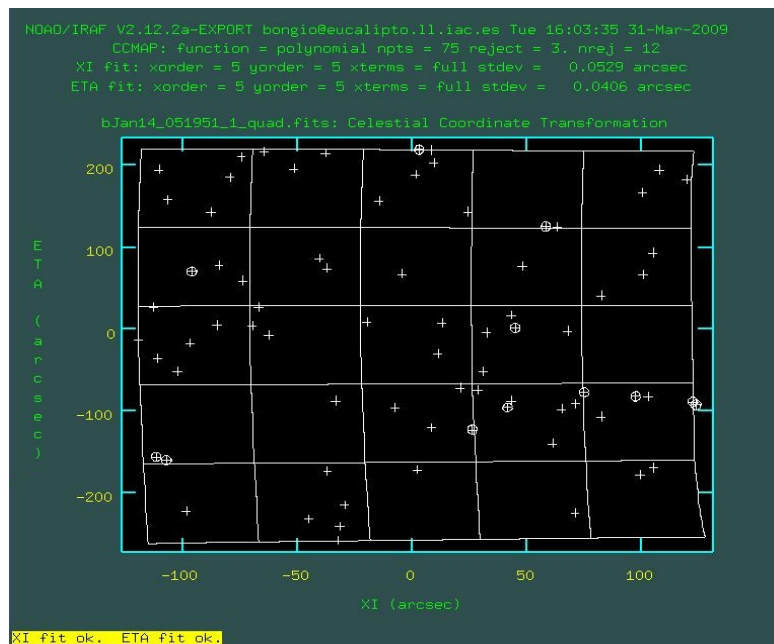


Figure 9.2.- Example of the IRAF task ccmmap solution.

The commands associated to the interactive option and further details are given in the task's help. If `update` parameter is turned to "yes", the task appends the parameters of the astrometric solution (here named `image.db`) to the image header. A `tnx` projection is highly recommended. As additional output, the file `image.res` contains a line for each astrometric object with the following structure:

Column 1: X (pixels)

Column 2: Y (pixels)

Column 3: Ra / Longitude (degrees)

Column 4: Dec / Latitude (degrees)

Column 5: Fitted Ra / Longitude (degrees)

Column 6: Fitted Dec / Latitude (degrees)

Column 7: Residual Ra / Longitude (arcseconds)

Column 8: Residual Dec / Latitude (arcseconds)

9.2.3 Mosaic Composition

To optionally create a mosaic in WCS from individually corrected frames, use first the `mscimage` task of the `mscred` package. This task puts in a common system both WCS referenced frames of any scientific image. Input images are the exposures to be resampled into a single image and the output must match the number of input images. Use a minimum of 30 grid points (`nx`, `ny`) over the input image to determine the mapping function. Also, the parameters `fitgeometry`, `function`, `x/y orders` and `x/y terms`, should match

those previously selected in the `ccmap` task. Once both frames are in a common reference system, you can combine both frames to obtain a single image using the task `imcombine`, setting before the parameter `offsets` to “`wcs`”. An example of a resulting mosaic is shown below (an astrometrically calibrated image of the Galactic cluster M67 with 2MASS point sources overlaid; standard deviation of the fit: 0.04 arcsec).

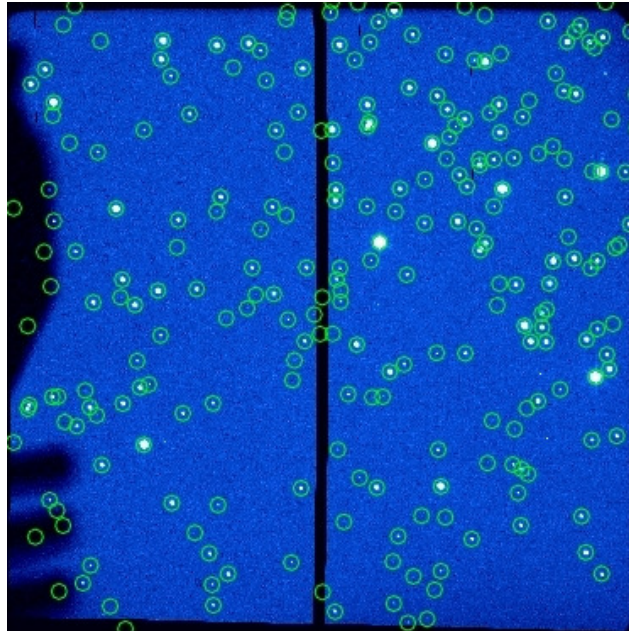


Figure 9.3.- Example of an OSIRIS mosaic.

9.2.4 Composing a first-order mosaic from raw data

To create a mosaic from the raw frames of a scientific image (valid up to first order), proceed as follows (assuming standard 2 x 2 binning):

- Create an empty fits image with 2110 × 2051 pixel.
- Rotate the CCD1 frame in 0.02386 degrees around the pixel (525.0,1026.0).
- Rotate the CCD2 frame in 0.04067 degrees around the pixel (525.0, 1026.0).
- Shift CCD2 in X=11.82013 and Y=1.64119 pixels.
- Copy the CCD1 frame in the region [1:1049, 1:2051] and the rotated CCD2 frame in the region [1050:2110, 1:2051] of the empty image recently created.
- Apply the instructions above to obtain a WCS solution for the whole mosaic.

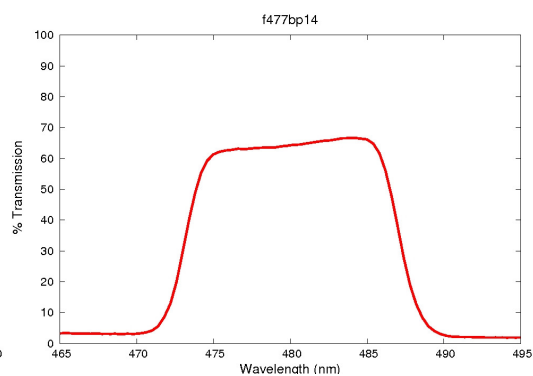
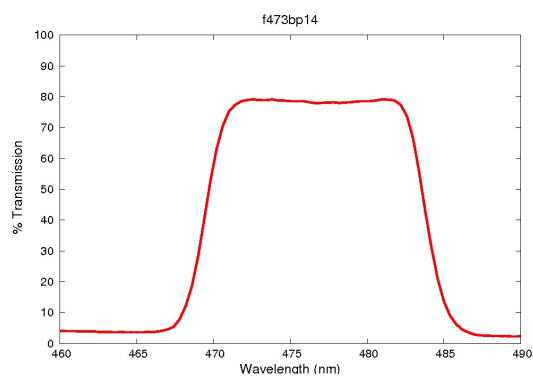
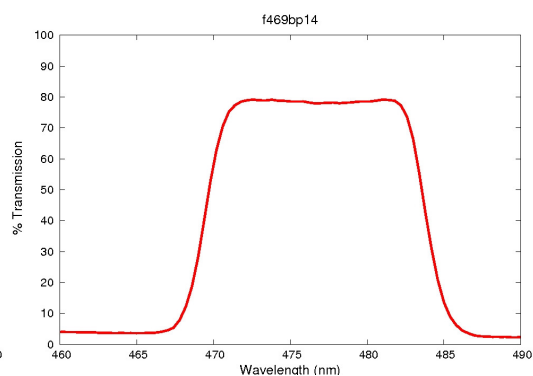
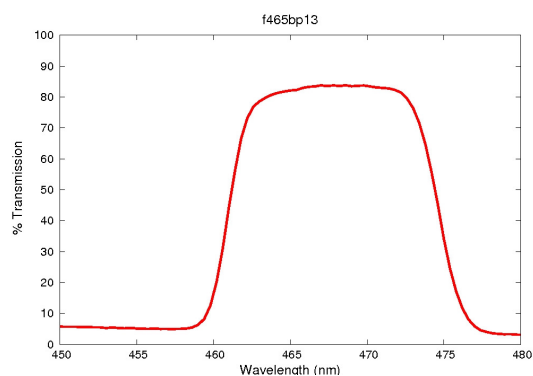
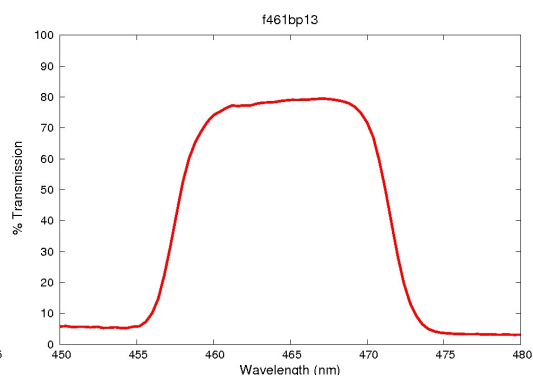
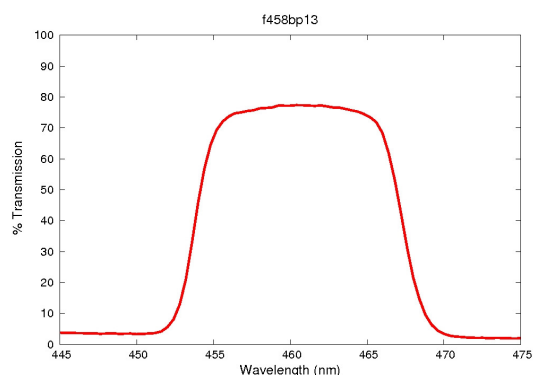
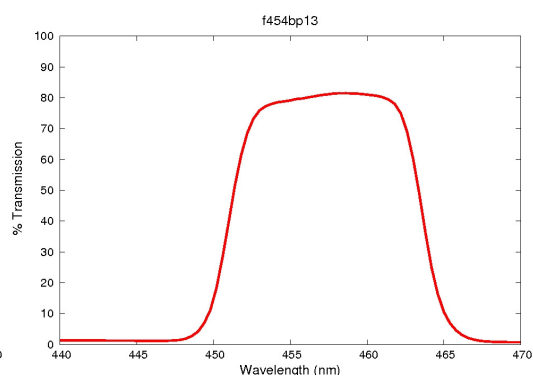
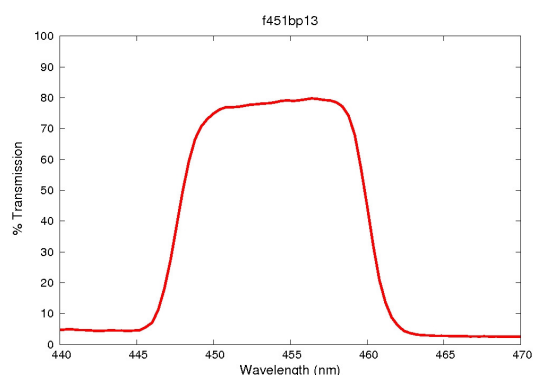
All this process can be executed in a direct way by using the pre-imaging MOS script (see Section 7.6.4.1). Also, note that from September 2012, a WCS solution is provided in OSIRIS FITS headers, hence a direct WCS mosaicking is possible. For a more precise astrometric solution, please follow the instructions described in Sections 9.2.2 and 9.2.3.

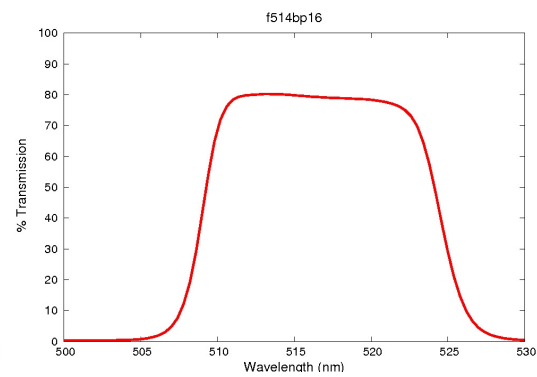
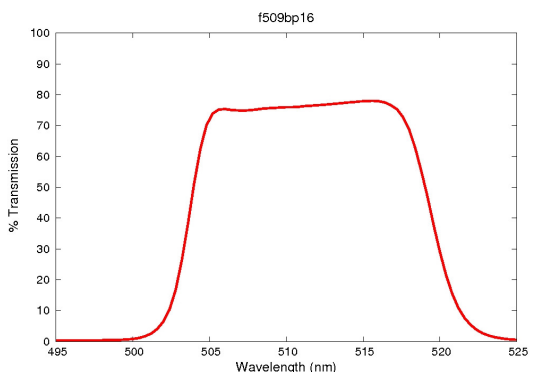
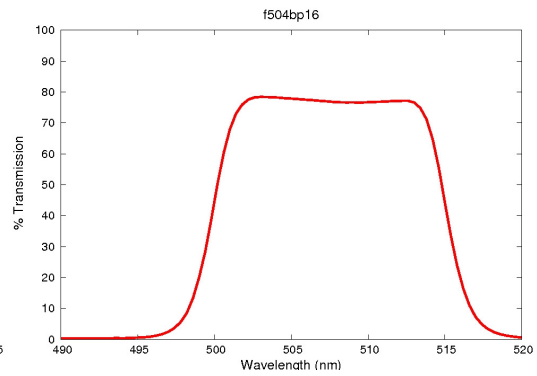
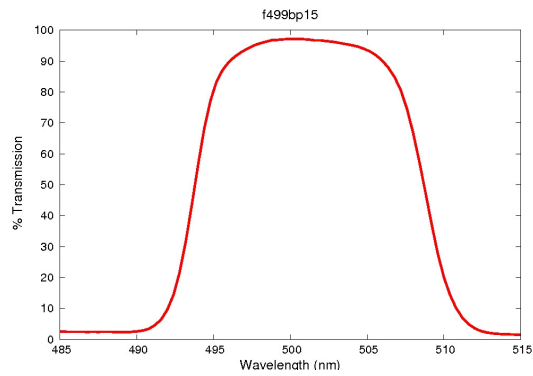
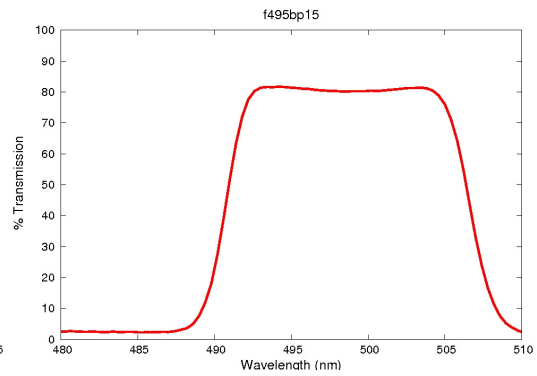
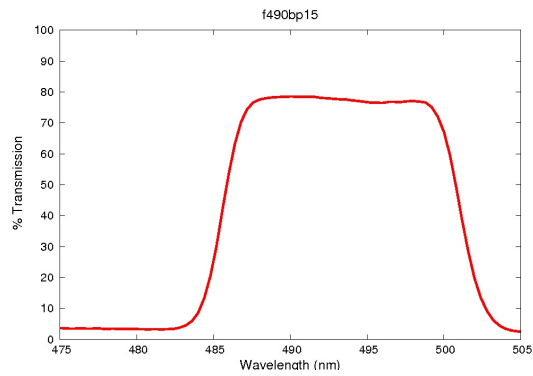
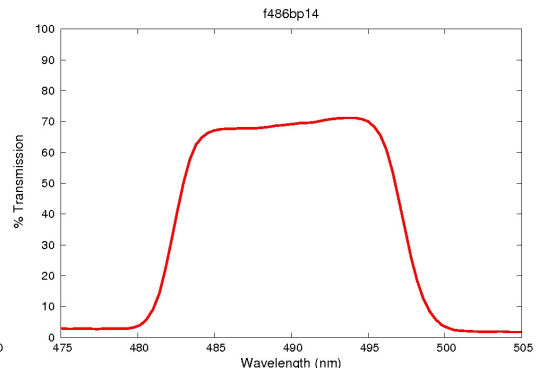
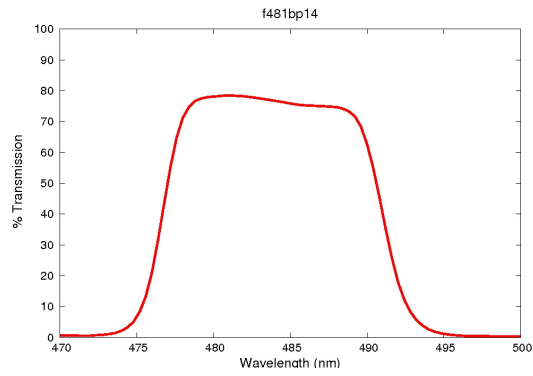
10 OSIRIS OS FILTER CHARACTERISTICS

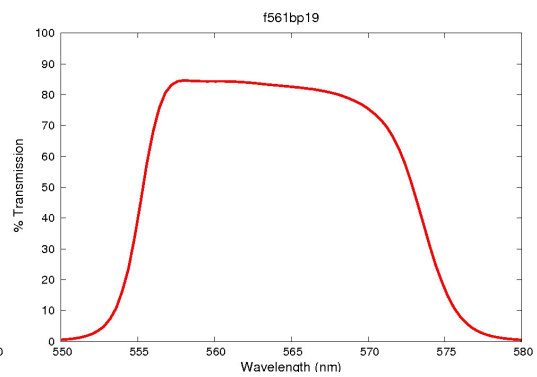
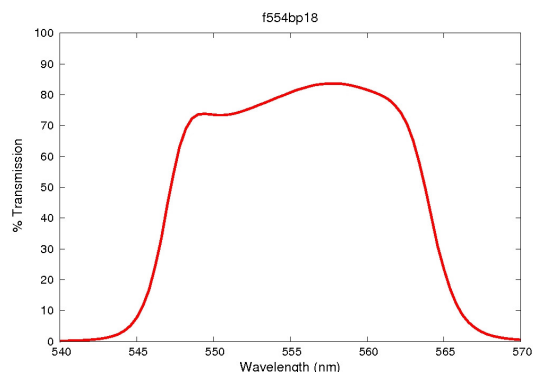
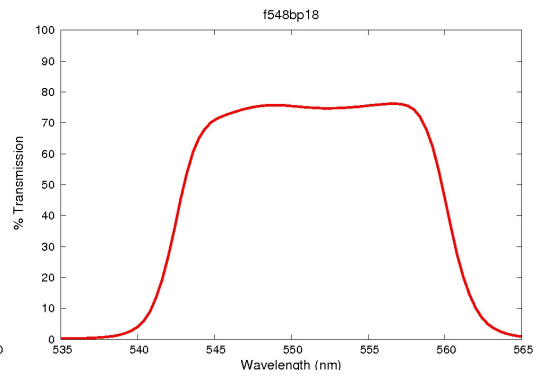
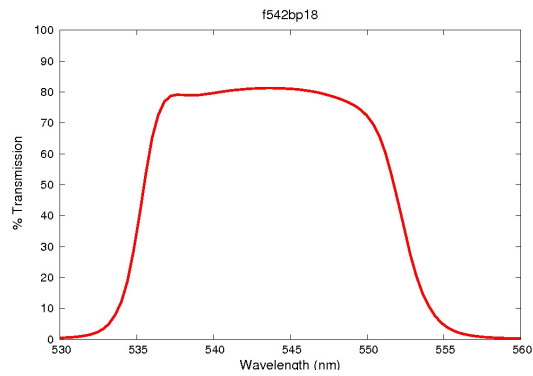
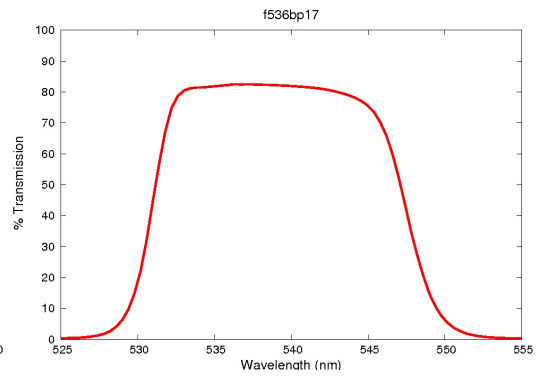
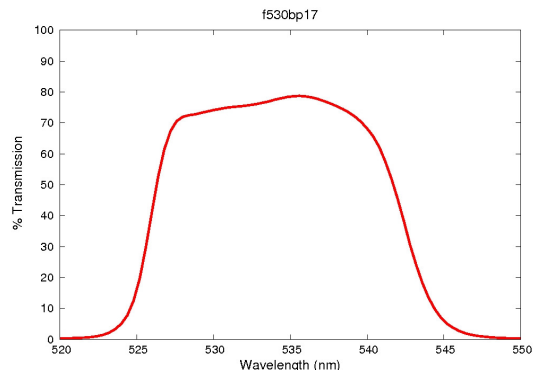
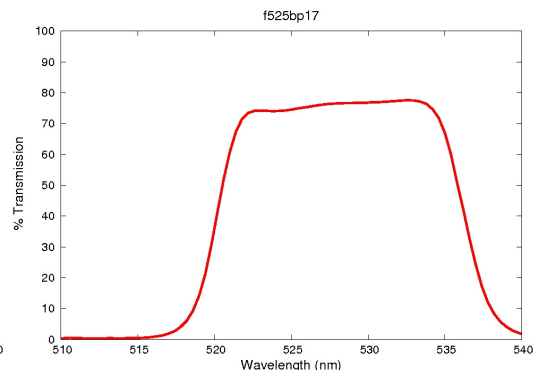
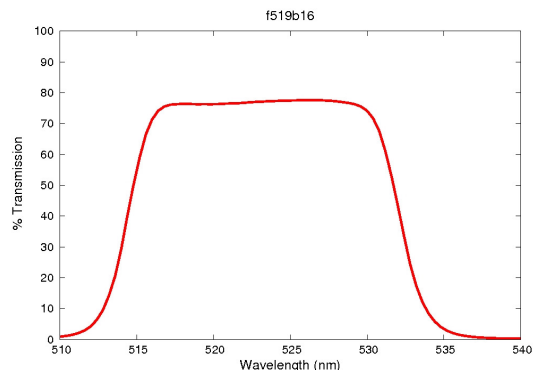
The following tables and figures list the complete OS filter set corresponding to OSIRIS Blue and Red Tunable Filters.

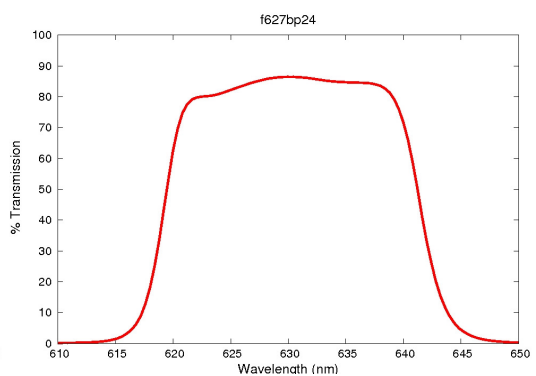
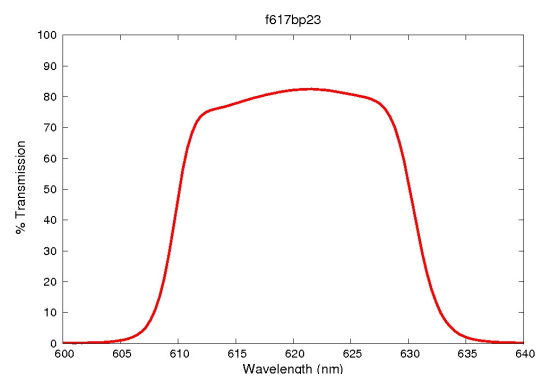
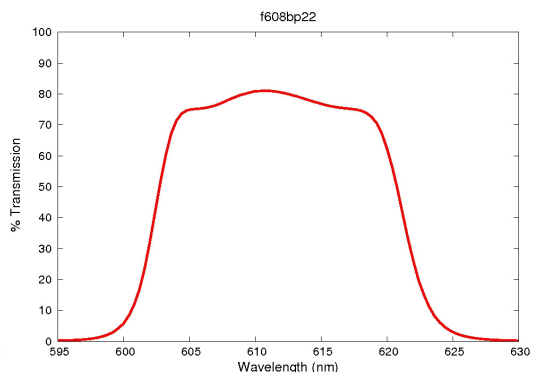
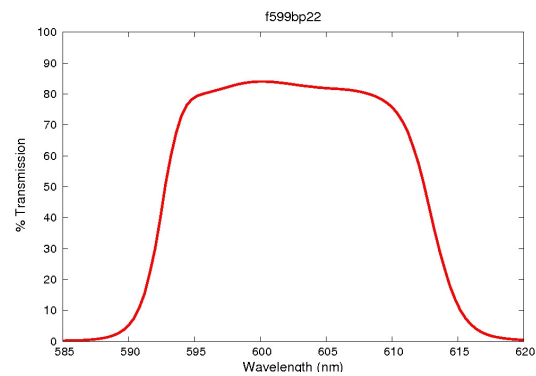
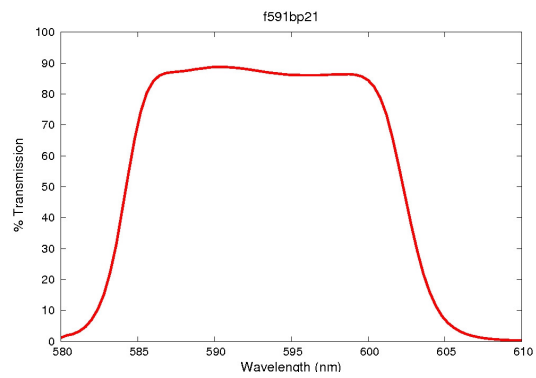
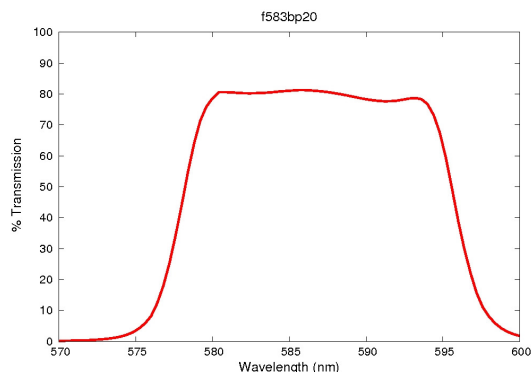
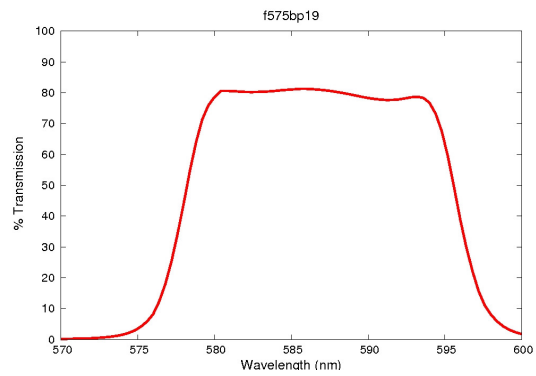
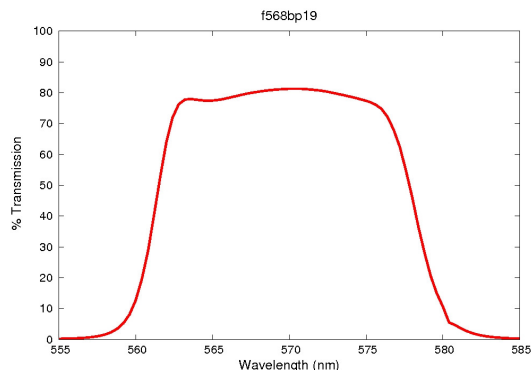
10.1 Blue Tunable Filter

Filter ID	λ (nm)	FWHM (nm)	TF λ range (nm)	Filter ID	λ (nm)	FWHM (nm)	TF λ range (nm)
f451/13	450.7	13.1	448 - 458	f525/17	524.6	16.7	528 - 533
f454/13	454.3	13.2	458 - 461	f530/17	530.1	16.8	533 - 538
f458/13	457.9	13.3	461 - 464	f536/17	535.7	17.0	538 - 543
f461/13	461.5	13.4	464 - 468	f542/18	541.6	17.8	543 - 550
f465/13	465.1	13.5	468 - 473	f548/18	547.8	18.0	550 - 556
f469/14	469.0	14.0	473 - 476	f554/18	554.1	18.2	556 - 562
f473/14	473.1	14.1	476 - 481	f561/19	560.8	19.0	562 - 569
f477/14	477.2	14.2	481 - 484	f568/19	567.9	19.2	569 - 576
f481/14	481.4	14.4	484 - 489	f575/19	575.0	19.5	576 - 584
f486/14	485.6	14.5	489 - 494	f583/20	582.6	20.4	584 - 593
f490/15	490.0	15.1	494 - 498	f591/21	590.5	20.7	593 - 600
f495/15	494.7	15.2	498 - 503	f599/22	599.0	21.8	600 - 610
f499/15	499.5	15.4	503 - 506	f608/22	607.9	22.1	610 - 618
f504/16	504.2	15.5	506 - 511	f617/23	617.4	23.3	618 - 628
f509/16	509.1	15.7	511 - 516	f627/24	627.4	23.7	628 - 638
f514/16	514.0	15.8	516 - 522	f638/25	638.0	25.0	638 - 649
f519/16	519.1	16.5	522 - 528				









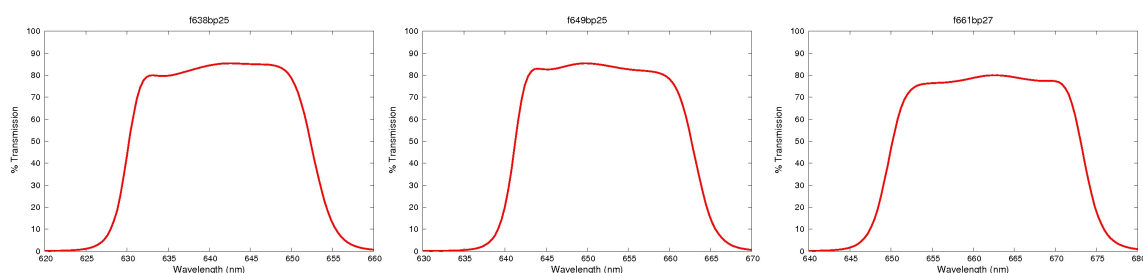
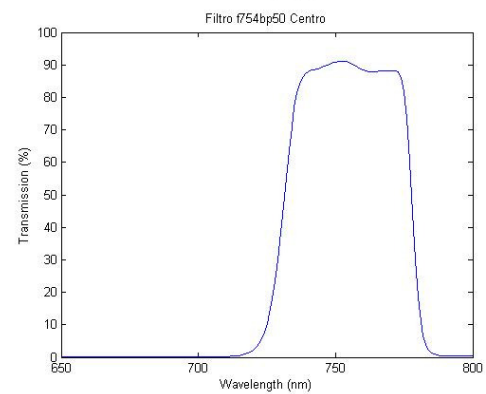
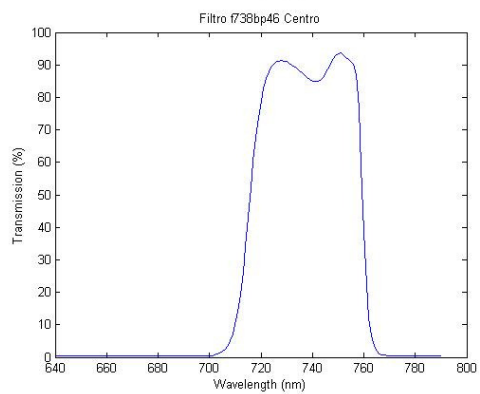
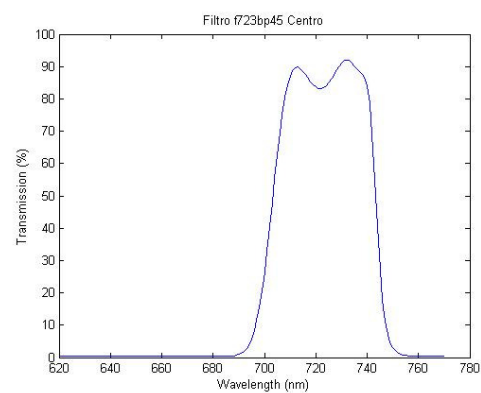
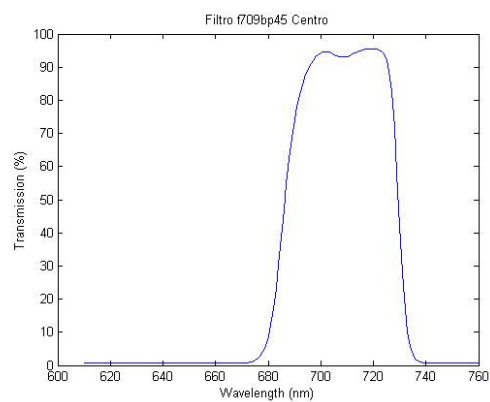
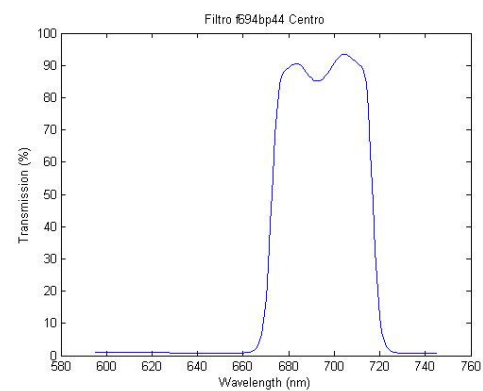
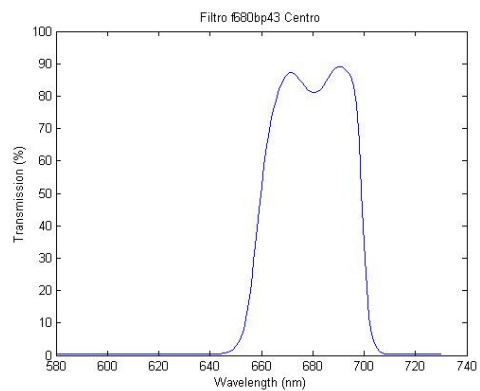
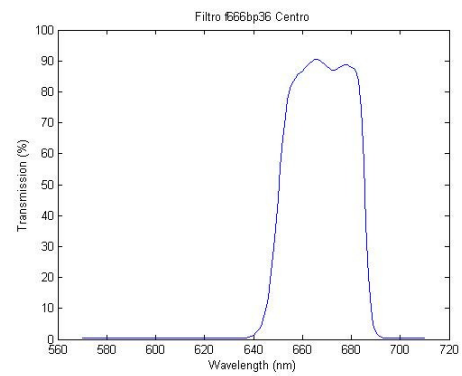
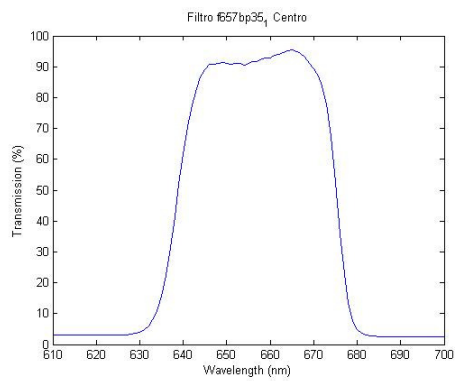
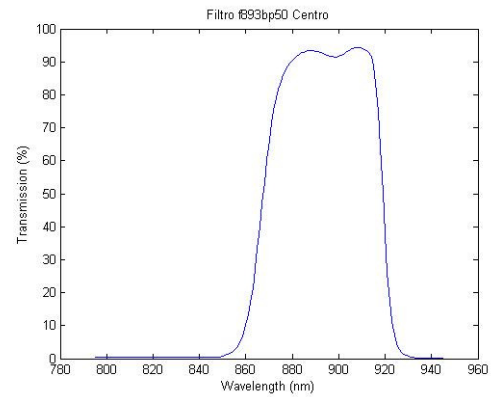
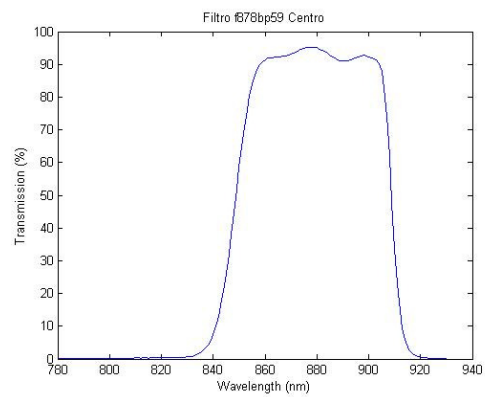
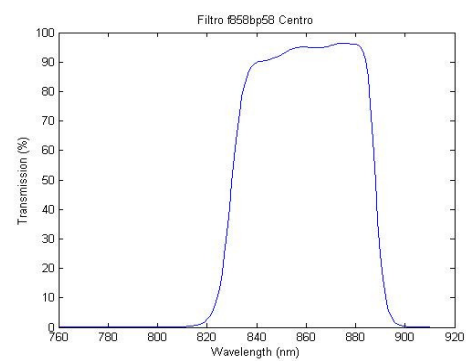
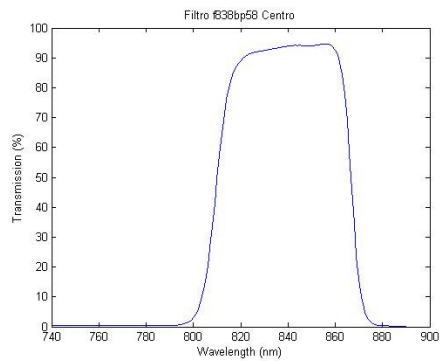
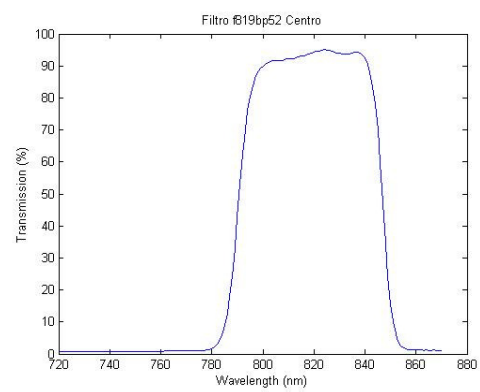
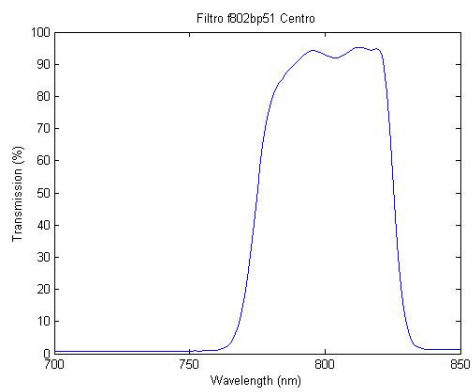
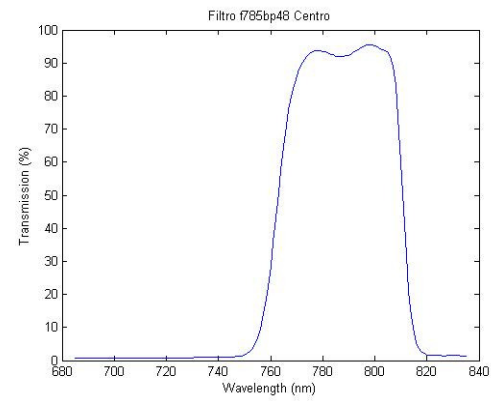
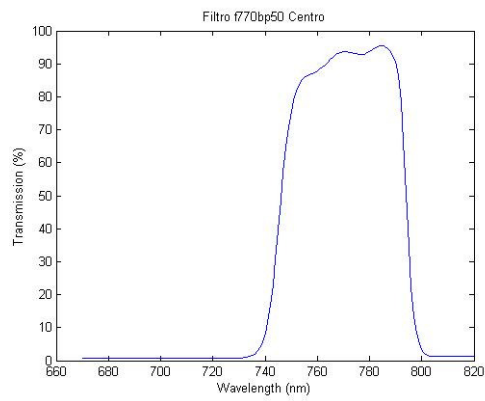


Figure 10.1.- From left to right and top to bottom: measured central spectral response of BTF Order Sorter Filters according to increasing wavelength, for normal incidence. Central wavelength and bandpass are indicated on top of each plot.

10.2 Red Tunable Filter

Filter ID	λ (nm)	FWHM (nm)	TF λ range (nm)	Filter ID	λ (nm)	FWHM (nm)	TF λ range (nm)
f657/35	657.20	35.0	649 - 660	f819/52	819.03	52.4	803 - 818
f666/36	666.84	35.5	660 - 670	f838/58	838.57	57.8	818 - 845
f680/43	680.21	43.2	670 - 685	f858/58	858.21	57.9	845 - 860
f694/44	694.38	44.0	685 - 695	f878/59	878.23	59.3	860 - 885
f708/45	708.84	44.9	695 - 710	f893/50	893.21	49.6	885 - 900
f723/45	723.29	45.2	710 - 725	f902/44	902.40	40.1	900 - 910
f738/49	737.98	46.1	725 - 735	f910/40	910.64	40.5	910 - 912
f754/50	754.25	49.6	735 - 755	f919/41	918.95	40.8	912 - 920
f770/50	770.57	49.7	755 - 770	f923/34	923.85	34.2	920 - 925
f785/48	785.58	47.6	770 - 788	f927/34	927.94	34.4	925 - 930
f802/51	802.02	51.3	788 - 803	f932/34	932.05	34.5	930 - 935





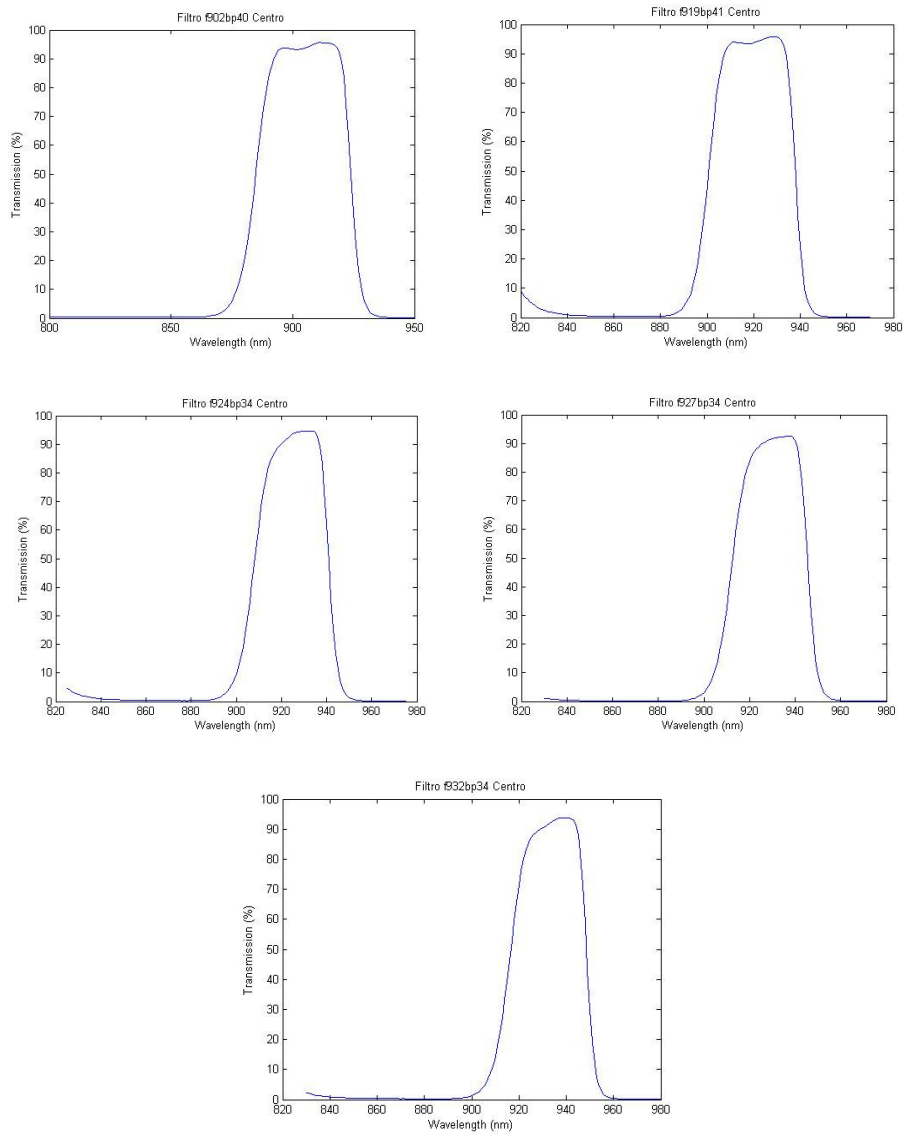
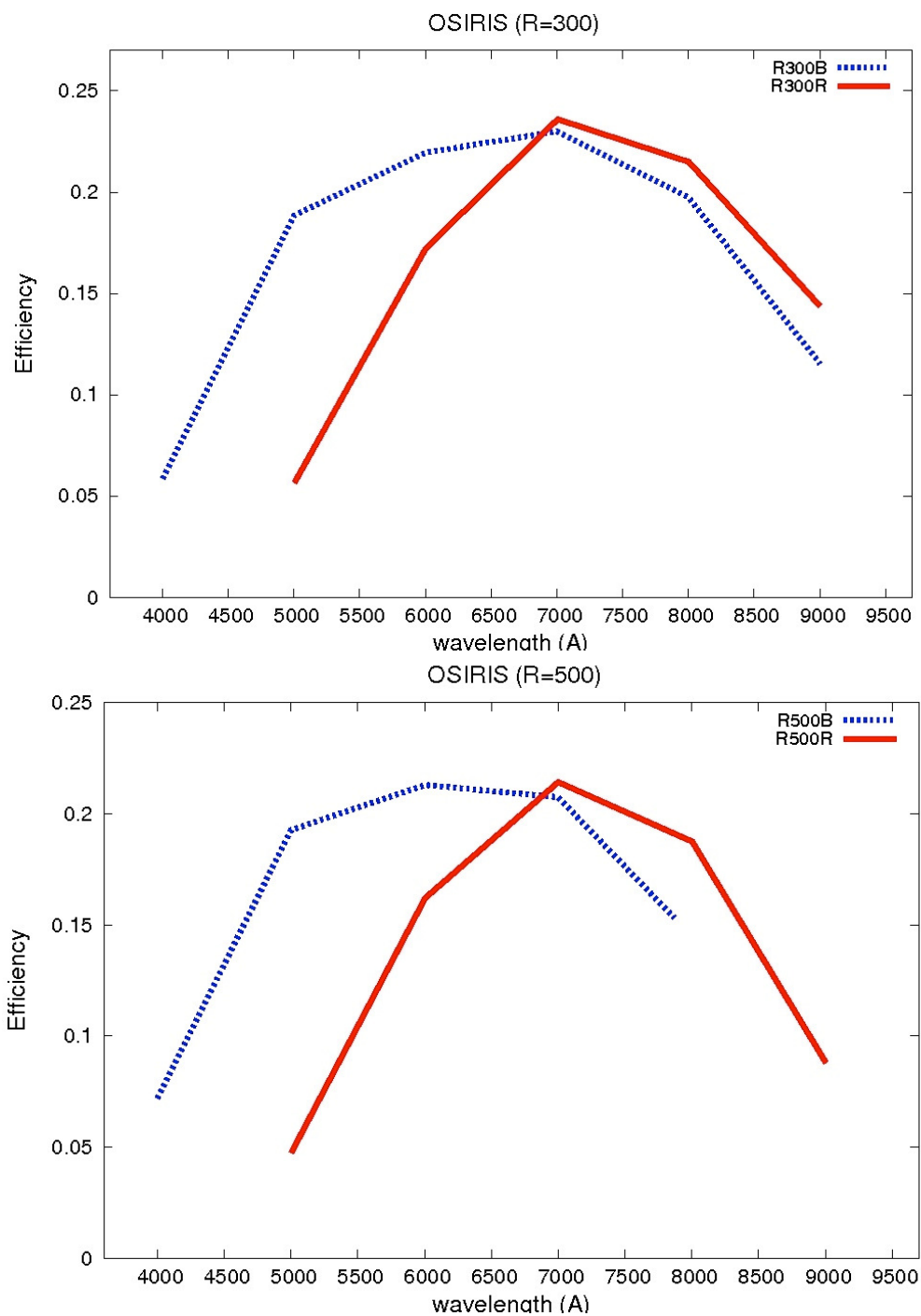
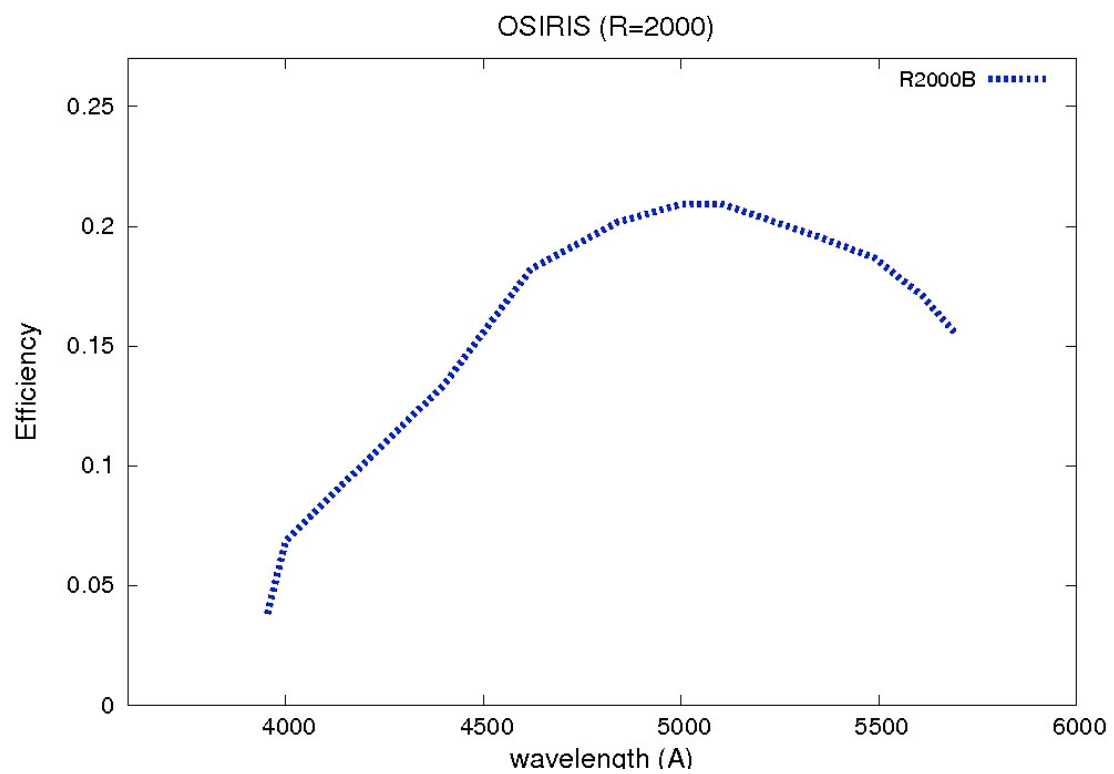
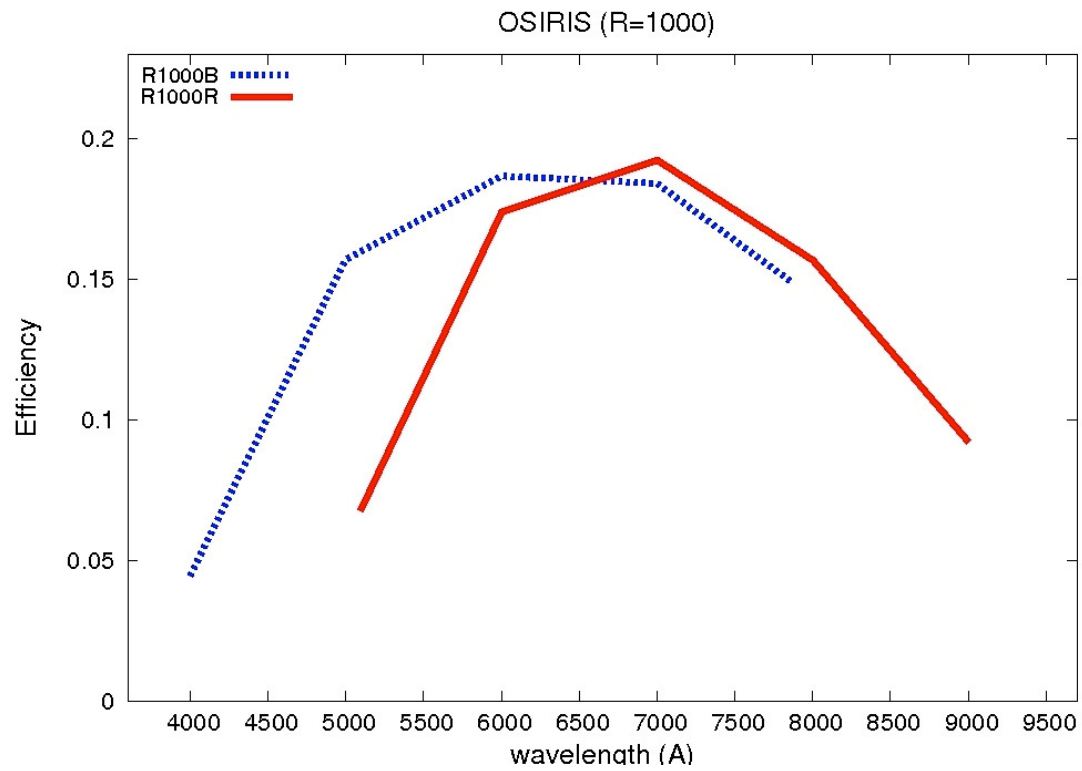


Figure 10.2.- From left to right and top to bottom: measured central spectral response of RTF Order Sorter Filters according to increasing wavelength, for normal incidence. Central wavelength and bandpass are indicated on top of each plot.

11 OSIRIS GRISMS/VPH EFFICIENCIES

Efficiency curves of the OSIRIS grisms/VPHs are measured using spectrophotometric standard stars observed through a wide slit, and are shown below. These transmission curves include all the system (telescope + OSIRIS optics + detectors):





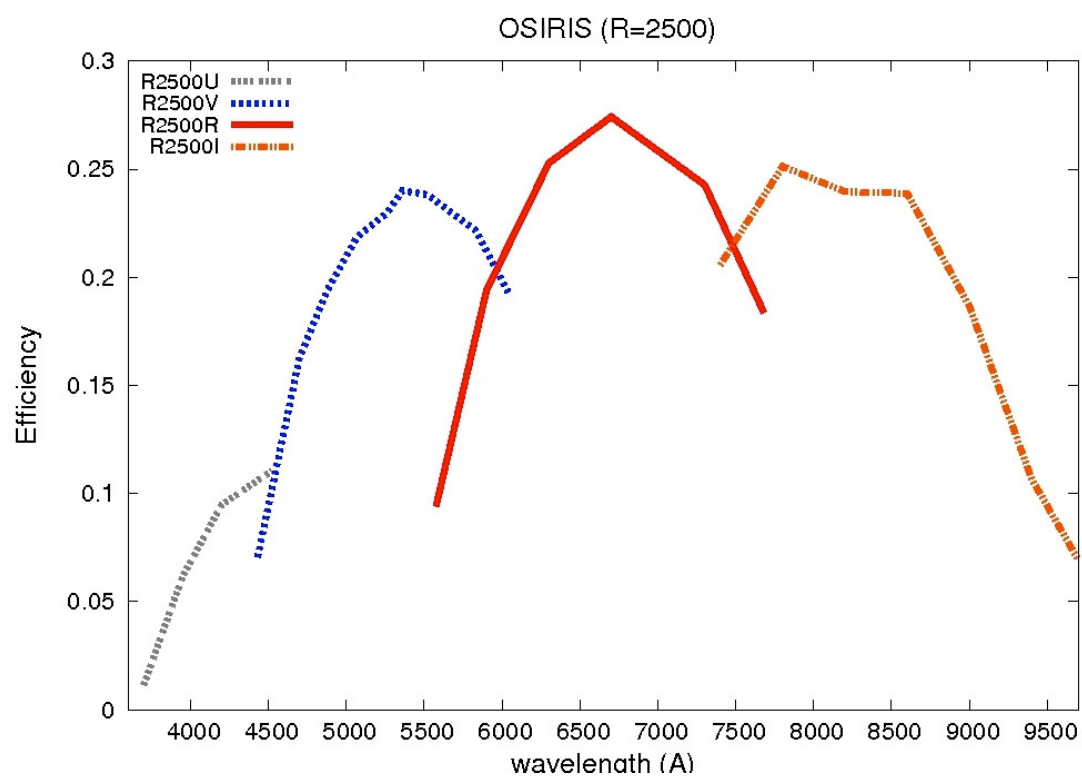
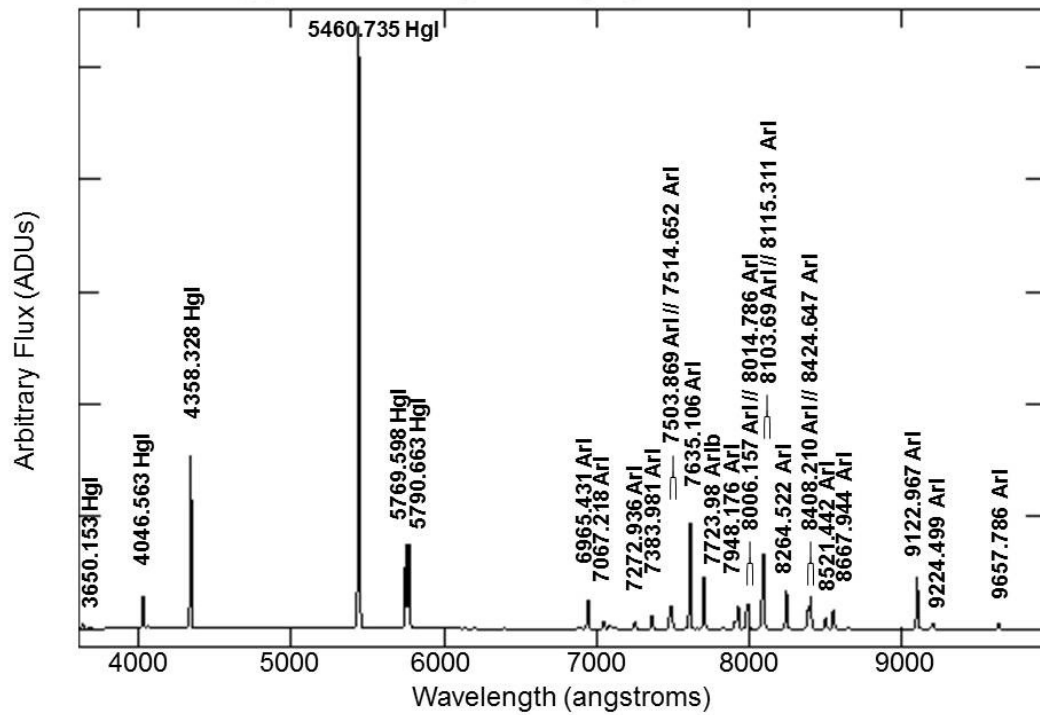


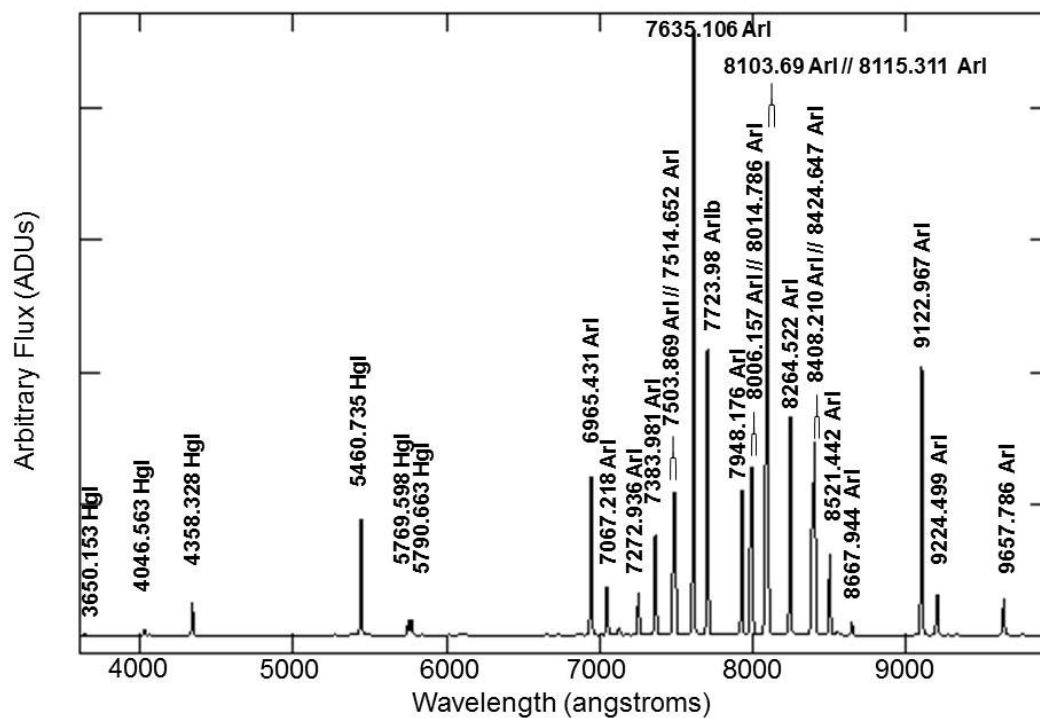
Figure 11.1.- From top to bottom, overall efficiencies for OSIRIS gratings/VPHs.

12 OSIRIS INDIVIDUAL ARC LINE MAPS

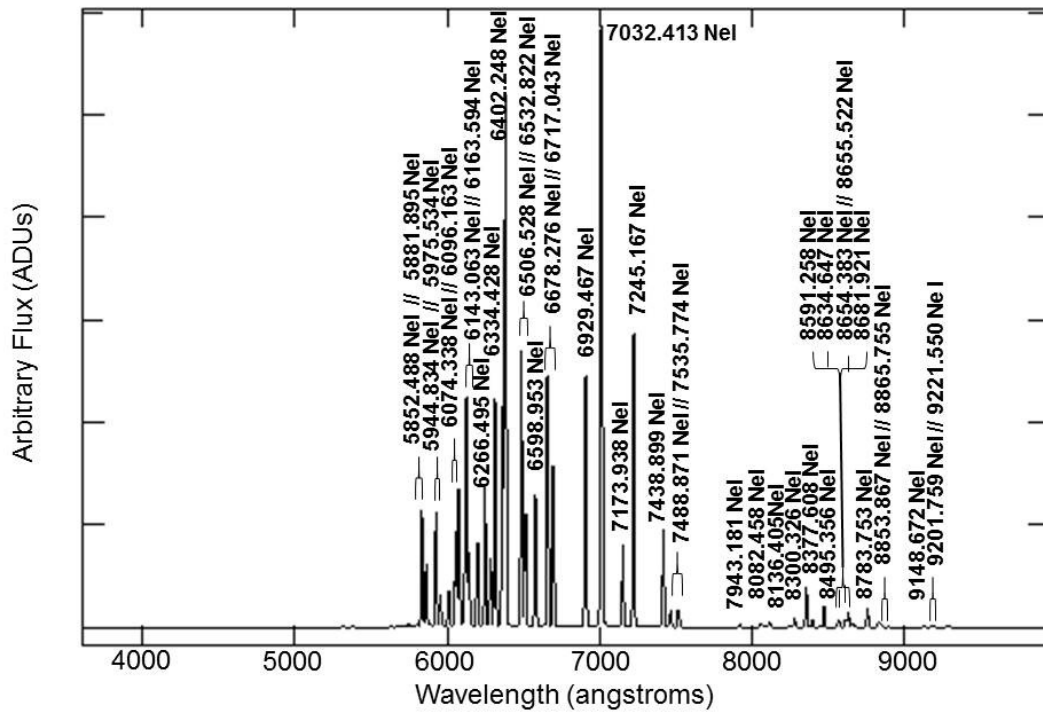
OSIRIS R300B: HgAr calibration lamp



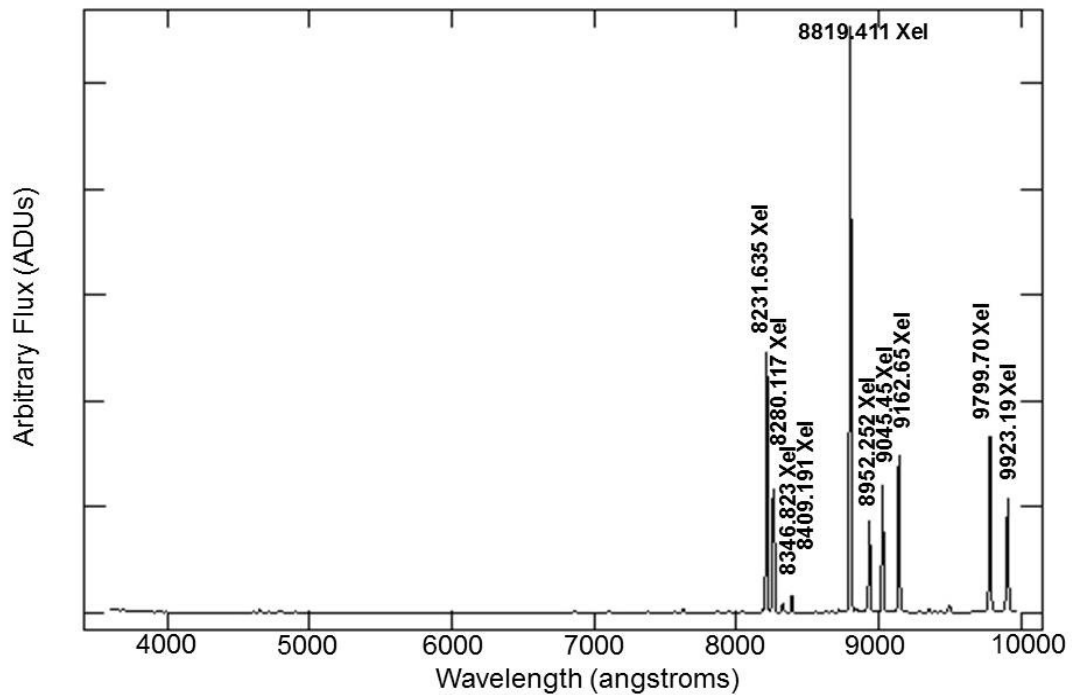
OSIRIS R300B: HgAr calibration lamp (Ar lines)



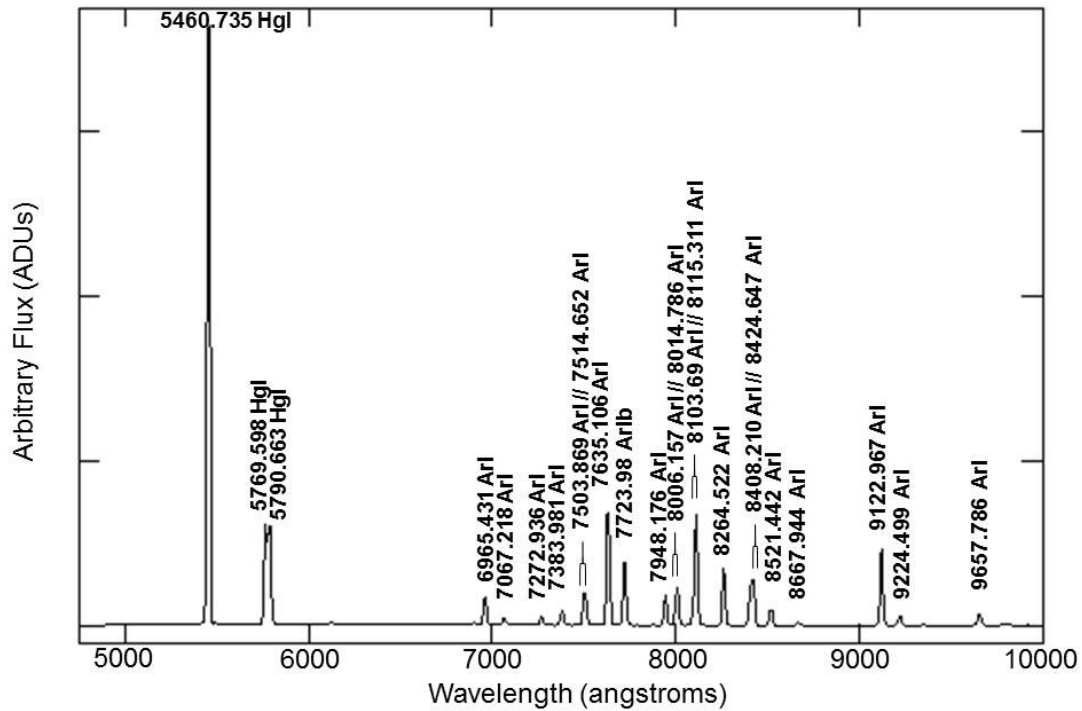
OSIRIS R300B: Ne calibration lamp



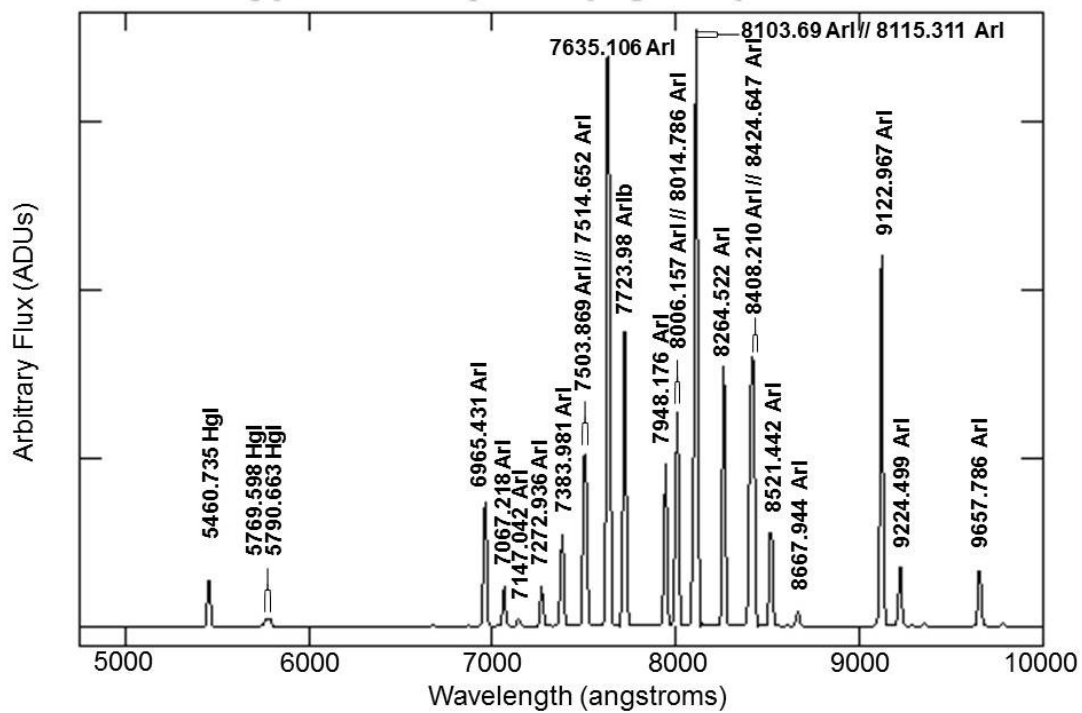
OSIRIS R300B: Xe calibration lamp



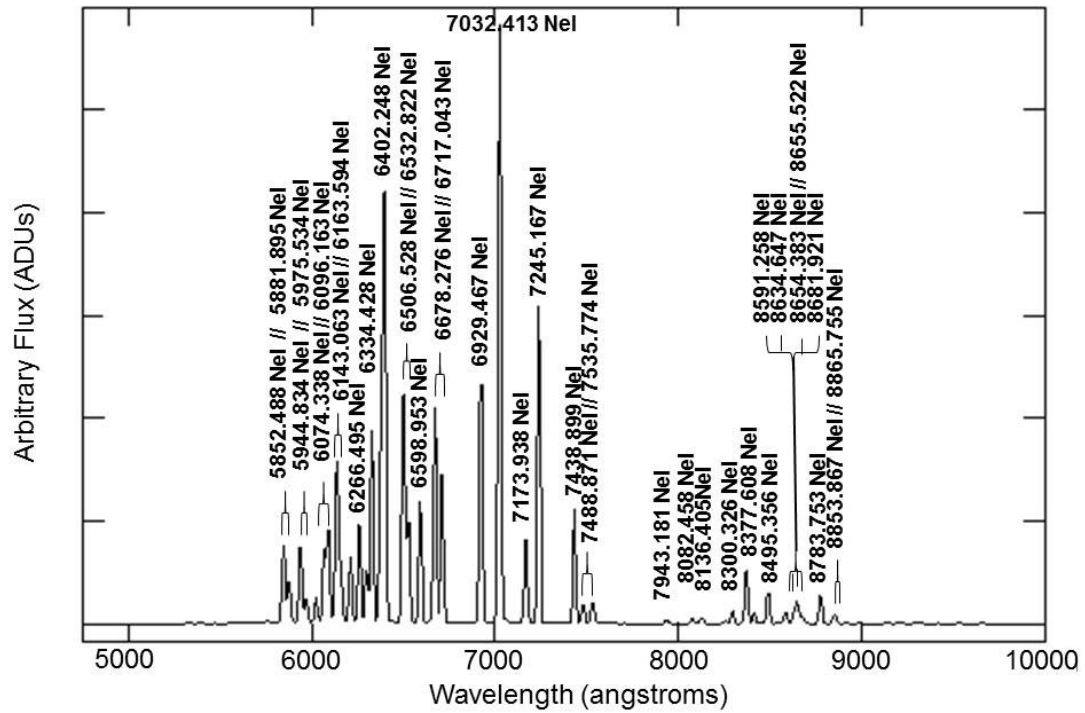
OSIRIS R300R: HgAr calibration lamp



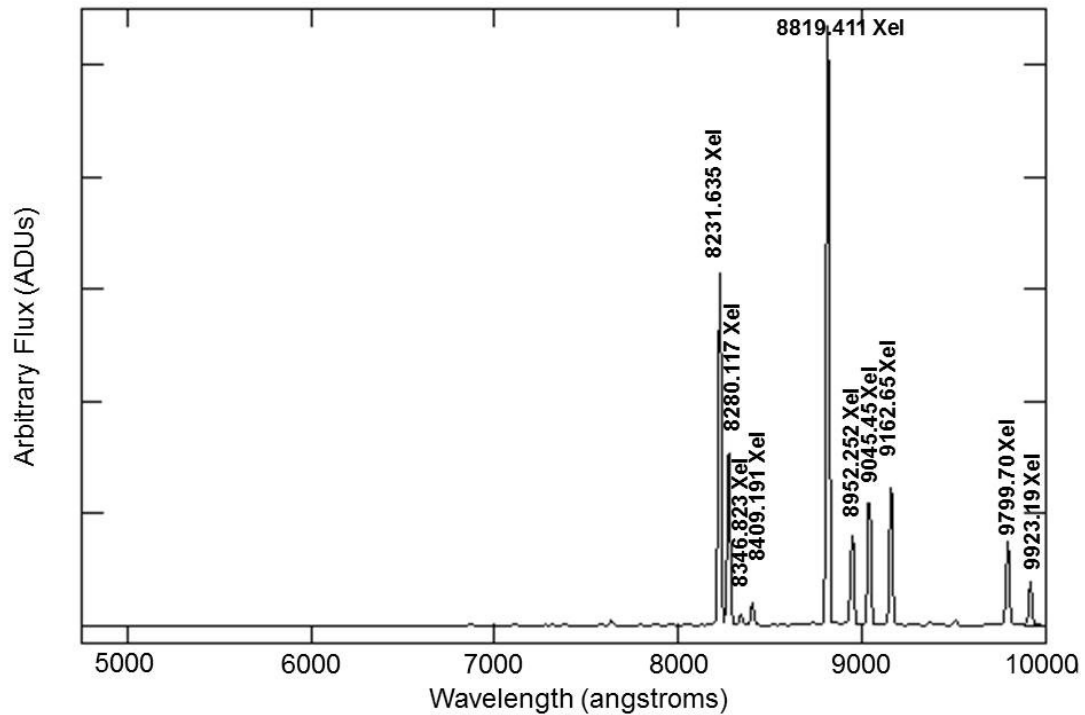
OSIRIS R300R: HgAr calibration lamp (Ar lines)



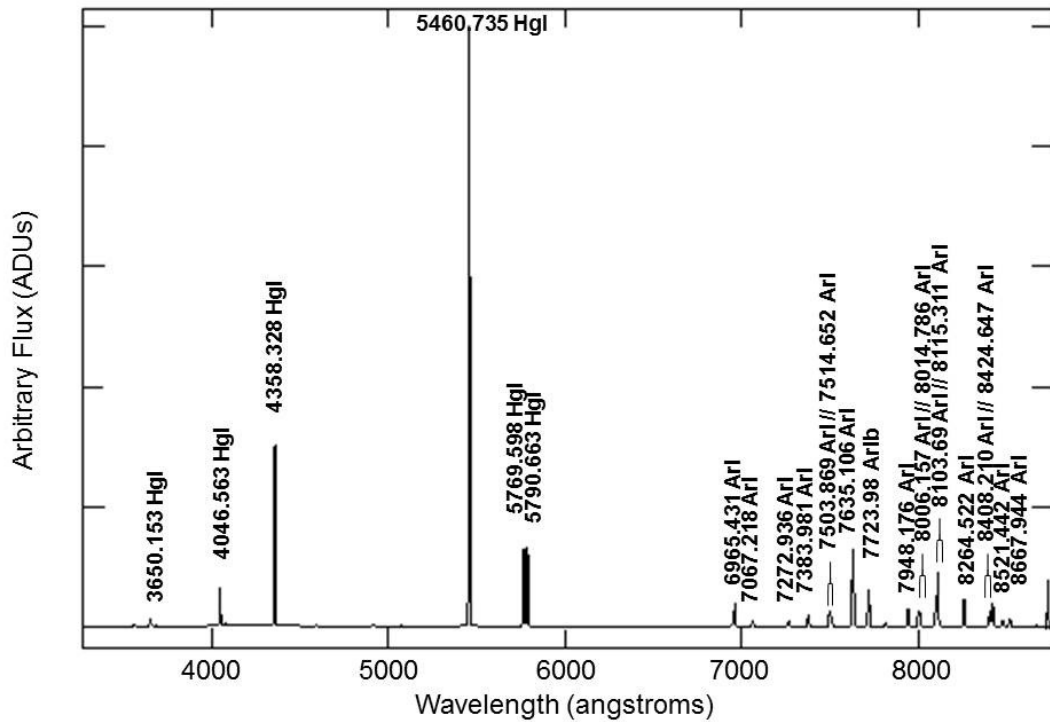
OSIRIS R300R: Ne calibration lamp



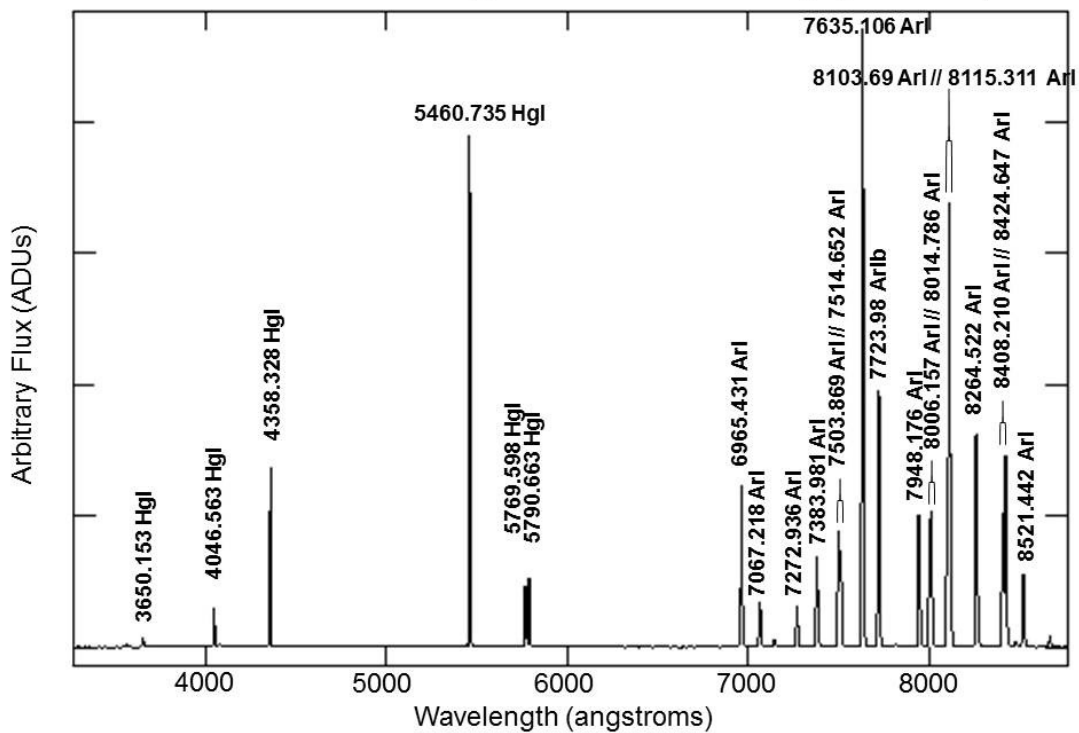
OSIRIS R300R: Xe calibration lamp



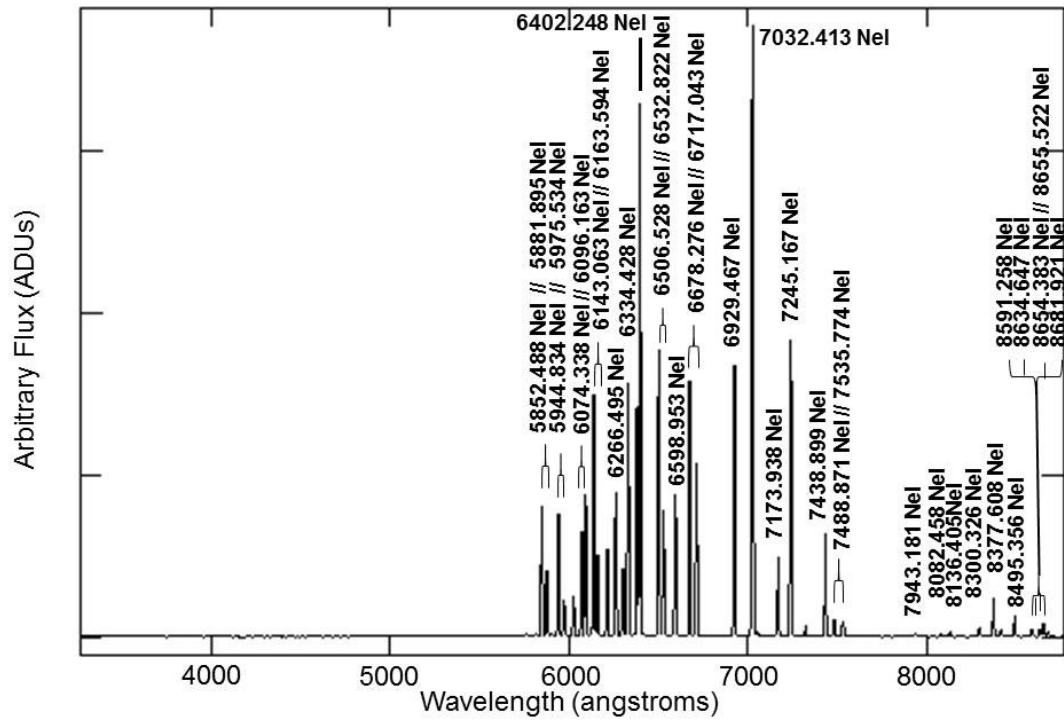
OSIRIS R500B: HgAr calibration lamp



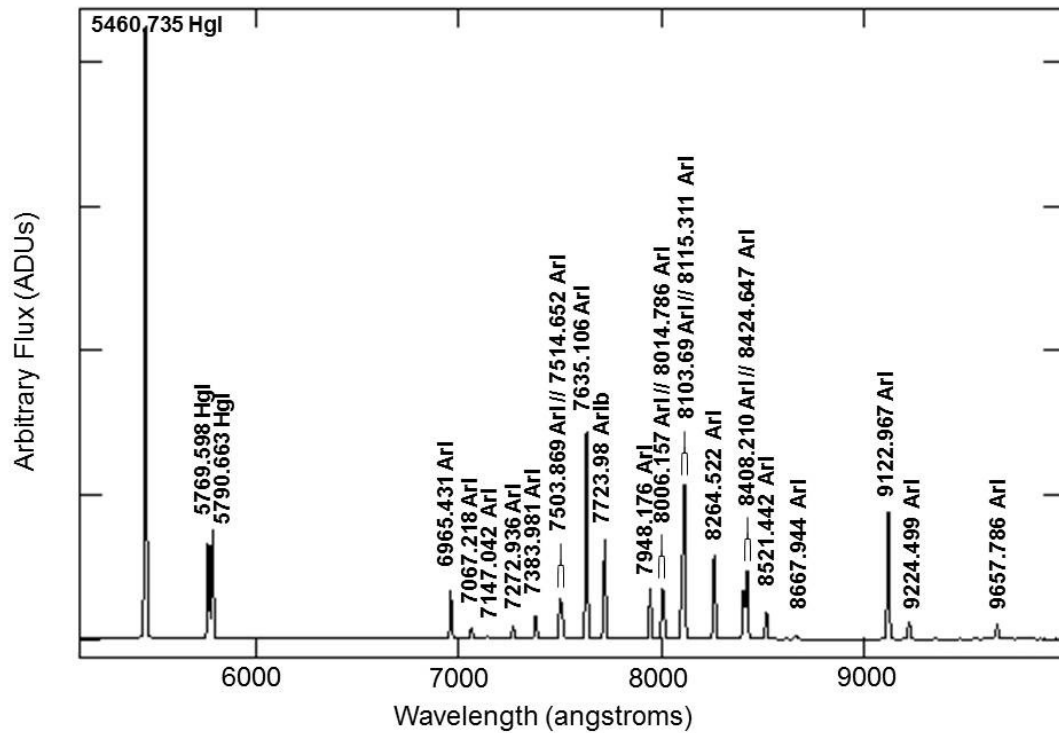
OSIRIS R500B: HgAr calibration lamp (Ar lines)



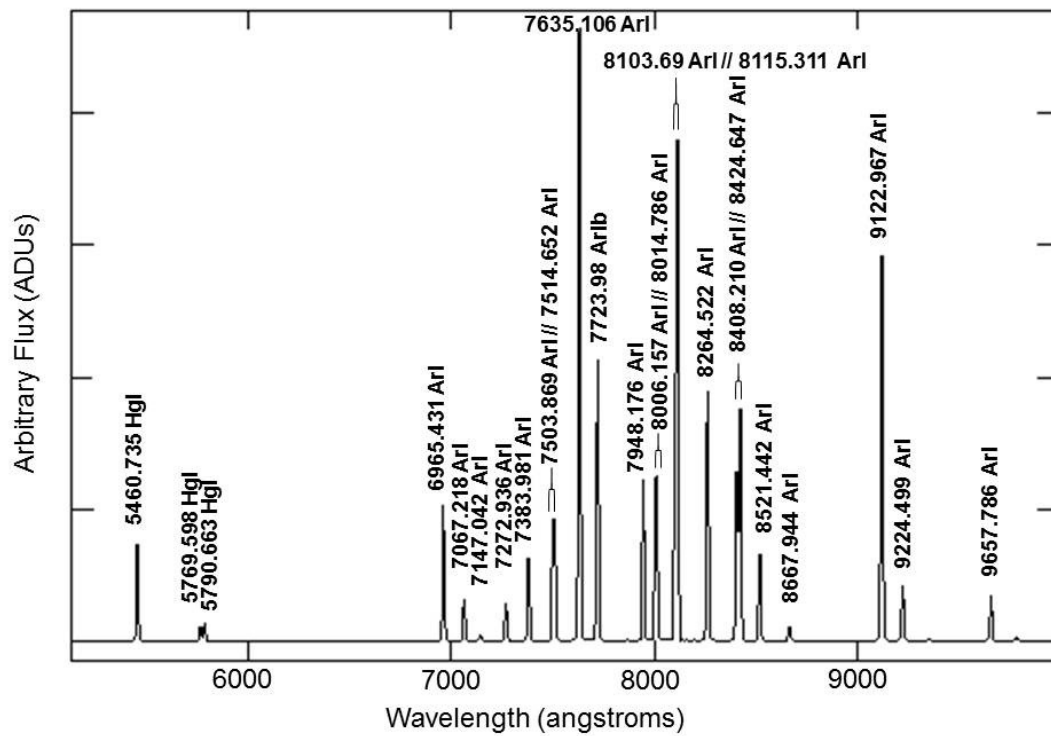
OSIRIS R500B: Ne calibration lamp



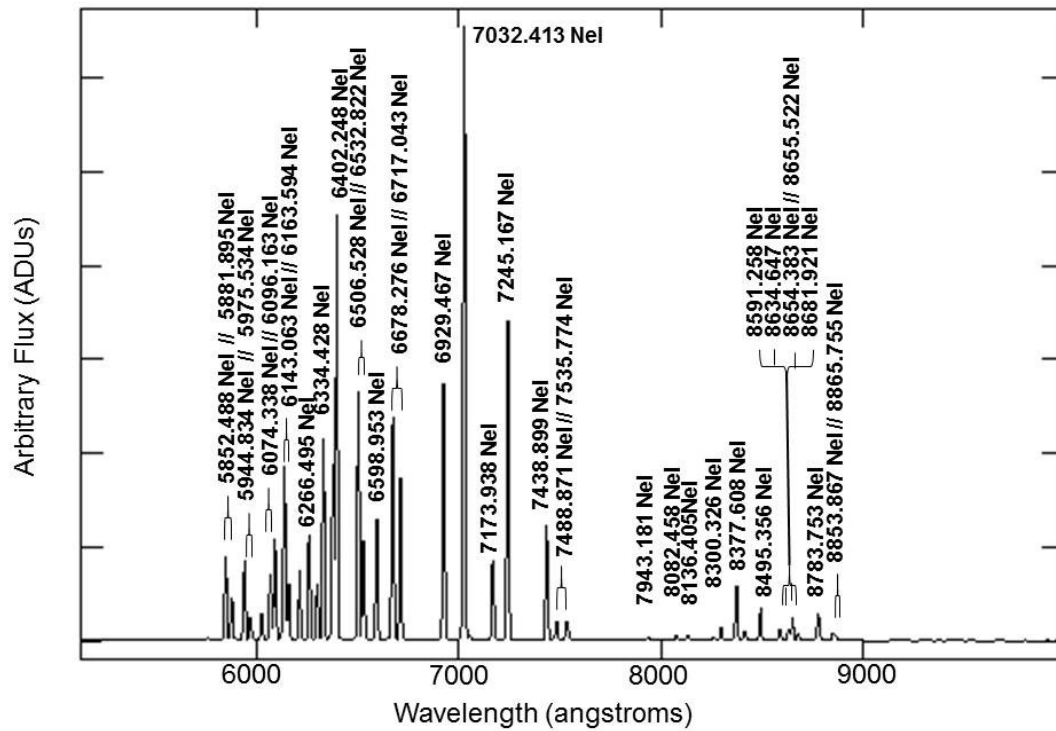
OSIRIS R500R: HgAr calibration lamp



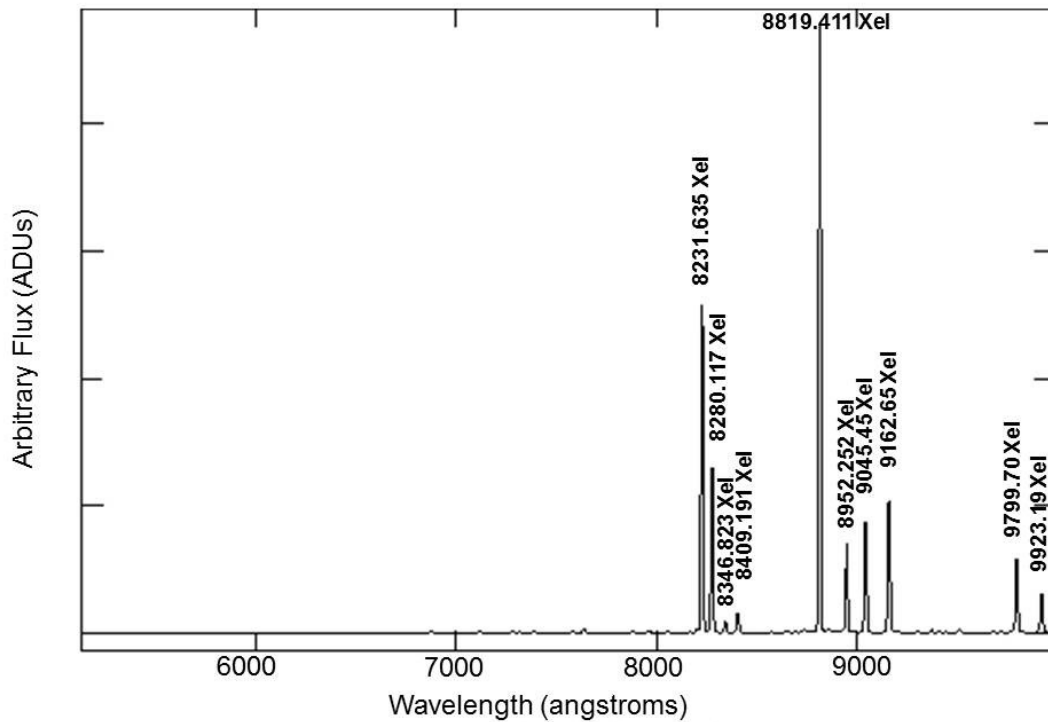
OSIRIS R500R: HgAr calibration lamp (Ar lines)

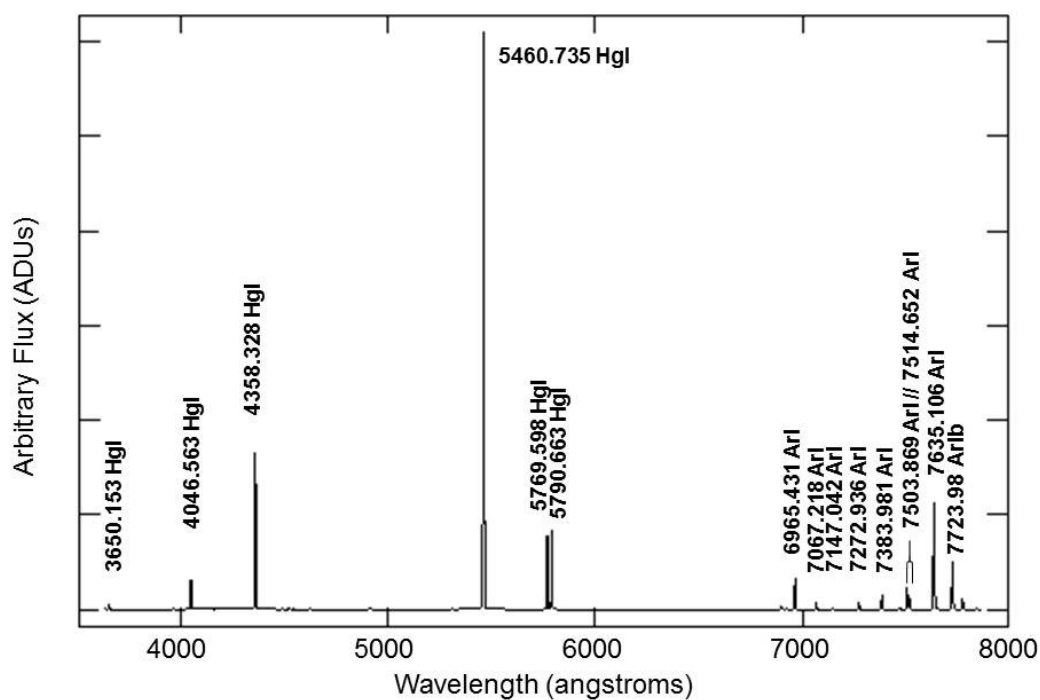
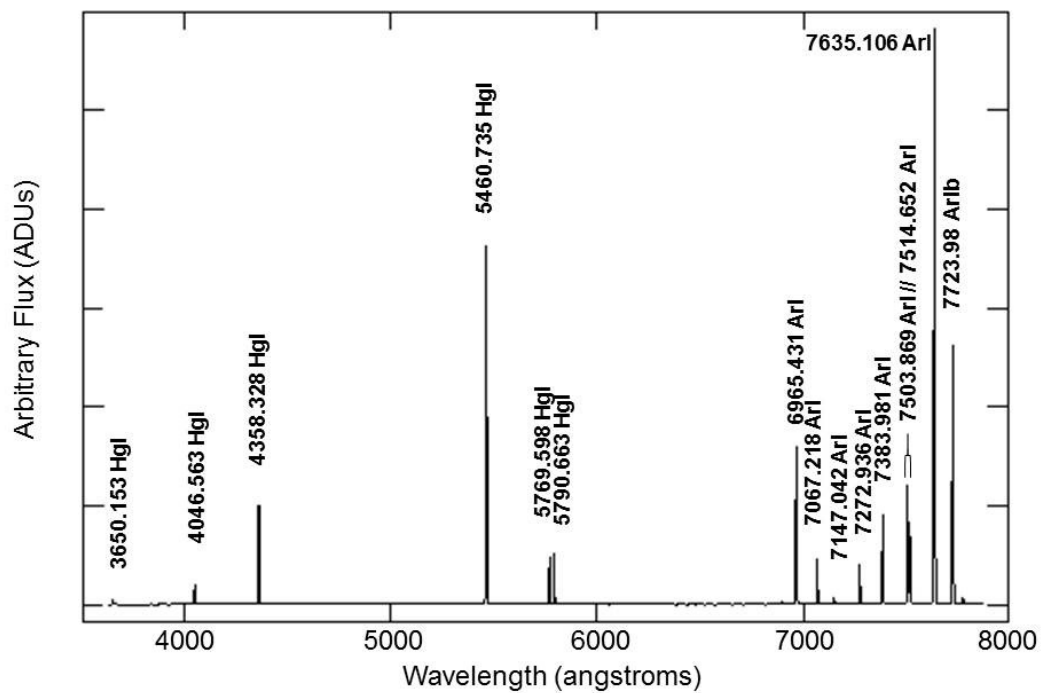


OSIRIS R500R: Ne calibration lamp

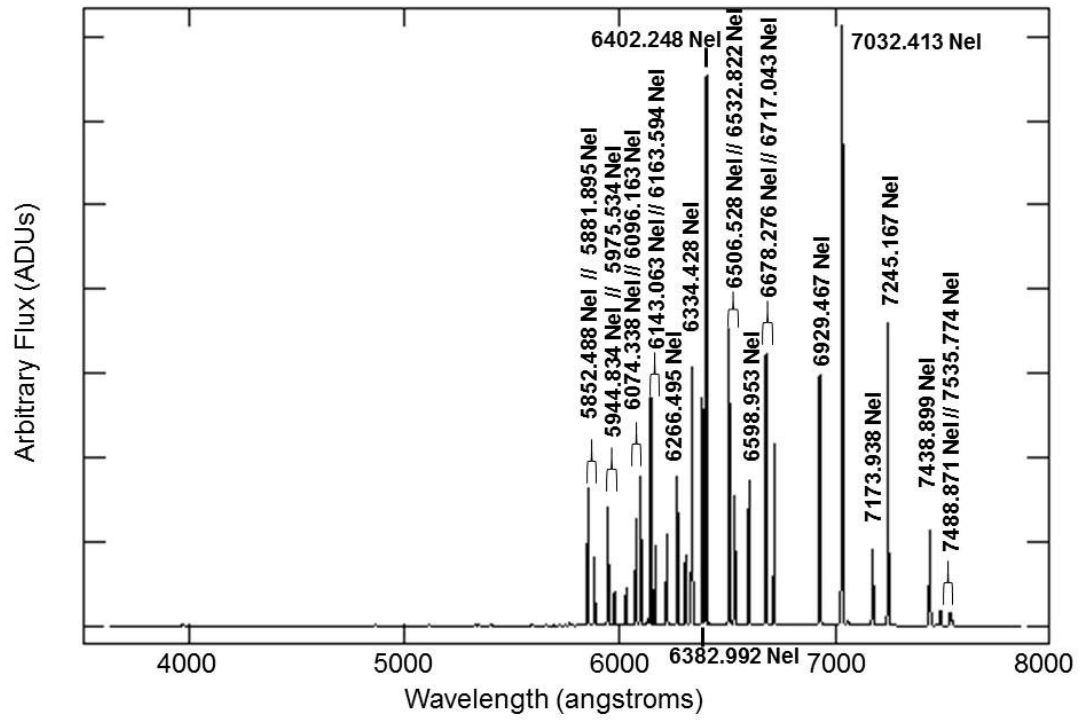


OSIRIS R500R: Xe calibration lamp

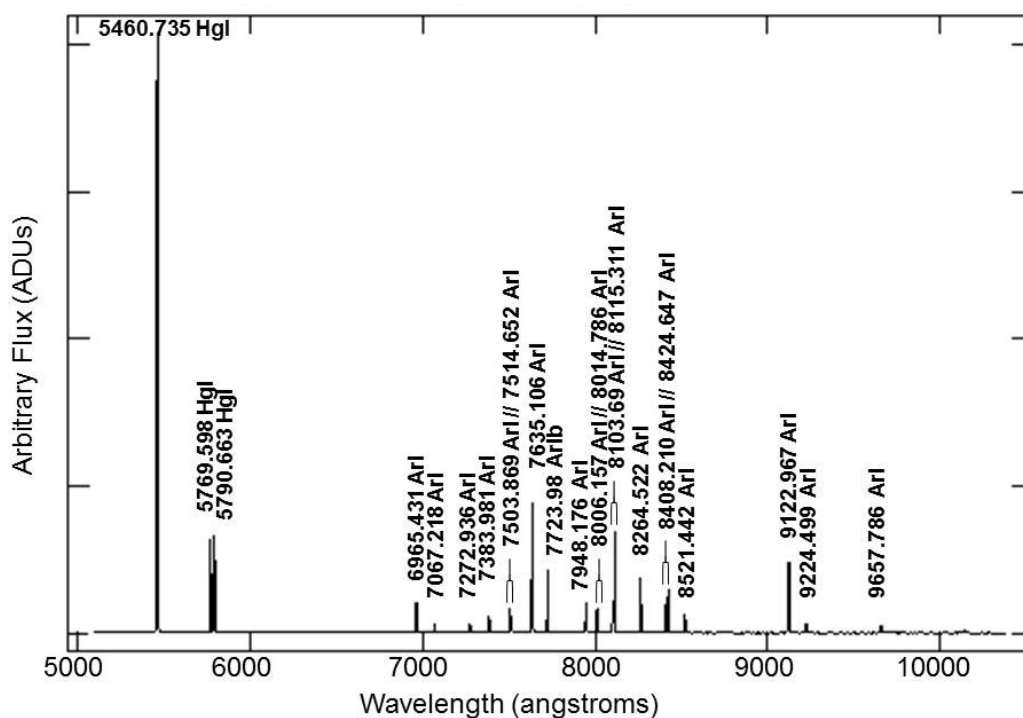


OSIRIS R1000B: HgAr calibration lamp**OSIRIS R1000B: HgAr calibration lamp (Ar lines)**

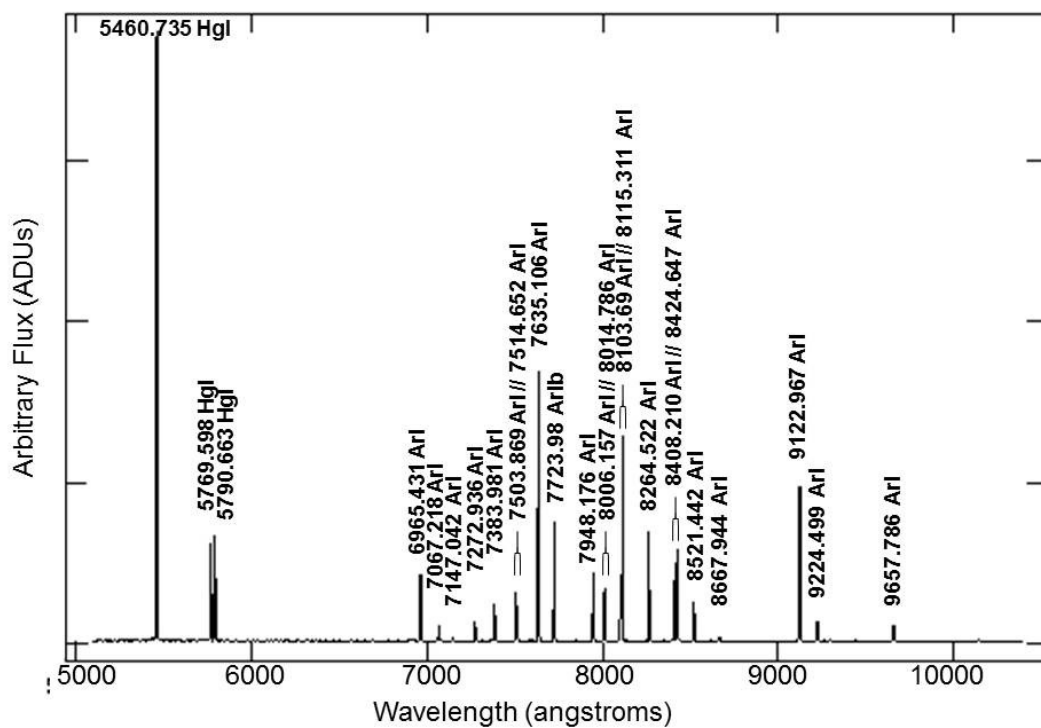
OSIRIS R1000B: Ne calibration lamp



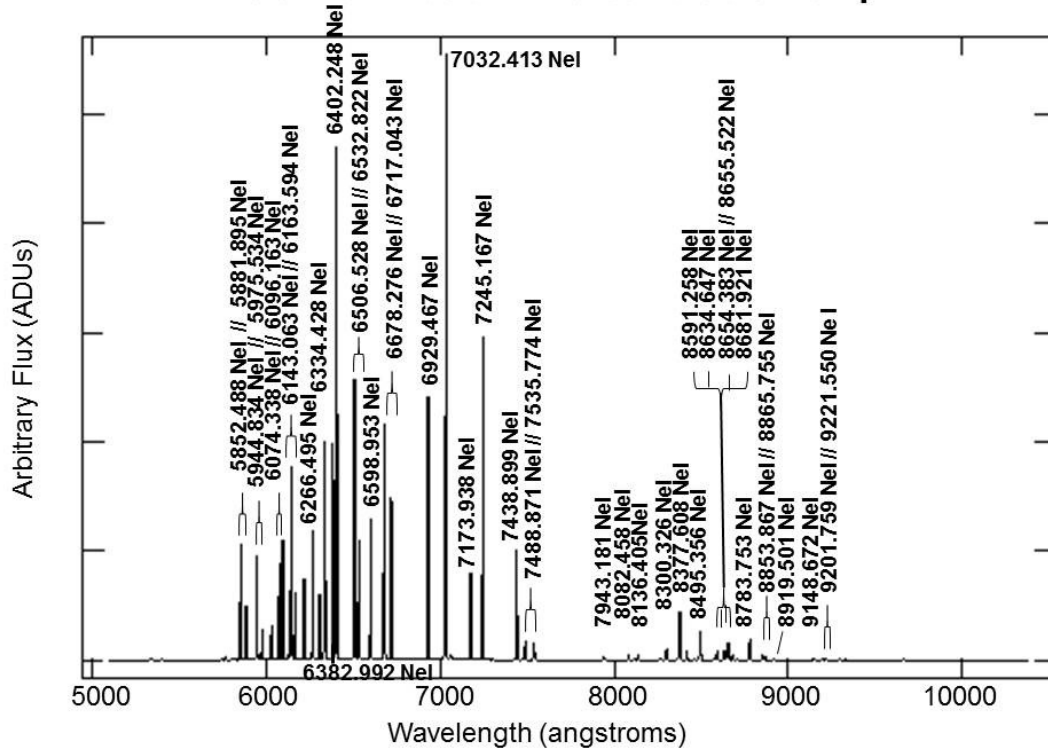
OSIRIS R1000R: HgAr calibration lamp



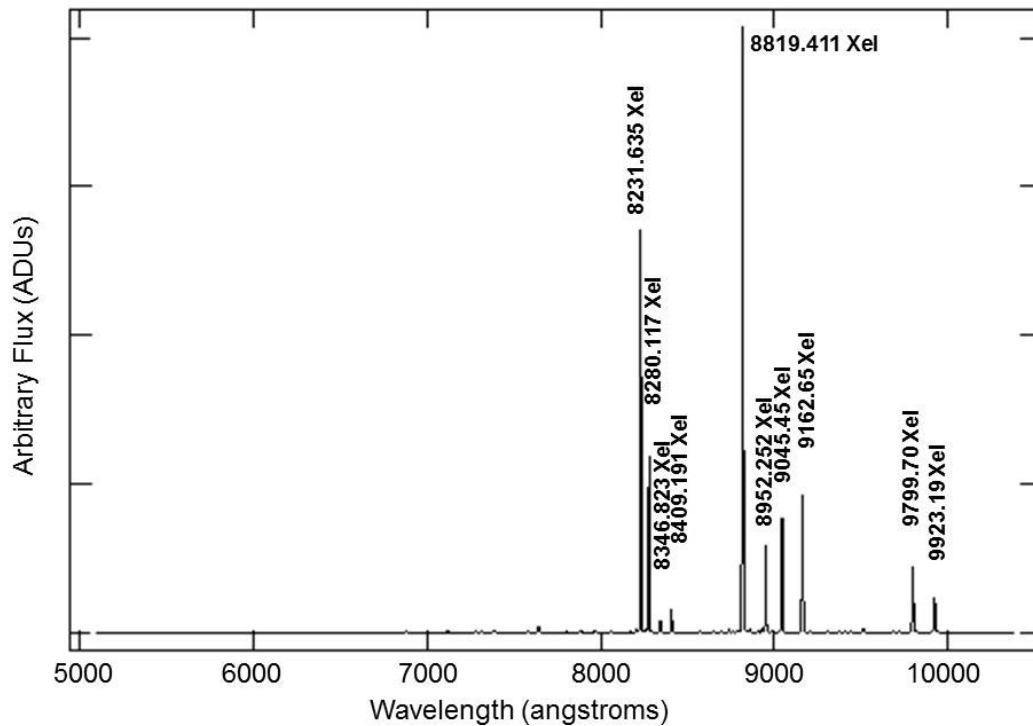
OSIRIS R1000R: HgAr calibration lamp (Ar lines)



OSIRIS R1000R: Ne calibration lamp



OSIRIS R1000R: Xe calibration lamp



13 OSIRIS SLOAN PHOTOMETRIC STANDARDS

Photometric calibration for OSIRIS Broad Band imaging is done via a Sloan standard set taken from Smith et al. (2002, AJ, 123, 2121):

Name	RA (J2000)	DEC (J2000)	r'	u'-g'	g'-r'	r'-i'	i'-z'
G 158-100	00:33:54.60	-12:07:58.9	14.691	1.101	0.510	0.222	0.092
SA 92 282	00:56:46.86	+00:38:30.9	12.936	1.000	0.136	0.021	-0.009
Feige 22	02:30:16.62	+05:15:50.6	13.024	0.050	-0.333	-0.303	-0.273
SA 95 193	03:53:20.59	+00:16:34.7	13.844	2.489	1.097	0.407	0.214
Ross 49	05:44:56.81	+09:14:32.2	11.163	1.130	0.467	0.162	0.049
Hilt 566	06:32:09.67	+03:34:44.4	10.787	1.125	0.673	0.341	0.211
Ru 149F	07:24:14.02	-00:31:38.2	13.119	2.469	0.867	0.317	0.166
SA 100 280	08:53:35.47	-00:36:41.0	11.689	1.143	0.308	0.084	0.003
PG0918+029D	09:21:21.94	+02:47:28.7	11.937	2.227	0.817	0.324	0.166
SA 101 316	09:54:52.03	-00:18:34.4	11.438	1.152	0.309	0.073	0.007
G 162-66	10:33:42.81	-11:41:38.7	13.227	-0.183	-0.387	-0.354	-0.303
Feige 34	10:39:36.73	+43:06:09.2	11.423	-0.509	-0.508	-0.347	-0.265
PG1047+003A	10:50:05.65	-00:01:11.3	13.303	1.385	0.519	0.212	0.087
G 163 50	11:07:59.97	-05:09:26.0	13.266	0.215	-0.277	-0.272	-0.271
Feige 66	12:37:23.52	+25:03:59.9	10.747	-0.345	-0.476	-0.367	-0.316
SA 104 428	12:41:41.31	-00:26:26.5	12.330	2.153	0.763	0.279	0.147
PG1323-086D	13:26:05.26	-08:50:35.7	11.928	1.210	0.397	0.132	0.032
Ross 838	14:01:44.47	+08:55:17.4	11.327	1.277	0.573	0.239	0.111
PG1528+062B	15:30:39.55	+06:01:13.1	11.828	1.235	0.419	0.143	0.036
G 15-24	15:30:41.76	+08:23:40.4	11.277	1.035	0.412	0.151	0.052
BD+33 2642	15:51:59.88	+32:56:54.3	10.979	-0.018	-0.332	-0.284	-0.212

Ross 530	16:19:51.66	+22:38:20.2	11.319	1.273	0.558	0.229	0.103
Wolf 629	16:55:25.66	-08:19:13.1	11.129	3.013	1.413	1.466	0.648
SA 109 381	17:44:12.26	-00:20:32.7	11.514	1.477	0.547	0.223	0.094
Ross 711	18:35:19.17	+28:41:55.3	11.295	0.837	0.282	0.104	0.015
SA 110 232	18:40:52.33	+00:01:54.8	12.287	1.390	0.552	0.237	0.094
SA 111 1925	19:37:28.62	+00:25:03.1	12.345	1.397	0.200	0.061	0.051
Wolf 1346	20:34:21.89	+25:03:49.7	11.753	-0.016	-0.351	-0.309	-0.291
SA 112 805	20:42:46.74	+00:16:08.4	12.174	1.183	-0.087	-0.135	-0.090
SA 113 260	21:41:48.03	+00:23:53.3	12.284	1.217	0.331	0.080	0.015
BD+28 4211	21:51:11.02	+28:51:50.4	10.750	-0.517	-0.511	-0.379	-0.313
G 93-48	21:52:25.37	+02:23:19.6	12.961	0.107	-0.308	-0.307	-0.261
SA 114 656	22:41:35.06	+01:11:09.8	12.326	1.961	0.756	0.293	0.156
GD 246	23:12:23.07	+10:47:04.2	13.346	-0.491	-0.504	-0.378	-0.367
PG2336+004B	23:38:38.26	+00:42:46.4	12.312	1.101	0.336	0.100	0.014

14 OSIRIS SPECTROPHOTOMETRIC STANDARDS

Flux calibration for OSIRIS Long Slit Spectroscopy, OSIRIS MOS and OSIRIS TF imaging is done via the following subset of standards taken from the ING spectrophotometric standards list:

Name	RA/DEC (J2000)	mag (5556)	Wavelength coverage	Reference
G158-100	00:33:54.5 -12:07:58	14.8	320-1000 nm	Oke 1990, AJ 99, 1621 Filippenko & Greenstein 1984, PASP 96, 530
GD50	03:48:50.06 -00:58:30.4	14.06	320-920 nm	Oke 1990, AJ 99, 1621
HZ15	04:40:39.32 +08:40:45.3	12.6	320-840 nm	Stone 1977, ApJ 218, 767
G191-B2B	05:05:30.6 +52:49:56	11.9	320-1000 nm	Oke 1974, ApJ Supp. 27, 21 Massey 1988, ApJ 328, 315 Oke 1990, AJ 99, 1621
GD71	05:52:27.51 +15:53:16.6	14.5	320-1000 nm	Bohlin et al. 1995, AJ 110, 1316
Hilt600	06:45:13.33 +02:08:14.1	10.4	320-1000 nm	Hamuy et al. 1994, PASP, 106, 566 Hamuy et al. 1992, PASP, 104, 533
He 3	06:47:37.99 +37:30:57.0	12.1	320-940 nm	Oke 1974, ApJ Supp. 27, 21
PG0823+546	08:26:49.4 +54:28:01	14.4	320-800 nm	Massey 1988, ApJ 328, 315
Feige 34	10:39:36.7 +43:06:10	11.3	320-900 nm	Stone 1977, ApJ 218, 767 Massey 1988, ApJ 328, 315 Oke 1990, AJ, 99, 1621
GD 140	11:37:05.1 +29:47:58	12.4	320-1000 nm	Massey 1988, ApJ 328, 315 Oke 1974, ApJ. Supp. 27, 21
HZ 21	12:13:56.6 +32:56:30	14.7	320-900 nm	Oke 1990, AJ 99, 1621
GD153	12:57:02.3 +22:01:56.0	13.3	320-1000 nm	Bohlin et al. 1995, AJ 110, 1316

GRW+70d5824	13:38:51.87 +70:17:08.5	12.77	320-920 nm	Oke 1990, AJ 99, 1621
GD190	15:44:20.0 +18:06.7	14.7	320-1000 nm	Oke 1974, ApJ. Supp. 27, 21
BD+33d2642	15:51:59.86 +32:56:54.8	10.81	320-920 nm	Oke 1990, AJ 99, 1621
Ross 640	16:28:25.03 +36:46:15.4	13.8	320-1000 nm	Oke 1974, ApJ. Supp. 27, 21
PG1708+602	17:09:15.9 +60:10:10	13.9	320-800 nm	Massey 1988, ApJ 328, 315
Grw+70 8247	19:00:10.25 +70:39:51.2	13.1	340-920 nm	Oke 1974, ApJ Supp. 27, 21
G24-9	20:13:55.7 +06:42:45	15.8	320-1000 nm	Oke 1990, AJ, 99, 1621 Filippenko & Greenstein 1990, PASP 96, 530
LDS749B	21:32:15.75 +00:15:13.6	14.67	320-920 nm	Oke 1990, AJ 99, 1621
GD248	23:26:06.59 +16:00:19.6	15.1	320-1000 nm	Oke 1990, AJ, 99, 1621 Filippenko & Greenstein 1984, PASP 96, 530
Feige110	23:19:58.39 -05:09:55.8	11.82	320-920 nm	Oke 1990, AJ 99, 1621

A. LIST OF REFERENCE DOCUMENTS

1	Lauer T. & Valdés F. 1997, NOAO Newsletter 52 (http://www.noao.edu/noao/noaonews/dec97/node23.html)
2	Valdés F. 2000, Mosaic Data Structures (http://iraf.noao.edu/projects/ccdmosaic)
3	<i>The Zen of IRAF</i> . A Spiritual User's Guide to the "Image Reduction and. Analysis Facility" for the LINUX Novice. A. Charles Pullen. A User's Guide to CCD Reductions with IRAF , Philip Massey, February 1997

B. REFERENCES

- Bertin, E, & Arnouts, S. 1996, A&AS 117, 393 (SEXtractor)
- Castro F.J. et al. 2007, *Optical Data of GTC*, GTC Internal Report
- Cuillandre et al. 1994, A&A 281, 503
- Filippenko, 1982, PASP 94, 715
- Francis P.J. & Bland-Hawthorn J. 2004, MNRAS 353, 301
- González-Serrano et al. 2004, Experimental Astronomy 18, 65
- Jester S. et al. 2005, AJ 130, 873
- Jones, Shopbell & Bland-Hawthorn 2002, MNRAS 329, 759
- Landolt A.U. 1992, AJ 104, 340
- Pérez-Gonzalez et al., 2013, ApJ, 762, 46 (SHARDS survey description)
- SESO 2006, Collimator Unit Measurement Report
- Smith et al. 2002, AJ, 123, 2121
- Szokoly, 2005, A&A 443, 703
- Veilleux S. et al. 2010, AJ 139, 145